Max-Planck-Institut
für Kolloid- und Grenzflächenforschung
Abteilung Theorie und Bio-Systeme

Universität Potsdam

On the Depolymerization of Actin Filaments

Dissertation

zur Erlangung des akademischen Grades
Doktor der Naturwissenschaften (Dr. rer. nat.)
in der Wissenschaftsdisziplin Theoretische Physik

eingereicht an der
Mathematisch-Naturwissenschaftlichen Fakultät
der Universität Potsdam

angefertigt in der
Abteilung Theorie und Bio-Systeme
des Max-Planck-Instituts
für Kolloid- und Grenzflächenforschung

von
Thomas Niedermayer

Potsdam, im Juli 2012

Published online at the
Institutional Repository of the University of Potsdam:
URL http://opus.kobv.de/ubp/volltexte/2013/6360/
URN urn:nbn:de:kobv:517-opus-63605
http://nbn-resolving.de/urn:nbn:de:kobv:517-opus-63605

Abstract

Actin is one of the most abundant and highly conserved proteins in eukaryotic cells. The globular protein assembles into long filaments, which form a variety of different networks within the cytoskeleton. The dynamic reorganization of these networks – which is pivotal for cell motility, cell adhesion, and cell division – is based on cycles of polymerization (assembly) and depolymerization (disassembly) of actin filaments. Actin binds ATP and within the filament, actin-bound ATP is hydrolyzed into ADP on a time scale of a few minutes. As ADP-actin dissociates faster from the filament ends than ATP-actin, the filament becomes less stable as it grows older. Recent single filament experiments, where abrupt dynamical changes during filament depolymerization have been observed, suggest the opposite behavior, however, namely that the actin filaments become increasingly stable with time. Several mechanisms for this stabilization have been proposed, ranging from structural transitions of the whole filament to surface attachment of the filament ends.

The key issue of this thesis is to elucidate the unexpected interruptions of depolymerization by a combination of experimental and theoretical studies. In new depolymerization experiments on single filaments, we confirm that filaments cease to shrink in an abrupt manner and determine the time from the initiation of depolymerization until the occurrence of the first interruption. This duration differs from filament to filament and represents a stochastic variable. We consider various hypothetical mechanisms that may cause the observed interruptions. These mechanisms cannot be distinguished directly, but they give rise to distinct distributions of the time until the first interruption, which we compute by modeling the underlying stochastic processes. A comparison with the measured distribution reveals that the sudden truncation of the shrinkage process neither arises from blocking of the ends nor from a collective transition of the whole filament. Instead, we predict a local transition process occurring at random sites within the filament.

The combination of additional experimental findings and our theoretical approach confirms the notion of a local transition mechanism and identifies the transition as the photo-induced formation of an actin dimer within the filaments. Unlabeled actin filaments do not exhibit pauses, which implies that, in vivo, older filaments become destabilized by ATP hydrolysis.

This destabilization can be identified with an acceleration of the depolymerization prior to the interruption. In the final part of this thesis, we theoretically analyze this acceleration to infer the mechanism of ATP hydrolysis. We show that the rate of ATP hydrolysis is constant within the filament, corresponding to a random as opposed to a vectorial hydrolysis mechanism.

Contents

1 Introduction

1.1 Dynamics of single actin filaments

From ancient times, motion has been considered as a measure of vitality. Life as defined by modern biological concepts – such as metabolism, mutation, and selection – heavily relies on the directed motion of many parts of the cellular machinery. An important example for such motion on the microscopic scale is the dynamics of actin filaments. In this thesis, we study the disassembly of single actin filaments and its relation to different states of the building blocks of the filament.

1.1.1 Actin as part of the cytoskeleton

Actin is one of the most abundant and highly conserved proteins in eukaryotic cells [1]. Its most prominent feature is the ability to self-assemble into long filaments that amount to a major part of the cytoskeleton, which maintains the cell's structure and shape [2], see figure 1.1(a). Networks of actin filaments are pivotal to cell motility in two distinct ways.

First, they serve as tracks for the family of myosin motors. This enables the transport of biological cargoes such as macromolecules, vesicles and different organelles through the highly viscous cytosol (cell fluid) of eukaryotic cells. In addition, myosin, acts as a linker between actin filaments. The generation of force by myosin motors that are, in a highly organized fashion, attached to actin filament, leads to muscle contraction. In fact, actin was first isolated in 1942 from muscles [3] where it constitutes up to 20% of the total protein mass [4]. With a mechanism similar to muscle contraction, many eukaryotic cells use a contractile ring of actin filaments and myosin to pinch themselves in two during cell division [5].

Second, the filament assembly itself constitutes directed motion 1.1(b)-(c). The assembly and disassembly of intricate actin networks in the vicinity of the plasma membrane locally controls the cell morphology. This process not only gives rise to cell locomotion with cell migration rates of up to 0.5 μm/s [6, 7], but also contributes to cell adhesion [2] and endocytosis, i.e., the uptake of molecules by the cell [8, 9]. The dissipative cycles of actin assembly and disassembly are coupled to ATP hydrolysis as discussed below, and a large number of regulatory actin binding proteins (ABPs) have been identified to play an essential role *in vivo* [10]. Filament assembly from monomers is often termed polymerization in the literature, despite the fact that an actin filament is not a polymer in the classical sense, but an assembly of identical polymers, each constituting a single copy of the actin protein. We adopt both the terms *polymerization* and *depolymerization* in this text.

In the following, we review the structure of globular (G-) and filamentous (F-)actin and discuss how binding of a nucleotide – either ATP or ADP – influences filament polymerization and depolymerization. In order to focus on aspects of relevance for our investigations, we

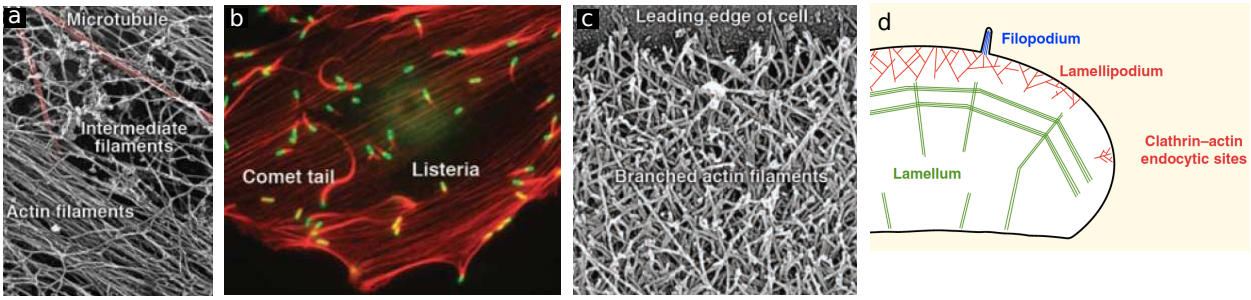

Figure 1.1 : Actin filament networks in cells. (a) Electron micrograph of the three types cytoskeleton polymers: Actin filaments, intermediate filaments, and microtubules (colored in red). (b) Fluorescence image of an animal epithelial cell infected with the bacterial pathogen Listeria. Actin filaments are shown in red and Listeria in green. Actin bundles, called stress fibers, bridge sites of adhesion to the substrate. Listeria assembles actin "comet tails" for locomotion through the cytoplasm. (c) Electron micrograph of the network of branched actin filaments at the leading edge (called the lamellipodium) of a motile cell. (d) Some examples of distinct networks of actin filaments in metazoan cells. Red: At the lamellipodium of migrating cells and at sites of endocytosis, dense networks of actin filaments are nucleated and crosslinked in branched arrays. Green: The lamellum is composed of linear arrays of actin filaments organized into longitudinal stress fibers. Blue: Filopodia are finger-like protrusions and contain linear bundled arrays of actin filaments. The images (a)-(c) are taken from [5], the schematic (d) is from [11].

restrict the introduction into actin dynamics threefold. First, we mainly consider actin *in vitro* and in particular do not discuss the myriads of proteins that regulate actin dynamics *in vivo*. Second, we focus on the results about single filaments and ignore the experimental and theoretical research on gels and actin networks *in vitro*. Third, we consider actin dynamics only in terms of filament polymerization and depolymerization and not in terms of the bending motion of these filaments.

1.1.2 Structure of globular and filamentous actin

The globular protein actin (*G-actin*) is folded into two major domains of similar size. The polypeptide consists of 375 residues and has a molecular weight of about 43 kDa. Most organisms have multiple actin genes. The known diversity of actin isoforms arises from these multiple genes rather than from alternative splicing of mRNAs. Even between highly divergent species, the sequences of pairs of actin isoforms are generally more than 90% identical. In living cells some isoforms are sorted into particular structures, for instance stress fibers or the lamellipodium, see figure 1.1(d). However, *in vitro* actin isoforms copolymerize in every case that was studied [1].

The first crystal structure of G-actin was determined by X-ray diffraction of actin co-crystallized with Deoxyribonuclease I which binds actin monomers with very high affinity and actin polymers with lower affinity [17]. Subsequently, more than 80 very similar crystal structures of actin have been reported, where polymerization was prevented by ABPs, small molecules, or by chemically modifying or mutating actin [14]. Actin is folded into two major domains with two clefts between these domains, see figure 1.2(a). One cleft, marked by

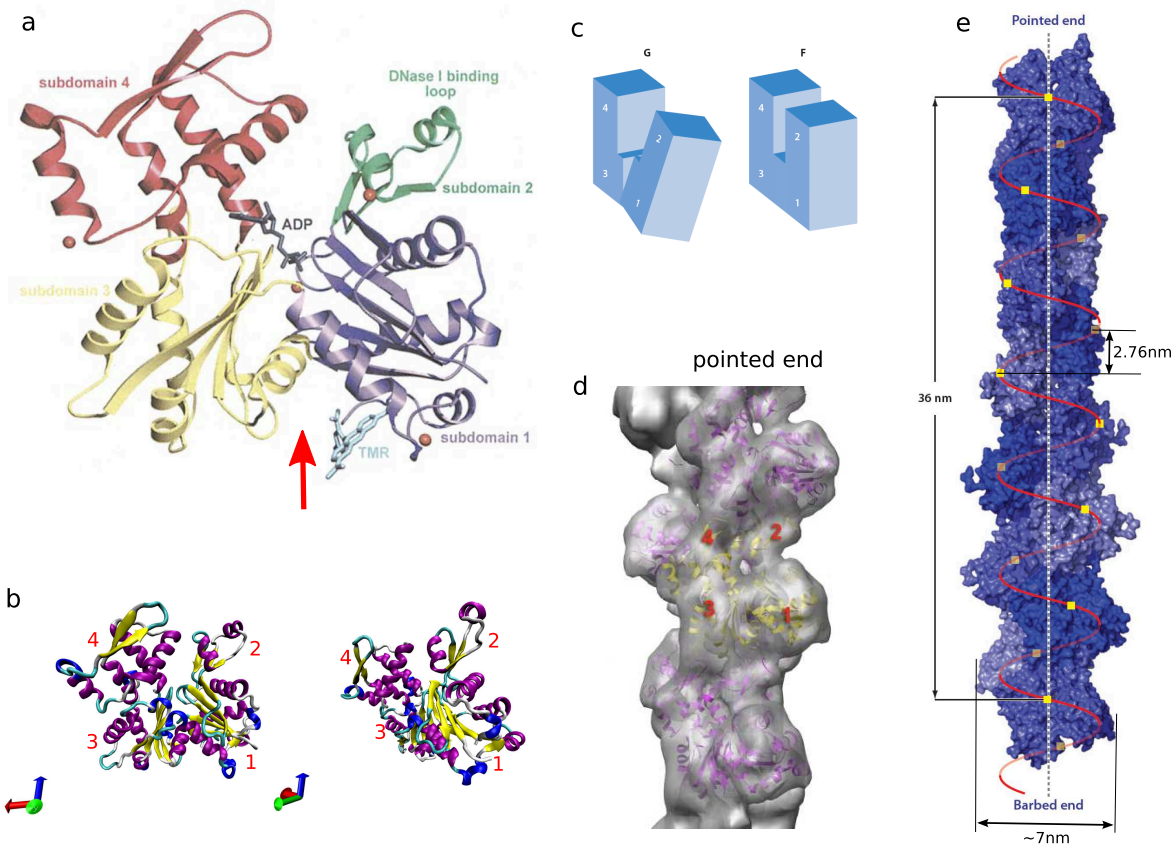

Figure 1.2 : Structure of globular (G-) and filamentous (F-) actin. (a) Crystal structure of G-actin with bound ADP, from [12]. Tetramethylrhodamine-5-maleimide (TMR) was covalently attached to Cysteine-374 to prevent polymerization and allow crystallization. Actin is folded into two major domains with two subdomains each. These four subdomains are represented in different colors. The nucleotide is bound at the center of the molecule, where the four subdomains meet. Nucleotide-dependent differences in this location may provide a mechanism to change the orientations of the actin subdomains relative to each other and explain the conformational differences between ATP- and ADP-actin [12, 13]. The four red spheres represent bound Ca^{2+} ions. One Ca^{2+} is binds in association with the nucleotide at the high-affinity binding site for divalent cations. The other three at some low-affinity binding sites at the surface of the molecule. The arrow indicates the small cleft that constitutes the major binding site for most ABPs. (b) Clockwise rotation of the G-actin molecule by about 45° around the vertical (blue) axis. The otherwise flat G-actin molecule exhibits a twist around the axis connecting the subdomains 1 and 3. The structure is from the protein data base (PDB code: 1J6Z) and illustrated with `VMD`. (c) A sketch of the relative twist, taken from [14]. Reducing this twist by a relative rotation of the two major domains by about 20° is the essence of the G-actin to F-actin transition. (d) Projection of the atomic model of the F-actin protomer (with the four labeled subdomains) into the three-dimensional filament reconstruction from cryo-electron microscopy (gray surface), with the pointed end at the top. The graphic is taken from [15]. (e) The helical structure of an actin filament derived from cryo-electron microscopy [16]. The figure is adapted from [14]. The filament can be envisaged as a single left-handed helix with approximately 13 actin molecules repeating every six turns in an axial distance of about 36 nm and a diameter of about 7 nm.

the arrow, is lined by hydrophobic residues and constitutes the major binding site for most ABPs. At the second, larger cleft a nucleotide (ATP or ADP) and an associated divalent cation bind the actin molecule and provide a linkage between the domains. Data from X-ray diffraction reveal that there are structural differences between ATP-actin and ADP-actin [12, 13]. Furthermore, polymerization assays suggest a slow conformational change that follows the replacement of Ca^{2+} by Mg^{2+} at the binding site near the bound nucleotide [18]. Besides this high-affinity binding site for divalent cations, where Ca^{2+} and Mg^{2+} bind with a dissociation constant in the nanomolar range, there are multiple low-affinity cation binding sites at the surface of G-actin, see figure 1.2(a). Physiological concentrations of mono- or divalent cations promote the polymerization of filaments because of the putative conformational changes induced by binding at these sites [18, 19].

An actin filament is a helical structure, see figure 1.2(e). It can be envisaged as a single left-handed helix with approximately 13 actin molecules repeating every six turns in an axial distance of 35.9 nm and a diameter of about 7 nm [14]. Thus, every subunit – which in reference to the term monomer is called protomer throughout this text – accounts for about 2.76 nm of the filament length. Because the twist per protomer is about $6 \times 360°/13 \simeq 166°$ and hence close to 180°, the filament can be pictured as two intertwined, slowly turning right-handed helices. Because of the head-to-tail arrangement of asymmetric protomers within the filament, the filament has a polarity with two distinct ends. Based on the arrowhead pattern created by the decoration with myosin [20], one end is called *barbed end* and the other *pointed end*. This polarity is key to the mechanism of actin assembly in cells where the barbed end is favored for growth [6].

Even though electron microscopy has been used to image actin filaments as early as in the 1940s [21] and revealed the double-helical structure in the 1960s [22], to date the structure of filamentous actin (*F-actin*) has not been resolved on an atomistic level. In fact, actin filaments cannot be crystallized because their symmetry with about 2.17 protomers per turn of the helix is incompatible with any crystal space group [15]. Models for the atomic structure of F-actin were constructed by docking the crystal structure of G-actin from Ref. [17] into lower resolution structures obtained by X-ray diffraction of oriented filament gels [23]. Quite recently, higher resolution data from X-ray fibre diffraction intensities obtained from well oriented sols of filaments allowed the construction of a refined filament model, which elucidates the nature of the transition from G- to F-actin [24]. In this model the major conformational transition is a relative rotation of the two major domains by about 20°, see figure 1.2(c).

1.1.3 Polymerization of actin

G-actin binds both Ca^{2+} and Mg^{2+} ions with nanomolar affinity [18, 25]. Given that the concentration of magnesium ions in cells is much higher than the one of calcium ions, G-actin *in vivo* is saturated with Mg^{2+}. Contrary to that, purified G-actin is typically kept in Ca^{2+} buffer. In typical polymerization assays this cation is replaced by Mg^{2+} shortly before the initiation of polymerization, see chapter 2. If not otherwise indicated, we consider the physiologically relevant Mg-actin throughout this text. The polymerization of actin *in vitro* requires a high concentration of cations, similar to the physiological salt conditions, to ensure

that the low-affinity cation binding-sites of G-actin are sufficiently occupied. In fact, the putative conformational changes induced by ions binding at these sites are associated with the activation of G-actin [18,19]. In typical experiments, either K^+ or Mg^{2+} at concentrations between 10 and 100 mM are used.

Nucleation is the rate-limiting step in spontaneous polymerization of actin, because actin dimers are extremely unstable. Trimers appear to be the critical nuclei, that is the smallest actin oligomers that are more likely to grow into a filament than to dissociate into monomers. Because of the extreme instability of dimers and trimers, the rate constants for their formation and decay cannot directly be measured, but are determined as parameters from kinetic models that reproduce the time course of the amount of polymerized actin [26, 27].

Because of the double-stranded structure of actin filaments, a fragmentation event involves the breakage of three bonds between protomers, while the dissociation of a protomer involves the breakage of only two bonds. Likewise, the end-to-end annealing of filaments involves the formation of three bonds, while the association of an monomer involves the formation of only two bonds. Therefore, the elongation and shortening of actin filaments takes place mainly at the ends [28]. In fact, the local rate of spontaneous fragmentation (measured per F-actin protomer) was estimated to be about seven or eight orders of magnitude smaller than the dissociation rate of protomers from the ends [29,30]. The filament polarity causes these two ends to be distinct and one consequence is that filament growth at the barbed end is faster than at the pointed end [31].

Actin polymerization is favored by increasing temperature and is thus endothermic [32]. The formation of hydrophobic bonds between protomers is driven by the increased entropy of the water released at the interface [30].

1.1.4 ATP hydrolysis and treadmilling

To provide a universal source of free energy, living cells maintain the ratio of ATP to ADP at a point that is ten orders of magnitude from equilibrium, i.e. the ATP concentration is about a thousandfold higher than the concentration of ADP [33]. Moreover, the affinity of ATP for G-actin at physiological salt concentrations is about 3-fold higher than the affinity of ADP for G-actin [34]. Therefore, the nucleotide binding pocket of G-actin *in vivo* is saturated with ATP. In fact, ATP is a functional group of G-actin. Its removal by dialysis results in a great loss of polymerizability [35] because of denaturation [36].

The polymerization of actin into a helical structure does not only alter the chemical properties of actin due to steric effects on the filament level but also by distortion of the protein conformation, see figure 1.2. As a consequence, nucleotide exchange is inhibited, but ATP hydrolysis is highly accelerated within the filament [37]. In fact, it was observed as early as 1950 that actin filaments contain ADP instead of ATP [35] and hypothesized that *"[polymerization and ATP hydrolysis] are expressions of one and the same thing: when actin polymerizes ATP disappears, and when [bound] ATP is decomposed, the actin polymerizes"* [35]. As we will see, however, it is essential for the non-equilibrium polymerization dynamics of actin, which drives cell motility, that the hydrolysis of bound ATP is not tightly coupled to the polymerization, but a delayed process, as directly shown in [38].

The structural differences between ATP-actin [13] and ADP-actin [12] give rise to different

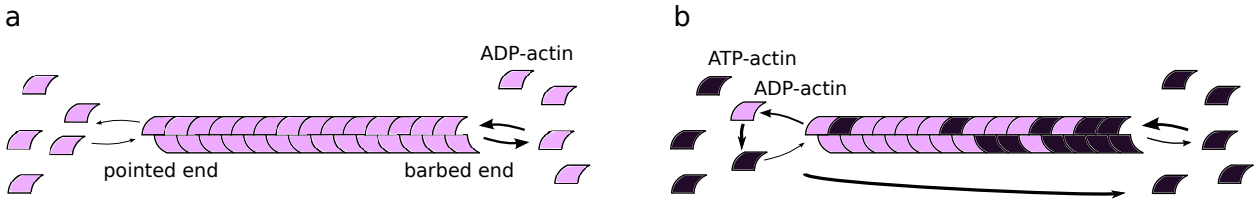

Figure 1.3 : Principle of treadmilling.(a) Sketch of an ADP-actin filament in equilibrium with a pool of ADP-actin monomers. The thickness of the arrows indicates the magnitude of the respective association or dissociation rate. Because of the structural differences, association and dissociation are slow at the pointed end and rapid at the barbed end, but conservation of free energy requires that the critical concentration is equal at both ends and thus the filament can not exhibit directed motion. (b) Treadmilling of a filament assembled from ATP-actin in a pool of ATP-actin monomers. At the barbed end, the association is faster than hydrolysis which transforms ATP-actin protomers (dark) into ADP-actin protomers (bright). In consequence, the protomer at the barbed end is in the ATP-actin conformation. In contrast, hydrolysis is more rapid than ATP-actin association at the pointed end, and therefore there is a higher probability that the protomer at this terminus binds ADP. The conformational difference between ATP- and ADP-actin does not only change the kinetic, but also the thermodynamics properties of the ends, i.e., the free energy difference for association, or equivalently the critical concentrations. ATP-actin has a considerably lower critical concentration at the barbed end than ADP-actin at the barbed end, and in consequence the critical concentration of an ATP-actin filament at its barbed end is lower than at its pointed end. For monomer concentrations in between, the filament grows at the barbed end (thus termed plus end) while it shrinks at the pointed end (termed minus end). At the critical concentration of the filament, growth and shrinkage are balanced and the filament "treadmills": it exhibits directed motion towards the barbed end side without net growth or shrinkage. The free energy for this process is provided by the ATP pool. Immediately after the dissociation of ADP-actin from the pointed end, its bound ADP is replaced by ATP. Diffusion of the monomer back to the barbed end then enables the next cycle of polymerization.

polymerization properties of the two types of monomers [39]. G-Actin with bound ADP polymerizes less rapidly than ATP-G-actin, and again, the barbed end appears to be more dynamic than the pointed filament end [40, 41].

A system – consisting of an ADP-actin filament, ADP-G-actin at the concentration c_{D}, the surrounding water and the solved ions – where a filament has been assembled by successive association of monomers at its pointed end, is identical to an analogous system where the filament has been polymerized at its barbed end. Therefore the conservation of free energy requires that the ratio of association rate $\omega_{\mathrm{on,D}}$ and dissociation rate ω_{D} of ADP-actin is identical at both ends and given by

$$\frac{\omega^{\mathrm{B}}_{\mathrm{on,D}}}{\omega^{\mathrm{B}}_{\mathrm{D}}} = \exp\left(-\frac{\Delta G}{k_{\mathrm{B}}T}\right) = \frac{\omega^{\mathrm{P}}_{\mathrm{on,D}}}{\omega^{\mathrm{P}}_{\mathrm{D}}}. \tag{1.1}$$

Here, the superscripts "B" and "P" denote the barbed and pointed ends. For monomer concentrations c_{D} within the experimentally relevant regime, that is below 100 μM, the association rates are proportional to the monomer concentration and defined as $\omega^{\mathrm{B}}_{\mathrm{on,D}} \equiv \kappa^{\mathrm{B}}_{\mathrm{on,D}} \times c_{\mathrm{D}}$, $\omega^{\mathrm{P}}_{\mathrm{on,D}} \equiv \kappa^{\mathrm{P}}_{\mathrm{on,D}} \times c_{\mathrm{D}}$, with the association rate constants $\kappa^{\mathrm{B}}_{\mathrm{on,D}}$ and $\kappa^{\mathrm{P}}_{\mathrm{on,D}}$ for the

barbed and pointed end, respectively. ΔG is the difference between the Gibbs free energy of the system after and before the association of the monomer. It is important to note that the free energy of the entire system, i.e. the filament, ADP-G-actin at the concentration c_{D}, the surrounding water and the solved ions, must be considered. As mentioned above, actin polymerization is endothermic, but without the surrounding water and the dissolved ions, a hypothetical monomer association would result in a decrease of the entropy. Thus, the free energy for the polymerization is provided by the water and/or the solved ions.

The *critical concentration* c^{crit} of a filament end is defined as the monomer concentration where the end neither shrinks nor grows, but is in equilibrium with the monomer pool:

$$c^{\mathrm{crit}} \equiv \frac{\omega_{\mathrm{off}}}{\kappa_{\mathrm{on}}}. \tag{1.2}$$

With eq. (1.1), the free energy change can be expressed in terms of the concentration relative to the critical concentration:

$$\frac{\Delta G}{k_{\mathrm{B}}T} = -\ln\left(\frac{c}{c^{\mathrm{crit}}}\right). \tag{1.3}$$

Conservation of free energy requires that this critical concentration is identical at both filament ends and an ADP-actin filament cannot exhibit directed motion. However, the filament polarity causes a difference between the barbed and the pointed end in terms of kinetics, with the former having the ability to grow or shrink more rapidly than the latter, see figure 1.3. This shows that the free energy barrier is lower for association and dissociation at the barbed end. At concentrations above c^{crit}, the filament grows at both ends, but more rapidly at the barbed end. At concentrations below c^{crit}, it shrinks at both ends, again more rapidly at the barbed end.

As Wegner has realized [42] and we will elaborate in the following, the differences in the association and dissociation kinetics at the ends are one of a few conditions for *treadmilling* – the simultaneous growth at the barbed and shrinkage at the pointed end – of ATP-actin filaments. A faster kinetics at the barbed end implies that on average less time has passed since the incorporation of the protomer at the barbed end with respect to the pointed end. So even in the absence hydrolysis, the barbed end is younger than the pointed end. If the monomer pool consists of ATP-actin, the probability for the presence of ATP-actin is higher at the barbed than at the pointed end, because of the irreversible hydrolysis of bound ATP.

The free energy change ΔG for the association, and thus the critical concentration c^{crit}, differs for the distinct protomer states induced by the bound nucleotide. ATP-actin has a considerably lower critical concentration than ADP-actin [41]. As a consequence, the critical concentration at the barbed end is lower than at the pointed end [41]. In the concentration regime between the two critical concentrations, the filament simultaneously grows at the barbed end and shrinks at the pointed end, thus moving into the direction defined by its polarity. The free energy for this directed motion is provided by the excess of ATP in solution: The ADP that is bound to dissociated G-actin is rapidly replaced by ATP. This enables another cycle of actin polymerization and depolymerization.

In summary, four properties of actin are essential for treadmilling: (i) The structural difference of the filament ends leading to distinct kinetics, (ii) the faster hydrolysis of ATP in F-actin with respect to G-actin, (iii) the conformational change induced by the hydrolysis manifested in a difference of the thermodynamic properties of ATP- and ADP-actin, and

(iv) the fast nucleotide exchange in G-actin, which is prohibited in F-actin. Treadmilling of single actin filaments was first demonstrated *in vitro* by Fujiwara et al. [43].

Treadmilling *in vitro* illustrates the principle but does not account for the velocity of actin turnover *in vivo*, where cell migration with velocities up to 0.5 μm/s, that is almost 200 protomers per second, is driven by treadmilling [6]. In contrast, at treadmilling conditions, the net elongation rate of the barbed end can be estimated to be of the order of 0.1 protomers per second, when using literature values of the *in vitro* rates for association, dissociation and hydrolysis. Furthermore, direct measurement [43] revealed a rate of 0.38 ± 0.31/s. The large enhancement of filament turnover *in vivo* can be rationalized by the function of actin destabilization factors (ADFs/cofilins), which preferentially bind ADP-actin [44, 45]. The destabilization of the filamented caused by these factors accelerates pointed-end disassembly and increases the pool of available monomers for barbed-end elongation.

1.1.5 ATP cleavage and phosphate release

The hydrolysis of F-actin bound ATP takes place in two sequential elementary steps, rapid cleavage of the γ-phosphate of ATP, followed by the slower release of phosphate from the nucleotide binding pocket [46]. The cleavage step is essentially irreversible [47], while the release of the inorganic phosphate (Pi) is reversible [48]. The reversible binding of Pi to ADP-F-actin also reveals that the barbed end dissociation of ADP-Pi-actin is about tenfold slower than the dissociation of ADP-actin [48].

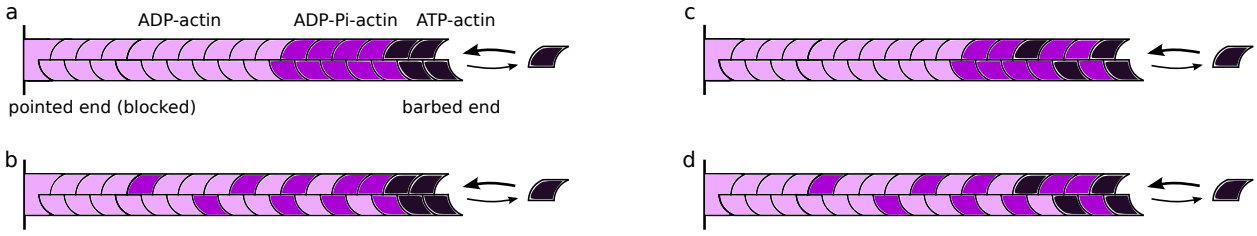

Figure 1.4 : Vectorial versus random mechanisms for ATP cleavage and Pi release. Filaments are assembled at their barbed ends. (a) Both ATP cleavage and phosphate release are governed by a vectorial mechanism, resulting in distinct ATP-, ADP-Pi-, and ADP-actin segments. (b) Vectorial cleavage and random release. (c) Random cleavage and vectorial release. (d) Both the cleavage and the release step follow a random mechanism, i.e., they occur with the same rate irrespective of their position along the filament.

The mechanisms of ATP cleavage and Pi release are still under debate [7]. For each of these processes, it is disputed whether it has equal rates at each protomers within the filament [1, 49, 50] ("random mechanism") or occur only at a protomer neighboring one where the process has already taken place [19, 39] ("vectorial mechanism"), see figure 1.4. The random and vectorial mechanisms can be seen as opposing limiting cases of the more general "cooperative" mechanism [39], where the process can take place at random positions, but is enhanced for the protomer next to sites where the process has already taken place. Both the vectorial and strongly cooperative mechanism may lead to characteristic segments consisting of only ATP-, ADP-Pi-, or ADP-actin protomers [19, 50, 51], see figure 1.4.

One reason for the ongoing controversy is that bulk solution measurements show evidence for uncoupling between the elementary reactions [46], but fail to distinguish between these different mechanisms, because they only detect the amount of F-actin – either by turbidity or by the increase of fluorescence of labeled actin upon polymerization [38,48] – and thus involve averaging over the whole filament population. Similarly, the observation of the assembly of individual filaments with fluorescence microscopy [43], or the measurement of filament lengths at different times by electron microscopy [41], do not probe the inner structure of the filaments. Hence the spatial distribution of ATP-, ADP-Pi- and ADP-actin protomers within the filament remains unknown. However, *in vivo* not only the filament ends, but also this protomer distribution influences filament dynamics as regulating proteins have a preference of binding to some of the actin species [10].

1.1.6 Experimental concepts and interpretation of dissociation rates

In order to determine the dissociation rates and association rate constants of actin monomers to filament ends, three kinds of experiments have been performed: (i) In bulk assays the increase of the amount of F-actin is measured [38]. The initial rate of this increase determines the elongation rate, as the initial filament number is defined by filament seeds. (ii) Filament lengths are measured at different points in time by electron microscopy [41]. (iii) Single filaments can directly be observed by fluorescence microscopy [52]. In all cases, the filament elongation velocity is measured for a range of monomer concentrations. Both the barbed and the pointed end can be blocked to measure the elongation at the distinct ends separately. If the same protomer species (ATP- or ADP-actin) is present at the filament end over the entire range of concentrations, plotting the elongation velocity versus the monomer concentration ideally yields a linear function, in which the slope determines the association rate constant, and the intercept with the vertical axis determines the dissociation rate, see for instance [41]. The nonlinearity of the elongation rate as a function of the monomer concentration indicates the presence of different protomer species at the ends. Determining the kinetic parameters then involves certain assumptions.

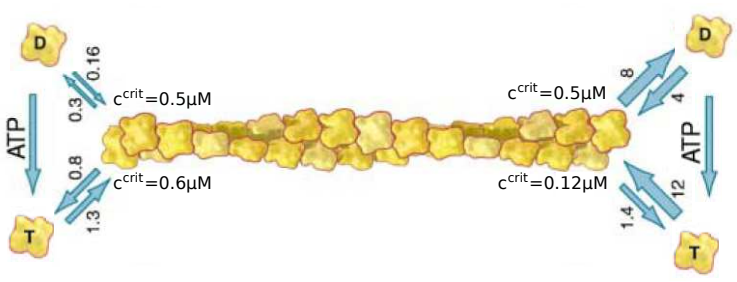

Figure 1.5 : Rates for dissociation (in units of s^{-1}) and rate constants of association (in units of $\mu M^{-1}s^{-1}$) for ATP-actin (T) and ADP-actin (D). The graph is taken from [6] and originated from the textbook [1]. The rates were originally published in [41]. The numerical values have to be interpreted with care, as discussed in the text.

Here, we briefly illustrate one common misinterpretation of the published dissociation

rates. In the most cited review article about the assembly of actin filaments [6], and in T.D. Pollard's book on cell biology [1], the association and dissociation rates for ATP-, and ADP-actin are illustrated as in figure 1.5. These rates originate from [41] and were measured with EM as described above. In the figure 1.5 they seem to represent the kinetic rates of the respective species. For ADP-actin, this is the case and the critical concentration is identical and given by 0.5 μM at both ends. For ATP-actin, however, the critical concentrations of the ends differ from each other, as discussed in [41,49]. This is because ATP hydrolysis gives rise to different protomer species at the two ends. Thus the depicted dissociation rates of ATP-actin can not be interpreted as such, but instead the probability for ATP-actin to be at the terminus must be weighted in.

However, it seems that the illustrations has mislead other researchers in this respect. In [53] for instance, where an integrative simulation model of actin filaments is presented, the rates measured for ATP-actin [41], as shown in figure 1.5, are used as the association and dissociation rates of the ATP-protomers. In consequence, the model in [53] could give rise to treadmilling filaments in the absence of ATP hydrolysis, and thus violates thermodynamics. In another theoretical study [54] the rates from figure 1.5 are also employed without questioning.

For a meaningful interpretation of the kinetic rates of figure 1.5, the following consideration, which is discussed in a similar manner in [49], is needed. The experiments in [41] were performed at monomer concentrations that are sufficient to ensure the presence of ATP-actin at the barbed ends of the filaments in solution. Furthermore, the association rates are pure ATP-actin rates, because of the excess of ATP in solution. Therefore, the critical concentration of $c^{\mathrm{crit}} = 1.4\,\mathrm{s}^{-1}/12\,\mu\mathrm{M}^{-1}\mathrm{s}^{-1} = 0.12\,\mu\mathrm{M}$ at the barbed end is indeed the critical concentration of pure ATP-actin. Conservation of free energy requires a value of $1.3\,\mu\mathrm{M}^{-1}\mathrm{s}^{-1} \times c^{\mathrm{crit}} = 0.16\,\mathrm{s}^{-1}$ for the pointed end dissociation rate of ATP-actin.

1.1.7 Theoretical approaches to filament polymerization

As for other processes of the cellular machinery, real time observation of the elementary processes involved in actin polymerization is not possible as there is no "nanoscope" available to date. In particular, the measurements of ATP cleavage and Pi release are rather indirect and thus give rise to controversy about the underlying mechanism [7]. Therefore, there is a natural need for theoretical models that make some assumption about the involved association, dissociation and hydrolysis processes and predict experimentally accessible quantities. In case of a useful model, the measurement of these quantities allows a falsification of the model. Furthermore, according to the principle of Occams razor – "entities are not to be multiplied unnecessarily" – models with minimal assumptions should be preferred over those that involve a variety of undetermined parameter. Here we briefly summarize some of the theoretical work that is particularly interesting.

In an encyclopedic article [55], Hill and Kirschner discussed the thermodynamics and kinetics of actin and microtubule polymerization, and considered a large range of hypothetical models. Pantaloni et al. [56] showed that a vectorial ATP hydrolysis model can explain the kinetic data obtained from bulk assays of actin polymerization, if additional assumptions are met: The hydrolysis rate must be zero at the terminal protomer, and the dissociation

rate must depend on the states of the penultimate and antepenultimate protomers. Hill studied this vectorial model in detail and analytically investigated the possibility of phase changes at an end of an actin filament, associated with the presence or absence of an ATP-cap in [57]. Flyvberg et al. [58] proposed a generic model of cooperative GTP hydrolysis in microtubules. As it does not contain details about the structure of microtubules, this model can be transferred to actin dynamics and it will turn out to be the coarse-grained version of one of the theoretical models that we will consider in chapter 3. Vavylonis et al. [59] considered a model of random ATP cleavage and random Pi release and computed the length fluctuations of single filaments at the barbed end. These fluctuations are largely enhanced compared to the fluctuations in the absence of hydrolysis, if the monomer concentration is slightly below the critical concentration. The reason for the large fluctuations lies in the different dissociation rates of the protomer species. The dissociation rates of ATP- and ADP-Pi-actin are assumed to be similar, whereas the dissociation rates of ADP-actin is assumed to be about 5 times higher. At the critical concentration, the cap of (ATP- and) ADP-Pi-actin protomers is stable, such that the length fluctuations are basically equal to the fluctuations in the absence of hydrolysis. At very low concentrations, there are very few association events and thus the dissociating protomer is typically in the ADP-state, giving rise to intermediate fluctuations. In contrast, slightly below the critical concentration, the ADP-Pi-actin cap is neither constantly present nor absent, but intermittently present, which creates much larger fluctuations. For the used (realistic) parameters these length fluctuations are very similar to those measured in fluorescence microscopy experiments with single filaments [43]. As the experiments in [43] were performed at the treadmilling concentration, which is above the critical concentration of the barbed end, the theory ultimately fails to explain the observations. However, it predicts an interesting quantity, namely the size of the fluctuations, that can in principle be tested experimentally.

Stukalin et al. [54] considered a vectorial hydrolysis model and found a very similar enhancement of length fluctuations at the critical concentration of the barbed end. Even though these enhanced fluctuations appear at a slightly higher monomer concentration when compared to the random model considered in [59], the similarity of the fluctuations prevent a reliable discrimination between the random and the vectorial hydrolysis mechanism. As mentioned earlier, the nonlinearity of the elongation rate as a function of the monomer concentration indicates the presence of different protomer species at the ends, and is thus a fingerprint for the existence of hydrolysis. Thus, the exact functional form of this nonlinear relation could – in principle – allow conclusions about the hydrolysis mechanism. In particular, the vectorial mechanism leads to a kinked relation, since the probability of finding ATP-actin is strictly one above a certain monomer concentration [54]. In contrast, for the random mechanism the growth velocity is a very smooth function of the monomer concentration. For small ATP-actin concentrations, this function asymptotically approaches the difference between the association rate of ATP-actin and the dissociation rate of ADP-actin. Likewise, it approaches the difference between the association and the dissociation rate of ATP-actin in the limit of large monomer concentrations where ATP-actin is present at the barbed end. However, apart from the kink, the growth velocity versus monomer concentration plots based on a vectorial or a random hydrolysis mechanism are qualitatively very similar and their quantitative features are very sensitive to the numerical values of the kinetic

rates [54]. Thus, it seems very difficult to discriminate a vectorial from a random hydrolysis mechanism using the experimentally found [18] nonlinear relation between elongation rate and actin concentration.

Vectorial and random hydrolysis mechanisms (more precisely the slow phosphate release that follows the rapid ATP cleavage) lead to fundamentally different ATP-caps (more precisely ADP-Pi-caps), see figure 1.4. In case of a vectorial mechanism, hydrolysis can not catch up with monomer association above a certain concentration and the ATP-cap grows infinitely [54]. In contrast, this cap is always finite for the random mechanism, since the overall hydrolysis rate increases with the number of protomers with non-hydrolyzed nucleotides [59]. Unfortunately, these caps can not be detected directly. Instead dilution experiments are required, which we present in chapter 6. Ranjith et al. [60] analyzed a vectorial hydrolysis model, similar to [54, 57], and discussed the combined effect of hydrolysis and a pushing force on the growth velocity if the monomer association rate is force dependent. Li et al. [51] studied a general hydrolysis model that discriminates between ATP cleavage and Pi release steps and assumes cooperative mechanisms for both of these processes. Many quantities, such as the cap structure in terms of ATP-, ADP-Pi, and ADP-actin, are calculated analytically for the steady state. In particular, the cleavage flux as a function of the G-actin concentration is compared between a strongly cooperative (for which the cleavage rate at random ATP-actin protomers was assumed to be by a factor of 3×10^{-6} smaller than the cleavage rate at the ATP-boundary), the random and the vectorial cleavage mechanism. For the latter mechanism this flux is limited to a certain value as there is only a single cleavage site. In contrast, for random cleavage, the flux increases with the monomer concentration. It may seem counterintuitive that the flux of the strongly cooperative mechanism turns out to be similar to the random case, even though the strong cooperativity implies an ATP- and ADP-Pi-actin distribution similar to the vectorial mechanism. This remarkable feature can be rationalized by considering that even a very strong cooperativity does not exclude nucleation of new cleavage sites where the vectorial process then can then set in, quickly creating islands of ADP-Pi-actin within large segments of ATP-actin.

Without knowledge about the molecular details, the association and dissociation processes at the filament ends as well as the cleavage and release processes can be described as Markov processes. Thus, the time evolution of the probability distribution that characterizes the system can be formulated in terms of a master equation [61]. In the studies listed above, the computed quantities, such as growth velocities, length fluctuations, cap lengths, or cleavage fluxes, are calculated under the assumption of certain non-equilibrium steady-states, which allows the analytical solution of the master equation. However, it is far beyond experimental time scales to reach some of these steady states. Furthermore, considering the transient situation often reveals more information about the underlying mechanism, as intermediate states are less hidden in the observables.

1.2 Research objectives

Many aspects of actin have been studied: A query with the `ISI Web of Knowledge` gives more than 2×10^5 results for "actin", and more than 1.5×10^3 results for "actin polymerization". For comparison, the estimated overall number of scientific articles ever produced is 5×10^7. Despite these impressive numbers, certain fundamental issues remain unsolved.

1.2.1 Interruption of depolymerization

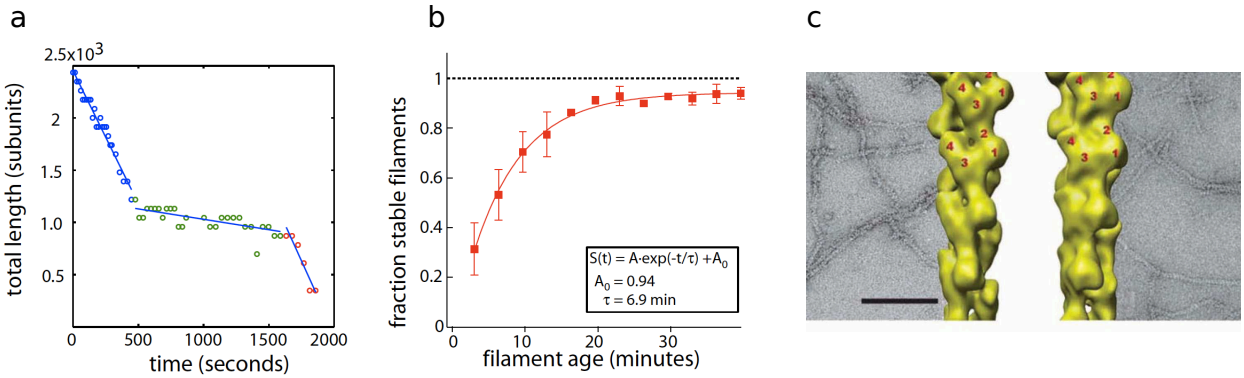

Figure 1.6 : Dynamic stabilization of actin filaments. Figures (a) and (b) are taken from [62]; figure (c) is taken from [63] and originally stems from the Egelman lab. (a) Filament length as a function of time for a single filament in buffer. Imaging was started 1-2 minutes after the initiation of depolymerization. The filament suddenly switches to a slow-shrinking state, and finally back to the fast-shrinking state. In the slow shrinkage state, disassembly only occurs from the pointed end [62]. (b) Fraction of filaments in the slow-shrinking state as a function of time. The exponential fit indicates that at the end only 6% of the filaments shrink from the barbed end. (c) Electron micrographs and 3D reconstructions of actin filaments. Left hand side: Shortly after polymerization, filaments appear ragged. Right hand side: After 2 hours, filaments appear smoothened. Kueh et al. proposed that the abrupt changes of the depolymerization velocity is caused by spontaneous transitions from the ragged to the smooth filament structure [62, 63].

The starting point for our investigations was the recent observation that the depolymerization of single actin filaments is suddenly slowed down, or interrupted after a few minutes [62], see figure 1.6(a). This observation seemed to imply that old filaments are more stable than young ones [62], and therefore seemed to challenge the established view of actin dynamics, in which the hydrolysis of the bound ATP causes actin filaments to become less stable as they grow older. In fact, earlier fluorescence microscopy studies of the dynamics of single filaments already reported pauses both during filament growth and shrinkage [43, 52], but simply attributed them to incidental blockage of filament ends on the glass surface and therefore excluded them from the analysis [52].

In contrast, Kueh et al. [62, 63] argued that the changing depolymerization velocity is an intrinsic effect of actin filaments – the "dynamic stabilization of actin filaments" – that

is correlated with the structural polymorphism or plasticity as reported in some [64, 65], but not all [16] electron microscopy studies. According to this view, the sudden slowdown of depolymerization is a consequence of a remodeling of the filament structure from an unstable, relatively disordered state of young filaments to the stable, conventional Holmes helix [23] as the filaments grow older, see figure 1.6(c). Such a remodeling would have far-reaching implications for many actin-related processes *in vivo*. For instance, certain age-dependent actin conformations could favor the binding of particular ABPs and thereby trigger the formation of particular actin networks [11, 66].

Li et al. [51] proposed another explanation for the abrupt dynamical changes which cause the different phases of depolymerization: The initial phase of shrinkage, cf. figure 1.6(a), was interpreted as the rapid depolymerization of an ATP-actin segment, the second phase as the slow depolymerization of an ADP-Pi-actin segment, and finally the third phase as the rapid depolymerization of ADP-actin. The distinct segments of ATP-, ADP-Pi-, and ADP-actin, which give rise to the abrupt transitions, are a fingerprint of strongly cooperative ATP cleavage and Pi release mechanisms: At random sites within the filament, the rates are very small and after nucleation, a vectorial mechanism sets in. As it abstains from proposing a new state, this explanation is tempting. However, it predicts that ultimately filaments depolymerize rapidly, as ADP-actin has the largest dissociation rate. Even though not all filaments may reach this state during the experiment, the fraction of stable filaments should decrease within the experimental time scale. Kueh et al. [62] found the opposite: The fraction of stable filaments approaches 94%, see figure 1.6(b).

Kueh et al. fitted the time-dependent fraction of stable filaments by an exponential, see figure 1.6(b). This implies that a transition from the unstable to the stable state consists of one rate-limiting step, see section 3.2 and [61]. For the suggested global transition of the filament helix, this means that the filament helix as a whole suddenly changes its state, or the transition propagates instantaneously – compared to time scales of the association and dissociation kinetics – along the filament, once it has been triggered.

The fact that both interpretations [51, 62] are not fully convincing – Kueh et al. [62] proposed a novel state of actin whose transitions seem to be very unphysical, while Li et al. [51] did not account for experimental observations – motivated our study of the intermittent depolymerization of actin filaments.

1.2.2 Mechanism of ATP hydrolysis

The cleavage of F-actin bound ATP is much faster than the subsequent phosphate release, and thus, except when growing very rapidly, an actin filament consists mainly of ADP-Pi- and ADP-actin. The mechanism of Pi release has remained elusive for 20 years, both the random as well as the vectorial model have been discussed, see section 1.1.5. This is because the kinetic assays which probe the phosphate release involve averaging over many filaments in solution. However, spatial information about the release step is required to infer the local composition of the filament in terms of ADP-Pi- and ADP-actin. This local composition may control or be affected by regulators of actin dynamics like profilin, capping proteins, or ADFs/cofilins that bind differently to ADP- or ADP-Pi-actin [44, 45].

Since ADP-Pi- and ADP-actin have different dissociation rates, depolymerization exper-

iments with single filaments can indirectly discriminate between the vectorial and random release mechanism. In fact, the former mechanism gives rise to a defined segment of ADP-actin, whereas the latter one leads to a continuous increase of ADP-actin during the course of depolymerization, see figure 1.4. Theoretical modeling again proves to be essential for conclusive answers about the release mechanism. In addition, it allow us to address the function of profilin during actin polymerization and depolymerization.

1.3 Outline of the thesis

Our work has strongly profited from the mutual stimulation of experimental and theoretical approaches. The interplay of experiment and theory is reflected in the organization of this thesis. In particular, we successively generalize our theoretical approach to accommodate observations from later experiments that in turn were motivated by the finding of the first theoretical approach. All experiments were carried out in the Carlier laboratory at the National Center for Scientific Research (CNRS) in Gif-sur-Yvette, France, but only the basic depolymerization experiments described in chapter 2 were performed by the author of this thesis. The more advanced setup, which involves a microfluidic device discussed in chapter 4, was subsequently developed by members of the Carlier lab.

In chapter 2, single filament experiments are presented, in which we first observed the interruption of depolymerization. Stochastic modeling, as discussed in chapter 3, then shows that various hypothetical mechanisms, which could cause the interruptions are characterized by distinct *distributions* of the interruption times. By comparison with the experimental data, a local transition mechanism at random sites within the filament is predicted.

In chapter 4, we first introduce a microfluidic device, which allows for a much more precise observation of filament depolymerization. First, we confirm that filaments depolymerize in an intermittent manner, that means that their shrinking is often interrupted for an extended period of time. Second, it turns out that the depolymerization of filaments grown from ATP-actin is continuously accelerated on a time scale of a few minutes. Third, more complicated depolymerization experiments give further insight into the mechanism of intermittent depolymerization. In chapter 5, we combine experimental findings with theoretical considerations to elucidate the molecular nature of the novel transition mechanism. We find that the transition indeed occurs only locally, leading to stable dimers within the filament.

The second research objective, namely the mechanism of ATP hydrolysis within filaments, is investigated in chapter 6. We use the shape of the depolymerization curve of ATP-actin filaments to determine the release mechanism and specify the respective rate constants. Again, we combine experimental data and theoretical modeling to draw quantitative conclusions. Chapter 6 can be read separately, since the acceleration of depolymerization caused by ATP hydrolysis is independent from the intermittent depolymerization of the filaments.

The last chapter provides a summary of the results, a discussion, and an outlook on possible research directions.

1.4 List of publications

The research presented in this thesis contributed to the following peer-reviewed publications:

- [67]: "Intermittent depolymerization of actin filaments is caused by photo-induced dimerization of actin protomers".
  Thomas Niedermayer, Antoine Jégou, Lionel Chièze, Bérengère Guichard, Emmanuèle Helfer, Guillaume Romet-Lemonne, Marie-France Carlier, and Reinhard Lipowsky *Proc. Natl. Acad. Sci.* **109**, 10769–10774 (2012)
  This article corresponds to the objective formulated in section 1.2.1.

- [68]: "Individual actin filaments in a microfluidic flow reveal the mechanism of ATP hydrolysis and give insight into the properties of profilin".
  Antoine Jégou, Thomas Niedermayer, József Orbán, Dominique Didry, Reinhard Lipowsky, Marie-France Carlier, and Guillaume Romet-Lemonne
  PLoS Biology **9**, e1001161 (2011)
  This article corresponds to the objective formulated in section 1.2.2.

Furthermore, the author of this thesis co-authored the following publication during the course of his PhD. Therein, the length distribution of labeled actin filaments within a pool of unlabeled actin is measured and we demonstrate that the dominating process at steady state is filament fragmentation. The topic of this paper was not included into this thesis, because it was thematically independent from our other investigations, as it does not deal with the depolymerization of single actin filaments.

- [69]: "Fragmentation is crucial for the steady-state dynamics of actin filaments".
  Kurt M. Schmoller, Thomas Niedermayer, Carla Zensen, Christine Wurm, and Andreas R. Bausch *Biophysical Journal* **101**, 803–808 (2011)

2 Depolymerization experiments with individual filaments

In this chapter, fluorescence microscopy experiments which probe the disassembly of single actin filaments are presented. In particular, we are interested to verify a phenomenon reported by Kueh et al. [62]: Actin depolymerization exhibits several dynamic phases. The initial fast-shrinking phase changes abruptly into a second phase which is characterized by essentially no shrinkage from the barbed end. This observation shaped the notion of a "dynamic stabilization" [62, 63] which challenges the classical view that filaments become less stable with age [1, 2].

In standard microscopy experiments with single actin filaments, ABPs like inactivated myosins [49, 52, 70] or filamins [62] attach the filaments to the coverslip. While this attachment seems to be unproblematic during filament polymerization [49, 52], it may stall the depolymerization process. In fact, it has been recently shown that filamin slows down the depolymerization of actin [71]. In addition, we performed preliminary experiments presented in section 2.1.2 which indicate that filaments attached by inactivated myosins or a biotin-antibiotin interaction are not able to depolymerize.

As the single filaments studied in [62] were attached by filamins, the abrupt changes in depolymerization velocity could be caused by specific interactions between actin and this actin binding protein (ABP). To avoid such interactions, we use spectrin-actin seeds to anchor the filaments only at their pointed ends while the rest of the filament could move freely. The experimental protocol consisted of two basic steps. First, the filaments were elongated by a buffer containing free actin monomers. Then, depolymerization was initiated by replacing this buffer by one without actin monomers. The latter buffer also contained methyl cellulose which prevented the filaments from bending out of the focal plane. This enabled us to use fluorescence microscopy to measure the filament length as a function of time.

The experiments in this chapter are rather basic – compared to the subsequent, advanced microfluidics experiments which are discussed in chapter 4 – and were performed by the author in the laboratory of Marie-France Carlier.

Readers not interested in the experimental details may skip the next two sections and proceed to the chapter summary in section 2.3.

2.1 Experimental realization

2.1.1 Proteins, buffers and imaging

Actin was purified from rabbit muscle [72] and its concentration was determined from ultraviolet absorption. As a fluorescent label, Alexa488 succinimidyl ester which binds to the surface lysines of the actin protein was used. A fraction of labeled actin (labeling fraction) of 10% was chosen. In some samples, 2% of the monomers were additionally labeled with n-(1-pyrenyl)iodoacetamid (pyrene) in order to optionally check the polymerization properties in bulk assays [73]. Instead of Alexa488, we used Alexa594 succinimidyl ester in certain assays. Spectrin-actin seeds were purified from human red blood cells [74].

G-actin was stored in G-buffer which consists of 2.5 mM $(HOCH_2)_3CNH_2$ (Tris), 0.2 mM adenosine triphosphate (ATP), 0.1 mM $CaCl_2$, 0.01% NaN_3, and 1 mM dithiothreitol (DTT). The pH of the buffers was adjusted to 7.8 by adding HCl. F*-buffer additionally contains 100 mM KCl, 1 mM $MgCl_2$, and 0.2 mM ethylene glycol tetraacetic acid (EGTA), to allow the formation of filaments. Standard polymerization/depolymerization experiments were performed in F-buffer which consists of F*-buffer with additionally 9 mM DTT and 1 mM 1,4-diazabicyclo[2.2.2]octane (DABCO) to limit photobleaching. In some instances, F-buffer was supplemented with 0.2 wt.% methyl cellulose M-0512 from SIGMA and/or 3 μM latrunculin A. Bovine serum albumin (BSA) from Sigma was used in F*-buffer.

We used total internal reflection fluorescence microscopy (TIRFM) to observe the filaments. An Olympus IX 71 microscope equipped with an oil immersion objective with a magnification of 60 and a numerical aperture of 1.42 was employed. A maximal resolution of 6 pixels per μm, corresponding to 62 F-actin subunits per pixel, was achieved. Images were acquired with a Cascade II EMCCD camera from Photometrics. Excitation was realized through the objective lens with a 25 mW laser from Cobolt, emitting at 473 nm. In the experiments with the Alexa594 label, we used a laser emitting at 561 nm instead. In both cases, an exposure time of 40 ms was chosen. Typically, the time interval between images was 20 s. The entire microscopy setup was controlled using Metamorph.

2.1.2 Different experimental approaches

In the depolymerization experiments reported in ref. [62], the cross-linker filamin was employed to attach the actin filaments to the surface of the coverslips. As this protein was not available in the lab, we tried three alternative approaches of linking filaments to the chamber wall.

1. Prior to filament polymerization, the flow cell was incubated with F*-buffer containing N-ethyl-maleimide (NEM)-inactivated myosin. NEM-myosin attaches the actin filaments to the chamber wall, but does not walk along their contour [52]. However, it turned out that the immobilization was not complete: The pivotal points, where the filaments were attached, seemed to move during microscope observation. In addition, the depolymerization seemed to be hindered at these points. This is presumably caused by myosin-actin interactions.
2. G-actin was labeled with biotin and the flow chamber was incubated with an anti-biotin antibody [75]. The interaction and thus attachment seemed to be quite strong

and again hindered the depolymerization process.

3. The cell was incubated with spectrin-actin seeds. Some of them stick to the surface and trigger the growth of filaments after injection of the G-actin into polymerization buffer. Individual filament are only attached on their pointed ends and thus their interactions with the surface are minimized.

It appears that only the third linking approach is feasible for the investigation of depolymerization dynamics. Since the filaments are only attached at their pointed ends, it is essential to supplement the F-buffer with methyl cellulose. These very long polymers prevent the filaments from bending out of the focal plane near the surface of the coverslip, but are believed not to influence the polymerization properties of actin [43]. In fact, we did not observe large fluctuations of the apparent –that is projected – filament length. Therefore one can conclude that the filaments remained within the range of TIRF excitation, i.e. their distance to the coverslip did not exceed 200 nm, see figure 2.1. Considering a persistence length of actin filaments which is of the order of 10 μm [76], this also ensures that the error from the projection is small.

To start polymerization, we mixed G-actin with F-buffer and adjusted the salt concentration within a micro tube. In most cases, a final G-actin concentration of 5 μM was chosen. Without delay, the solution was flushed into the flow chamber and filaments began to grow from the seeds. Depending on the concentration of G-actin, the filaments were allowed to elongate for one to five minutes. After this period, we intended to stop polymerization and initiate depolymerization by rinsing the chamber with F-buffer without G-actin. The initial idea was that rinsing with several times the volume of the chamber would remove both the G-actin as well as the filaments which were not attached, as described in ref. [62].

In practice, this turned out to be infeasible, as the buffers were supplemented with 0.2 wt.% methyl cellulose and thus too viscous for efficient rinsing. Therefore, we omitted methyl cellulose in all buffers except for the buffer finally flushed in. In consequence, only the depolymerization, but not the growth of filaments could be observed in standard assays.

However, even after washing with 10 times the cell volume, we could only observe very slow depolymerization with rates of 0.2 ± 0.1 protomers per second. In fact, we observed a high density of filaments near the edge of the flow cell which can not be removed by perfusion since the flow velocity in the vicinity of the boundary is too low. These filaments provide a continuous source of G-actin which diffuses and, in principle, could associate to the observed filaments. To resolve this issue, we added an excess of latrunculin A into the final depolymerization buffer. This agent binds in a 1:1 stoichiometry to actin monomers with an equilibrium dissociation constant of about 0.2 μM [77]. In appendix A.2.2 we show that replacing the buffer by one containing 3 μM of latrunculin A ensures that practically all actin monomers are sequestered. As no association can occur, the dissociation process is represented by the shrinkage of individual filaments.

2.1.3 Working experiment

Taking into account the issues described in the last section, the following protocol turned out to be suitable to observe the depolymerization of actin filaments.

We used parafilm, multiply cleaned coverslips, and microscopy slides to assemble flow

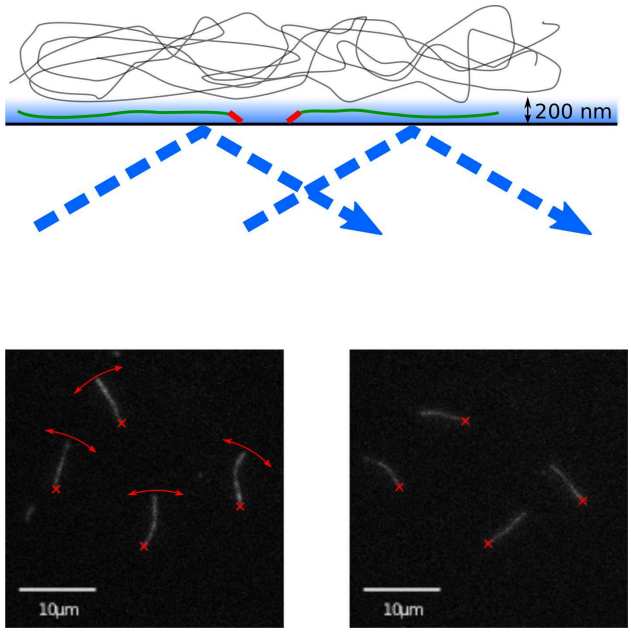

Figure 2.1: TIRFM experiment: On the top, a side-view of the experimental setup is shown. The blue gradient displays the evanescent wave from the totally reflected laser beam. Actin filaments are shown in green with red seeds at their pointed ends. The curly lines represent methyl cellulose which confines the filaments to the vicinity of the coverslip where they are visualized by the evanescent wave. On the bottom, two microscopy images of the same region, but at different points in time are shown to indicate the lateral filament fluctuations around the anchoring points which are marked by the red crosses. Since the filaments are observed as continuous lines, we can conclude that they reside within a boundary of 200 nm from the coverslip, and only a negligible projection error is made when measuring their lengths.

chambers with a volume of about $8-10$ μl. Each flow chamber was incubated with spectrin-actin seeds that were dissolved in F*-buffer. We worked out that a seed concentration of $1-2$ pM and an incubation time of 5 min are suitable for a density of filaments which is both small enough to avoid overlapping filaments, and big enough to ensure the presence of at least a few filaments in the field of view. This holds for standard assays where we polymerized actin at 5 μM for about 90 s. Then we rinsed the chamber extensively and incubated it for another minute with F*-buffer containing 1 wt.% bovine serum albumin (BSA). This protein is expected to coat the chamber surface and prevent nonspecific interactions. After rinsing and exchanging the buffer for the F-buffer, the chamber was prepared for the polymerization experiment.

We first adjusted the salt concentration of the F-buffer to account for the later addition of G-buffer which contains a much lower salt concentration. Next, a micro tube was used to mix the adjusted F-buffer with G-buffer containing the monomeric actin. Without delay, the flow chamber was rinsed with this solution and the timer was started. As mentioned, we have chosen a final G-actin concentration of 5 μM and a polymerization time of 90 s in standard assays. At this concentration, not more than 10% of the actin monomers are lost by spontaneous nucleation of filaments, see figure 4 of ref. [27]. Furthermore, the monomer pool is not considerably depleted by association, see appendix A.2.1 for details. If the product of monomer concentration and polymerization time is considerable larger than $5\,\mu\text{M} \times 90\,\text{s} = 450\,\mu\text{M}\,\text{s}$, the filaments become too long and break as soon as the chamber is rinsed. If the product is much smaller, the filaments are too short to be observed.

To stop polymerization, we used 60 μl F-buffer (without methyl cellulose) to extensively rinse the chamber. The rinsing has to be done very gently and not as quickly as possible since otherwise the filaments break or are ripped off the surface by the flow. Immediately after this intermediate step which is needed to remove all G-actin and also the filaments

which are not attached well, we flushed in F-buffer that contains 0.2 wt.% methyl cellulose and 3 μM latrunculin A. The latter procedure takes longer than the one before since methyl cellulose strongly increases the viscosity of the buffer. The entire rinsing process typically takes between 30 and 60 s. Another 30 to 60 s are needed to focus and find a suitable field of vision. Therefore, the image acquisition can be started at the earliest after one minute after the start of depolymerization which is two and a half minutes after the start of polymerization. The experiment was performed at room temperature.

2.1.4 Image processing

Since the filaments are only attached at their pointed end and not on the whole contour as in ref. [62], their interaction with the surface is minimal and they fluctuate within the focal plane. The filaments that did not exhibit these fluctuations were excluded from the image analysis since they apparently interact with the glass surface. The disadvantage of the fluctuations is that one can not proceed via the standard kymograph analysis to determine the filament length as a function of time. Instead, we used two alternative procedures.

In the first approach, the sequence of microscopy images was processed with ImageJ as follows. A threshold is set to get a stack of binary (black-and-white) images. This was done such that the "sketetonizing" step described below gives a minimal number of holes and branches within an identified filament. Then, first the black and then the white outliers were removed. Subsequently, a "skeletonizing" operation was performed, that means the foreground regions are reduced to a skeletal remnant that largely preserves the extent and connectivity of the original region while removing most of the original foreground pixels. Ideally, this operation changes the appearance of a filament from an elongated object with a variable width of a few pixels to a line with a width of only one pixel. Then, we manually filled the "holes" and removed the "branches" of the filaments. The filament length can now be determined by automatically analyzing the perimeter of the lines.

In the second approach, we used a Java based tracking program, that was developed in the Vavylonis lab [78]. The tracking program applies an open active contour model, to automatically measure the length of filaments. Unfortunately, it was not available when we started analyzing the data, making the first procedure necessary.

Both approaches lead to very similar length-vs-time curves. We only consider the curves obtained by means of the automatic tracking approach for the subsequent analysis. As most traces appear to be biphasic, see 2.2, we automatically determined a continuous and piecewise linear function with one kink that provided the best fit using the method of least squares. Details are given in appendix A.2.3. The kink of the fitting function determines the duration τ of the initial shrinkage phase.

2.1.5 Additional depolymerization experiments

As an attempt to understand the mechanism of the observed biphasic depolymerization (see section 2.2.1), we performed the following additional experiments.

ADP-P*-actin

Inorganic phosphate (Pi) binds rapidly to ADP-F-actin and restores the ADP-Pi state. The phosphate that has restored the ADP-Pi-state dissociates much faster from the filaments than the Pi which is produced by ATP cleavage [79]. Therefore, there must be an intermediate step, which kinetically limits Pi release after ATP cleavage. In fact, this step is the isomerization of penta-coordinated bi-pyramidal phosphate in the transition state ADP-P* into tetra-coordinated phosphate in ADP-Pi-F-actin [79]. Hence, the relatively persistent nucleotide state before Pi release is ADP-P* which can be mimicked by ADP-BeF_3, as discussed in [79, 80]. We followed the same strategy and added 9 mM of NaF and 100 μM of $BeCl_2$ into the buffers to get an excess of BeF_3^-.

ADP-Pi-actin

We also investigated the depolymerization of filaments in a buffer supplemented with an excess of Pi. In this case, Pi release is not directly prevented, but the excess of Pi binds rapidly to ADP-F-actin and restores the ADP-Pi state. In our standard assays described above, a pH of 7.8 was chosen and thus Pi is mainly present as HPO_4^{2-}. However, because it is the $H_2PO_4^-$-species which interacts with F-actin [48], we had to decrease the pH in all buffers to a value of about 7. Thus, the standard buffers were altered as follows. (A) The F-buffer was supplemented with 25 mM Pi. In practice, we mixed KH_2PO_4 and K_2HPO_4 solutions of identical concentrations. To yield pH 7.0, 61% of KH_2PO_4 solution and 39% of K_2HPO_4 solution were taken, see appendix A.2.2 for the computation. According to [48, 49], the numerical value of the dissociation constant of Pi and an ADP-actin protomer is given by $K_D \simeq 1.5$ mM at pH 7.0. As the concentration of F-actin is at most in the μM range, binding of Pi does not considerably deplete the pool of free Pi. Therefore, we have $c_{\text{ADP-Pi-actin}}/c_{\text{ADP-actin}} \simeq 25\,\text{mM}/1.5\,\text{mM} \simeq 17$, which means that essentially all F-actin is in the ADP-Pi state. (B) The pH in all buffers was changed from 7.8 to 7.0 by addition of HCl.

Lower pH

As a control for the assays with ADP-Pi-actin, where we have used 25 mM phosphate at pH 7, another experiment with the same pH and the same ionic strength is needed. In this case, the potassium phosphate was replaced by potassium sulfate K_2SO_4. For the same ionic strength, 15 mM of K_2SO_4 is needed, see appendix A.2.2 for the computation. The pH in all buffers was changed from 7.8 to 7.0 simply by adding HCl.

Ca-actin

We also probed the depolymerization properties of Ca-ATP-actin, where Ca^{2+} instead of Mg^{2+} is the tightly-bound divalent cation of actin. Accordingly, EGTA must be omitted in all buffers, and $MgCl_2$ was replaced by the same amount of $CaCl_2$. Apart from these changes, we followed the standard experimental protocol.

2.2 Results

2.2.1 Biphasic depolymerization

We were able to observe filaments not later than 2 min after depolymerization was initiated. This lag time varied between individual assays, see section 2.1.3. By inspection of the length-vs-time traces, we find that for about two-thirds of the filaments ($N_\mathrm{f} = 57$), the depolymerization process consists of a fast-shrinkage phase (*phase I*) followed by a phase of very slow shrinkage (*phase II*). The change in shrinkage velocity occurs very abruptly and typically after a few minutes. Since this notion of a biphasic depolymerization may be subjective, we checked it by the minimization procedure described in appendix A.2.3. The other third of the filament population appears to shrink very slowly from the beginning of observation, see figure 2.2 for an example.

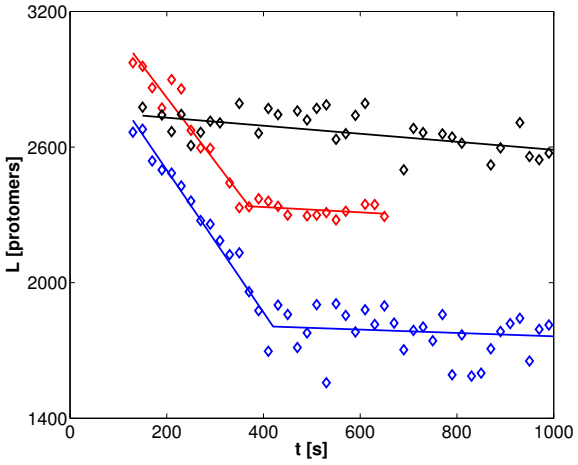

Figure 2.2: Depolymerization curves (length versus time) for three filaments. The time is taken from the initiation of depolymerization. The measured lengths are shown as diamonds and the piecewise linear fits as continuous lines. The kinks o these lines determine the durations τ of phase I. About two-thirds of the filaments ($N_\mathrm{f} = 57$) displays biphasic depolymerization, with the duration τ exhibiting some fluctuations.

The shrinkage velocity in phase I is measured to be $v_\mathrm{I} = 2.7 \pm 1.2$ protomers per second. The two numerical values denote the mean and the standard deviation of the filament population, respectively. For phase II, the apparent shrinkage velocity is measured to be $v_\mathrm{II} = 0.08 \pm 0.17$ protomers per second. These values are calculated by taking both phase II of the initially fast-shrinking filaments and the filaments which shrink slowly from the beginning into account.

The quantity τ is defined as the duration of phase I, measured from the beginning of the depolymerization. Our experimental approach requires a certain time between the beginning of the depolymerization (defined by the exchange of the buffer containing actin monomers) and the start of the imaging. This time varied between assays but did not exceed 2 min. Another 40 s are needed to detect the sudden drop of the shrinkage velocity. Therefore, we could only reliably detect durations τ which are not smaller than the lag time of $t_\mathrm{lag} = 160$ s. We found $\langle\tau\rangle_\mathrm{obs} = 5.4$ min for the average of τ, calculated for the filaments that exhibited both phases of depolymerization. In principle, the filaments that shrink only slowly from the beginning of the observation, could also exhibit a biphasic behavior when observed from the very beginning of the depolymerization process. Therefore, one may expect that $\langle\tau\rangle_\mathrm{obs}$ overestimates the average over the whole filament population. The measured standard

deviation of τ is calculated to be $s_{obs}(\tau) = 2.4$ min, where again we can only consider the filaments with an observable biphasic behavior.

Note that the lag time which prevents the observation of the very early stage of depolymerization is not a particular feature of the discussed experiment, but is an intrinsic problem of experiments involving microscopy perfusion chambers. In particular, in ref. [62] a lag time of $1.5 - 3$ min was indicated. In our advanced experimental setup, which is presented in chapter 4, the classical perfusion chamber is replaced by a microfluidic setup. This allows us to basically eliminate the lag time.

Our observations are in qualitative agreement with Kueh et. al [62]: On a time scale of $5 - 10$ min, filaments suddenly stop to shrink rapidly. In [62], the shrinkage velocity of phase I is reported to be 1.8/s, i.e. somewhat smaller than $v_I = 2.7 \pm 1.2$/s. We believe that the difference is due to the filamin anchors used in [62], which can slow down actin depolymerization as reported in [71].

2.2.2 Biphasic depolymerization is not caused by ATP cleavage

As discussed in the introduction, the dissociation rates of protomers depend on the state of the bound nucleotide [41, 48]. In particular, ATP-actin is believed to dissociate considerably faster from the barbed end than ADP-Pi-actin [49] and ADP-actin is measured to have a barbed end dissociation rate which is about one order of magnitude larger than the respective rate of ADP-Pi-actin [41,48,49]. Furthermore, the initially bound ATP is rapidly cleaved into ADP-Pi, followed by a slower release of Pi [46, 48]. Li et al. [51] interpreted the different phases of depolymerization which were reported by Kueh et al. [62] by the different depolymerization rates of ATP-, ADP-Pi-, and ADP-actin. In particular, the fast shrinking at the beginning was proposed to be caused by the rapid dissociation of ATP-actin and an effectively vectorial ATP cleavage mechanism with a very low cleavage rate was thought to account for the abrupt drop of the shrinkage rate. In this section, we falsify this hypothesis by the analysis of different experiments.

Filaments in phase I are already in the ADP-state

In a first set of experiments which we described in section 2.1.5, the existence of a transition state between ATP-actin and ADP-Pi-actin is exploited to prevent phosphate release. For the population of $N_f = 6$ filaments, we found constantly slow shrinkage with an apparent velocity of $v_a = 0.04 \pm 0.08$ protomers per second. In a second set of experiments, detailed in section 2.1.5, this release step was inhibited by a sufficiently large excess of phosphate in the buffers. Again, no biphasic, but constantly slow shrinkage with an apparent shrinkage velocity of $v_b = 0.17 \pm 0.09$ subunits per second was observed ($N_f = 13$). However, if the abrupt transition from phase I to II had arisen from ATP cleavage, the biphasic depolymerization should still be visible, even if the subsequent phosphate release was prevented. Therefore, our observations can be explained in an alternative way. Since Pi release is prevented, the ADP-actin state, which gives rise to fast depolymerization, is not reached and one only observes the slow dissociation of ADP-Pi-actin. Furthermore, the abrupt transition which gives rise to phase II cannot be detected since the shrinkage velocities v_{II}, v_a, and v_b are rather similar. Note, that we do not conclude that every protomer that dissociates in phase I

is ADP-actin. We rather claim that the majority is already in the ADP-state since otherwise suppressing Pi release would not have such a pronounced effect.

Ca-actin filaments exhibit qualitatively the same behavior

We performed depolymerization experiments with Ca-actin as described in section 2.1.5. We found that 14 out of the $N_f = 18$ observable filaments have initially depolymerized fast with an apparent shrinkage of $v_{I,Ca} = 3.7 \pm 0.6$ protomers per second, that is they exhibited phase I. For 5 of these filaments, we were also able to observe the abrupt switch to phase II. 4 filaments were shrinking slowly from the beginning of the observation, i.e. exhibited only phase II. In consequence, we used $5 + 4 = 9$ filaments to calculate $v_{II,Ca} = 0.18 \pm 0.11$ protomers per second. Contrary to the physiologically relevant Mg-actin which we investigated so far, it is generally believed that ATP cleavage is a random process in Ca-actin [39]. Such a random cleavage process should lead to a continuous decrease of the shrinkage velocity. However, we again observed an abrupt transition from phase I to phase II, which provides additional evidence that the transition is not caused by ATP cleavage.

Consequently, there must be yet another structural transition.

2.2.3 More dynamic phases at lower pH

We also performed experiments at a pH which is lower than the standard pH of 7.8. As described in section 2.1.5, we intended to choose a pH of 7.0 and a slightly increased ionic strength. However, some later tests revealed that the actual pH was heavily fluctuating around 7.3. The most likely reason for this is that we kept Tris ($pK_a = 8.2$ at 20°C) as the buffering agent, instead of replacing it by HEPES which has a pK_a of 7.5 and is therefore much more suitable for buffering at pH 7.0.

Thus the following results should only be interpreted qualitatively. All $N_f = 28$ filaments were in phase I (i.e. shrinking rapidly with a velocity of $v_{pH} = 2.5 \pm 1.2$ protomers per second) from the beginning of the observation. For 12 filament phase II could not be observed because of the limited observation time caused by bleaching. For the remaining cases, phase I lasts for 6.4±3.4 min. Strikingly, we observed 8 filaments which exhibited not only two but four dynamic phases. We used the minimization procedure described in appendix A.2.3 to confirm the notion of four phases. The first and the third phase were characterized by a large shrinking velocity of about 3 protomers per second. The second and the fourth phase exhibit only very slow shrinkage with a rate of about 0.1 protomers per second.

Apparently, the slightly lower pH, that is the higher concentration of hydronium ions, facilitates the reversal to the fast-shrinking phase. This dependence on pH is not surprising. Reports based both on structural data [81] and on biochemical experiments [82–86], conclude that actin filaments are very sensitive to pH.

2.3 Summary

We have improved the standard experiments which probe the depolymerization of single actin filaments in two ways. First, we attached the individual actin filaments not along their

contour, but only at their pointed ends. Second, we have supplemented the depolymerization buffers with latrunculin A which sequesters G-actin. By avoiding both the possible stalling of the shrinkage process due to crosslinking and the slowdown of the shrinkage process by association of free G-actin, we have shown that the depolymerization of single actin filaments is indeed characterized by at least two dynamic phases. In phase I, a filament shrinks rapidly with a velocity of a few protomers per second. A couple of minutes after the initiation of depolymerization, it switches to phase II which is characterized by an apparent shrinkage velocity of about 0.1 protomers per second. We have shown that this abrupt transition is not caused by ATP cleavage, as assumed in [51]. Instead, most protomers dissociating from the barbed end in phase I are already in the ADP-state. At a pH that is slightly lower than the standard of 7.8, we have observed occasional reversals from phase II to phase I.

The shrinkage velocity in phase I is consistent with known barbed end dissociation rates [41, 48]. In contrast, we have shown that phase II cannot be rationalized by the known slow dissociation of ADP-Pi-actin [49]. In addition, the slow-shrinking filaments observed in [62] are reported to shrink from their pointed ends only, i.e. the dissociation from the barbed end is completely interrupted. To account for this, it makes sense to assume that the apparent shrinkage we observe in phase II is caused by bleaching of the fluorescent label and not by dissociation of protomers. In fact, we will see in later experiments (cf. chapter 4) that phase II is indeed characterized by a constant length.

3 Stochastic modeling of interrupted depolymerization

We have seen in the last chapter, that a single actin filament with a blocked pointed end and a free barbed end exhibits two distinct dynamical phases, when kept in a buffer containing no free monomers. In phase I, the filament depolymerizes with a velocity which is consistent with biochemical rates. Then, it abruptly switches to phase II, where the shrinkage is halted. This interruption is not caused by the known protomer states which are determined by the bound nucleotide. Therefore, it is required to postulate another entity that influences the filament dynamics.

Since the actin filament has a helical structure, see figure 1.2(e), the dissociation of a single protomer from a filament end requires the disintegration of two bonds between protomers whereas the detachment of an oligomer requires that at least three such bonds are broken. Because of the essentially exponential dependence of the reaction rate on the barrier of free energy, the disassembly of actin filaments occurs almost exclusively by successive dissociation events of the terminal subunits, see section 1.1.3.

Almost all studies on actin dynamics presume that only the state of the ultimate protomer determines the dissociation rate. However, the fact that the terminal protomer is in contact with both the penultimate protomer and the antepenultimate protomer implies that the dissociation rate depends on the states of all these protomers, or more precisely on the state of the two interfaces of the terminal protomer, see figure 3.1. In our model for barbed end dissociation, the state of the terminal protomer solely determines the dissociation rate as well, but we interpret this state as a combined state of the two interfaces of the barbed end protomer.

To account for the observed interruptions theoretically, we propose a novel protomer state, which we term *state 2*. By definition, protomers in state 2 are characterized by their vanishing barbed end dissociation rate, but we are agnostic about the chemical details that may cause this property. In contrast, protomers in state 1 dissociate from the barbed end with a rate that is consistent with the published rates [41, 48]. We have seen that such a dissociation event involves the disintegration of two protomer bonds. However, since we cannot experimentally resolve the dissociation of single protomers, we consider it as a single transition in a Markov process, in agreement with the notion of the intrinsic state of the terminal protomer itself. By definition, a filament switches from phase I to phase II, as soon as a protomer in state 2 appears at the barbed end, see figure 3.2. Note, that the abstract notion of state 2 contains the proposed "dynamic stabilization" [62, 63], and the idea that a contaminating capping protein is responsible for the interruptions [52] as special cases.

The actin bound nucleotide, namely ATP, ADP-Pi, or ADP, also influences the dissociation rates of the protomers [41, 48]. However, at the barbed end, the dissociation rates that

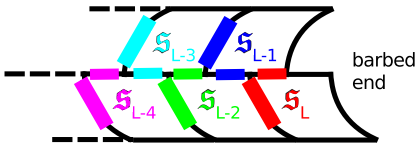

Figure 3.1 : Sketch of the barbed end side of an actin filament. Because of the helical filament structure, each protomer within the filament is in contact with four others, while the terminal protomer is in contact with the penultimate and the antepenultimate protomer. Therefore the barbed end dissociation rate is determined by the combined state of the interfaces marked in red and we define this state as the state $\mathfrak{s}_L$ of the barbed end protomer. For consistency, the state $\mathfrak{s}_i$ of the i-th protomer is determined by the interfaces of this protomer with the $(i-1)$-th protomer and the $(i-2)$-th protomer.

characterize these states are relatively similar to each other when compared to the vanishing dissociation rate of state 2. This is reflected by our observation, that during phase I, a filament shrinks with a velocity that varies only little. In consequence, we consider the known nucleotide states to be substates of state 1. In principle, state 2 could also contain a collection of substates which are determined by the bound nucleotide. However, as a protomer in state 2 does not dissociate from the barbed end by definition, these substates are intrinsically hidden to depolymerization experiments, and we are not able to consider them. On the other hand, the substates of state 1 are in principle observable during phase I, but because of the lag phase in the experiments discussed in the last chapter, most protomers are already in the ADP-actin state when their dissociation is observed. Thus, we will choose a coarse-grained description and ignore the substates.

In this chapter, we will employ stochastic modeling to investigate the interruption of the depolymerization process. Within our simplified model, the state of a filament is represented by the sequence

$$\mathfrak{S}(t) \equiv (\mathfrak{s}_1, \mathfrak{s}_2, \ldots, \mathfrak{s}_L), \tag{3.1}$$

where $\mathfrak{s}_i(t) = \{1, 2\}$ is the state of the i-th protomer. The state of the pointed and barbed end is denoted as $\mathfrak{s}_1(t)$ and $\mathfrak{s}_L(t)$, respectively. Note, that the length of the sequence $L = L(t)$ is an unbounded stochastic variable giving rise to 2^L filament states. Association and dissociation of state-1-protomers at the barbed end are described as Markov processes [61] with rates ω_{on} and ω_{off}, respectively. Furthermore, a transition from state 1 to state 2 is also a Markov process characterized by the rate ω.

We will consider the following alternative mechanisms for transitions from state 1 to state 2, which all give rise to the appearance of a state-2-protomer at the barbed end, see figure 3.2.

a) **Global transitions.** The filament helix as a whole suddenly switches to state 2 at a random point in time. As this instantaneous transition appears unphysical, one can equivalently imagine a random distortion that propagates very fast – compared to time scales of the association and dissociation kinetics – along the filament. The model of a global transition is implicit in the idea of "dynamic stabilization" which was proposed by Kueh et al. [62] and further discussed in recent reviews [11, 63].

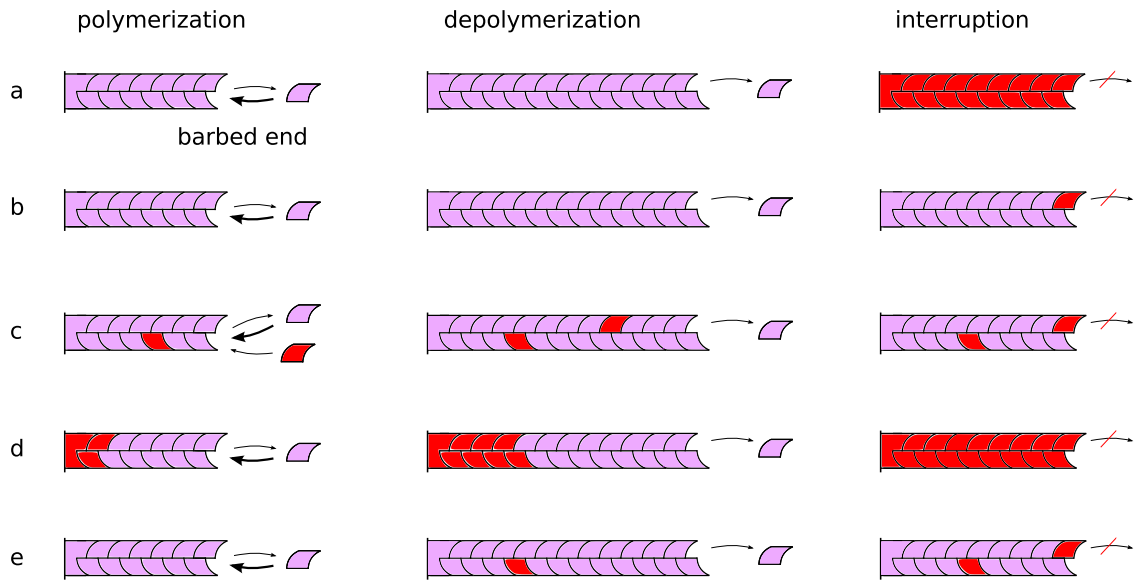

Figure 3.2 : Alternative mechanisms that give rise to the appearance of state 2 at the barbed end. Protomers in state 1 are shown in purple; protomers in state 2 in red. During polymerization, monomer association takes place with a larger rate than dissociation of state-1-protomers. During depolymerization, free monomers are absent and no association events take place. As soon as a protomer in state 2 reaches the barbed end, depolymerization is interrupted. Five mechanisms for such an event can be discriminated, see main text for details. Each mechanism leads to a different time-dependent pattern of state-2-protomers within the filament. However, this pattern is experimentally not accessible.

b) **Transitions at the barbed end.** The transitions from state 1 to state 2 occur only at the depolymerizing barbed end. For instance, small concentrations of capping proteins may contaminate the depolymerization buffer. The binding of these proteins to the terminus may effectively prevent further depolymerization. Alternatively, a random contact of the filament tip with the chamber wall or the surrounding methyl cellulose could cause the transition.

c) **Transitions during polymerization.** As the transition to state 2 may only occur during the elongation process, the sequence of protomer states along the filament is time-independent during depolymerization. Assuming a uniform polymerization process, the probability that a certain protomer is in state 2 is constant along the filament. Furthermore, this probability must be very small, since typically a few hundreds of protomers dissociate before phase II is reached.

   Transitions during polymerization could arise in various scenarios. For instance, a transition might be coupled to the association process which involves the relative rotation of the two major domains of the actin molecule [24] and gives rise to the F-actin conformation. With a certain, very low probability, another conformation which is represented by our state 2 is attained instead of the F-actin conformation. Thus, the transition can be regarded as an imperfection of the polymerization process.

Our model also contains the possibility of co-polymerization of actin and some contaminating protein (or equally actin that has been modified in some way) which does not dissociate from the filament end. Equivalently, state 2 might represent a persistent contact of a cross-linking protein with the filament helix. Since the filaments in our experiments were only attached at their pointed ends, we could readily exclude the last scenario. Nevertheless, we consider it for completeness.

d) **Vectorial transition mechanism.** Starting from the seed at the pointed end, which represents a filament segment of infinite age, protomers successively undergo transitions from state 1 to 2. Phase I ends when a protomer in state 2 finally reaches the barbed end and the remaining filament consists only of state 2 protomers.

e) **Random transition mechanism.** Each protomer within the filament may undergo the transition independently. Then, the probability that a certain protomer is in state 2 depends only on its age, that is on the time period since it has been incorporated into the filament.

3.1 Distributions of the duration of shrinking

The pattern of state 1 and state 2 protomers within a filament is obviously quite different between each case, see figure 3.2, but apparently these patterns cannot be measured directly. Instead, we measure the duration τ of phase I, i.e. the time interval from the initiation of depolymerization until a protomer in state 2 appears at the barbed end. The quantity τ is a random variable, see figure 2.2, and can be characterized by its distribution function. Specifically, the cumulative distribution function (cdf)

$$P(t) \equiv \text{prob}(\tau \leq t) \tag{3.2}$$

describes the probability that τ is found at a value less than or equal t. Equivalently, the distribution of τ can be represented by the probability density function (pdf), which is defined as the derivative of the cdf:

$$p(t) \equiv \partial_t P(t) \equiv \lim_{dt\to 0} \frac{P(t+dt) - P(t)}{dt} = \lim_{dt\to 0} \frac{\text{prob}(t < \tau \leq t+dt)}{dt}. \tag{3.3}$$

From this definition, $p(t)dt$ can be interpreted as the probability of τ falling within the interval $(t, t+dt]$.

As the cdf of τ is a probability, the conditional cdf is defined by

$$P(t\ |B) \equiv \text{prob}\,(\tau \leq t\ |B) \equiv \frac{\text{prob}\,(\tau \leq t, B)}{\text{prob}\,(B)}, \tag{3.4}$$

where B is a random event, and $\text{prob}\,(\tau \leq t, B)$ is the joint probability for both $\tau \leq t$ and B. For convenience, we also define a conditional pdf for τ by

$$p(t\ |B) \equiv \partial_t P(t\ |B). \tag{3.5}$$

In the next sections, we will derive analytical expressions for $p(t)$ – and equivalently $P(t)$ – for each of the listed transition mechanism. In general, these formulae will depend on the transition rate ω from state 1 to state 2 and on the polymerization and depolymerization kinetics of the filament.

Readers not interested in the details of the calculations may skip the next sections and proceed to the summary of the theoretical results in section 3.7.

In the experiments presented in chapter 2, every filament has exhibited an interruption before it had the chance to depolymerize completely. Therefore, in our computations, we will first assume that a state-2-protomer eventually appears at the barbed end. This means that we exclude the hypothetical case that the filament depolymerize entirely by neglecting the finiteness of its length. Later, in section 3.6, we will use some results obtained in the meantime to extend our theory to the case that the depolymerization is not interrupted until the filament has vanished. At the end of this chapter, we will compare our theoretical results with the distribution of the experimentally determined τ. It will turn out that only one particular transition mechanism is consistent with the experimental data.

3.2 Global transitions or transitions at the barbed end

A global transition, see figure 3.2(a), or a transition to state 2 that occurs at the barbed end, see figure 3.2(b), directly interrupts the depolymerization process. Therefore, the duration τ of phase I is simply given by the time interval until such a transition occurs. For a Markov process [61], the pdf for the occurrence of a single, random transition is given by

$$p(t) = \omega e^{-\omega t}, \tag{3.6}$$

where the transition rate $\omega \equiv 1/\langle\tau\rangle$ is the inverse of the mean dwell time in the initial state. The corresponding cdf reads

$$P(t) = 1 - e^{-\omega t}. \tag{3.7}$$

Consistently with this abstract description, alternative physical interpretations of the transition rate ω are possible. The rate ω could characterize the global transition of the filament, or the binding of a capping protein to the barbed end with the rate $\omega \equiv k_{\mathrm{on}}^{\mathrm{cap}} c_{\mathrm{cap}}$, where $k_{\mathrm{on}}^{\mathrm{cap}}$ and c_{cap} are the association rate constant and the concentration of the capping protein, respectively. A third possibility is that of random contacts of the barbed end with the chamber wall or the surrounding methyl cellulose. In that case, ω is to be interpreted as the product of the frequency of such contacts and the probability that a contact causes a transition to state 2.

Formally, the simple exponential time dependence in eq.(3.6) follows from the fact that a single transition is *memoryless*. Implicitly, we have assumed that the lifetime τ of state 1 is time-invariant. This means that if the transition has not occurred until time t_1, the probability that it does not occur until time t_1+t_2 is the same as the unconditional probability that it does not occur until time t_2. Formally, this is expressed by

$$\mathrm{prob}(\tau > t_1 + t_2 \,|\tau > t_1) = \mathrm{prob}(\tau > t_2). \tag{3.8}$$

By definition of the conditional probability, we have

$$\text{prob}(\tau > t_1 + t_2 \,|\tau > t_1) \equiv \frac{\text{prob}(\tau > t_1 + t_2 \,, \tau > t_1)}{\text{prob}(\tau > t_1)} = \frac{\text{prob}(\tau > t_1 + t_2)}{\text{prob}(\tau > t_1)}, \tag{3.9}$$

where the last equality holds, since $\tau > t_1 + t_2$ implies $\tau > t_1$. In consequence, the survival function

$$S(t) \equiv \text{prob}(\tau > t) \tag{3.10}$$

of a memoryless random variable τ must obey the functional equation

$$S(t_1)S(t_2) = S(t_1 + t_2), \tag{3.11}$$

which is uniquely satisfied by an exponential

$$S(t) = a^t = e^{\ln\left(a^t\right)} = e^{t\ln(a)} = e^{-\omega t}, \tag{3.12}$$

with $\omega > 0$, since $S(t)$ is required to be a monotonically decreasing function. Equation (3.6) follows from the definition of $S(t)$.

3.3 Transitions during polymerization

The transitions to state 2 are assumed to occur randomly at the growing barbed end. During depolymerization, the probability that a certain protomer is in state 2, is time-independent and constant along the filament, see figure 3.2(c). Since typically hundreds of protomers dissociate before state 2 reaches the barbed end, this probability Q must be very small. Depending on the scenario, Q might be interpreted as the probability that a monomer is incorporated into the filament in state 2, which could be a variation of the F-actin conformation, or alternatively Q might be the probability that a protomer is anchored to the surface. As mentioned, the model also contains the possibility of co-polymerization of actin and some contaminating protein which does not dissociate from the barbed end. In this case, Q represents the fraction of contaminations on the overall number of protomers within the filament.

The depolymerization of a filament is a stochastic process. It consists of many dissociation events of state-1-protomers. However, we expect the length fluctuation to be small compared to the shortening of the filament, since there are typically hundreds of identical events in phase I. In consequence, we anticipate that the stochasticity of the depolymerization process is small compared to the stochasticity of distributing transformed state-2-protomers along the filament. We will verify this notion by comparing the exact result for the pdf of τ with two simplifications, where either the shrinkage process or the distribution of state-2-protomers along the filament is assumed to be deterministic. We additionally consider a continuous model for the depolymerization process. The calculations are presented with a large amount of detail, as intermediate results are needed in later sections, when considering more intricate transition mechanisms.

3.3.1 Direct solution

Before starting to discuss the stochastic system in detail, we first give a direct solution for our problem to find the pdf of τ. The probability that a filament is in phase I is given by $1-P(t)$, where $P(t)$ is the cdf for the duration τ. At the beginning of the depolymerization process, at time $t=0$, we have $P(0)=Q$ as the probability that the very first protomer is in state 2 is given by Q. Phase I is terminated in an abrupt manner, when a protomer in state 2 reaches the barbed end. The rate at which such an event occurs is given by the probability Q that the penultimate protomer is in state 2 multiplied by the dissociation rate ω_{off}. Therefore, the time evolution of $P(t)$ is governed by

$$\partial_t \left(1-P(t)\right) = -Q\,\omega_{\text{off}}\left(1-P(t)\right), \tag{3.13}$$

and with the initial condition $P(0)=Q$, we find

$$\begin{aligned} P(t) &= 1-(1-Q)\;e^{-Q\,\omega_{\text{off}}\,t} && (3.14)\\ &= Q+(1-Q)\left(1-e^{-Q\,\omega_{\text{off}}\,t}\right). && (3.15)\end{aligned}$$

In eq. (3.15), the exceptional case of filaments initially being in phase II is reflected by the first term. The corresponding pdf is given by

$$p(t) = Q\delta(t) + (1-Q)\,Q\,\omega_{\text{off}}\;e^{-Q\,\omega_{\text{off}}\,t}, \tag{3.16}$$

where the first term, with the *Dirac delta function* $\delta(t)$, accounts for this particular case. Note that the normalization

$$\int_0^\infty dt\; p(t) = Q\int_{-\infty}^{\infty} dt\;\Theta(t)\,\delta(t) + (1-Q) = 1, \tag{3.17}$$

where $\Theta(t)$ is the *Heaviside step function*, is fulfilled if $\Theta(0)\equiv 1$ is chosen.

The mean and variance of the duration τ are given by:

$$\begin{aligned} \mu &\equiv \langle\tau\rangle \equiv \int_0^\infty dt\; t\; p(t) = \frac{1-Q}{Q\,\omega_{\text{off}}}, && (3.18)\\ \sigma^2 &\equiv \langle\tau^2\rangle - \langle\tau\rangle^2 = \frac{1-Q}{\left(Q\,\omega_{\text{off}}\right)^2}. && (3.19)\end{aligned}$$

As the average value $\langle\tau\rangle$ was experimentally found to be of the order of a few hundred seconds and the ω_{off} is of the order of a few protomers per second, Q is expected to be of the order of 10^{-3}. Thus, for the relevant parameter regime, very good approximations are given by

$$\begin{aligned} p(t) &= Q\,\omega_{\text{off}}\,e^{-Q\,\omega_{\text{off}}\,t}, && (3.20)\\ P(t) &= 1-e^{-Q\,\omega_{\text{off}}\,t}, && (3.21)\\ \mu &= \frac{1}{Q\,\omega_{\text{off}}}, && (3.22)\\ \sigma^2 &= \frac{1}{\left(Q\,\omega_{\text{off}}\right)^2}. && (3.23)\end{aligned}$$

3.3.2 Systematic analysis of discrete model

The depolymerization process is a succession of stochastic dissociation events. The number N_0 of protomers that dissociate, before a state-2-protomer appears at the terminus depends on the distribution of such protomers along the filament, see figure 3.2(c), and is thus a random variable. Even though the pdf of τ can be calculated directly, as we have seen above, a systematic solution is presented here, since intermediate concepts and results can be used in later sections. Let us first consider all realizations of N_0 that can contribute to the pdf of τ:

$$p(t) = \sum_{m=0}^{\infty} p(t \mid N_0 = m)\ \mathrm{prob}(N_0 = m). \tag{3.24}$$

The first term in this sum is the conditional pdf for τ, given that m protomers dissociate in phase I. The second term is the probability that m protomers dissociate in phase I and is given by

$$\mathrm{prob}(N_0 = m) = \mathrm{prob}(\mathfrak{s}_1 = 1, \ldots, \mathfrak{s}_m = 1, \mathfrak{s}_{m+1} = 2) = (1-Q)^m Q, \text{ for } m \geq 0. \tag{3.25}$$

As discussed before, we implicitly assume here that phase I is ended by a protomer in state 2 and not by the depolymerization of the whole filament.

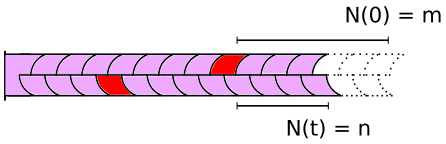

Figure 3.3 : Filament segment which consists of m state-1-protomers at the initiation of depolymerization and of n such protomers after time t. State-2-protomers are shown in red. Already dissociated protomers are framed by dotted lines. The time-dependent number of protomers $N(t)$ in the segment represents a random variable. When this variable reaches $N(t) = 0$, the depolymerization is interrupted.

In order to compute the conditional pdf $p(t \mid N_0 = m)$, we have to investigate the depolymerization of a segment that initially consists of m state-1-protomers. First, we will exclude the case that no protomer is initially in this segment – that is $m = 0$ – and consider the time-dependent number $N(t) \in \{0, 1, \ldots, m\}$ of protomers in the depolymerizing segment, with $N(0) \equiv N_0 > 0$. We define

$$P_n^{(m)}(t) \equiv \mathrm{prob}(N(t) = n \mid N(0) = m) \tag{3.26}$$

as the probability that n protomers are in the segment at time t, given that m protomers were initially present, see figure 3.3. $N(t)$ performs a random walk on the natural numbers and, by its definition, phase I ends, when $N(t) = 0$ is reached. The master-equation for $P_n^{(m)}(t)$ reads

$$\partial_t P_n^{(m)} = \omega_{\mathrm{off}}(P_{n+1}^{(m)} - P_n^{(m)}), \text{ for } n \geq 1 \tag{3.27}$$

$$\partial_t P_0^{(m)} = \omega_{\mathrm{off}} P_1^{(m)}, \tag{3.28}$$

where a filament in phase II is described by the state $n = 0$. Before solving this equation, we eliminate the inconvenient boundary of the random walk as follows. Since there are only transitions from $n + 1$ to n, we can extend the master equation to all integers n:

$$\partial_t P_n^{(m)} = \omega_{\text{off}}(P_{n+1}^{(m)} - P_n^{(m)}), \text{ for all } n, \tag{3.29}$$

and simultaneously consider a filament to be in phase II if and only if $n \leq 0$, that is

$$\text{prob}(\tau < t \mid N_0 = m) = \sum_{n=-\infty}^{0} P_n^{(m)}. \tag{3.30}$$

The standard procedure [61] to solve a master equation like eq. (3.29) is to introduce a generating function

$$G^{(m)}(z,t) \equiv \sum_{k=-\infty}^{\infty} P_k^{(m)}(t)\, z^k \tag{3.31}$$

and to rewrite the master equation (3.29) as a differential equation for this generating function:

$$\partial_t G^{(m)}(z,t) = \omega_{\text{off}}(1/z - 1)G^{(m)}(z,t). \tag{3.32}$$

The intial condition $P_n^{(m)}(0) = \delta_{m,n}$ translates to $G^{(m)}(z,0) = z^m$, and we find

$$G(z,t) = z^m e^{\omega_{\text{off}}(1/z-1)\,t}. \tag{3.33}$$

By expanding $e^{\omega_{\text{off}}\,t/z}$ in powers of z^{-1}, we can transform back to the probability

$$P_n^{(m)}(t) = e^{-\omega_{\text{off}}\,t}\frac{(\omega_{\text{off}}\,t)^{m-n}}{(m-n)!} \quad \text{for all } n. \tag{3.34}$$

Using eq. (3.30), we find

$$\text{prob}(\tau < t \mid N_0 = m) \equiv \sum_{n=-\infty}^{0} P_n^{(m)}(t) = 1 - \sum_{n=1}^{\infty} P_n^{(m)}(t) = 1 - e^{-\omega_{\text{off}}\,t}\sum_{k=0}^{m-1}\frac{(\omega_{\text{off}}\,t)^k}{k!}, \tag{3.35}$$

and the pdf reads

$$p(t \mid N_0 = m) \equiv \partial_t \text{ prob}(\tau < t \mid N_0 = m) = \omega_{\text{off}}\; e^{-\omega_{\text{off}}\,t}\;\frac{(\omega_{\text{off}}\,t)^{m-1}}{(m-1)!}, \text{ for } m \geq 1. \tag{3.36}$$

This distribution is termed *Erlang distribution.* It was first derived for an equivalent problem in *queueing theory* [87].

In the exceptional case that the first protomer is already in state 2, the filament is in phase II from the beginning and we have

$$p(t \mid N_0 = 0) = C\,\delta(t), \tag{3.37}$$

where the prefactor $C \equiv 1$ is determined by the normalization of the conditional pdf, since

$$\int_0^\infty dt\; p(t \mid N_0 = 0) \equiv C\int_{-\infty}^{\infty} dt\; \Theta(t)\,\delta(t) \equiv C\,\Theta(0) \equiv C \tag{3.38}$$

holds, where again $\Theta(0) \equiv 1$ is chosen. Inserting eqs. (3.25) and (3.36) into eq. (3.24), and considering the exceptional case brings us back to the solution in eq. (3.16):

$$\begin{aligned} p(t) &= Q\,\delta(t) + \sum_{m=1}^{\infty} \omega_{\text{off}}\; e^{-\omega_{\text{off}}\, t} \frac{(\omega_{\text{off}}\, t)^{m-1}}{(m-1)!} (1-Q)^m Q \\ &= Q\,\delta(t) + (1-Q)Q\,\omega_{\text{off}}\; e^{-\omega_{\text{off}}\, t} \sum_{m=0}^{\infty} \frac{(\omega_{\text{off}}\, t)^m}{m!} (1-Q)^m \\ &= Q\,\delta(t) + (1-Q)Q\,\omega_{\text{off}}\; e^{-Q\,\omega_{\text{off}}\, t}. \end{aligned} \tag{3.39}$$

This equation incorporates both the randomness caused by the random distribution of state-2-protomers along the filament, and the randomness resulting from the stochastic depolymerization, cf. eq. (3.24). Next, we aim to clearly distinguish between these two sources of stochasticity of τ.

Deterministic distribution of state-2-protomers

First, we neglect the randomness of distributing state-2-protomers along the filament, but do consider depolymerization as a stochastic process. This means that we assume that a fixed number of protomers dissociate, before the shrinkage of a filament is interrupted at a given state-2-protomer. We choose this number as the rounded mean number $\langle N_0 \rangle$ of protomers that dissociate in a stochastic model and use eq. (3.25) to compute it:

$$[\langle N_0 \rangle] = \left[\sum_{m=0}^{\infty} m(1-Q)^m Q \right] = \left[\frac{1-Q}{Q} \right], \tag{3.40}$$

where $[z]$ denotes the rounded value of z. With eq. (3.36), we retrieve the Erlang distribution for the pdf of τ, and the corresponding cdf:

$$p(t) = \omega_{\text{off}}\; e^{-\omega_{\text{off}}\, t}\; \frac{(\omega_{\text{off}}\, t)^{[\langle N_0 \rangle]-1}}{([\langle N_0 \rangle]-1)!}, \tag{3.41}$$

$$P(t) = 1 - e^{-\omega_{\text{off}}\, t} \sum_{k=0}^{[\langle N_0 \rangle]-1} \frac{(\omega_{\text{off}}\, t)^k}{k!} \tag{3.42}$$

In the case of small Q, $[\langle N_0 \rangle]$ is large, and thus the pdf is very narrow.

Deterministic depolymerization

Now we consider the counterpart of the previously discussed case: We neglect the randomness of the depolymerization process, but consider the random distribution of state-2-protomers. Thus, eq. (3.25) remains valid, but the conditional pdf for τ, given that m protomers dissociate is altered to

$$p(t \mid N_0 = m) = \delta\left(t - \frac{m}{\omega} \right). \tag{3.43}$$

With eq. (3.24), we find

$$p(t) = Q \sum_{m=0}^{\infty} (1-Q)^m \; \delta\left(t - \frac{m}{\omega}\right), \tag{3.44}$$

and

$$P(t) = Q \sum_{m=0}^{\infty} (1-Q)^m \; \int_0^t dt' \; \delta\left(t' - \frac{m}{\omega}\right) = 1 - (1-Q)^{1+\lfloor \omega_{\text{off}}\, t \rfloor}, \tag{3.45}$$

where $\lfloor z \rfloor$ is the *floor function*. We retrieve both the mean, eq. (3.18), as well as the variance, eq. (3.19), of the exact solution. Furthermore, for small Q, the cdf simplifies to eq. (3.21).

3.3.3 Systematic analysis of continuous model

In later sections, we will take advantage of a continuous description of filament depolymerization. Thus, we already introduce the continuous filament model here in the context of the transitions that occur during polymerization. In a continuous model of the filament, the concept of discrete subunits – the protomers – ceases to exist. Instead, certain sites along the continuous filament are assumed to be in state 2. We define q as the number density of these sites, such that the product qL is the number of sites in state 2 within a filament of length L. Depolymerization is interrupted at the state-2-site which is closest to the barbed end. Thus, we define

$$X_0 \equiv \min_{1 \le i \le qL} \{\Delta_i\}, \tag{3.46}$$

where Δ_i is the distance of the i-th state-2-site to the barbed end. As state 2 is equally distributed along the filament, the continuous random variable Δ_i is distributed according to

$$\text{prob}(\Delta_i \le x_0) = \frac{x_0}{L}, \text{ for } x_0 \le L. \tag{3.47}$$

We now assume an infinite filament length, $L \to \infty$, to ensure that a state-2-site always appears at the barbed end. In section 3.6, we will relax this assumption and realize that the pdf of τ does not change considerably. In the limit $L \to \infty$, the probability distribution of the random variable X_0 can be calculated as follows.

$$\text{prob}(X_0 > x_0) = \lim_{L\to\infty} \prod_{i=1}^{qL} \text{prob}(\Delta_i > x_0) = \lim_{L\to\infty} \left(1 - \frac{x_0}{L}\right)^{qL} = e^{-x_0\, q}. \tag{3.48}$$

We define the pdf of X_0 by

$$p_{X_0}(x_0) \equiv \partial_{x_0} \text{prob}(X_0 \le x_0) = q e^{-q\, x_0}, \tag{3.49}$$

and interpret $p_{X_0}(x_0)dx_0$ as the probability that the site at which depolymerization is interrupted is within the infinitesimal interval $(x_0, x_0 + dx_0]$. For the pdf of τ, we then have

$$p(t) = \int_0^\infty dx_0 \; p(t \;|X_0 = x_0) \; p_{X_0}(x_0), \tag{3.50}$$

where the first term within the integral is the conditional pdf of τ, given that the interruption occurs at $X_0 = x_0$. To determine this quantity, a reformulation of the stochastic depolymerization dynamics in a continuous state space is required. Again, we present the computations in some detail, since intermediate results will be used in later sections.

The discrete depolymerization process can be modeled by the master eq. (3.29). That equation can be understood to describe a random walker that moves from the right to the left of a one-dimensional lattice and here we intend to find a reformulation for this on the real axis. Because we need the result for later computations, we first generalize eq. (3.29) to include transitions into the other direction

$$\partial_t P_n(t) = -(\omega_{\mathrm{R}} + \omega_{\mathrm{L}})P_n(t) + \omega_{\mathrm{R}} P_{n-1}(t) + \omega_{\mathrm{L}} P_{n+1}(t), \tag{3.51}$$

where ω_{R} and ω_{L} are the transition rates to the right and to the left of the lattice, respectively. In order to describe the random walk in a continuous state space, we consider the distance $X(t)$ between the barbed end and the first state-2-site. That is, $X(t)$ denotes the length of the state-1-segment at the barbed end, and, in particular, we have $X(t) = \ell N(t)$ where $\ell = 2.7$nm is the extend of one protomer within the filament and $N(t)$ was defined as the number of protomers in that segment. We define the probability density function

$$p(x,t) \equiv \partial_x \mathrm{prob}(X(t) \leq x) \tag{3.52}$$

and choose the normalization

$$\int_{-\infty}^{\infty} dx\ p(x,t) = 1, \tag{3.53}$$

which means that we allow for negative $X(t)$. All measured filament lengths are specified in the units of protomers. Thus, we set $\ell \equiv 1$ protomers, or simply $\ell \equiv 1$, and obtain

$$P_n(t) = \int_{(n-\frac{1}{2})\ell}^{(n+\frac{1}{2})\ell} dx\ p(x,t) \approx \ell p(n,t) \equiv p(n,t), \tag{3.54}$$

and with the expansion

$$p(n \pm 1, t) = p(n,t) \pm \partial_x p(x,t)\Big|_{x=n} \ell + \frac{1}{2}\partial_x^2 p(x,t)\Big|_{x=n} \ell^2 + \mathcal{O}(\partial_x^3 p(x,t)\ \ell^3), \tag{3.55}$$

we write down the continuous counterpart of eq. (3.51):

$$\partial_t p(x,t) = \omega_{\mathrm{R}}(-\partial_x p(x,t) + \frac{1}{2}\partial_x^2 p(x,t)) + \omega_{\mathrm{L}}(\partial_x p(x,t) + \frac{1}{2}\partial_x^2 p(x,t)) + \mathcal{O}(\partial_x^3 p(x,t)). \tag{3.56}$$

Neglecting the higher order derivatives, this represents a diffusion equation [88]

$$\partial_t p(x,t) = -u\partial_x p(x,t) + D\partial_x^2 p(x,t), \tag{3.57}$$

where

$$u \equiv \omega_{\mathrm{R}} - \omega_{\mathrm{L}}, \text{ and} \tag{3.58}$$

$$D \equiv (\omega_{\mathrm{R}} + \omega_{\mathrm{L}})/2 \tag{3.59}$$

are the drift and diffusion coefficient, respectively. For the initial distribution

$$p(x,0) = \delta(x - x_0), \tag{3.60}$$

the solution of the diffusion equation is given by

$$p(x,t\ |x_0) = \frac{1}{\sqrt{4\pi D t}} \exp\{-\frac{(x - x_0 - ut)^2}{4Dt}\}. \tag{3.61}$$

In order to calculate the first passage time distribution

$$p(t) \equiv \partial_t \,\mathrm{prob}(\tau \leq t\ |X(0) = x_0), \tag{3.62}$$

we follow the strategy of Cox [88]. Introducing an absorbing boundary at the origin allows us to identify the probability that the random walk has not yet reached the origin with the probability that it is on the positive half of the real axis:

$$\mathrm{prob}(\tau > t\ |X(0) = x_0) = \mathrm{prob}(\hat{X}(t) > 0\ |\hat{X}(0) = x_0). \tag{3.63}$$

The hat indicates that the variable $\hat{X}(t)$ represents a random walk which is absorbed at $x = 0$. Thus, we have to solve the diffusion equation, eq. (3.57), with the initial condition eq. (3.60) and the additional boundary condition

$$p(0,t) = 0 \tag{3.64}$$

which accounts for the absorption. The standard method [88] to account for absorption is to envisage that the absorption site mirrors the initial probability density $p(x,0) = \delta(x - x_0)$ and induces an "image" given by $p(x,0) = \delta(x + x_0)$. If we neglect the drift for a moment ($u = 0$), subtracting the probability density created by the image from $p(x,t\ |x_0)$ then results in a zero probability at the origin. Because of the linearity of the diffusion equation, this superposition also constitutes a solution. However, since the random walker has a certain drift ($u \neq 0$), we need to introduce a prefactor $C(u,D,x_0)$ of the "mirrored" solution to ensure $\hat{p}(0,t\ |x_0) = 0$ for all t. Thus, the solution for a random walk that starts at $x_0 > 0$ and is absorbed at $x = 0$ is given by

$$\hat{p}(x,t\ |x_0) = p(x,t\ |x_0) + C(u,D,x_0)\ p(x,t\ |-x_0), \tag{3.65}$$

where $p(x,t\ |x_0)$ is the solution of the diffusion equation without an absorbing boundary. By substituting eq. (3.61) and setting $\hat{p}(0,t\ |x_0) = 0$, we find

$$\hat{p}(x,t\ |x_0) = \frac{1}{\sqrt{4\pi D t}} \left(\exp\{-\frac{(x - x_0 - ut)^2}{4Dt}\} - \exp\{-\frac{ux_0}{D} - \frac{(x + x_0 - ut)^2}{4Dt}\} \right). \tag{3.66}$$

To compute the first passage time distribution, we can now use eq. (3.63) and find

$$\begin{aligned} p(t\ |X(0) = x_0) &= -\partial_t\ \mathrm{prob}(\hat{X}(t) > 0\ |\hat{X}(0) = x_0) & (3.67)\\ &= -\partial_t \int_0^\infty dx\ \hat{p}(x,t\ |x_0) = \frac{x_0}{\sqrt{4\pi D t^3}}\ \exp\{-\frac{(x_0 + ut)^2}{4Dt}\}. & (3.68) \end{aligned}$$

For our special case, where $u \equiv -\omega_{\text{off}}$ and $D \equiv \omega_{\text{off}}/2$, we obtain

$$p(t \mid X(0) = x_0) = \frac{x_0}{\sqrt{2\pi\omega_{\text{off}}\, t^3}} \exp\{-\frac{(x_0 - \omega_{\text{off}}\, t)^2}{2\omega_{\text{off}}\, t}\}. \tag{3.69}$$

This result and eq. (3.49) are finally inserted into the integral in eq. (3.50). As $\ell \equiv 1$ was chosen, numerical value of the number density q is identified with the respective value for the probability Q that a certain protomer is in state 2, i.e. $q \equiv Q$. Using an integral table [89], the resulting integral is computed:

$$\begin{aligned} p(t) &= \frac{Q}{\sqrt{2\pi\omega_{\text{off}}\, t^3}} e^{-\omega_{\text{off}}\, t/2} \int_0^\infty dx_0 \; x_0 \exp\left(-\frac{x_0^2}{2\omega_{\text{off}}\, t} - (Q-1)\, x_0\right) \qquad (3.70) \\ &= Q\, \omega_{\text{off}} e^{-(1-Q/2)Q\,\omega_{\text{off}}\, t} \left[\frac{e^{-(1-Q)^2\omega_{\text{off}}\, t/2}}{\sqrt{2\pi\omega_{\text{off}}\, t}} + \frac{1-Q}{2}\left(1 + \text{erf}\left((1-Q)\sqrt{\frac{\omega_{\text{off}}\, t}{2}}\right)\right)\right], \end{aligned}$$

where $\text{erf}(z) \equiv \frac{2}{\sqrt{\pi}} \int_0^z dt \; e^{-t^2}$ is the *error function*. We have verified the normalization of $p(t)$ by computing the respective integral and some lengthy algebra. In the same line, we compute the mean, the variance and the cdf of the duration τ:

$$\int_0^\infty dt \; p(t) = 1, \tag{3.71}$$

$$\mu \equiv \langle\tau\rangle \equiv \int_0^\infty dt \; t \; p(t) = \frac{1}{Q\, \omega_{\text{off}}}, \tag{3.72}$$

$$\begin{aligned} \sigma^2 &\equiv \langle\tau^2\rangle - \langle\tau\rangle^2 = \frac{Q^4 - 22Q^3 + 16Q - 16}{\omega_{\text{off}}^2\, Q^2\, (Q-2)^3} - \frac{1}{Q^2\, \omega_{\text{off}}^2} \\ &= \frac{Q^4 - 23Q^3 + 6Q^2 + 4Q - 8}{Q^2\, \omega_{\text{off}}^2\, (Q^3 - 6Q^2 + 12Q - 8)} = \frac{1}{Q^2\, \omega_{\text{off}}^2} \left(1 + Q + \mathcal{O}(Q^3)\right), \qquad (3.73) \end{aligned}$$

$$\begin{aligned} P(t) &= \int_0^t dt' \; p(t') = \frac{1}{2-Q}\left[\text{erf}\left(\sqrt{\frac{\omega_{\text{off}}\, t}{2}}\right)\right. \\ &+ \left.(1-Q)\left(1 - e^{-(1-Q/2)Q\,\omega_{\text{off}}\, t}\left[1 + \text{erf}\left((1-Q)\sqrt{\frac{\omega_{\text{off}}\, t}{2}}\right)\right]\right)\right]. \qquad (3.74) \end{aligned}$$

For $\omega_{\text{off}}\, t \gg 1$, the equations (3.70) and (3.74) can be approximated asymptotically by

$$p(t) \approx (1-Q)Q\, \omega_{\text{off}} \exp\left(-(1-Q/2)Q\, \omega_{\text{off}}\, t\right), \text{ and} \tag{3.75}$$

$$P(t) \approx 1 - \frac{1-Q}{1-Q/2} \exp\left(-(1-Q/2)Q\, \omega_{\text{off}}\, t\right). \tag{3.76}$$

3.3.4 Comparison and validation

In the last subsections, we have considered the case that the pattern of state-2-protomers is time-independent during filament shrinkage, as transitions to state 2 already occurred during polymerization. We have discussed different ideas to characterize and approximate

the stochastic processes that lead to the appearance of state-2-protomers at the barbed end and have derived the following four probability density functions for the duration τ of phase I, i.e. the time interval until a protomer in state 2 appears at the barbed end:

$$p(t) = Q\,\delta(t) + (1-Q)Q\,\omega_{\text{off}}\; e^{-Q\,\omega_{\text{off}}\,t} \tag{3.77}$$

$$p(t) = Q\,\omega_{\text{off}}\, e^{-(1-Q/2)Q\omega_{\text{off}}t}\left[\frac{e^{-(1-Q)^2\omega_{\text{off}}t/2}}{\sqrt{2\pi\omega_{\text{off}}t}} + \frac{1-Q}{2}\left(1+\text{erf}\left((1-Q)\sqrt{\frac{\omega_{\text{off}}\,t}{2}}\right)\right)\right] \tag{3.78}$$

$$p(t) = \omega_{\text{off}}\; e^{-\omega_{\text{off}}\,t}\;\frac{(\omega_{\text{off}}\,t)^{[(1-Q)/Q]-1}}{([(1-Q)/Q]-1)!} \tag{3.79}$$

$$p(t) = Q\sum_{m=0}^{\infty}(1-Q)^m\;\delta\left(t-\frac{m}{\omega}\right) \tag{3.80}$$

$$p(t) = Q\,\omega_{\text{off}}\; e^{-Q\,\omega_{\text{off}}\,t}. \tag{3.81}$$

The pdf given by eq. (3.77) is derived from an exact stochastic description of the underlying processes, that is transitions to state 2 during polymerization, and dissociation of state-1-protomers during depolymerization phase I. The other three distributions involve different approximations: Eq. (3.78) is the exact solution for a continuous approximation of the filament. In eq. (3.79), depolymerization was exactly described as a stochastic process, but the number of protomers that dissociate before a state-2-protomer appears at the barbed end is not a random number, but determined by the average number of protomers in state 2. Eq. (3.80) represents the counterpart, as the state-2-protomers are randomly distributed along the filament, but the depolymerization is described deterministically. Finally, eq. (3.81) is an asymptotic approximation for eqs. (3.77), (3.78), or (3.80) for small Q.

In figures a.2 - a.4 (shown in appendix A.3.1), we compare the pdfs given by eqs. (3.77) - (3.81) with each other and with the results from stochastic simulations. We have used the Gillespie algorithm [90] to simulate all stochastic processes. In the depolymerization experiments discussed in the last chapter, the typical dissociation rate was a few protomers per second and the depolymerization was typically interrupted after a few hundred seconds. With eq. (3.18), we can therefore conclude that a realistic value for the fraction Q of state-2-protomers is given by $Q = 0.001$.

In a first set of simulations, see figure a.2, we have chosen this value for Q and the dissociation rate $\omega_{\text{off}} = 4/\text{s}$. All approximation formulas, apart from eq. (3.79), nicely match the simulation result. This means that the randomness of the depolymerization process can be easily neglected, whereas the stochasticity of τ arising from the fact that the number of protomers that dissociate is a random variable, must be definitely taken into account. After our detailed analysis in the previous subsections, this can be easily understood: The probability distribution for the number of dissociating protomers, given by eq. (3.25), broadens for small Q. In fact, the ratio between standard deviation and mean value of this distribution approaches unity as Q approaches zero. In contrast, the pdf for τ, under the condition that a fixed number $[\langle N_0\rangle]$ of protomers dissociate, is the Erlang distribution, see (3.41), which quickly narrows with increasing $[\langle N_0\rangle]$, that is decreasing Q. We can rationalize this behavior from the notion that the stochastic nature of an individual dissociation event can be expected to be obscured on the filament level.

We will utilize this idea – i.e. considering the transitions to state 2 as a proper stochastic process while approximating the depolymerization process – when discussing more involved models, which are not analytically tractable in a full stochastic description. In fact, whenever the transitions from state 1 to state 2 occur locally within the filament, the linear topology of filaments implies that there are much less transition events than dissociation events

In order to illustrate the limit of the approximations, we have performed another set of simulations, see figure a.3, where $\omega_{\text{off}} = 4/\text{s}$ was retained and the fraction of state-2-protomers was increased to the unrealistic value $Q = 0.1$. Again, eq. (3.79) completely fails to match the simulations, which means that we cannot neglect the stochasticity from randomly distributing state-2- protomers along the filament. The other three approximations, match the simulation result reasonably well, indicating that the transition to state 2 is still the most pronounced stochastic process in the system. However, we also notice that the deviation from the simulation results, or equivalently from the exact solution eq. (3.77), is larger than in the case $Q = 0.001$. This is because all three approximations rely on the assumption that the typical number of protomers that dissociate is much larger than one. However, in the present case of one out of ten protomers being in state 2, there are only 9 protomers that dissociate on average. The exact result match the simulations, with deviations arising merely from the finite number of simulated filaments.

In a last set of simulations, see figure a.4, we further increased the fraction of state-2-protomers to the extreme value $Q = 0.5$, to demonstrate the failure of all the approximations. On average, only one protomer dissociates before a state-2-protomer appears at the barbed end. Therefore, the stochasticity arising from the depolymerization is as pronounced as the stochasticity from randomly distributed state-2-protomers along the filament. In consequence, eqs. (3.79) and (3.80) exhibit a comparable deviation from the simulation results. In fact, they both fail to describe the simulations, and only the exact solution matches the simulations.

3.4 Vectorial transition mechanism

According to the vectorial mechanism, the transition from state 1 to state 2 may only occur at protomers adjacent to one where the process has already taken place. Thus, protomers successively undergo transitions from state 1 to 2, starting from the seed at the pointed end, which represents a filament segment of infinite age. Phase I ends when a protomer in state 2 reaches the barbed end, that is the last protomer in state 1 has been dissociated, see figure 3.2. Thousands of subsequent and independent transitions from state 1 to 2 as well as association/dissociation events must have occurred at that moment to explain both the observed shortening of the filament and its remaining length, see figure 2.2. Thus, the stochastic nature of an individual transition can be expected to be obscured on the filament level and the fluctuations in the duration τ are expected to be relatively small compared to $\langle\tau\rangle$.

To calculate the distribution of τ, we will use the approach and the results discussed in the last section when considering the simpler case of a time-independent pattern of protomers in state 2. At the end of phase I, the number of protomers in state 2 is of the same order of magnitude as the number of associated/dissociated protomers. Unlike in the transition

mechanisms discussed before, the stochasticity of the protomer transitions can therefore not be assumed to be much larger than the stochasticity from the association and dissociation processes. In consequence, we must take every stochastic event into account: Association of monomers during the growth phase with rate $\omega_{\text{on}} \equiv k_{\text{on}} c_{\text{actin}}$, dissociation of protomers during the growth phase with rate $\omega_{\text{off}}^{\text{pol}}$, dissociation of protomers during depolymerization phase I with rate ω_{off}, as well as transitions from state 1 to state 2 with rate ω at the boundary between the shrinking state-1-segment and the growing state-2-segment of the filament. Note, that the dissociation rate $\omega_{\text{off}}^{\text{pol}}$ during polymerization is smaller than the respective rate ω_{off} during depolymerization, because in the former case the barbed end is expected to consist of ATP-actin, whereas in the latter case it consists mainly of ADP-actin [19]. As mentioned, we do not explicitly consider ATP hydrolysis here, as we use a coarse-grained model for the protomer states. However, we simply implement the well-known difference of the dissociation rates during polymerization and depolymerization. The pure coarse-grained model which ignores the nucleotide states can be easily retrieved by setting $\omega_{\text{off}}^{\text{pol}} = \omega_{\text{off}}$.

3.4.1 Discrete model

For an exact stochastic description, the state space of a filament is discrete. As only vectorial transitions from state 1 to state 2 may occur, a filament consists of two segments: At the side of the barbed end, there is a segment of $N_1(t)$ protomters in state 1. At the pointed end, there is an older segment of $N_2(t)$ protomers in state 2, see figure 3.4. Thus, the state space of a filament is given by $\{0, 1, 2, \dots\} \otimes \{0, 1, 2, \dots\}$. However, as we are only interested in the duration τ of phase I, it is useful to restrict our considerations to the stochastic dynamics of $N(t) \equiv N_1(t)$. The dynamics of $N(t)$ can be described as a random walk on the one-dimensional lattice $\{0, 1, 2, \dots\}$. During the depolymerization phase I, there are only transition to the left of the lattice, caused by dissociation events at the barbed end or transition events at boundary between the two segments, see figure 3.4. Thus, the overall transition rate is given by $\omega_1 \equiv \omega + \omega_{\text{off}}$. During the polymerization phase, the transition rate to the right is given by $\omega_2 \equiv \omega_{\text{on}} \equiv k_{\text{on}} c_{\text{actin}}$, and the transition rate to the left by $\omega_3 \equiv \omega + \omega_{\text{off}}^{\text{pol}}$.

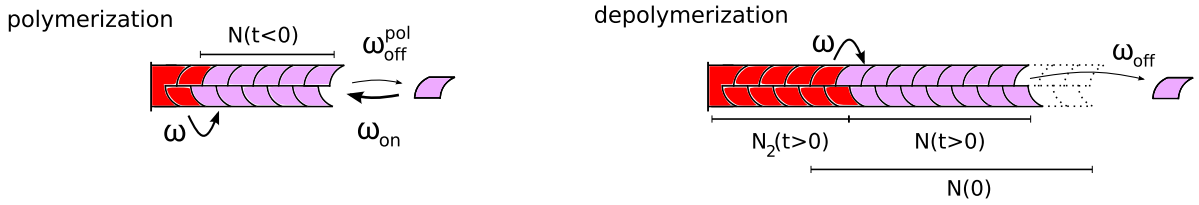

Figure 3.4 : The vectorial transition mechanism gives rise to a state-2-segment (red) toward the pointed end and a state-1-segment (purple) toward the barbed end. $N(t)$ denotes the number of protomers in the state-1-segment. This quantity performs a random walk on the one-dimensional lattice $\{0, 1, 2, \dots\}$. During polymerization, i.e. $t < 0$, the transition rate to the right of this lattice is given by ω_{on}, whereas the transition rate to the left is given by $\omega + \omega_{\text{off}}^{\text{pol}}$. During depolymerization, i.e. $t > 0$, only transitions to the left occur with the rate $\omega + \omega_{\text{off}}$.

Now, we can exploit the results discussed on page 34 and the following. As all realizations of $N(t) = N(0)$ at the beginning of depolymerization at $t = 0$ contribute to the pdf of τ, we have

$$p(t) = \sum_{m=0}^{\infty} p(t \mid N(0) = m) \text{ prob}(N(0) = m \mid N(-t_\text{p}) = 0). \tag{3.82}$$

The first term is the conditional pdf for τ, given that a filament contains m state-1-protomers at the beginning of depolymerization. The second term is the probability that a filament contains m state-1-protomers at the beginning of depolymerization, given the natural assumption that there was no state-1-protomer at the beginning of polymerization at $t = -t_\text{p}$.

First, we aim to calculate $p(t \mid N(0) = m)$. We have already investigated the problem of finding the pdf of the first passage time for a shrinking segment, see page 34 ff.. Here, the shrinkage rate is given by $\omega_1 \equiv \omega + \omega_\text{off}$ and thus the corresponding Erlang distribution reads

$$p(t \mid N(0) = m) = \omega_1 e^{-\omega_1 t} \frac{(\omega_1 t)^{m-1}}{(m-1)!}. \tag{3.83}$$

As a next step, we will compute the length distribution

$$\tilde{P}_m(t_\text{p}) \equiv \text{prob}(N(0) = m \mid N(-t_\text{p}) = 0) \tag{3.84}$$

of state-1-segments at the beginning of depolymerization. Recall, that during the elongation process, $N(t)$ increases with the rate $\omega_2 \equiv \omega_\text{on} \equiv k_\text{on} c_\text{actin}$ and decreases with the rate $\omega_3 \equiv \omega_\text{off}^\text{pol} + \omega$, where $\omega_\text{off}^\text{pol}$, is not necessarily identical to the dissociation rate ω_off during depolymerization phase I. Hence, the master-equation for $\tilde{P}_m(t)$ reads

$$\begin{aligned} \partial_t \tilde{P}_m &= \omega_2 \tilde{P}_{m-1} + \omega_3 \tilde{P}_{m+1} - (\omega_2 + \omega_3)\tilde{P}_m, \ m \geq 1 & (3.85) \\ \partial_t \tilde{P}_0 &= \omega_3 \tilde{P}_1 - \omega_2 \tilde{P}_0. & (3.86) \end{aligned}$$

These equations describe a *biased random walk* of a particle on a lattice, which has a *reflecting boundary* preventing transitions to $m = -1$ [61]. Equivalently, this master-equation characterizes the time evolution of a *queue* [87], where ω_2 and ω_3 are the arrival and service time respectively. In queueing theory, the general solution to this problem has been worked out [87,91–93]. However, our particular situation allows us to avoid the lengthy and complex general solution. In fact, a filament typically shrinks for about half of its length before a protomer in state 2 reaches the barbed end. Therefore, the transition rate ω for a vectorial transition mechanism can not be of a larger order of magnitude than the dissociation rate ω_off, which in turn is of the order of a few protomers per second. Again, the rate $\omega_\text{off}^\text{pol}$ is even smaller. In contrast, the association rate $\omega_\text{on} \equiv k_\text{on} c_\text{actin}$ is one order of magnitude larger. In consequence, the relation $\omega_2 \gg \omega_3$ holds, which means that the random walker quickly moves away from the reflecting boundary. Considering also the overall number of random steps, this means that reflections at the boundary are extremely rare. Therefore, we do not take this boundary into account. This means that within our model filaments that do not have protomers in state 1 can however loose such a state-1-protomer by a transition or dissociation event during the elongation phase. By comparison with stochastic simulations

at the end of this section, we will double-check the validity of this approximation which gives rise to the simplified master-equation

$$\partial_t \tilde{P}_m = \omega_2 \tilde{P}_{m-1} + \omega_3 \tilde{P}_{m+1} - (\omega_2 + \omega_3)\tilde{P}_m, \text{ for all } m, \tag{3.87}$$

with the initial condition

$$\tilde{P}_m(t) = \delta_{0,m}. \tag{3.88}$$

This equation can once again be solved by means of a generating function

$$\tilde{G}(z,t) \equiv \sum_{k=-\infty}^{\infty} \tilde{P}_k(t) z^k. \tag{3.89}$$

In analogy to the derivation on page 35, one gets

$$\tilde{G}(z,t) = e^{[\omega_2(z-1)+\omega_3(1/z-1)]\ t} \tag{3.90}$$

and finally

$$\tilde{P}_m(t) = e^{-(\omega_2+\omega_3)t} \sum_{k=0}^{\infty} \frac{\omega_2^{k+m}\ \omega_3^k\ t^{2k+m}}{(m+k)!k!} = e^{-(\omega_2+\omega_3)t} \left(\frac{\omega_2}{\omega_3}\right)^{m/2} I_m(2\sqrt{\omega_2\omega_3}t), \tag{3.91}$$

where

$$I_\nu(z) \equiv \sum_{k=0}^{\infty} \frac{\left(\frac{z}{2}\right)^{2k+\nu}}{\Gamma(k+\nu+1)k!}, \text{ and} \tag{3.92}$$

$$\Gamma(\nu) \equiv \int_0^\infty dx\ e^{-x} x^{\nu-1} \tag{3.93}$$

are the *modified Bessel function of the first kind* and the *Gamma function*, respectively [94]. The distribution $\tilde{P}_m(t)$ in eq. (3.91) is named *Skellam distribution*, after J. G. Skellam who first derived this general results in 1946 for the distribution of the difference between two independent Poisson-distributed random variables [95]. The time dependent distribution $\tilde{P}_m(t)$ can be illustrated by the mean $\langle m \rangle(t)$ and standard deviation $\sqrt{\langle m^2 \rangle(t) - \langle m \rangle^2(t)}$. Using the following relations for the modified Bessel functions of the first kind [89],

$$\sum_{\nu=-\infty}^{\infty} t^\nu I_\nu(z) = \exp\left(\frac{z}{2}(t + \frac{1}{t})\right) \tag{3.94}$$

$$\nu I_\nu(z) = \frac{z}{2}\left(I_{\nu-1}(z) - I_{\nu+1}(z)\right), \tag{3.95}$$

we obtain

$$\sum_{m=-\infty}^{\infty} \tilde{P}_m(t) = 1, \tag{3.96}$$

$$\langle m \rangle(t) = \sum_{m=-\infty}^{\infty} m\tilde{P}_m(t) = (\omega_2 - \omega_3)t, \tag{3.97}$$

$$\langle m^2 \rangle(t) = \sum_{m=-\infty}^{\infty} m^2 \tilde{P}_m(t) = (\omega_2 + \omega_3)t + ((\omega_2 - \omega_3)t)^2, \text{ and} \tag{3.98}$$

$$\sqrt{\langle m^2 \rangle(t) - \langle m \rangle^2(t)} = \sqrt{(\omega_2 + \omega_3)\ t}. \tag{3.99}$$

The ratio of standard deviation and mean value,

$$\frac{\sqrt{\langle m^2\rangle(t_\mathrm{p}) - \langle m\rangle^2(t_\mathrm{p})}}{\langle m\rangle(t_\mathrm{p})} = \frac{\sqrt{\omega_2+\omega_3}}{(\omega_2-\omega_3)\sqrt{t_\mathrm{p}}} \tag{3.100}$$

indicates a very narrow length distribution after the polymerization time $t = t_\mathrm{p}$. Note that this distribution is nevertheless broader than a corresponding Poisson distribution, where the ratio is given by $1/\sqrt{(\omega_2-\omega_3)t_\mathrm{p}}$.

Now, we combine eqs. (3.83) and (3.91) to calculate the sought probability density function in eq. (3.82):

$$\begin{aligned} p(t) &= \sum_{m=0}^{\infty} p(t\ |N(0)=m)\ \mathrm{prob}(N(0)=m\ |N(-t_\mathrm{p})=0) \\ &= \sum_{m=0}^{\infty} p(t\ |N(0)=m)\ \tilde{P}_m(t_\mathrm{p}) \qquad (3.101) \\ &= t^{-1}\ e^{-(\omega_2+\omega_3)t_\mathrm{p}-\omega_1 t} \sum_{m=0}^{\infty} \frac{\beta_1^m(t) I_m(\beta_2)}{(m-1)!} \\ &= \omega_1\sqrt{\frac{\omega_2}{\omega_3}}\ e^{-(\omega_2+\omega_3)t_\mathrm{p}-\omega_1 t} \sum_{m=0}^{\infty} \frac{\beta_1^m(t) I_{m+1}(\beta_2)}{m!} \qquad (3.102) \end{aligned}$$

where

$$\begin{aligned} \beta_1(t) &\equiv \sqrt{\frac{\omega_2}{\omega_3}}\omega_1 t, \text{ and} \qquad (3.103) \\ \beta_2 &\equiv 2\sqrt{\omega_2\omega_3}t_\mathrm{p}. \qquad (3.104) \end{aligned}$$

The sum of Bessel functions can be simplified according to [96], and we obtain:

$$p(t) = \omega_1\sqrt{\frac{\omega_2}{\omega_3}}\ I_1(\beta_2\gamma(t))\ \gamma^{-1}(t)\ e^{-\omega_1 t-(\omega_2+\omega_3)t_\mathrm{p}}, \tag{3.105}$$

where

$$\gamma(t) \equiv \sqrt{1+\frac{2\beta_1(t)}{\beta_2}} = \sqrt{1+\frac{\omega_1 t}{\omega_3 t_\mathrm{p}}}. \tag{3.106}$$

For the special case, that the dissociation rate of state 1 protomers does not change upon depolymerization, that is for $\omega_\mathrm{off} = \omega_\mathrm{off}^\mathrm{pol}$, we have $\omega_1 = \omega_3$ and the distribution simplifies to

$$p(t) = \sqrt{\frac{\omega_1\omega_2}{1+t/t_\mathrm{p}}}\ I_1\left(2\sqrt{\omega_1(t+t_\mathrm{p})\omega_2 t_\mathrm{p}}\right)\ e^{-\omega_1 t-(\omega_1+\omega_2)t_\mathrm{p}}. \tag{3.107}$$

Next, we will successively simplify the general result for the pdf of τ, given by eq. (3.105). First, we use the properties $\beta_2 \gg 1$ and $\gamma(t) > 1$ to employ the asymptotic expansion

$I_\nu(z) \approx e^z/\sqrt{2\pi z}$ [94] of the Bessel function, and to yield the asymptotic expansion of eq. (3.105):

$$p(t) \approx \sqrt{\frac{\omega_2}{\omega_3}}\ \frac{\omega_1}{\sqrt{2\pi\beta_2\gamma^3(t)}}\ \ e^{-(\omega_2+\omega_3)t_\mathrm{p}-\omega_1 t+\beta_2\gamma(t)}. \tag{3.108}$$

For a further step of approximation, we will now study the properties of the functions given by of eqs. (3.105) and (3.108). According to eq. (3.91), there is a finite probability for having state-1-segments with negative length m after the polymerization phase. Since eq. (3.83) does not account for these exceptional cases, the normalization of the pdf (3.105) is expected to be not exact. However, by expanding the sum in eq. (3.101) to negative m, and using the results from eqs. (3.96)-(3.98), the exact normalization of $p(t)$ becomes evident. Along these lines, we also calculate the mean μ and variance σ^2 of the stochastic variable τ:

$$\begin{aligned}
\int_0^\infty dt\ p(t) &= \int_0^\infty dt \sum_{m=-\infty}^{\infty} p(t\ |N(0)=m)\ \tilde{P}_m(t_\mathrm{p}) \\
&= \sum_{m=-\infty}^{\infty} \tilde{P}_m(t_\mathrm{p}) \int_0^\infty dt\ p(t\ |N(0)=m) = 1, && (3.109)\\
\mu \equiv \langle\tau\rangle &= \int_0^\infty dt\ t \sum_{m=-\infty}^{\infty} p(t\ |N(0)=m)\ \tilde{P}_m(t_\mathrm{p}) \\
&= \sum_{m=-\infty}^{\infty} \tilde{P}_m(t_\mathrm{p}) \frac{m}{\omega_1} = \frac{\omega_2-\omega_3}{\omega_1} t_\mathrm{p}, && (3.110)\\
\langle\tau^2\rangle &= \int_0^\infty dt\ t^2 \sum_{m=-\infty}^{\infty} p(t\ |N(0)=m)\ \tilde{P}_m(t_\mathrm{p}) \\
&= \sum_{m=-\infty}^{\infty} \tilde{P}_m(t_\mathrm{p}) \frac{m^2+m}{\omega_1^2} = \frac{2\omega_2 t_\mathrm{p} + (\omega_2-\omega_3)^2 t_\mathrm{p}^2}{\omega_1^2}, && (3.111)\\
\sigma^2 &\equiv \langle\tau^2\rangle - \langle\tau\rangle^2 = \frac{2\omega_2 t_\mathrm{p}}{\omega_1^2}. && (3.112)
\end{aligned}$$

When using the asymptotic expansion – eq. (3.108) – instead of the exact result – eq. (3.105) – to check the normalization and to calculate the mean μ and variance σ^2, we find the same results in the limits of $\omega_2/\omega_3 \to \infty$ and $\omega_2 t_\mathrm{p} \to \infty$. The somewhat technical derivation can be found in appendix A.3.2. The position t_max of the maximum of the distribution is determined via the derivation of the asymptotic expansion, eq. (3.108). We find

$$t_\mathrm{max} \approx \frac{\omega_2-\omega_3}{\omega_1} t_\mathrm{p} = \mu, \tag{3.113}$$

which indicates that the mean μ also marks the maximum of the function. Since we have $\sigma/\mu \ll 1$, the function given by eq. (3.108) is narrowly centered around its maximum. This is also where the value of the exponential part in eq. (3.108) reaches its maximum. Therefore, it makes sense to expand the logarithm in eq. (3.108) into a power series around

$t = \mu$:

$$\begin{aligned} f(t) &\equiv \log p(t) \\ &= \log\left(\frac{\omega_1}{\sqrt{4\pi\omega_2 t_\mathrm{p}}}\right) - \frac{3\omega_1}{4\omega_2 t_\mathrm{p}}(t-\mu) + \frac{\omega_1^2}{4\omega_2 t_\mathrm{p}}\left(\frac{3}{2\omega_2 t_\mathrm{p}} - 1\right)(t-\mu)^2 + \mathcal{O}((t-\mu)^3), \end{aligned}$$

to finally find

$$p(t) \approx \frac{\omega_1}{\sqrt{4\pi\omega_2 t_\mathrm{p}}} \exp\left(-\frac{3}{4\omega_2 t_\mathrm{p}}\left(\omega_1 t - (\omega_2 - \omega_3)\, t_\mathrm{p}\right) - \frac{1}{4\omega_2 t_\mathrm{p}}\left(\omega_1 t - (\omega_2 - \omega_3)\, t_\mathrm{p}\right)^2\right). \quad (3.114)$$

With the relations $\omega_1 t \gg 1$ and $\omega_2 t_\mathrm{p} \gg 1$, we can approximate this expansion by a Gaussian distribution with mean and variance given by (3.110) and (3.112) respectively:

$$p(t) \approx \frac{\omega_1}{\sqrt{4\pi\omega_2 t_\mathrm{p}}}\ \exp\left(-\frac{(\omega_1 t - (\omega_2 - \omega_3)t_\mathrm{p})^2}{4\omega_2 t_\mathrm{p}}\right). \quad (3.115)$$

As several approximations have been employed to yield the last equation, we will later cross-check its validity by simulating the stochastic variable τ. Furthermore, we note that eq. (3.115) has been derived for large $\omega_2 t_\mathrm{p}$ and large $\omega_1 t$, corresponding to many association, dissociation and transition events. Thus, the problem could have been treated continuously from the beginning by employing a corresponding diffusion equation with a drift term. As we will see, this allows us to retrieve eq. (3.115).

3.4.2 Continuous model

We have seen before, that the stochastic dynamics of the segment of protomers in state 1 can be modeled by a master equation for a one-dimensional random walk on a lattice

$$\partial_t P_n(t) = -(\omega_\mathrm{R} + \omega_\mathrm{L})P_n(t) + \omega_\mathrm{R} P_{n-1}(t) + \omega_\mathrm{L} P_{n+1}(t), \quad (3.116)$$

where ω_R and ω_L are the transition rates to the right and to the left of the lattice, respectively. We also convinced ourselves that, for the considered problem, the reflecting boundary at the origin does not play a role and the master equation holds for all integers n. In the last section (page 38 ff.), we have transformed that master equation into a diffusion equation

$$\partial_t p(x,t) = -u\partial_x p(x,t) + D\partial_x^2 p(x,t), \quad (3.117)$$

for the continuous variable $X(t)$, where we defined

$$p(x,t) \equiv \partial_x \mathrm{prob}(X(t) \leq x) \quad (3.118)$$

and

$$u \equiv \omega_\mathrm{R} - \omega_\mathrm{L}, \text{ and} \quad (3.119)$$

$$D \equiv (\omega_\mathrm{R} + \omega_\mathrm{L})/2 \quad (3.120)$$

are the drift and diffusion coefficient, respectively. For the initial distribution

$$p(x,0) = \delta(x - x_0), \tag{3.121}$$

the solution of the diffusion equation is given by

$$p(x,t\ |x_0) = \frac{1}{\sqrt{4\pi Dt}} \exp\left(-\frac{(x - x_0 - ut)^2}{4Dt}\right). \tag{3.122}$$

In order to calculate the pdf $p(t)$ of the duration τ, we will once again consider the elongation and shrinkage processes separately. First, we will determine the density

$$p_{X_0}(x_0) \equiv \partial_{x_0} \mathrm{prob}(X(0) \leq x_0\ |X(-t_\mathrm{p}) = 0) \tag{3.123}$$

of the random walkers at the beginning of the shrinkage process, given that elongation takes place between $t = -t_\mathrm{p}$ and $t = 0$. In a second step, we will write down the pdf $p(t\ |X(0) = x_0)$ of the times τ of first hitting the origin, given that the random walker starts at the position x_0. The growth of the state1-segment is described by a diffusion process that starts at the origin and whose drift and diffusion terms are given by

$$u_+ \equiv \omega_2 - \omega_3 \equiv \omega_\mathrm{on} - \omega_\mathrm{off}^\mathrm{pol} - \omega, \tag{3.124}$$

$$D_+ \equiv (\omega_2 + \omega_3)/2 \equiv (\omega_\mathrm{on} + \omega_\mathrm{off}^\mathrm{pol} + \omega)/2. \tag{3.125}$$

When dealing with the discrete case, we have argued that the reflecting boundary at the origin does not play a role for our set of parameter values. Therefore, we again neglect this boundary and allow the random walker to diffuse along the entire real axis. We can then use the general result, given by eq. (3.122), to determine the density $p_{X_0}(x_0)$ as defined by eq. (3.123):

$$p_{X_0}(x_0) = \frac{1}{\sqrt{2\pi(\omega_2 + \omega_3)t_\mathrm{p}}} \exp\left(-\frac{(x_0 - (\omega_2 - \omega_3)t_\mathrm{p})^2}{2(\omega_2 + \omega_3)t_\mathrm{p}}\right). \tag{3.126}$$

The shrinkage of the state1-segment is described by a diffusion process that starts at x_0 and whose drift and diffusion terms are given according to eqs. (3.119) and (3.120):

$$u_- \equiv -\omega_1 \equiv -\omega_\mathrm{off} - \omega, \tag{3.127}$$

$$D_- \equiv \omega_1/2 \equiv (\omega_\mathrm{off} + \omega)/2. \tag{3.128}$$

From our previous result for the distribution of the first-passage times, eq. (3.68), we find

$$p(t\ |X(0) = x_0) = \frac{x_0}{\sqrt{2\pi\omega_1 t^3}}\ \exp\left(-\frac{(x_0 - \omega_1 t)^2}{2\omega_1 t}\right). \tag{3.129}$$

Recall, that this result only holds for $x_0 > 0$. As we deal with drift to the left hand side, $u_- \equiv -\omega_1 < 0$, random walkers that start from negative x_0 might escape to negative infinity and never reach the origin. This can be seen from eq. (3.129) by considering the inverse situation of a random walk that starts at positive x_0 and also has a positive drift

$u_- \equiv -\omega_1 > 0$. The probability that such a random walk reaches the origin at all is given by

$$\int_0^\infty dt\, p(t\ |X(0) = x_0) = \int_0^\infty dt \frac{x_0}{\sqrt{4\pi D_- t^3}} \exp\left(-\frac{(x_0 + u_- t)^2}{4D_- t}\right) = \exp\left(-\frac{x_0}{2D_-}\left(u_- + |u_-|\right)\right),$$

which is smaller than unity for $u_- \equiv -\omega_1 > 0$. In our case $u_- \equiv -\omega_1$ is negative, and the distribution at the beginning of depolymerization is given by eq. (3.126), where $(\omega_2 - \omega_3)\, t_\mathrm{p} \gg 1$, meaning that negative x_0 basically do not occur. Thus, in the following, we may safely ignore the exotic cases of random walks that never reach the origin and formally extend the validity of eq. (3.129) to $x_0 < 0$. Now, to obtain the pdf of τ, we again integrate over all possible x_0, and find via a table in [89]:

$$p(t) = \int_{-\infty}^\infty dx_0\ p(t\ |X(0) = x_0)\ p_{X_0}(x_0) \tag{3.130}$$

$$= \sqrt{\frac{2}{\pi}} \frac{\omega_1 \omega_2 t_\mathrm{p}}{\left(\omega_1 t + (\omega_2 + \omega_3)\, t_\mathrm{p}\right)^{3/2}} \exp\left(-\frac{\left(\omega_1 t - (\omega_2 - \omega_3)\, t_\mathrm{p}\right)^2}{2\left(\omega_1 t + (\omega_2 + \omega_3)\, t_\mathrm{p}\right)}\right). \tag{3.131}$$

In close analogy to the discrete model, we aim to simplify this expression to have a clear picture of the distribution. First, we calculate the mean $\mu \equiv \langle\tau\rangle$, variance $\sigma^2 \equiv \langle\tau^2\rangle - \langle\tau\rangle^2$, and the position of the maximum of $p(t)$:

$$\langle\tau\rangle \equiv \int_0^\infty dt\ t\ p(t) = \int_{-\infty}^\infty dx_0\ p_{X_0}(x_0) \int_0^\infty dt\ t\ p(t\ |X(0) = x_0) = \frac{\omega_2 - \omega_3}{\omega_1} t_\mathrm{p} \tag{3.132}$$

$$\langle\tau^2\rangle \equiv \int_0^\infty dt\ t^2\ p(t) = \frac{2\omega_2 t_\mathrm{p}}{\omega_1^2} + \frac{(\omega_2 - \omega_3)^2}{\omega_1^2} t_\mathrm{p}^2 \tag{3.133}$$

$$\sigma^2 = \frac{2\omega_2 t_\mathrm{p}}{\omega_1^2} \tag{3.134}$$

$$t_\mathrm{max} \approx \frac{\omega_2 - \omega_3}{\omega_1} t_\mathrm{p} = \mu. \tag{3.135}$$

Since these results match the corresponding findings for the discrete model, the pdf is again narrowly centered around its maximum and we proceed as before by expanding the logarithm of eq. (3.131). After some calculation, we retrieve eq. (3.114), which again can be approximated by the Gaussian distribution, eq. (3.115).

3.4.3 Comparison and validation

In the last subsections, we have considered the case of a vectorial transition mechanism both in a discrete as well as in a continuous filament description. With various approximations, we obtained the following four alternative results for the pdf $p(t)$.

$$p(t) = \omega_1 \sqrt{\frac{\omega_2}{\omega_3}}\ I_1(\beta_2 \gamma(t))\ \gamma^{-1}(t)\ e^{-\omega_1 t - (\omega_2 + \omega_3) t_\mathrm{p}}\ , \tag{3.136}$$

where $\gamma(t) \equiv \sqrt{1+\omega_1 t/(\omega_3 t_\mathrm{p})}$, and $\beta_2 \equiv 2\sqrt{\omega_2\omega_3}t_\mathrm{p}$,

$$p(t) = \sqrt{\frac{\omega_2}{\omega_3}}\,\frac{\omega_1}{\sqrt{2\pi\beta_2\gamma^3(t)}}\,e^{-(\omega_2+\omega_3)t_\mathrm{p}-\omega_1 t+\beta_2\gamma(t)}, \tag{3.137}$$

$$p(t) = \sqrt{\frac{2}{\pi}}\frac{\omega_1\omega_2 t_\mathrm{p}}{\left(\omega_1 t+(\omega_2+\omega_3)\,t_\mathrm{p}\right)^{3/2}}\,\exp\left(-\frac{\left(\omega_1 t-(\omega_2-\omega_3)\,t_\mathrm{p}\right)^2}{2\left(\omega_1 t+(\omega_2+\omega_3)\,t_\mathrm{p}\right)}\right), \tag{3.138}$$

$$p(t) = \frac{\omega_1}{\sqrt{4\pi\omega_2 t_\mathrm{p}}}\,\exp\left(-\frac{\left(\omega_1 t-(\omega_2-\omega_3)t_\mathrm{p}\right)^2}{4\omega_2 t_\mathrm{p}}\right). \tag{3.139}$$

The first equation is the result for the discrete model. The only approximation that we employed was to neglect the reflecting boundary in the random walk described by eq. (3.87). The second equation is the asymptotic expansion of the first one, for large $\beta_2\gamma(t)$. The third equation is the result for the continuous filament model, where again the reflecting boundary during polymerization was neglected. The last equation is a Gaussian approximation of both the discrete as well as the continuous filament model.

In figures a.5-a.7 (shown in appendix A.3.3), we compare these results with each other and with stochastic simulations. For realistic parameter values, we find a very good agreement between all analytical results and the simulations, cf. figure a.5. When the duration of polymerization t_p is considerably reduced as in figure a.6, the approximation by a Gaussian, eq. (3.139), deviates from the other results and from the simulations. When we additionally reduce the association rate, see figure a.7, all analytical results overestimate the density $p(t)$ for small times t, since neglecting the reflecting boundary in the random walk described by eq. (3.87) is not feasible, but leads to an overestimation of the probability of short state-1-segments in eq. (3.91). However, as we can exclude such parameter values, even our crudest approximation – the Gaussian distribution – describes the pdf very well. Its corresponding cumulative distribution function (cdf) is given by

$$P(t) = \int_0^t dt'\,\frac{\omega_1}{\sqrt{4\pi\omega_2 t_\mathrm{p}}}\exp\left(-\frac{\left(\omega_1 t'-(\omega_2-\omega_3)t_\mathrm{p}\right)^2}{4\omega_2 t_\mathrm{p}}\right) = \frac{1}{\sqrt{2\pi}}\int_{-\mu/\sigma}^{(t-\mu)/\sigma} dy\; e^{-y^2/2}, \tag{3.140}$$

where

$$\mu = \frac{\omega_\mathrm{on}-\omega_\mathrm{off}^\mathrm{pol}-\omega}{\omega_\mathrm{off}+\omega}t_\mathrm{p},\ \text{and} \tag{3.141}$$

$$\sigma^2 = \frac{2\omega_\mathrm{on}}{(\omega_\mathrm{off}+\omega)^2}t_\mathrm{p}. \tag{3.142}$$

Since the Gaussian distribution is very narrow, $\mu/\sigma \gg 1$, this can be written as

$$P(t) = \Phi\left(\frac{t-\mu}{\sigma}\right), \tag{3.143}$$

with the *standard normal integral*

$$\Phi(z) \equiv \frac{1}{\sqrt{2\pi}}\int_{-\infty}^{z} dy\; e^{-y^2/2}. \tag{3.144}$$

3.5 Random transition mechanism

In a random transition mechanism, the transitions to state 2 occur at any protomer with the same transition rate ω. Therefore, the probability that a certain protomer is in state 2 depends only on its age, that is on the time period since it has been incorporated into the filament. In a typical experiment, there are of the order of one thousand protomers which dissociate, before a single protomer in state 2 appears at the barbed end and blocks the depolymerization process. Thus, the order of magnitude of ω can be estimated by $10^3\omega\langle\tau\rangle = \mathcal{O}(1)$, giving a transition rate ω of the order of 10^{-6}/s to 10^{-5}/s. Compared to the association and dissociation events, the very rare protomer transitions have a much bigger stochastic effect on the system, as discussed in section 3.3. Consequently, we will not consider the full stochastic process in order to calculate the pdf $p(t)$, but consider both polymerization and depolymerization as deterministic processes. While we can infer from the previous sections that this will lead to a negligible error in $p(t)$, the result will be cross-checked by stochastic simulations.

In analogy to section 3.4, we may derive an expression for the pdf of τ by considering the number of state-1-protomers in the filament segment that extends from the barbed end until the first state-2-protomer, see figure 3.3. Adapting a continuous description of this number, we could proceed in three steps: First, we derive the distribution of this number after the polymerization time t_p. For realistically large times t_p, this distribution can be approximated by its steady-state which can be calculated in analogy to the steady-state length distribution of GTP-tubulin caps in microtubules, see [58]. In the second step, we determine the conditional pdf for τ, given a fixed length of the segment of state-1-protomers, again using a result from [58]. Thirdly, we integrate over all possible segment lengths, in analogy to eq. (3.130). At the end of this procedure, we find the same result as given by eq. (3.157).

However, a different approach is taken here, since it can be easily generalized, for instance in section 4.6. We start by recalling that the polymerization velocity v_pol is the difference between the barbed end association rate ω_on and dissociation rate $\omega_\mathrm{off}^\mathrm{pol}$, and that we have allowed the dissociation rate during depolymerization ω_off (which equals the depolymerization velocity v_dep) to be different from the dissociation rate $\omega_\mathrm{off}^\mathrm{pol}$ during polymerization. Note that in the experiments discussed in the last chapter, v_dep is observed directly, but v_pol must be estimated from the filament length at the beginning of observation. However, the experimental setup introduced in the next chapter allows us to observe both quantities directly.

In general, the transition rate $\hat{\omega}$ from a filament state with a state-1-protomer at the barbed end (depolymerization phase I) to a filament state with a state-2-protomer at the barbed end (depolymerization phase II) is given by

$$\hat{\omega} = \omega + \omega_\mathrm{off}\, Q \tag{3.145}$$

where $Q \equiv \mathrm{prob}(\mathfrak{s}_{L-1} = 2)$ is defined as the probability that the penultimate protomer is in state 2. The first summand accounts for transitions from state 1 to state 2 that occur directly at the terminus, whereas the second describes dissociation events which lead to the

appearance of a state-2-protomer at the barbed end. The equation

$$\partial_t \left(1 - P(t)\right) = -\hat{\omega}(t) \left(1 - P(t)\right) \tag{3.146}$$

describes the time-evolution of the probability $\text{prob}\left(\tau > t\right) \equiv 1 - P(t)$ of a filament to be in phase I. Formal integration with the initial condition $P(0) = 0$ yields the general expression

$$P(t) = 1 - \exp\left(-\int_0^t dt' \; \hat{\omega}(t')\right), \tag{3.147}$$

which we will use later in a broader context. Note that the transition rate $\hat{\omega}$ is a random variable as the probability Q depends on the exact realization of the stochastic process. In general, eq. (3.147) does not solve our problem, because $\hat{\omega}$ is not simpler to compute than the cdf. For a random transition mechanism, the probability Q is determined by the age A of the penultimate protomer, which in turn is a random variable. For a fixed age, the conditional probability for the penultimate protomer to be in state 2 reads

$$\lim_{da \to 0} \text{prob}(\mathfrak{s}_{L-1} = 2 \; | a < A \leq a + da) = 1 - e^{-\omega a}. \tag{3.148}$$

Therefore, we have

$$Q = \int_0^\infty da \; p_A(a) \; (1 - e^{-\omega a}), \tag{3.149}$$

where $p_A(a)$ is the probability density function of the age A. In general, the computation of $p_A(a)$ is very intricate, as it involves the consideration of the stochastic nature of all association and dissociation processes.

3.5.1 Deterministic age

As mentioned, we simplify the problem by approximating both polymerization and depolymerization as deterministic processes. In consequence, the age $A = a$ of the penultimate protomer is not a random variable any more, but an explicit function of the time t, and given by

$$a(t) = \left(1 + v_{\text{dep}}/v_{\text{pol}}\right) t, \tag{3.150}$$

see figure 3.5. With the corresponding pdf

$$p_A(a) = \delta\left(a - \left(1 + v_{\text{dep}}/v_{\text{pol}}\right) t\right), \tag{3.151}$$

the probability Q can also be written as an explicit function of time t:

$$Q(t) = 1 - \exp\left(-\omega \left(1 + v_{\text{dep}}/v_{\text{pol}}\right) t\right). \tag{3.152}$$

With the identity $\omega_{\text{off}} \equiv v_{\text{dep}}$, eq. (3.147) can be concretized to

$$P(t) = 1 - \exp\left(-\omega t - v_{\text{dep}} t + \frac{v_{\text{dep}}}{\omega \left(1 + v_{\text{dep}}/v_{\text{pol}}\right)} \left(1 - e^{-\omega\left(1 + v_{\text{dep}}/v_{\text{pol}}\right)t}\right)\right), \tag{3.153}$$

$$p(t) = \left(\omega + v_{\text{dep}} \left(1 - e^{-\omega\left(1 + v_{\text{dep}}/v_{\text{pol}}\right)t}\right)\right) \times \exp\left(-\omega t - v_{\text{dep}} t + \frac{v_{\text{dep}}}{\omega \left(1 + v_{\text{dep}}/v_{\text{pol}}\right)} \left(1 - e^{-\omega\left(1 + v_{\text{dep}}/v_{\text{pol}}\right)t}\right)\right). \tag{3.154}$$

Figure 3.5: Neglecting the length fluctuations of the filament leads to an explicit expression for the age $a(t)$ of the penultimate protomer as a function of time. The filament length during polymerization and depolymerization is shown in green. As the size of a single protomer is negligible compared to this scale, this length also represents the distance of the penultimate protomer to the pointed end, where polymerization started. The age of the penultimate protomer is given by $a(t) = t + t'$, where t' is the time from the incorporation of the protomer into the filament until the initiation of depolymerization at $t = 0$. The equality $t'/t_\mathrm{p} = v_\mathrm{dep} t/(v_\mathrm{pol} t_\mathrm{p})$ leads to $a(t) = (1 + v_\mathrm{dep}/v_\mathrm{pol})\, t$.

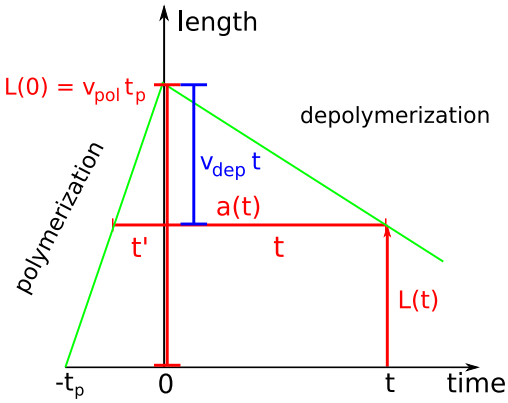

In the experimental situation, we have $\omega < 10^{-5}/\mathrm{s}$, $v_\mathrm{dep} < v_\mathrm{pol}$, and $t < 10^3 \mathrm{s}$. Therefore, $\omega\,(1 + v_\mathrm{dep}/v_\mathrm{pol})\, t \ll 1$ holds, and eq. (3.152) simplifies to

$$Q(t) \approx \omega\,(1 + v_\mathrm{dep}/v_\mathrm{pol})\, t. \tag{3.155}$$

According to eq. (3.145), transitions occurring directly at the terminus only play a role at the very beginning of the shrinkage process, where $t^{-1} \gtrsim v_\mathrm{dep}\,(1 + v_\mathrm{dep}/v_\mathrm{pol})$ – which means in our experiments $t \lesssim 0.2\,\mathrm{s}$ – holds. Therefore, we neglect these transitions and find

$$\hat{\omega}(t) \approx v_\mathrm{dep}\,\omega\,(1 + v_\mathrm{dep}/v_\mathrm{pol})\, t. \tag{3.156}$$

The probability density function of τ then simplifies to the Rayleigh distribution:

$$p(t) \approx \alpha\,\omega\, t\, \exp\left(-\alpha\,\omega\, t^2/2\right), \tag{3.157}$$

where the parameter

$$\alpha \equiv v_\mathrm{dep}\,(1 + v_\mathrm{dep}/v_\mathrm{pol}) \tag{3.158}$$

characterizes the polymerization and depolymerization curve, see figure 3.5. With this simplification, the $n-$th moment of τ can be computed as

$$\begin{aligned} \langle \tau^n \rangle &= \alpha\,\omega \int_0^\infty dt\; t^{n+1} \exp\left(-\alpha\,\omega\, t^2/2\right) \\ &= \left(\frac{2}{\alpha\,\omega}\right)^{n/2} \int_0^\infty dt'\; (t')^{n/2}\, e^{-t'} = \left(\frac{2}{\alpha\,\omega}\right)^{n/2} \Gamma\left(\frac{n}{2} + 1\right), \end{aligned} \tag{3.159}$$

where $\Gamma(z)$ is again the Gamma function [94]. With the mean μ and the variance σ^2 given by

$$\mu \equiv \langle \tau \rangle = \sqrt{\frac{\pi}{2\,\alpha\,\omega}} \tag{3.160}$$

$$\sigma^2 \equiv \langle \tau^2 \rangle - \langle \tau \rangle^2 = \frac{4 - \pi}{2\,\alpha\,\omega}, \tag{3.161}$$

we find that the ratio σ/μ is independent of the parameter $\alpha\,\omega$:

$$\frac{\sigma}{\mu} = \sqrt{\frac{4 - \pi}{\pi}} \simeq 0.523. \tag{3.162}$$

3.5.2 Comparison and validation

Next, we compare the densities given by the eqs. (3.154) and (3.157) with the results from stochastic simulations. In figure a.8 (shown in appendix A.3.4), realistic parameter values are considered, that is $\langle\tau\rangle = 5\,\mathrm{min}$, $v_{\mathrm{pol}} = \omega_{\mathrm{on}} - \omega_{\mathrm{off}}^{\mathrm{pol}} = 34/\mathrm{s}$, $v_{\mathrm{dep}} = \omega_{\mathrm{off}} = 4/\mathrm{s}$, which leads to $\alpha = 4.47/\mathrm{s}$, and with eq. (3.160) to the transition rate $\omega = 3.9 \times 10^{-6}/\mathrm{s}$. Eqs. (3.154) and (3.157) coincide and agree very well with the simulations, except for $t > 700\,\mathrm{s}$, where apparently a neglected effect leads to an additional small peak in the distribution. This effect will be discussed in the next section.

When the transition rate ω is increased to unrealistic values which are comparable to the association and dissociation rates, the simple estimate in eq. (3.156) is no longer valid. Thus, the approximation (3.157) fails, as can be seen in figure a.9. Furthermore, our core assumption, namely that the age of the penultimate protomer does not depend on the realization of the stochastic association and dissociation processes, but is simply given by the pdf in eq. (3.151), looses its justification. This is because only a few dissociation events occur in depolymerization phase I, and thus the randomness caused by the stochastic dissociation events is comparable to the randomness of the transitions. When we also decrease the association rate ω_{on}, the random character of the polymerization process also plays a role and leads to a broad age-distribution instead of the δ-function in eq. (3.151). As can be seen in figure a.9, our analytical results fail to match the simulations in this case.

3.6 Finite filaments lengths

For all discussed transition mechanisms, apart from the vectorial mechanism, filaments might depolymerize completely before a state-2-protomer appears at the barbed end. In that case, the complete depolymerization, instead of the state-2-protomer causes the termination of phase I. Thus, the finiteness of the filament lengths modifies the probability density function. The simulation results in figure a.8 which describe the pdf for a random transition mechanism with realistic parameter values, are an example for such a modification. Here, we will address this problem in general, and derive modified pdfs.

For clarity, the following definitions are introduced. The duration of phase I is denoted by the random variable τ, which is determined by

$$\tau \equiv \min\left(\tau_1, \tau_2\right), \tag{3.163}$$

where τ_1 denote the point in time where a state-2-protomes appears at the barbed end, and τ_2 denotes the instant of complete depolymerization. The random variables τ_1 and τ_2 are independent from each other and distributed according to the following cumulative distribution functions (cdfs) or probability density functions (pdfs):

$$P_1(t) \equiv \mathrm{prob}\left(\tau_1 \leq t |\ \tau_2 > t\right), \quad p_1(t) \equiv \partial_t P_1(t), \tag{3.164}$$

$$P_2(t) \equiv \mathrm{prob}\left(\tau_2 \leq t |\ \tau_1 > t\right), \quad p_2(t) \equiv \partial_t P_2(t). \tag{3.165}$$

The expressions for $p_1(t)$ have beed derived in the previous sections. As only very low transition rates can give rise to complete depolymerization, the approximations for $p_1(t)$ that

have beed derived in the previous sections are entirely adequate. For finding an analytical expression for $p_2(t)$, we recall the discussion of the vectorial transition mechanism. In fact, we can identify the segment of state-1-protomers with the entire filament whose disappearance gives rise to the end of phase I. Arguing along the same lines, the pdf is again approximated well by a Gaussian, as in eq. (3.115). As there are no transitions now, the growth rate ω_2 of the segment during the polymerization process, is given by the association with rate $\omega_{\rm on}$, and the shrinkage rate ω_3 is simply the dissociation rate $\omega_{\rm off}^{\rm pol}$. The shrinkage rate during depolymerization ω_1 is now given by the dissociation rate $\omega_{\rm off}$. Therefore, we have

$$p_2(t) \approx \frac{\omega_{\rm off}}{\sqrt{4\pi\omega_{\rm on}t_{\rm p}}} \exp\left(-\frac{\left(\omega_{\rm off}t - (\omega_{\rm on}-\omega_{\rm off}^{\rm pol})t_{\rm p}\right)^2}{4\omega_{\rm on}^{\rm pol}t_{\rm p}}\right) = \frac{1}{\sqrt{2\pi\sigma_{\rm cd}^2}} \exp\left(-\frac{(t-\mu_{\rm cd})^2}{2\sigma_{\rm cd}^2}\right), \quad (3.166)$$

where the index "cd" stands for "complete depolymerization" and the mean $\mu_{\rm cd}$ and variance $\sigma_{\rm cd}^2$ are given by:

$$\mu_{\rm cd} \equiv \langle\tau_2\rangle = \frac{\omega_{\rm on}-\omega_{\rm off}^{\rm pol}}{\omega_{\rm off}}t_{\rm p} = \frac{v_{\rm pol}}{v_{\rm dep}}t_{\rm p}, \quad (3.167)$$

$$\sigma_{\rm cd}^2 \equiv \langle\tau_2^2\rangle - \langle\tau_2\rangle^2 = \frac{2\omega_{\rm on}t_{\rm p}}{\omega_{\rm off}^2}. \quad (3.168)$$

We now put together the cdf

$$\begin{aligned} P(t) &\equiv \text{prob}\,(\tau \le t) = 1 - \text{prob}\,(\tau > t) = 1 - \text{prob}\,(\tau_1 > t, \tau_2 > t) \\ &= 1 - (1-P_1(t))\,(1-P_2(t)) = P_1(t) + P_2(t) - P_1(t)P_2(t) \end{aligned} \quad (3.169)$$

and the pdf of τ:

$$\begin{aligned} p(t) \equiv \partial_t P(t) &= p_1(t)\,(1-P_2(t)) + p_2(t)\,(1-P_1(t)) \\ &\approx \frac{p_1(t)}{2}\left(\text{erfc}\left(\frac{\mu_{\rm cd}}{\sqrt{2\sigma_{\rm cd}^2}}\right) + \text{erfc}\left(\frac{t-\mu_{\rm cd}}{\sqrt{2\sigma_{\rm cd}^2}}\right)\right) + \frac{1-P_1(t)}{\sqrt{2\pi\sigma_{\rm cd}^2}} \exp\left(-\frac{(t-\mu_{\rm cd})^2}{2\sigma_{\rm cd}^2}\right) \end{aligned} \quad (3.170)$$

where $\text{erfc}(z) \equiv \frac{2}{\sqrt{\pi}}\int_z^\infty dt\; e^{-t^2} = 1 - \text{erf}(z)$ is the *complimentary error function*. For global transitions or transitions that occur at the barbed end during depolymerization, the pdf $p_1(t)$ is a simple exponential function, with the transition rate ω as the decay constant. For transitions that occur during the polymerization process, we recall that the pdf can also be approximated by an exponential function, where the decay constant is given by $Q\,\omega_{\rm off}$, with the time-independent probability Q that a protomer is in state 2 during depolymerization. This approximation works formidable for $Q \ll 1$ which must be fulfilled to allow the occasional complete depolymerization. For a random transition mechanism, finally, $p_1(t)$ is given by eq. (3.157).

In figure a.10 (shown in appendix A.3.5), we compare the results from stochastic simulations of transitions that occur during polymerization to eq. (3.170) with an exponential $p_1(t) = Q\,\omega_{\rm off}\exp(-Q\,\omega_{\rm off}\,t)$. Likewise, in figure a.11 stochastic simulations of the random transition mechanism are compared to eq. (3.170) with the Rayleigh distribution $p_1(t) = \alpha\,\omega\,t\exp(-\alpha\,\omega\,t^2/2)$. In both cases, we find formidable agreement.

To assess the importance of the refinement by the extended expression in eq. (3.170), that is the relative importance of the local peak for instance in figure a.8, we finally calculate the probability that a filament depolymerizes completely:

$$\text{prob}\,(\tau_2 < \tau_1) = \int_0^\infty dt\; p_1(t) P_2(t) = \int_0^\infty dt\; p_2(t)\,(1 - P_1(t))\,. \tag{3.171}$$

For all transition mechanisms which give rise to exponential pdfs $p_1(t)$, we find

$$\text{prob}\,(\tau_2 < \tau_1) \approx \frac{1}{2}\left(1 + \text{erf}\left(\frac{\mu_{\text{cd}} - \tilde{\omega}\sigma_{\text{cd}}}{\sqrt{2\sigma_{\text{cd}}^2}}\right)\right) \times \exp\left(-\tilde{\omega}\left(\mu_{\text{cd}} - \tilde{\omega}\sigma_{\text{cd}}^2/2\right)\right), \tag{3.172}$$

where $\tilde{\omega} \equiv \omega$ for global transitions, or transitions of the depolymerizing terminus, and $\tilde{\omega} \equiv Q\,\omega_{\text{off}}$ for transitions that are coupled to polymerization. In a realistic situation, we have $\tilde{\omega}\,\sigma_{\text{cd}}^2 \ll \mu_{\text{cd}}$ and $\sigma_{\text{cd}} \ll \mu_{\text{cd}}$, and thus

$$\text{prob}\,(\tau_2 < \tau_1) \approx \exp\left(-\tilde{\omega}\,\mu_{\text{cd}}\right) \approx \exp\left(-\frac{\mu_{\text{cd}}}{\langle\tau\rangle}\right). \tag{3.173}$$

The latter approximation holds as long as most filaments exhibit an interruption of depolymerization before they vanish. Then the unknown $\tilde{\omega}$ can still be estimated by $\langle\tau\rangle^{-1}$. For the realistic parameter values chosen in figures a.2 and a.10, we have $\mu_{\text{cd}} = v_{\text{pol}} t_{\text{p}}/v_{\text{dep}} \simeq 790\,\text{s}$ and $\langle\tau\rangle \simeq 250\,\text{s}$, leading to $\text{prob}\,(\tau_2 < \tau_1) \simeq 4\%$. For a random transition mechanism which gives rise to a Rayleigh distribution, we find

$$\begin{aligned} \text{prob}\,(\tau_2 < \tau_1) \;&\approx\; \frac{1}{2\sqrt{\alpha\omega\sigma_{\text{cd}}^2 + 1}}\left(1 + \text{erf}\left(\frac{\mu_{\text{cd}}}{\sqrt{2\sigma_{\text{cd}}^2}\sqrt{\alpha\omega\sigma_{\text{cd}}^2 + 1}}\right)\right) \\ &\times\; \exp\left(\frac{-\alpha\omega\mu_{\text{cd}}^2}{2\,(\alpha\omega\sigma_{\text{cd}}^2 + 1)}\right). \end{aligned} \tag{3.174}$$

For the realistic parameter values, we have $\alpha\,\omega\,\sigma_{\text{cd}}^2 \ll 1$, $\sigma_{\text{cd}} \ll \mu_{\text{cd}}$, and thus

$$\text{prob}\,(\tau_2 < \tau_1) \approx \exp\left(-\frac{\alpha\omega\mu_{\text{cd}}^2}{2}\right) \approx \exp\left(-\frac{\pi\mu_{\text{cd}}^2}{4\langle\tau\rangle^2}\right), \tag{3.175}$$

where the latter approximation is valid as long as most filaments exhibit an interruption of depolymerization before they vanish. Then, the transition rate can be still estimated from eq. (3.160). Given the measured average duration $\langle\tau\rangle$ of phase I, and the inequality $\mu_{\text{cd}} > \langle\tau\rangle$, it is less probable that a filament disassembles completely in case of a random transition mechanism than in case of transition mechanism which gives rise to an exponential distribution. In fact, for the realistic parameter values chosen in figure a.8, we find $\text{prob}\,(\tau_2 < \tau_1) \simeq 0.6\%$, which also evaluates the approximation in eq. (3.157) to be appropriate. As we have inspected less than 100 filaments in the experiments discussed in the last chapter, it is not surprising that not a single instance of complete depolymerization was observed, if we assume that the unknown transition is indeed governed by a random transition mechanism.

3.7 Summary of theoretical results

We have introduced stochastic models for several hypothetical transition mechanisms which all lead to the appearance of a state-2-protomer at the barbed end and thus, the termination of depolymerization phase I. Starting from the simple case where the transitions occur already during the polymerization process, and the distribution of state-2-protomers along the filament is constant during depolymerization, we have elaborated various approximation schemes for the involved stochastic sub-processes. The idea that the stochasticity caused by the association and dissociation events is – in most cases – small compared to the stochasticity caused by the transition from state 1 to state 2, allowed us to get an insight to the more intricate models and to obtain analytical expressions for the probability density function of the duration τ of phase I. For realistic parameter values, it turns out that even our most simple approximations excellently match the exact analytical results as shown in figure 3.6. We have then extended our computations to account for the termination of phase I by complete depolymerization. For reasonably long filaments, this finite size effect leads only to small modifications of the pdfs. All analytical results were confirmed by extensive stochastic simulations using the Gillespie algorithm [90].

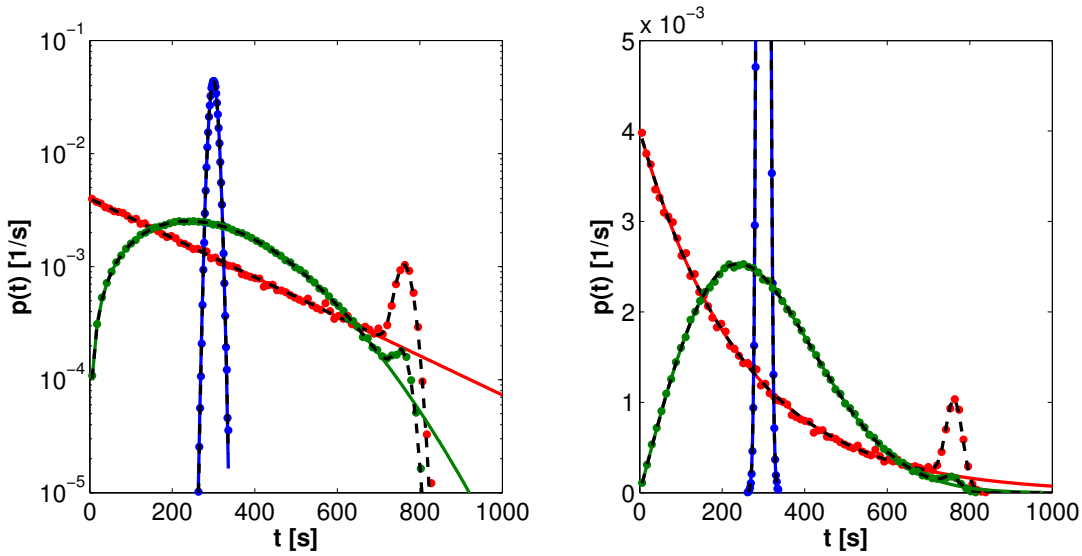

Figure 3.6 : Summary and comparison of theoretical results for the probability density functions $p(t)$ of the duration τ. For clarity, the results are plotted both on a logarithmic scale (left hand side) and on a linear scale (right hand side). Shown are the results for global transitions, transitions at the barbed end, transitions during polymerization (all in red), vectorial transitions (blue), and random transitions (green). Analytical results that neglect the finiteness of the filaments are displayed as continuous colored lines. For the chosen realistic parameter values, they match even our most simple approximations given by eqs. (3.176), (3.177), and (3.180), respectively. The extended expressions, which account for complete depolymerization due to finite filament lengths, are shown as dashed black lines. They perfectly match the simulation results which are shown as colored dots. For transitions during polymerization, the finite size effect is more pronounced than in the other cases, but still pretty small.

In summary, the different mechanisms for the transition from the protomer state 1 to the protomer state 2 lead to three qualitatively distinct pdfs, as shown in figure 3.6. Within the range of realistic parameter values, these pdfs can be approximated by the following simple functions. Global transitions of the whole filament, transitions that occur only at the depolymerizing terminus, as well as transitions during polymerization all lead to an exponentially decaying pdf,

$$\boxed{p(t) = \omega \exp\left(-\omega\, t\right)}\,. \tag{3.176}$$

In case of transitions coupled to polymerization, we have $\omega \equiv Q\,\omega_{\rm off}$, where Q is the time-independent probability that a protomer is in state 2 during depolymerization and $\omega_{\rm off}$ is the dissociation rate. For global transitions, or transitions at the depolymerizing terminus, ω is simply the transition rate. In eq. (3.176), ω is expected to be of the order of 10^{-3} to 10^{-2}/s. The vectorial transition mechanism, according to which the protomers successively undergo the transitions until the barbed end is reached, gives rise to a sharp Gaussian peak around the average duration $\langle\tau\rangle$.

$$\boxed{p(t) = \frac{1}{\sqrt{2\pi\sigma^2}}\ \exp\left(-\frac{\left(t-\langle\tau\rangle\right)^2}{2\sigma^2}\right)}\,, \tag{3.177}$$

where

$$\langle\tau\rangle \;\equiv\; \frac{\omega_{\rm on} - \omega_{\rm off}^{\rm pol} - \omega}{\omega_{\rm off}+\omega}\ t_{\rm p} \equiv \frac{v_{\rm pol}-\omega}{v_{\rm dep}+\omega}\ t_{\rm p}, \tag{3.178}$$

$$\sigma^2 \equiv \langle\tau^2\rangle - \langle\tau\rangle^2 \;\equiv\; \frac{2\,\omega_{\rm on}}{\left(\omega_{\rm off}+\omega\right)^2}\ t_{\rm p} \equiv \frac{2\left(v_{\rm pol}+\omega_{\rm off}^{\rm pol}\right)}{\left(v_{\rm dep}+\omega\right)^2}\ t_{\rm p} \tag{3.179}$$

The kinetic parameters $\omega_{\rm on}$, $\omega_{\rm off}^{\rm pol}$, and $\omega_{\rm off}$ are the association rate, the dissociation rate during polymerization, and the dissociation rate during shrinkage, respectively. Both the polymerization time $t_{\rm p}$, and the depolymerization velocity $v_{\rm dep}$ are known from experiment. The polymerization velocity $v_{\rm pol}$ can be inferred from the measured filament lengths and $t_{\rm p}$. The dissociation rate during polymerization $\omega_{\rm off}^{\rm pol}$ is of the same order as $\omega_{\rm off}$. If we neglect the presence of an ATP-cap during polymerization, these dissociation rates are identical. For the vectorial transition mechanism, the unknown transition rate ω must be of the order of 1 to 10/s to match the observed depolymerization curves. Finally, the random transition mechanism leads to a Rayleigh distribution, that grows linearly for small times t and decays slowly for large t, with a broad maximum in-between:

$$\boxed{p(t) = \alpha\,\omega\,t \exp\left(-\alpha\,\omega\,t^2/2\right)}\,, \tag{3.180}$$

where

$$\alpha \equiv v_{\rm dep}\left(1 + v_{\rm dep}/v_{\rm pol}\right) \tag{3.181}$$

can be inferred from the depolymerization curves. For the random transition mechanism, the unknown transition rate is expected to be very small and of the order of 10^{-6} to 10^{-5}/s.

3.8 Comparison with experiment

In order to infer on the transition mechanism that leads to the interruption of depolymerization, we will compare the three distinct theoretical distributions for the duration τ to our experimental results. We consider the cumulative distribution functions $P(t)$ instead of the probability densities $p(t)$ to circumvent any binning effects. From the experimentally determined durations $\{\tau_i\}_{i=1,\ldots,N_\mathrm{f}}$ of N_f observed filaments, we calculate the empirical cumulative distribution function (ecdf) $\hat{P}(t)$ as the fraction of filaments that already exhibited an interruption before time t:

$$\hat{P}(t) \equiv \frac{1}{N_\mathrm{f}} \sum_{i=1}^{N_\mathrm{f}} \Theta(t - \tau_i), \tag{3.182}$$

where $\Theta(z)$ is the Heaviside step function as defined before.

Due to the experimental setup, it was not possible to start filament observation at the initiation of depolymerization. In fact, the delay varied between assays, but did not exceed 2 min. Furthermore, the depolymerization had to be observed for at least 40 s to detect the sudden drop of the shrinkage velocity and to determine τ. In consequence, the ecdf $\hat{P}(t)$ is unknown for times t that are smaller than the lag time $t_\mathrm{lag} = 160$ s. We observed that 21 out of $N_\mathrm{f} = 57$ filaments were not shrinking at time t_lag.

For these non-shrinking filaments, it is plausible to assume that they are already in phase II and that a state-2-protomer has appeared at the barbed end before time t_lag. Therefore the particular value $\hat{P}(t_\mathrm{lag}) = 21/57 \simeq 0.37$ is fixed and marked by the black cross in figure 3.7(a). Apparently, the vectorial transition mechanism is in conflict with this notion, since it gives rise to a sharp increase of $P(t)$ at $t = \langle\tau\rangle$ and thus cannot account for filaments already in phase II at time t_lag. Comparing $\hat{P}(t)$ to the analytical distributions $P(t)$ involves fixing of the unknown rate ω for each of the transition mechanisms. To determine ω, we can not simply use the average $\langle\tau\rangle_\mathrm{obs} = 5.4$ min of the filaments exhibiting an interruption, because filaments which are already in phase II at time t_lag have lower but unknown values for τ. Instead, the relation $P(t_\mathrm{lag} = 160\mathrm{s}) = 21/57$ for each of the analytical cdfs determines ω. Alternatively ω can be considered as a free fitting parameter, see figure 3.7(a). The latter procedure naturally gives a better estimate for ω.

A different assumption for the non-shrinking filaments is that they have not been stabilized by the mechanism that gives rise to the interruptions. We believe that this is less plausible since filaments that were apparently attached to the glass surface with their barbed ends were excluded from our analysis. However if we yet postulate another mechanism leading to the stability of the 21 filaments, we must exclude these filaments from the statistics. In this case $\langle\tau\rangle = \langle\tau\rangle_\mathrm{obs} = 5.4$ min holds and determines the transition rate ω for each mechanism via the equations (3.22), (3.178), and (3.160).

Irrespective of the assumption for the non-shrinking filaments, the cumulative Rayleigh distribution describes the data best, see figure 3.7. Therefore, we conclude that the abrupt interruption of depolymerization is caused by a transition that occurs locally at random sites within the filament. Since the assumption of another mechanism for the non-shrinking filaments leads to comparably poor fits, see figure 3.7(b), we further infer that at least most of these filaments exhibited an interruption before time t_lag, caused by the same transition mechanism.

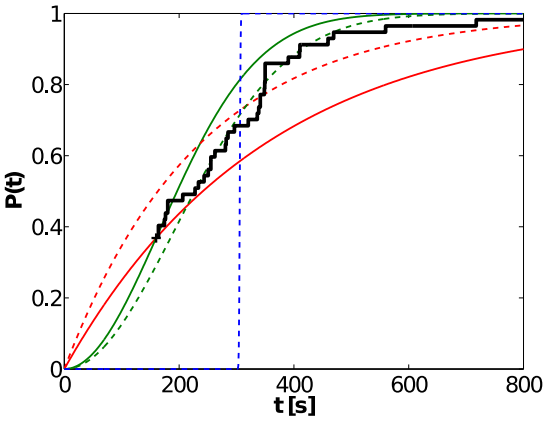

(a) Here we assume that the 21 non-shrinking filaments are already in phase II at time $t_{\mathrm{lag}} = 160\mathrm{s}$ and thus $\hat{P}(t_{\mathrm{lag}}) = 21/57 \simeq 0.37$, as marked by the black cross. The continuous (red and green) curves were drawn with transition rates ω that were determined by the equality $P(t_{\mathrm{lag}} = 160\mathrm{s}) = 21/57$. The dashed lines were obtained by least-square-fitting of the respective distributions to the empirical cdf involving only one fit parameter provided by ω. The green curves describe the data best and the transition rates for the solid and dashed curves are given by $\omega \simeq 1.3 \times 10^{-5}/\mathrm{s}$ and $\omega \simeq 9.3 \times 10^{-6}/\mathrm{s}$, respectively.

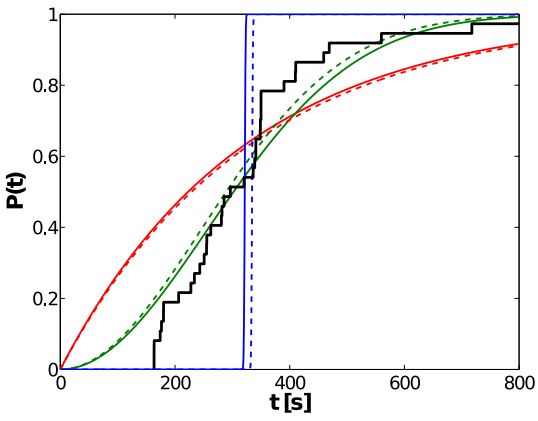

(b) Here the 21 non-shrinking filaments have been excluded from the statistics, according to the assumption that they have been stabilized by another cause. The continuous (red, blue, and green) lines were drawn with transition rates ω that were determined from the average value $\langle\tau\rangle = \langle\tau\rangle_{\mathrm{obs}} = 5.4\mathrm{min}$. The dashed lines are again least-square-fits. The green curves describe the data better than the blue and red curves. However, excluding all 21 non-shrinking filaments leads to poor fits which indicates that the assumption of another stabilization cause is not correct.

Figure 3.7 : Comparison of theoretical and experimental results for the cumulative distribution function $P(t)$ of the duration τ. The data for the black empirical curve $\hat{P}(t)$ were obtained from $N_{\mathrm{f}} = 57$ filaments, polymerized from ATP-actin using the simple setup discussed in chapter 2. The exponential cdf corresponding to eq. (3.176) is shown in red, the cdf corresponding to the sharp Gaussian peak in eq. (3.177) is displayed in blue, and the cdf of the Rayleigh distribution, eq. (3.180), is shown in green.

3.9 Conclusion

To account for the observed biphasic depolymerization of actin filaments, we have proposed a transformed protomer state ("state 2") which is defined by its vanishing rate of dissociation from the barbed end. The known nucleotide states of actin protomers are subsumed to "state 1" which has a dissociation rate of the order of 1/s as expected from bulk measurements. The dissociation of state-1-protomers explains the initial shrinking of filaments. As soon as a transformed state-2-protomer reaches the barbed end, the depolymerization is interrupted.

We considered a variety of possible mechanisms for the transition from protomer state 1 to state 2. These mechanism can not directly be probed by the depolymerization of single filaments. However, they give rise to three qualitatively different distributions for the dura-

tion τ of the initial fast-shrinking phase. Global transitions of the whole filament, transitions that occur only at the depolymerizing terminus, as well as transitions during polymerization all lead to exponentially distributed durations τ. A vectorial transition mechanism, according to which the protomers successively undergo the transitions until the barbed end is reached, gives rise to a narrow Gaussian distribution around the average duration $\langle\tau\rangle$. Local transitions of random protomers within the filament lead to a Rayleigh distribution, see eq. (3.180), that grows linearly for small and decays slowly for large times with a broad maximum in-between.

A comparison with the durations that we determined in the experiment discussed in the last chapter reveals that only localized random transitions within the filament can explain the biphasic depolymerization. In particular, our analysis rules out a global mechanism that is implicitly assumed in the idea of "dynamic stabilization" which was proposed by Kueh et al. [62]. Therefore in contrast to the view expressed in [63], the biphasic depolymerization does not reflect the structural polymorphism or plasticity of actin filaments observed in EM [65]. We can also rule out that any transitions that occur at the shrinking barbed end cause the interruption of depolymerization. In principle, such transitions could be triggered by random contacts of the filament tip with the chamber wall as suggested in [52] or could reflect the binding of capping proteins that have contaminated the solution. Furthermore, transitions that are coupled to the polymerization process or the copolymerization of actin with small amounts of contaminating protein can be excluded as the origin of the interruptions.

In the experiments discussed in the last chapter, imaging was started up to two minutes after the initiation of depolymerization. Furthermore, the point in time of the initiation of depolymerization is not precisely defined, since the buffer exchange involves several rinsing steps. These experimental deficits weaken the quality of the data for the distribution of the duration τ. First, the distribution is unknown for times smaller than 160 s. In particular, the sigmoidal shape of the cumulative distribution function that is expected for the random transition mechanism can not be observed, see figure 3.7. Second, the measurements of τ may contain considerable systematic errors due to the imprecise execution of the rinsing procedure by the experimenter (the author of this thesis) and the difficulty to rinse the perfusion cell with highly viscous buffer. Members of the Carlier lab overcame these hurdles by using a microfluidics setup which allows the exact measurement of the durations τ and many other insightful experiments which are presented in the following chapters.

4 Filaments in a microflow

In order to further investigate filament depolymerization, members of the Carlier lab developed a microfluidics setup which allows for the monitoring of individual actin filaments with light microscopy while rapidly changing their chemical environment. An apparent advantage of this approach compared to our experiments discussed in chapter 2 is the very small lag time, defined as the period between initiation of depolymerization and start of observation. In addition, the buffers do not have to contain methyl cellulose to prevent the filaments from bending out of the focal plane, since the microflow is sufficient to align the filaments. The lowered viscosity of the depolymerization buffer is a crucial advantage, as it enables the buffer to be exchanged at any point in time. In particular, it will turn out to be useful to expose filaments, which have already exhibited an interruption, to G-actin in order to elongate them again.

4.1 Monitoring depolymerization of actin filaments

With the microfluidic setup shown in figure 4.1, the following experiments were performed to investigate the dynamics of filament depolymerization. Spectrin-actin seeds were adsorbed to the surface of the glass coverslip, at the bottom of the flow cell. At the beginning of the experiment, the flow rate of the channel containing a fluorescently labeled G-actin solution was chosen to be higher than the rates from the other inlets, allowing the G-actin solution to occupy most of the flow cell, see figure 4.1(b). The steady growth of filaments at the seeds was observed by TIRFM. After a few minutes, switching to the flow channel that contained no actin triggered the depolymerization from the free barbed ends of filaments in the field of view. This local exchange of the chemical conditions took less than a second, see figure 4.1(d)-(f). During depolymerization, epifluorescence microscopy could be used due to the absence of fluorescent background from solution. Filaments are aligned by the flow, making the monitoring of their contour length and the derivation of kymographs straightforward and accurate. In the conditions of our experiments, no pointed end elongation of filaments from the spectrin-actin seeds was detected. It was verified that in the used range, the fraction of labeled actin, exposure time, and flow rate did not affect the kinetic parameters at the barbed end, see appendix A.4.

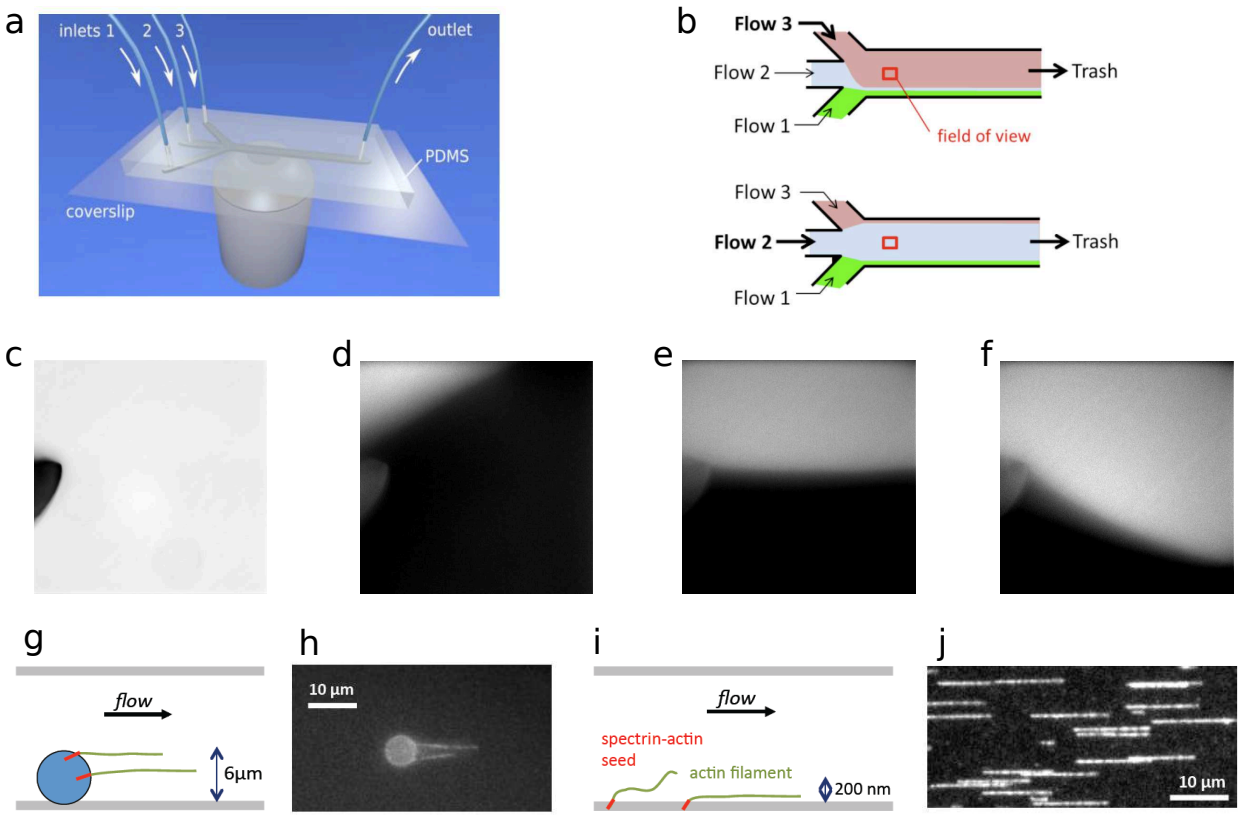

Figure 4.1 : Microfluidics setup. (a) Flow-cell with three entry channels on a microscope objective. (b) Bird's-eye view of the flow-cell. The dominant laminar flow determines which medium occupies most of the flow-cell and in particular the field of view. Transverse diffusion is too slow to balance a difference in protein concentration of adjacent flow channels, see [97] for computation. (c) Phase contrast image of the region close to the junction of two entry channels. (d)-(f) Epifluorescence images of the same corner indicate the absence of turbulent mixing. Fluorescently labeled G-actin flows through the upper channel, buffer streams the lower channel. (d) Flow rates are 1.3μL/min and 5.7μL/min for the upper and lower channel, respectively. The lower flow is dominant and no actin is present at the microscopic field of view on the right border of the image. (e) Flow rates are balanced with 5.0μL/min and 4.9μL/min. (f) Flow rates are 6.8μL/min and 3.1μL/min for the upper and lower channel, respectively. The upper flow dominates and the actin concentration at the microscopic field of view is identical to the concentration in the upper channel, since turbulence is absent and diffusion is negligible. We verified that switching between the conditions in (d) and (f) takes less than a second. (g) Side view of the flow-cell with spectrin-actin seeds anchored to a 6-μm-diameter bead. The high flow velocity a few microns above the glass coverslip easily aligns the filaments and enables imaging (h) with epifluorescence microscopy. (i) Side view of the flow-cell with spectrin-actin seeds anchored to the glass coverslip. Because of the parabolic velocity profile of the laminar flow [97], the microflow has to be sufficiently large to align filaments in the vicinity of the coverslip. (j) Epifluorescence microscopy image of these filaments. Alternatively, TIRF microscopy can be used, as the filaments are close enough to the coverslip.

4.2 Intermittent depolymerization

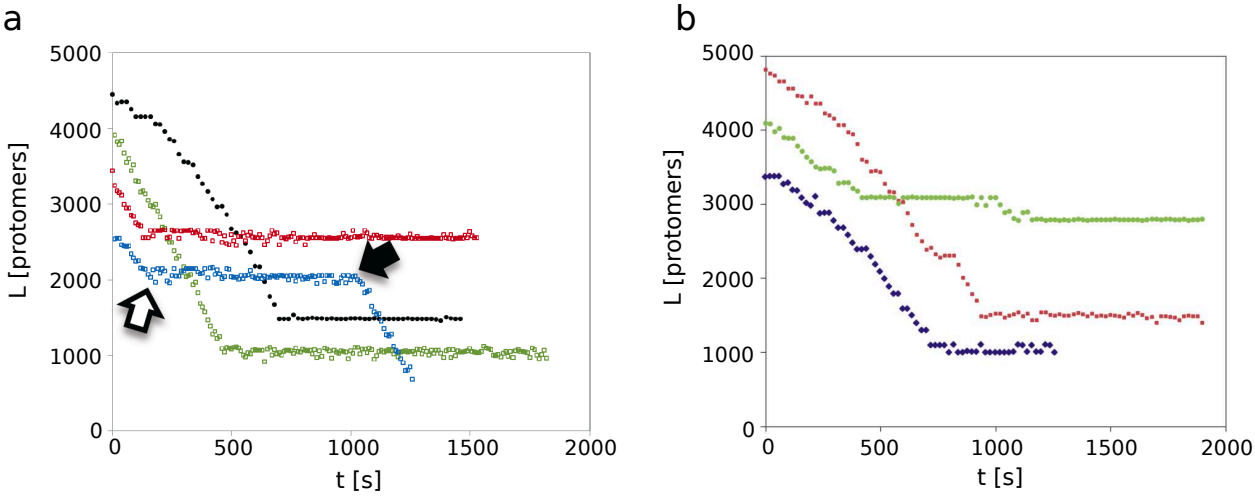

Figure 4.2 : Intermittent depolymerization. (a) Depolymerization curves (filament length versus time) of filaments attached to the coverslip as shown in figure 4.1(i). Black data points correspond to a filament grown from ATP-actin and exhibit an initial acceleration of the depolymerization which we will discuss in section 4.6. The red, green and blue data points which were obtained for three filaments grown from ADP-actin display a constant depolymerization velocity. All filaments exhibit pauses. A long, but finite pause is marked by the white and black arrow. (b) In control experiments in which the filaments were kept far from the coverslip (cf. figure 4.1(g)) the intermittency was also observed. All three depolymerization curves were obtained for filaments grown from ATP-actin.

Consistent with our earlier findings in chapter 2, filament depolymerization is typically interrupted after a few hundred seconds, see figure 4.2. Under standard conditions (see appendix A.4), the shrinking (phase I) lasts for an average of 7.6min. The pause of depolymerization (phase II), in which the filament length remains constant, lasts for an extended, but finite period of time. Subsequently, filaments switch back to a shrinking phase. More pauses occur if the remaining filament length is sufficient. Thus, we use the term *"intermittent"* to characterize the depolymerization behavior of single actin filaments. The intermittency was also observed for filaments kept a few micrometers away from the surface of the coverslip and, thus, in the absence of any filament-surface interactions, see figures 4.1(g) and 4.2(b).

Filaments elongated from Mg-ATP-actin, Ca-ATP-actin, profilin-Mg-ATP-actin, or Mg-ADP-actin all display the characteristic interruptions during depolymerization. In addition, depolymerizing Mg-ADP-Pi-actin filaments, maintained in the ADP-Pi state by large bulk concentrations of Pi, and Cr-ADP-Pi-actin filaments, which cannot release their Pi [98], also exhibit pauses. Altogether, these results directly confirm the findings of chapter 2: Intermittent depolymerization is not coupled to ATP hydrolysis, but caused by another, yet unknown mechanism.

4.3 Distribution of interruption times

Recall that the duration τ of phase I (which lasts until a filament exhibits its first interruption of depolymerization) is a stochastic variable. We have shown in the previous chapter, that the distribution of τ allows us to infer the transition mechanisms from protomer state 1 (regular state determined by the bound nucleotide) to the postulated state 2 which is defined by its very low barbed end dissociation rate.

Here, we proceed in analogy to section 3.8, but use the values of τ as measured with the microflow setup. We determine the empirical cumulative distribution function (ecdf) employing eq. (3.182) and compare it to the three alternative analytical cdfs corresponding to an exponential, a narrow Gaussian and a Rayleigh distribution, see figure 4.3. It turns out that the random transition mechanism describes the data best. Its cdf is given by

$$P(t) \equiv \text{prob}\,(\tau \leq t) = 1 - \exp\left(-\alpha\,\omega\,t^2/2\right) \tag{4.1}$$

where $\alpha \equiv v_{\text{dep}}(1 + v_{\text{dep}}/v_{\text{pol}})$ and v_{pol}, v_{dep} denote the polymerization and depolymerization velocities, respectively. The ecdf obtained here, resembles the ecdf found by our simple setup, compare figures 3.7(a) and 4.1. As the microfluidic setup allows for the observation of filaments with virtually no lag time, the ecdf can also be specified for small times t. This permits the identification of the characteristic sigmoidal shape of the cdf of the random model.

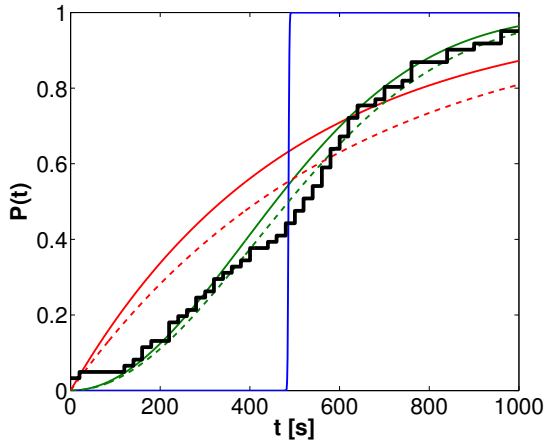

Figure 4.3 : Comparison of theoretical and experimental results for the cumulative distribution function $P(t)$ of the duration τ. The data for the black experimental curve were obtained from $N_{\text{f}} = 61$ filaments, polymerized from ATP-actin using the microfluidics setup shown in figure 4.1i. The exponential distribution is shown in red, the distribution corresponding to the vectorial transition mechanism in blue, and the distribution corresponding to the random transition mechanism is shown in green. The continuous (red, blue and green) curves were plotted with transition rates ω that were determined by the experimental mean duration $\langle\tau\rangle$. The dashed (red and green) lines were obtained by least-square-fitting of the respective distributions to the experimental distribution using the transition rate ω as the only fit parameter. The green curves fit the data best and the fitted transition rate is given by $\omega \simeq 10^{-6}/\text{s}$.

4.4 Repeated polymerization

The microfluidic setup makes it possible to exchange the buffer at any point in time during the experiment. When pausing filaments were again exposed to G-actin and regrown by a few microns before switching back to depolymerization conditions, the second shrinking process was typically interrupted at the same position, at which the initial pause had occurred, see figure 4.4. In fact, such a repeated interruption at the same filament position was observed for 86% of $N_{\mathrm{f}} = 131$ regrown filaments. This provides further evidence that the interruptions are caused by local, non-propagating changes in the filament structure.

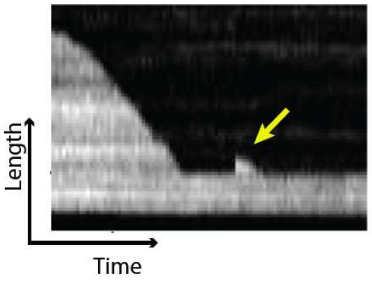

Figure 4.4: Kymograph of the repeated polymerization of a filament. After the interruption of initial depolymerization, we switched first to polymerization conditions for a short time period and then back to depolymerization conditions. The depolymerizing filament displayed a second interruption at precisely the same position, at which the first interruption had occurred, see small "shark fin" indicated by the arrow.

4.5 Accelerating depolymerization of ATP-actin

The very small lag time and precise length measurement due to the suppressed filament undulations enables the detection of another, independent phenomenon. Filaments assembled from ATP-actin depolymerize at a pace that accelerates progressively on a time scale of a few minutes, see black curve in figure 4.2 as an example. On the other hand, filaments grown from ADP-actin depolymerize with a constant velocity. These observation can be rationalized by the hydrolysis of the bound ATP. ADP-Pi-actin is the major intermediate of the hydrolysis process which consists of the cleavage and release steps [46, 48, 49, 99]. As ADP-actin dissociates considerably faster from the barbed end than ADP-Pi-actin [41, 48, 49], the depolymerization velocity increases with time as the filament ages. Since ATP hydrolysis is independent from the shrinking intermittency but also crucial for the depolymerization dynamics, we postpone its detailed analysis to chapter 6. The effect of the acceleration on the distribution function $P(t)$ will be analyzed the next section.

4.6 Effect of acceleration on distribution functions

Recall that in order to model the interruptions, we postulated a protomer state 1 which dissociates with a rate ω_{off} from the barbed end, see chapter 3. The known nucleotide states were considered as substates of this state. With the microfludics setup we are able to detect these substates since the accelerated depolymerization velocity reflects the difference in their dissociation rates, see chapter 6.

In this section, we aim to refine our course-grained analysis of the cumulative distribution functions $P(t)$ to account for the acceleration of depolymerization. In fact, we expect a

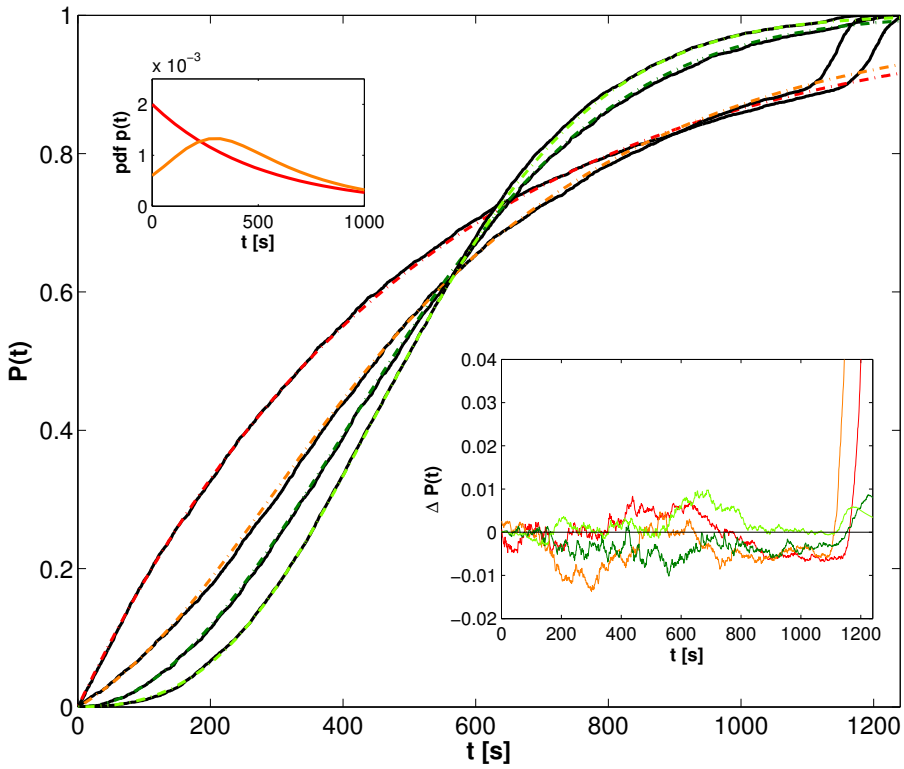

Figure 4.5 : Effect of hydrolysis on the cumulative distribution functions $P(t)$. In the absence of hydrolysis, the cumulative distribution function $P(t)$ is described by the red lines for the case of transitions that are coupled to the polymerization process and dark green lines for the random transition mechanism. When the hydrolysis process is included in the theoretical analysis, $P(t)$ is determined by eqs. (4.4) for transitions that are coupled to the polymerization process (orange line) and (4.8) for the random transition mechanism (lime green line). The corresponding results from stochastic simulations are displayed as solid black lines. The inset displays the small differences $\Delta P(t)$ between the analytical results and the stochastic simulations, which confirm the analytical expressions. For $t \gtrsim 1100$ s the finite lengths of the filaments cause a fast convergence of the simulated $P(t)$ to unity as discussed in section 3.6. Comparison of the red and the orange lines shows that the presence of hydrolysis leads to the appearance of an inflection point of $P(t)$, the distribution becomes more similar to the sigmoidal curve of the random transition mechanism. Correspondingly, the pdf $p(t)$ exhibits a maximum, see upper inset. On the other hand, the dark green and the lime green lines exhibit only small differences. We have chosen the parameter values in such a way to clearly illustrate the effect the hydrolysis, but in agreement with the experimentally determined values, see chapter 6: Duration of polymerization $t_{\mathrm{p}} = 300$ s, association rate $\omega_{\mathrm{on}} = 21/\mathrm{s}$, $Q = 10^{-4}$ for the transition coupled to polymerization and $\omega = 10^{-6}/\mathrm{s}$ for the random transition rate. In absence of hydrolysis (red and dark green lines), the other parameter values are $\omega_{\mathrm{off}}^{\mathrm{pol}} = 1/\mathrm{s}$ for the dissociation rate during the elongation phase (see chapter 3), and $\omega_{\mathrm{off}} = 5/\mathrm{s}$ for the dissociation rate during phase I. In presence of hydrolysis, we have taken the rates from chapter 6: Effective dissociation rate $\omega_{\mathrm{DPD}} = 1.5/\mathrm{s}$ of ADP-Pi-actin, dissociation rate $\omega_{\mathrm{D}} = 6.2/\mathrm{s}$ of ADP-actin, cleavage rate $\omega_{\mathrm{c}} = 0.3/\mathrm{s}$, phosphate release rate $\omega_{\mathrm{r}} = 7 \times 10^{-3}/\mathrm{s}$.

certain shift for cdfs that describe localized transitions within the filament: Because the depolymerization velocity is smaller at the beginning of the shrinking process, a state-2-protomer that is comparably close to the barbed end appears later at the terminus than expected for a constant shrinking velocity. Taking the acceleration into account thus shifts small interruption times τ to slightly larger values.

For the analysis, we anticipate the result of chapter 6. It turns out that ATP hydrolysis within actin filaments is governed by random release of inorganic phosphate (Pi) and that the length as a function of time $L(t)$ is implicitly described by the differential equation

$$\partial_t L(t) = \frac{-1}{\frac{1}{\omega_\mathrm{D}} + \left(\frac{1}{\omega_\mathrm{DPD}} - \frac{1}{\omega_\mathrm{D}}\right) \exp\left(-\omega_\mathrm{r}\left(t + t_\mathrm{p} - L(t)/v_\mathrm{pol}\right)\right)} \tag{4.2}$$

where ω_DPD, ω_D, and ω_r are the effective ADP-Pi-actin dissociation rate, the ADP-actin dissociation rate, and the phosphate release rate, respectively. Both the duration t_p and the velocity v_pol of the polymerization process represent control parameters that may vary for different experiments.

The exponential distribution, eq. (3.176), which arises from global transitions of the filament or transitions that take place at the barbed end only is not influenced by the variable depolymerization velocity. Furthermore, the variable velocity leads only to a small length dispersion of the filaments, see chapter 6. Therefore the narrow Gaussian distribution, eq. (3.177), will not considerably broaden by the ATP hydrolysis. In consequence, we restrict our generalization on eq. (3.176) for the case of transitions that are coupled to the polymerization process (i.e. $\omega \equiv Q\,\omega_\mathrm{off}$, where Q is the time-independent probability that a protomer is in state 2 during depolymerization) and on eq. (3.180) for the random transition mechanism.

We anticipate chapter 6 and approximate both polymerization and depolymerization as deterministic processes. Recalling section 3.5 and eq. (3.147) allows us to generalize the time evolution of the cdf to the case of a time-dependent depolymerization velocity $v_\mathrm{dep}(t)$:

$$P(t) = 1 - \exp\left(-\int_0^t dt'\; v_\mathrm{dep}(t')\; Q(t')\right). \tag{4.3}$$

Note that for clarity we have neglected the very rare case that the transitions occur directly at the barbed end. The depolymerization velocity is implicitly given by eq. (4.2) via $v_\mathrm{dep}(t) \equiv -\partial_t L(t)$.

For the case of transitions that are coupled to the polymerization process, the probability $Q(t)$ that the penultimate protomer is in state 2 is constant and eq. (4.3) simplifies to

$$P(t) = 1 - \exp\left(-Q\left(v_\mathrm{pol} t_\mathrm{p} - L(t)\right)\right), \tag{4.4}$$

where $v_\mathrm{pol} t_\mathrm{p}$ denotes the average filament length at the initiation of depolymerization and $L(t)$ is implicitly given by eq. (4.2). Note that in contrast to the exponential $P(t)$ which ignores the effect of hydrolysis and assumes a constant depolymerization velocity, the cdf as given by eq. (4.4) may have an inflection point like the sigmoidal distribution for the random transition mechanism, see figure 4.5.

From the general eq. (4.3) we see that the condition for the existence of an inflection point of the cdf, or equivalently an extremum of the pdf is given by

$$\partial_t^2 P(t) = \left(v_{\mathrm{dep}}\ \partial_t Q + Q\ \partial_t v_{\mathrm{dep}} - Q^2 v_{\mathrm{dep}}^2\right) \exp\left(-\int_0^t dt'\ v_{\mathrm{dep}}(t')\ Q(t')\right) \stackrel{!}{=} 0. \tag{4.5}$$

Since both $v_{\mathrm{dep}}(t)$ and $Q(t)$ are positive, at least one of these quantities must increase with time to allow an inflection of $P(t)$. For the random transition mechanism, this necessary condition is fulfilled by the increasing $Q(t)$, leading to the sigmoidal shape of $P(t)$. For the mechanism in which the transitions are coupled to polymerization and Q is constant during filament shrinkage, the depolymerization needs to be accelerated to enable an inflection point, see figure 4.5.

Within the scope of our usual assumption that polymerization and depolymerization can be approximated by a deterministic description, the probability that the penultimate protomer is in state 2 is for the random transition mechanism given by

$$Q(t) = 1 - \exp\left(-\omega\, a(t, L)\right), \tag{4.6}$$

where age $a(t, L)$ of the penultimate protomer is given by

$$a(t, L) = t + t_{\mathrm{p}} - L(t)/v_{\mathrm{pol}}, \tag{4.7}$$

see eq. (6.7). This leads to

$$P(t) = 1 - \exp\left(\int_0^t dt'\ \partial_{t'} L(t')\ \left[1 - \exp\left(-\omega\left(t + t_{\mathrm{p}} - L(t)/v_{\mathrm{dep}}\right)\right)\right]\right), \tag{4.8}$$

where the filament length $L(t)$ is implicitly given by eq. (4.2).

4.7 Improved analysis of the cumulative distribution function

In the last section, we have refined our theoretical description of the interruption of filament depolymerization to account for the accelerated depolymerization caused by ATP hydrolysis. Based on this refined model, we have derived analytical expressions $P(t)$ for the two relevant transition mechanisms: Transitions that occur during polymerization, see eq. (4.4), and transitions that occur at random protomers within the filament, see eq. (4.8). We have realized that including hydrolysis into our analysis of the transitions that occur during polymerization causes the appearance of an inflection point of $P(t)$. Thus for the case of ATP-actin filaments, the cdfs of the two transition mechanisms become qualitatively similar and we can not simply use the existence of an inflection of the experimental cdf as an argument to exclude transitions that occur during polymerization. Instead, we need a more quantitative comparison with the experimental data.

Thus, we also need to refine the expression for the empirical distribution function $\hat{P}(t)$. In fact, eq. (3.182) which gives the fraction of filaments that already exhibited an interruption before time t, presumes that all filaments in the experiment can be observed until

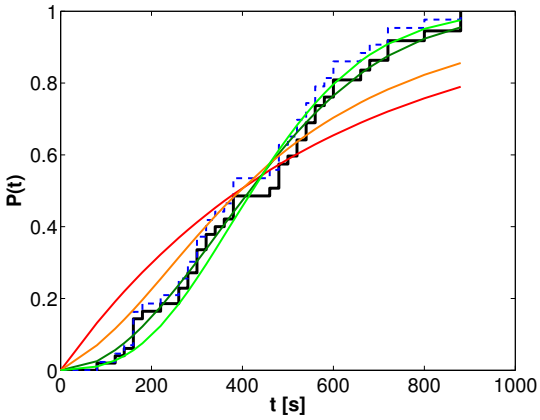

Figure 4.6 : Comparison of theoretical and experimental results for $P(t)$ taking into account the acceleration of depolymerization caused by ATP hydrolysis. The empirical distribution function $\hat{P}(t)$ for $N_\mathrm{f} = 51$ ATP-actin filaments is computed with the Kaplan-Meier estimator, eq. (4.10), and displayed in black. For comparison, we used the same data set but discarded all filaments that detached/fragmented before exhibiting an interruption. Using the simple eq. (3.182) we obtained the dashed blue line which systematically overestimates the cdf. The colored lines were obtained by least-square-fitting the following theoretical distributions $P(t)$ to the empirical distribution function $\hat{P}(t)$. The only fit parameter is provided by ω and the other parameters were fixed at the values discussed in the caption of figure 4.5. The red and orange lines correspond to transitions that occur during polymerization. For the red line hydrolysis was ignored, corresponding to a simple exponential. For the orange line it was taken it into account, cf. eq. (4.4). The green lines display $P(t)$ for random transitions, both in the absence (dark green, Rayleigh distribution) and presence (line green, eq. (4.8)) of hydrolysis. Even though the hydrolysis qualitatively changes $P(t)$ for the transitions that occur during polymerization as it gives rise to an inflection point, our earlier result remains valid: The data are best described by the distribution of a random transition mechanism. Furthermore, the value of the fitted parameter ω is not changed significantly, if realistic values for the other parameters are assumed. In the displayed case, we found $\omega \simeq 1.2 \times 10^{-6}$/s both with and without hydrolysis.

this time t. However, the microflow leads to a small number of filaments that fragment or detach from the coverslip at a random time τ_df before exhibiting the interruption. For certain experimental settings, see next chapter, the interruption times τ are large and the number of filaments with $\tau_\mathrm{df} < \tau$ becomes significant. For the elementary analysis performed above, we have simply discarded these filaments, and applied eq. (3.182) for the remaining filaments. However, since this analysis ignores the fact that the interruption of depolymerization of such a filament has certainly not occurred before its detachment/fragmentation, it systematically overestimates $P(t)$. In statistics, the fragmentation/detachment event is referred to as *right-censoring*, because the event of interest, the interruption, cannot be observed after fragmentation/detachment. The best nonparametric estimate for the cdf $P(t)$ of right-censored data is the Kaplan-Meier estimator $\hat{P}(t)$ [100, 101]. Its computation for N_f filaments involves the ordering of both the detachment/fragmentation times τ_df and the

durations τ

$$\tau_1 \leq \tau_2 \leq \cdots \leq \tau_{N_\mathrm{f}}, \tag{4.9}$$

where τ_i is the minimum of τ_df and τ of the i-th filament. The Kaplan-Meier estimator is given by

$$\hat{P}(t) = 1 - \prod_i \frac{N_\mathrm{f} - i}{N_\mathrm{f} - i + 1} \tag{4.10}$$

where i assumes those values for which $\tau_i < t$ and for which τ_i measures a duration τ of the i-th filament [100]. We have used eq. (4.10) to compute the empirical distribution functions in figure 4.6.

4.8 Summary

The key observation that motivated our study is also found in the microflow experiments: After a few minutes, the shrinking of filaments is suddenly interrupted for an extended period of time and the duration τ of the initial shrinking phase strongly differs from filament to filament. It turns out that the depolymerization is intermittent, meaning that after the interruption, filaments typically switch back to a shrinking phase which can be followed by another interruption.

The microflow setup facilitates the imaging of filaments during the whole course of the experiment and the precise determination of the distribution of τ from the beginning of depolymerization. Comparing this distribution with our analytical expressions for the various transition mechanisms confirms that local transitions at random protomers cause the interruptions. The transition rate is of the order of 10^{-6}/s. Further evidence that the interruptions are caused by local, non-propagating changes in the filament structure is provided by additional experiments in which pausing filaments were again exposed to actin monomers and regrown by a few microns before switching back to depolymerization conditions. In these experiments, the second shrinking process was typically interrupted at the same position at which the initial pause had occurred.

The microflow setup also enabled us to detect that filaments assembled from ATP-actin depolymerize at a pace that accelerates progressively, on a time scale of a few minutes. This observation can be rationalized by the hydrolysis of the bound ATP. In chapter 6, we will see that the analysis of the acceleration enables us to infer the mechanism of ATP hydrolysis in actin filaments. The increase of the depolymerization velocity effects the distribution of the duration τ. We have refined the stochastic modeling approach of chapter 3 to include this effect and have generalized the analytical expressions for the distribution of τ. From a comparison of the generalized expressions with the empirical distribution we conclude that our earlier result remains valid: The data are best described by the distribution of a random transition mechanism.

In conclusion, the microflow setup provides an excellent tool to investigate the depolymerization of single actin filaments. In combination with the theoretical analysis, it allowed us to confirm and refine the notion that a local transition of random protomers within the filament causes the interruption of depolymerization. In the next chapter, additional experiments will elucidate this local transition mechanism.

5 Elucidation of the local transition mechanism

In the last chapters, we have shown that local transitions of random protomers within the filament cause the interruption of depolymerization. So far we are agnostic about the nature of the transitions and the protomer states 1 and 2 are fairly abstract concepts. In this chapter, we elucidate the local transition mechanism by additional experiments and generalized expressions for the cdf $P(t)$. This will lead to a precise interpretation of the protomer state 2. In particular we will show that *in vivo* no intermittency of depolymerization is expected, as state 2 is absent.

5.1 Transitions of single, fluorescently labeled protomers

To elucidate the molecular nature of the transformed protomer states, both the fraction X_{fl} of the fluorescently labeled actin protomers and the laser illumination intensity were varied, see appendix A.5.1 for details. Our analytical expressions for the cumulative distribution of the duration τ enable us to determine the transition rate ω as a function of these experimental parameters. In the last chapter, we have seen that incorporating the effects of ATP hydrolysis does neither qualitatively change the functional form of $P(t)$ for the random transition mechanism, nor does it significantly alter the fitted parameter ω, if realistic parameter values for the hydrolysis are used. Thus, we will employ the simple expression (4.1) in the following. It turns out that the fitted ω increases monotonically both with increasing fraction X_{fl}, see figure 5.1(a), and with the time-averaged illumination intensity E, see figure 5.1(b). The data for small labeling fractions $X_{\mathrm{fl}} = 0.07$, 0.1, and 0.15 are well described by the linear relation

$$\omega \approx C X_{\mathrm{fl}}. \tag{5.1}$$

The numerical value of the constant is given by $C \simeq 10^{-5}/\mathrm{s}$ for a time-averaged illumination intensity of $E = 2.54\,\mathrm{mW/mm^2}$, see figure 5.1(a). If we assume that only the labeled protomers may undergo the random transitions, the expression for the probability that the penultimate protomer is in state 2, eq. (3.152), is modified into

$$Q(t) = X_{\mathrm{fl}}\left(1 - \exp\left(-\omega_{\mathrm{fl}}\left(1 + v_{\mathrm{dep}}/v_{\mathrm{pol}}\right)t\right)\right) \approx X_{\mathrm{fl}}\omega_{\mathrm{fl}}\left(1 + v_{\mathrm{dep}}/v_{\mathrm{pol}}\right)t, \tag{5.2}$$

where ω_{fl} denotes the transition rate of the labeled protomers. In consequence, the functional form of eq. (4.1) remains unchanged, but $\omega \equiv X_{\mathrm{fl}}\omega_{\mathrm{fl}}$ is interpreted as an effective rate. Identifying ω_{fl} with the empirical constant $C \simeq 10^{-5}/\mathrm{s}$, allows us to conclude that only the labeled protomers contribute to the transitions. In fact, the linear relation (5.1) also implies that the local transitions typically involve only a single fluorescently labeled protomer as a

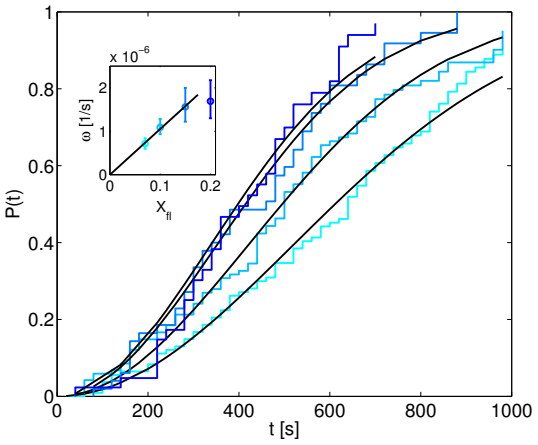

(a) Variation of labeling fraction for constant time-averaged illumination intensity of $E = 2.54\,\mathrm{mW/mm^2}$. The four blue empirical distribution functions correspond to labeling fractions $X_{\mathrm{fl}} = 0.07$, 0.1, 0.15, and 0.2 (bottom to top). The black lines were obtained by least-square-fitting of eq. (4.1) to the experimental distributions using the transition rate ω as the only free parameter. In the inset, ω is plotted as a function of X_{fl}.

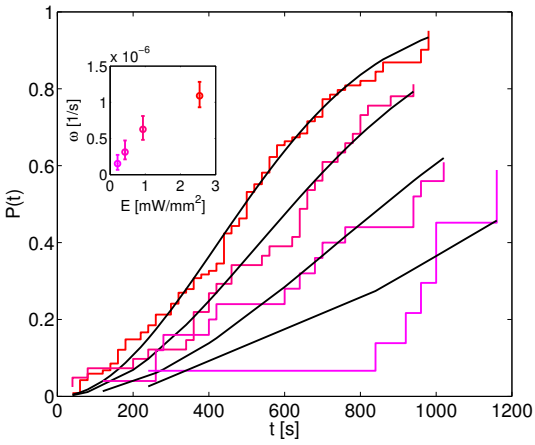

(b) Variation of time-averaged illumination intensity for constant labeling fraction $X_{\mathrm{fl}} = 0.1$. The four reddish empirical distribution functions correspond to time-averaged illumination intensities of $E = 0.21$, 0.42, 0.93, and $2.54\,\mathrm{mW/mm^2}$ (bottom to top). The black lines were again obtained by least-square-fitting of eq. (4.1) to the experimental distributions. In the inset, ω is plotted as a function of the intensity E.

Figure 5.1 : Cumulative distribution functions $P(t)$ for varying labeling fraction and illumination. Epifluorescence microscopy with the experimental setup shown in figure 4.1(i) was used to determine the durations τ. We used the Kaplan-Meier estimator, eq. (4.10), to compute the experimental distribution functions (ecdfs), since a significant number of right-censoring events were detected, especially for low illumination. The ecdfs are displayed as colored step functions and the black lines were obtained by represent least-square fitting of eq. (4.1). The error bars in the insets indicate confidence intervals for the transition rate ω of at least 50%, as computed with the method discussed in appendix A.5.2.

putative interaction between two such protomers would lead to a quadratic dependence of the protomer transition rate ω on the labeling fraction X_{fl}.

The microfluidics setup also enabled us to investigate the depolymerization of unlabeled filament segments that were only briefly exposed to light, see figure 5.2. The latter experiments indicate that no transitions occur within unlabeled and unexposed actin filaments. This conclusion was confirmed by control experiments on unexposed filament solutions, see section 5.6, which also demonstrated that no dimers were formed in unexposed and labeled F-actin.

From these combined finding we conclude that single, fluorescently-labeled protomers undergo photo-induced transitions that caused the intermittency of the filament depolymerization. Because of the low value of ω_{fl}, less than 1% of the fluorescently labeled actin is typically transformed in standard single filament microscopy assays.

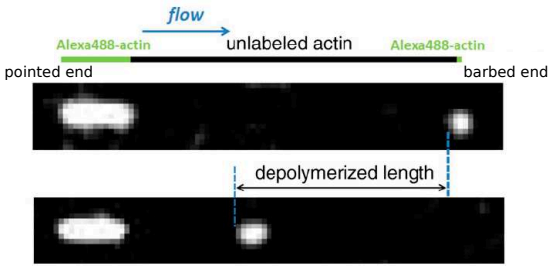

(a) Upper image: A labeled segment, a long unlabeled segment, and a very short labeled segment were successively polymerized. Lower image: The filament was then depolymerized for for a fixed time of 15 min, before again polymerizing a short labeled segment. The imaging and thus illumination took only place before and after depolymerization. This protocol enables us to infer the depolymerization length of the unlabeled segment that was only briefly exposed to light.

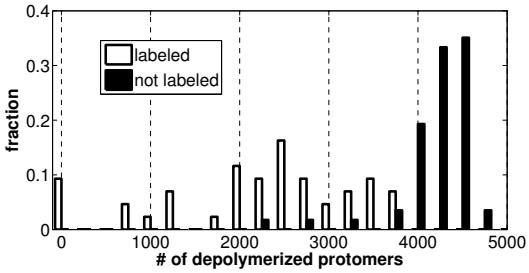

(b) Histogram of the number of depolymerized protomers. During the depolymerization phase of 15 min, almost all unlabeled segments lost about 4000 to 4500 protomers (black bars), as expected for a depolymerization velocity of $v_{\mathrm{dep}} \simeq 5/\mathrm{s}$ indicating that unlabeled filaments, which were only briefly exposed to light, depolymerize without interruptions. For comparison, the number of protomers lost by labeled filaments under standard illumination conditions (white bars) is governed by a broad distribution indicating interruptions at different filament sites.

Figure 5.2 : Depolymerization of unlabeled filament segments.

5.2 Reversibility of the transitions

Recalling that the depolymerization process is intermittent (see figure 4.2) and phase II has also a finite, stochastic duration τ_{II}, the random transitions from state 1 to state 2 might be reversible on experimental time scales.

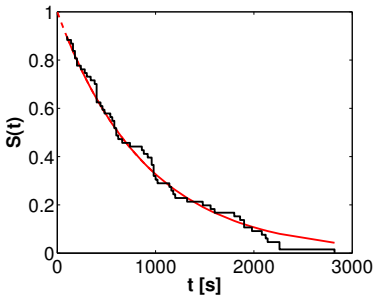

Figure 5.3: The survival function $S(t) \equiv \mathrm{prob}\,(\tau_{\mathrm{II}} > t)$ of the pause durations τ_{II} describes the probability that pause durations last for time periods that exceed t. The black data correspond to the filaments analyzed in figure 4.3. Pause durations below about 80 seconds cannot be reliably detected because of the limited resolution of the optical microscope, see appendix A.4.4. The data are well fitted by an exponential function $S(t) = \exp(-\Omega\, t)$ with $\Omega \simeq 1.1 \times 10^{-3}/\mathrm{s}$.

5.2.1 Distribution of pause durations

The microflow setup facilitates an extended observation time and allows us to study the distribution of τ_{II}. It turns out that τ_{II} is exponentially distributed with an inverse time of $\Omega \simeq 1.1 \times 10^{-3}/\mathrm{s}$, see figure 5.3. In general, a pause ends when the state-2-protomer at the barbed end dissociates with the rate $\omega_{\mathrm{off},2}$, or it first undergoes a reverse transition with the

rate ω_{21} before dissociating as a state-1-protomer with the rate ω_{off}. In our standard depolymerization experiments, these two routes are indistinguishable and Ω must be interpreted as an effective rate for which

$$\Omega = \omega_{\text{off},2} + \omega_{21} \tag{5.3}$$

holds, since the dissociation of state-1-protomers occurs instantaneously on the time scale of the pause duration. Hence, the measurement of the pause durations τ_{II} only allows us to determine the upper limit of the reverse transition rate ω_{21}.

5.2.2 Distribution functions for delayed depolymerization

One idea to disentangle the reverse transitions from the dissociation events of state-2-protomers is to keep the filaments at the critical G-actin concentration for an extended period of time before initiating depolymerization. In these delayed depolymerization experiments, one allows a significant number of reverse transitions before a state-2-protomer appears at the barbed end and interrupts the depolymerization.

Let us derive an analytical expression for the cdf of the duration τ which includes both reverse transitions as well as the delayed depolymerization. Recall that if the stochasticity of the polymerization and depolymerization as well as the acceleration of shrinking due to ATP hydrolysis is neglected, the cdf is given by

$$P(t) = 1 - \exp\left(-v_{\text{dep}} \int_0^t dt'\; Q(t')\right), \tag{5.4}$$

where $Q(t)$ is the probability that the penultimate protomer is in state 2. If we allow for reverse transitions with the rate ω_{21}, we find

$$Q(t) = \frac{\omega}{\omega + \omega_{21}} \left(1 - e^{-(\omega+\omega_{21})\, a(t)}\right), \tag{5.5}$$

where the age $a(t)$ of the penultimate protomer is the time since it has been incorporated into the filament. If the depolymerization is immediately initiated after the filament growth, that is without any delay, eq. (3.150) holds. Including a delay time t_{cc},

$$a(t) = (1 + v_{\text{dep}}/v_{\text{pol}})\, t + t_{\text{cc}}, \tag{5.6}$$

leads to the explicit expression for the generalized cdf:

$$P(t) = 1 - \exp\left(-\frac{v_{\text{dep}}\, \omega}{\tilde{\omega}^2} \left(\tilde{\omega}\, t - \frac{e^{-\tilde{\omega}\, t_{\text{cc}}}}{1 + v_{\text{dep}}/v_{\text{pol}}} \left(1 - e^{-\tilde{\omega}\left(1+v_{\text{dep}}/v_{\text{pol}}\right) t}\right)\right)\right), \tag{5.7}$$

where $\tilde{\omega} \equiv \omega + \omega_{21}$. Note that our initial theoretical description which implicitly required that no reverse transitions occur on the experimental time scale is consistent with this generalization. Because the pause durations set an upper limit for the reverse transition rate of $\omega_{21} \simeq 10^{-3}/\text{s}$, very few reversals occur before a state-2-protomer appears at the barbed end and gives rise to an interruption. Thus $P(t)$ changes only slightly when including these reversals, see blue lines in figure 5.4, which also means that the numerical value $\omega \simeq 10^{-6}/\text{s}$ remains valid as an approximation in the presence of reversals.

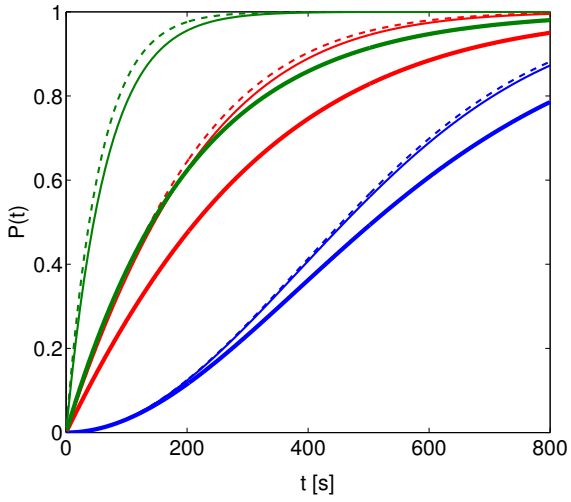

Figure 5.4: Cdfs of τ with reverse transitions as given by eq. (5.7). The blue, red and green curves display $P(t)$ for immediate depolymerization ($t_{cc} = 0$), for a delay time $t_{cc} = 900\,\mathrm{s}$, and for $t_{cc} = 3600\,\mathrm{s}$, respectively. The reverse transition rate ω_{21} is chosen to be zero for the dashed lines and $\omega_{21} = 10^{-4}/\mathrm{s}$ for the thin solid lines. The maximal value, that is $\omega_{21} = 10^{-3}/\mathrm{s}$, was assumed for the thick lines. Reverse transitions that occur with a rate of the order of $10^{-4}/\mathrm{s}$ or below do not significantly alter $P(t)$. The other parameter values for the plots are given by $\omega = 10^{-6}/\mathrm{s}$, $v_{dep} = 5/\mathrm{s}$, and $v_{pol} = 15/\mathrm{s}$.

The effect of the reversals becomes more apparent, if the filaments are kept at the critical concentration for a delay time of at least $t_{cc} = 15$ min. However, ω_{21} must be at least of the order of $10^{-3}/\mathrm{s}$ that is at its upper limit to significantly alter $P(t)$, see figure 5.4. We simultaneously fitted the empirical distribution functions from experiments without delay and with $t_{cc} = 15$ min (data not shown). We found $\omega \simeq 3 \times 10^{-7}/\mathrm{s}$, as expected for low illumination, and a negative value for ω_{21} which indicates that the positive true value is close to zero. Since values below $10^{-4}/\mathrm{s}$ can not be discriminated by these delay experiments, see figure 5.4, we conclude $\omega_{21} \lesssim 10^{-4}/\mathrm{s}$. Furthermore a quantitative analysis of the experiments involving the repeated polymerization of filament, see section 4.4, consistently suggest that an undetectable small value of ω_{21}. Increasing t_{cc} to one hour would allow a better estimate. However, in any case we can only determine ω_{21} for protomers within the filament whereas ω_{21} in eq. 5.3 denote the reverse rate at the barbed end which – in principle – could be different. We will see in the next section that the transitions are indeed irreversible on experimental time scales.

5.3 Formation of stable dimers

So far we revealed that localized photo-induced transitions occur at random labeled protomers within the filament. Once such a transformed protomer (state 2) appears at the barbed end it causes the interruption of depolymerization as it is more tightly bound to at least one of its neighbors within the helical filament. Therefore, it seems evident to envisage the transition of state 1 into state 2 as the dimerization of two adjacent protomers. In this section, we present a series of additional experiments which show that the photo-induced transitions indeed lead to the formation of stable actin dimers within the filament.

5.3.1 Incorporation of preformed dimers

Actin monomers were copolymerized with preformed lateral dimers that were obtained by covalent, pPDM-induced crosslinks [102] between two protomers [103], see appendix A.5.3.

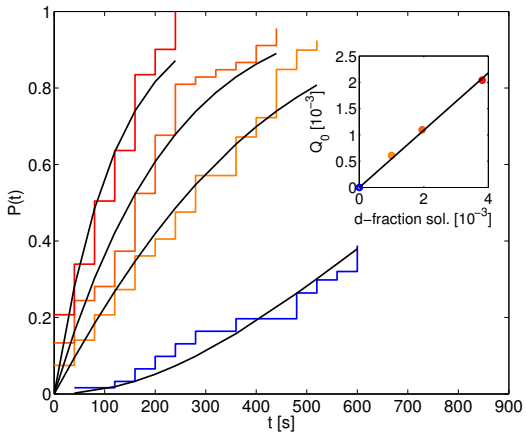

(a) Cumulative distribution functions for the occurrence of pauses during the depolymerization of filaments grown from actin monomers and preformed actin dimers. The empirical distributions functions (colored curves) were computed as discussed in appendix A.5.4. The blue curve was obtained in the absence preformed dimers and the three sets of reddish curves in the presence 2, 4, and 8 nM preformed dimers. The black lines represent fits of eq. (5.9) to the empirical distributions functions where the transition rate ω was determined in the absence of preformed dimers from the blue data. For the reddish data ω was fixed at this value and the fraction Q_0 of preformed dimers within the filament was fitted, as described in appendix A.5.4. In the inset the fitted value of Q_0 is shown as a function of the mole fraction of the dimers in the polymerization solution. As expected, Q_0 is proportional to the latter mole fraction.

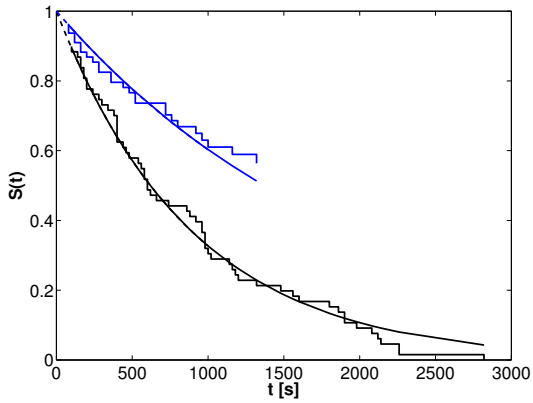

(b) Distribution of the pause durations caused by state-2-protomers and preformed dimers. Survival function $S(t)$ of terminal dimer for filaments elongated by copolymerization of actin monomers with 4 nM preformed actin dimers (blue step function). The data correspond to the filaments analyzed in figure 5.5(a) (intermediate reddish line). For comparison the survival function of state-2-protomers for filaments elongated from monomers alone is shown as the black step function (same as in figure 5.3). Pause durations below about 80s cannot be reliably detected because of the limited resolution of the optical microscope, see appendix A.4.4. The data are well fitted by an exponential function $S(t) = \exp(-\Omega\, t)$ with $\Omega = \omega_{\text{off},2} \simeq 1.1 \times 10^{-3}$/s for filaments with photo-induced state-2-protomers only (black line) and $\Omega = \tilde{\omega}_{\text{pre}} \simeq 5.1 \times 10^{-4}$/s for filaments that also contain preformed dimers.

Figure 5.5 : Pauses caused by photo-induced state-2-protomers and preformed dimers.

The preformed dimers induce additional pauses during depolymerization. Assuming that both the preformed dimers and photo-induced state-2-protomers at the barbed end cause interruptions, we generalize the cumulative distribution $P(t)$. The time-dependent probability $Q(t)$ that a dimer or state-2-protomer is at the penultimate position is given by

$$Q(t) = Q_0 + (1 - Q_0)\,(1 - \exp(-\omega\ (1 + v_{\text{dep}}/v_{\text{pol}})\ t)) \approx Q_0 + \omega\ (1 + v_{\text{dep}}/v_{\text{pol}})\ t \qquad (5.8)$$

where Q_0 is the fraction of dimers which are present in the filament at the initiation of depolymerization, and ω is the local transition rate. The approximated expression holds for

$Q_0 \ll 1$, $v_{\mathrm{dep}} < v_{\mathrm{pol}}$ and $\omega t \ll 1$. The cumulative distribution follows:

$$P(t) = 1 - \exp\left(-v_{\mathrm{dep}} \int_0^t dt'\; Q(t')\right) \approx 1 - \exp\left(-v_{\mathrm{dep}}\, Q_0\, t + \alpha\, \omega\, t^2/2\right), \qquad (5.9)$$

where $\alpha \equiv v_{\mathrm{dep}}(1 + v_{\mathrm{dep}}/v_{\mathrm{pol}})$ as usual. For filaments that were assembled by the copolymerization of actin monomers with various concentrations of preformed dimers, eq. (5.9) describes the occurrence of pauses. As expected, the fraction Q_0 is proportional to the mole fraction of preformed dimers in the polymerization solution and interestingly, the ratio of these fractions is about 0.5 indicating that the association rate of the dimers is about half the association rate of the monomer, see figure 5.5(a).

We also analyzed the distribution of the pause durations caused by preformed dimers. Filaments that were grown by the copolymerization of 2 μM monomers with 4 nM dimers exhibit an average pause duration of $\langle \tau_{\mathrm{II}} \rangle = \Omega^{-1} = \tilde{\omega}_{\mathrm{pre}}^{-1} \simeq 2.0 \times 10^3\,\mathrm{s}$. These filaments contain not only preformed dimers but also photo-induced state-2-protomers which also cause pauses. However, we conclude from figure 5.5(a) that in this case at least three out of four pauses are caused by preformed dimers. Thus we can estimate the dissociation rate ω_{pre} of a preformed dimer by

$$\frac{1}{\tilde{\omega}_{\mathrm{pre}}} \gtrsim \frac{3}{4\,\omega_{\mathrm{pre}}} + \frac{1}{4\,\omega_{\mathrm{off},2}} \quad \Rightarrow \quad \omega_{\mathrm{pre}} \gtrsim \frac{3}{4/\tilde{\omega}_{\mathrm{pre}} - 1/\omega_{\mathrm{off},2}} \simeq 4.3 \times 10^{-4}/\mathrm{s}, \qquad (5.10)$$

which implies that the dissociation rates of preformed dimers and photo induced state-2-protomers differ only slightly and the ratio $\omega_{\mathrm{off},2}/\omega_{\mathrm{pre}}$ is smaller than 2.6. Assuming that the pre-exponential factor in the Arrhenius equation is equal in both cases implies that the free energy barriers for the dissociation of photo-induced and preformed dimers differ by less than $1\,k_{\mathrm{B}}T$.

Therefore the preformed dimers indeed behave as a second species of transformed protomers that were present from the beginning of depolymerization. Vice versa we conclude that the protomer state 2 indeed represents a stable dimer within the filament which causes an interruption of depolymerization when it reaches the barbed end.

5.3.2 Gel electrophoresis of actin solutions

Finally, solutions of fluorescently labeled actin filaments were illuminated and subsequently analyzed via gel electrophoresis and immunodetection, as described in appendix A.5.5. It turns out that stable actin dimers are present and the apparent molecular mass of these dimers is similar to the one of preformed pPDM-dimers, see figure 5.6. For constant illumination, the dimer-to-monomer ratio increased linearly with the labeling fraction, see figure a.12 in the appendix, as expected from eq. (5.1) for the state-2-protomers.

5.4 Summary

In this chapter we first presented experiments demonstrating that the intermittency of depolymerization depends both on the fraction of labeled actin and on the intensity of the

illumination. By means of the analytical expression for the occurrence of pauses, we found a linear relation between the labeling fraction and the transition rate which allowed us to infer that transitions of single fluorescently labeled protomers lead to the local formation of state-2-protomers within the filament. *In vivo* these transitions and the depolymerization intermittency are expected to be absent.

The transitions appear to be photo-induced and irreversible on the experimental time scale. Every pause of depolymerization ends when the state-2-protomer dissociates from the barbed end according to a first order kinetics with the rate $\omega_{\text{off},2} \simeq 1.1 \times 10^{-3}/\text{s}$.

Preformed actin dimers that were incorporated into the filament by copolymerization with monomeric actin behaved as state-2-protomers. Their appearance at the barbed end during depolymerization caused very similar interruptions. This indicates that the transformed protomers form stable dimers within the filament. Gel electrophoresis revealed that very stable dimers are indeed present in illuminated solutions of fluorescently labeled actin filaments.

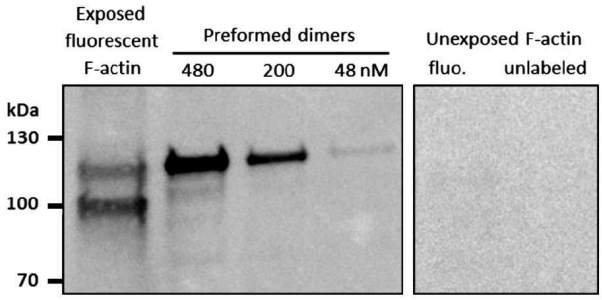

Figure 5.6 : Western blots obtained with an actin antibody. The apparent molecular masses of the photo-induced state-2-protomers (left column) are compared with the corresponding masses of the preformed dimers (three columns on the right corresponding to three different bulk concentrations of preformed actin dimers). The similarity of the apparent molecular masses implies that state-2-protomers are indeed actin dimers. Since the cross-links lead to a branched polypeptide chain, the apparent mass exceeds their true dimer mass of 86 kDa. Right: No state-2-protomers could be detected in labeled or unlabeled F-actin solutions that were not exposed to light.

In the experiments described so far, we primarily used the fluorophore Alexa488 bound to lysines on the surface of the actin filament. Additional experiments, in which actin was labeled with different fluorophores and on a different actin residue (see section A.5.6), revealed similar intermittent depolymerization and formation of dimers. Similar control experiments have shown that photo-induced dimerization can also take place in illuminated solutions of labeled G-actin, see section A.5.7 and figure a.12 in the appendix. This process should be negligible in conventional microscopy experiments and certainly played no role in our microfluidics experiments because the filaments elongated from fresh G-actin that constantly entered the flow cell, without being previously illuminated. In fact, if G-actin dimers were present and incorporated into the filaments, they would affect the cdf $P(t)$ in the same way as the preformed dimers. The distribution would no longer have a sigmoidal shape as in figure 4.3 but rather a convex shape as the three upper curves in figure 5.5(a).

Both a summary and a discussion of the last four chapters – dealing with the interruption of depolymerization of single actin filaments – is presented at the end of this thesis in chapter 7.

6 Mechanism of ATP hydrolysis

In filaments grown from ATP-actin, the initially bound ATP is rapidly cleaved into ADP-Pi, followed by a slower release of inorganic phosphate [46, 48]. Furthermore, the dissociation rates of protomers depend on the state of the bound nucleotide [41, 48]. In particular, ADP-actin is known to have a barbed end dissociation rate which is about one order of magnitude larger than the respective rate of ADP-Pi-actin [41, 48, 49]. This destabilization of the actin-actin bonds, caused by Pi release, leads also to a lower rigidity of the polymer [76, 104]. However, the molecular mechanism of Pi release in actin filaments grown from the physiologically relevant (Mg-)ATP-actin has remained elusive [39, 50]. As we have discussed in section 1.1.5 of the introduction, it is unclear if Pi release is governed by a vectorial mechanism – as shown in figures 1.4(a) and 1.4(c) – or by a random mechanism, as shown in figures 1.4(b) and 1.4(d). *In vivo* not only the filament ends, but also the distribution of ADP-Pi- and ADP-actin protomers influences filament dynamics as regulating proteins have a preference of binding to some of the actin species [10]. Since this distribution is determined by the mechanism of Pi release, see figure 1.4, the latter mechanism is of fundamental importance.

As the time scale of Pi release is comparable with the time scale in our depolymerization experiments, the increased dissociation rate of ADP-Pi-actin should become manifest in an accelerating depolymerization. In fact, in the microflow experiments discussed in chapter 4, the accelerating depolymerization is apparent, whereas the relatively large lag time in our early experiments (discussed in chapter 2) obstructed the observation of the acceleration. In the present chapter, we use the time-dependence of the depolymerization velocity to infer the spatial distribution of ADP-Pi- and ADP-actin protomers within the filament, and therefore the mechanism of Pi release.

For this purpose, we will first present a theoretical analysis which allows us to infer analytical expressions for the filament length as a function of time in case of the random as well as the vectorial phosphate release mechanism. A systematic comparison with the experimental depolymerization curves will then reveal the actual release mechanism and the corresponding parameter values. Subsequently, stochastic simulations are performed to justify the approximations made for the analytical calculations. Finally, the still elusive effect of profilin on actin dynamics is studied. Additional theoretical results are briefly presented in the corresponding appendix A.6.1.

6.1 Accelerating depolymerization of ATP-actin

In the last chapters, we have seen that the photo-induced formation of stable dimers within the filament causes the interruption of depolymerization. The resulting pauses did not affect the depolymerization curves up to the interruption, see figure 6.1(b). Therefore, we pref-

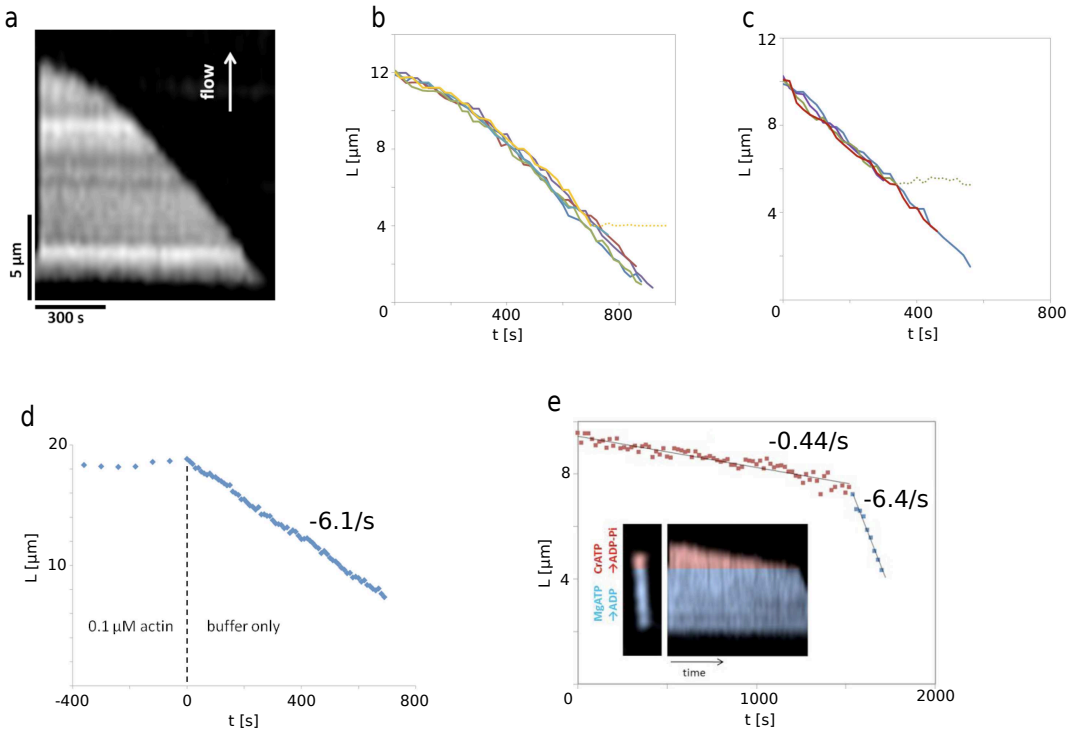

Figure 6.1 : (a) Kymograph of a depolymerizing actin filament: The filament extension (bright region) is plotted in vertical direction versus the time in horizontal direction. (b)-(e) Length versus time plots obtained from kymographs: (b) The depolymerization of ATP-actin accelerates on a time scale of a few minutes. (c) ADP-actin filaments shrink with a constant velocity corresponding to a dissociation rate of $\omega_{\mathrm{D}} = 5.8 \pm 0.4/\mathrm{s}$. (d) A filament that was assembles from ATP-actin and then kept at the critical concentration of 0.1 μM for 400 s subsequently disassembles with the dissociation rate of ADP-actin. (e) A filament that was sequentially grown from standard (Mg-)ATP-actin and then Cr-ATP-actin (which cannot release its Pi [98]) displays a sharp transition from slow to rapid depolymerization. The inset shows a fluorescence image of the filament with the ADP-Pi and ADP regions in pseudo colors, and the kymograph of its depolymerization.

erentially chose depolymerization curves with a long duration of the initial shrinking phase for the following analysis of ATP hydrolysis. Filaments assembled from ATP-actin depolymerize at a pace that accelerates progressively, on a time scale of a few minutes, see figure 6.1(a,b). On the other hand, filaments grown from ADP-actin disassemble with a constant rate $\omega_{\mathrm{D}} = 5.8 \pm 0.4/\mathrm{s}$ (mean and standard deviation of the population of $N_{\mathrm{f}} = 11$ filaments), see figure 6.1(c). Filaments assembled from ATP-actin that were kept at a constant length in a flow of 0.1 mM G-actin – the barbed end critical concentration – subsequently depolymerized at this constant rate as well, see figure 6.1(d). ADP-Pi-actin filaments exhibited another, but also constant depolymerization rate. For $N_{\mathrm{f}} = 13$ filaments depolymerizing in the presence of a saturating concentration of 100 mM Pi, $\omega_{\mathrm{DP}} = 0.16 \pm 0.07/\mathrm{s}$ was measured. For $N_{\mathrm{f}} = 21$ filaments grown from Cr-ATP-actin which cannot release it Pi [98], a rate of $\omega_{\text{Cr-DP}} = 0.33 \pm 0.16/\mathrm{s}$ was measured. Altogether, these dissociation rates confirm earlier measurements in bulk solution [48] as well as measurements on single actin filaments [49].

Recall, that in the simple experiments discussed in chapter 2, we found a shrinkage velocity of $v_{\mathrm{I}} = 2.7 \pm 1.2/\mathrm{s}$ for filaments in phase I, that is before the interruption. The rather large standard deviation is probably caused by the differing length of the depolymerization curves: In short depolymerization traces, a considerable amount of ADP-Pi-actin contributes to the shrinkage, whereas long traces represent almost exclusively the depolymerization of ADP-actin. However, mainly because of the long lag period, the data from these experiments are not suitable for further analysis. Kueh et al. [62] have reported even slower rates for ADP-actin, possibly because of filament-surface interactions. Also, there is no evidence in [62] for an accelerated depolymerization, as the lag time between initiation of depolymerization and imaging was too long. The observed depolymerization velocities can be explained as follows. The ATP in actin filaments is quickly cleaved [46, 105] and thus the dissociation of ATP-actin from the barbed end cannot be detected. The ADP-Pi-actin species, on the other hand, is the major intermediate [46,48,49,99]. ADP-Pi-actin dissociates considerably slower from the barbed end than ADP-actin [41, 48, 49]. The increasing depolymerization velocity of ATP-actin reflects the increasing probability to find ADP-actin instead of ADP-Pi-actin at the barbed end. As the shrinkage appears to increase continuously rather than discretely, we suspect that Pi release is a random mechanism, meaning the release rate ω_{r} does not depend on the position of the protomer in the filament. We will validate this hypothesis in the next sections by comparing the experimental depolymerization curves with corresponding analytical expressions for both vectorial and random release. This will also allow us to determine numerical values for the involved rates. To mimic the effect of vectorial Pi release, an ADP-Pi cap was constructed by elongating filaments sequentially from standard Mg-ATP-actin and then Cr-ATP-actin which cannot release its Pi [98]. These artificial filaments exhibited a sharp transition from slow to rapid depolymerization, see figure 6.1(e), differing from the smooth increase in depolymerization rate observed for standard filaments assembled from Mg-ATP-actin, see figure 6.1(a),(b). Evidence for an decreasing proportion of ADP-Pi-actin on the dissociating protomers was later also observed in bulk solution measurements using pyrenyl-actin fluorescence [73]. Filaments growing in a synchronous fashion from spectrin-actin seeds and ATP-actin displayed an accelerating depolymerization when they were switched to depolymerizing conditions in early stages of assembly, see figure a.13 in the appendix. By contrast, the filaments exhibited only constant (rapid) depolymerization when switched to depolymerizing conditions upon approaching steady state (figure a.13). In the latter case, Pi release has caught up with polymerization and the filaments consist almost exclusively of ADP-actin. However, the rapid depolymerization of ADP-actin was followed by a decline in rate that is probably caused by averaged effect of a intermittent depolymerization similar to the photo-induced intermittency discussed above. As these depolymerization pauses and in addition the discrimination between pointed and barbed end are not identifiable in the bulk of filaments, the kinetic analysis is feasible only on individual filaments and is discussed in the next sections.

6.2 Theoretical analysis

In order to infer the mechanism of hydrolysis from the measured quantity – the length L of an individual filament as a function of time t – and to determine the values of the relevant

parameters, we need to derive analytical expressions which relate the time evolution $L(t)$ with these parameters both for a random and a vectorial hydrolysis mechanism. During depolymerization, $L(t)$ is determined by the barbed end depolymerization velocity $v_{\mathrm{dep}}(t)$ which itself depends on the dynamics of the nucleotide state of the terminal protomer. ATP is quickly cleaved, so we may only consider ADP-Pi-actin and ADP-actin protomers, respectively. The self-consistency of this simplification will be validated in section 6.4.

Both a vectorial mechanism, where a phosphate can only be released from an ADP-Pi-protomer adjacent to an ADP-protomer and a random mechanism, where any ADP-Pi-protomer can release its phosphate with the same rate, are considered. We will see later that the vectorial mechanism does not fit the experimental data, and thus we will not use it to determine the numerical values of the involved parameters. Consequently we do not need a mathematical expression for the ensemble average of the depolymerization curves, but an expression for a typical curve. On the other hand, the random mechanism fits the experimental data and we will use the average $L(t)$ to determine the numerical values of the parameters.

6.2.1 Enhanced phosphate release at the barbed end

The phosphate release rate at the filament termini can be expected to differ from the respective rate within the filament. In fact, single filament experiments with varying phosphate concentrations in the buffer indicate that Pi release is strongly enhanced at the barbed end [49]. Furthermore, the initial slope of a typical depolymerization curve in our experiment appears to be larger than the constant slope for filaments that do not release the bound phosphate, indicating that a substantial number of ADP-Pi-protomers do not dissociate directly, but on another pathway.

Therefore, when considering the dissociation of ADP-Pi-actin, we must take two pathways into account: An ADP-Pi-protomer can either dissociate directly with the rate ω_{DP}, or first release its phosphate with the rate $\omega_{\mathrm{r}}^{\mathrm{B}}$ and then dissociate as ADP-actin with the rate ω_{DP}, see figure 6.2. In depolymerization experiments, these two pathways are indistinguishable. Thus, we define an effective ADP-Pi-actin dissociation rate ω_{DPD} as the inverse of the mean time that it takes for an ADP-Pi-protomer to depart from the barbed end. It can be computed considering the following. The fraction $\omega_{\mathrm{DP}}/\left(\omega_{\mathrm{r}}^{\mathrm{B}}+\omega_{\mathrm{DP}}\right)$ of the ADP-Pi-subunits at the barbed end dissociate directly, while the fraction $\omega_{\mathrm{r}}^{\mathrm{B}}/\left(\omega_{\mathrm{r}}^{\mathrm{B}}+\omega_{\mathrm{DP}}\right)$ first releases its phosphate before dissociating as ADP-actin. The dwell time of the initial ADP-Pi-state is given by $1/\left(\omega_{\mathrm{r}}^{\mathrm{B}}+\omega_{\mathrm{DP}}\right)$, and the dwell time of the ADP-state is given by $1/\omega_{\mathrm{D}}$. In consequence, the combination of the two routes leads to

$$\frac{1}{\omega_{\mathrm{DPD}}}=\frac{\omega_{\mathrm{DP}}}{\omega_{\mathrm{r}}^{\mathrm{B}}+\omega_{\mathrm{DP}}}\cdot\frac{1}{\omega_{\mathrm{r}}^{\mathrm{B}}+\omega_{\mathrm{DP}}}+\frac{\omega_{\mathrm{r}}^{\mathrm{B}}}{\omega_{\mathrm{r}}^{\mathrm{B}}+\omega_{\mathrm{DP}}}\cdot\left(\frac{1}{\omega_{\mathrm{r}}^{\mathrm{B}}+\omega_{\mathrm{DP}}}+\frac{1}{\omega_{\mathrm{D}}}\right) \tag{6.1}$$

and thus to

$$\omega_{\mathrm{DPD}}=\frac{\left(\omega_{\mathrm{DP}}+\omega_{\mathrm{r}}^{\mathrm{B}}\right)\omega_{\mathrm{D}}}{\omega_{\mathrm{D}}+\omega_{\mathrm{r}}^{\mathrm{B}}}. \tag{6.2}$$

Alternatively, this result can be derived formally by first computing the distribution of the first-passage times for the departure of the ADP-Pi-protomer and then averaging over

this distribution. The calculation also reveals the expected fact that the departure times are non-exponentially distributed. ADP-protomers that reach the barbed end, the setting is much simpler as these protomers dissociate directly with the rate ω_{D}, giving rise to a depolymerization velocity v_{D}.

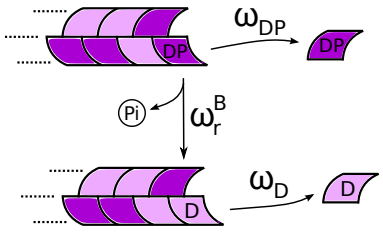

Figure 6.2: An ADP-Pi-protomer at the barbed end can either directly dissociate with rate ω_{DP}, or release its Pi with rate $\omega_{\mathrm{r}}^{\mathrm{B}}$ and then dissociate as ADP-actin with rate ω_{D}. Since the depolymerization experiments do not distiguish between these two pathways, we define an effective ADP-Pi-actin dissociation rate ω_{DPD} as the inverse of the mean time that it takes for an ADP-Pi-protomer to depart from the barbed end.

6.2.2 Random phosphate release

Our main objective is to calculate the average of the filament length, as we intend to compare our model with the experimental data. Thus we consider the average depolymerization velocity of an ensemble of N_{f} filaments

$$v_{\mathrm{dep}}(t) \equiv \frac{1}{N_{\mathrm{f}}} \sum_{i=1}^{N_{\mathrm{f}}} v_{\mathrm{dep}}^{i}(t) = \mathcal{P}_1(t)\, \omega_{\mathrm{DPD}} + (1 - \mathcal{P}_1(t))\, \omega_{\mathrm{D}}, \tag{6.3}$$

where the individual depolymerization velocities $v_{\mathrm{dep}}^{i}(t)$ are solely determined by the state of the protomer at the barbed end of the i-th filament, and $\mathcal{P}_1(t)$ is the probability that the terminal protomer is in the ADP-Pi-state when it appears at the barbed end . We have chosen this definition for $\mathcal{P}_1(t)$, since phosphate release on the barbed end is not considered explicitly, but via the effective dissociation rate ω_{DPD}. $(1 - \mathcal{P}_1(t))$ is the probability that the terminal protomer is in the ADP-state. The time evolution of $\mathcal{P}_1(t)$ is governed by

$$\partial_t \mathcal{P}_1(t) = -\omega_{\mathrm{DPD}} \mathcal{P}_1(t)\, (1 - \mathcal{P}_2(t)) + \omega_{\mathrm{D}}\, (1 - \mathcal{P}_1(t))\, \mathcal{P}_2(t), \tag{6.4}$$

where $\mathcal{P}_2(t)$ is the probability that the penultimate protomer is in the ADP-Pi-state. The first term on the right hand side of the equation accounts for the dissociation of an ADP-Pi-protomer (both direct dissociation and phosphate release followed by dissociation of an ADP-protomer, see eq. (6.2)) and an ADP-protomer on the penultimate position. The second term accounts for the opposite situation, dissociation of an ADP-protomer followed by an ADP-Pi-protomer.

During fast elongation, a cap of ATP-actin is present at the growing barbed end (see section 6.2.5) and prevents the exposure of ADP-Pi-protomers to the barbed end which would result in enhanced phosphate release. Thus the probability for the penultimate protomer to be in the ADP-Pi-state decays exponentially with its age $A(t)$, i.e. the time since it has been incorporated into the filament:

$$\mathcal{P}_2 = \int_0^\infty da\; p_A(a)\; e^{-\omega_{\mathrm{r}} a}, \tag{6.5}$$

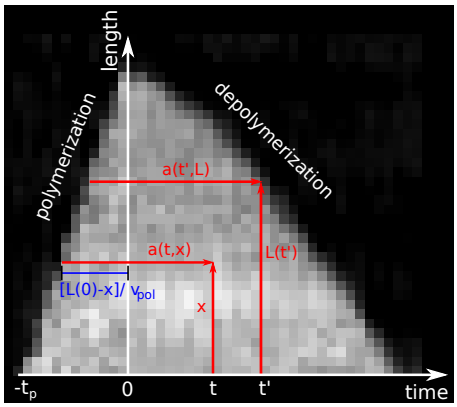

Figure 6.3: Calculation of the deterministic age $a(t,x)$. Shown is the kymograph of a filament during polymerization and depolymerization. Assuming a constant polymerization velocity v_{pol} and neglecting length fluctuations, the age of a protomer – defined as the elapsed time since its incorporation into the filament – at the beginning of depolymerization is given by $[L(0)-x]/v_{\mathrm{pol}} = t_{\mathrm{p}} - x/v_{\mathrm{pol}}$, with the position x measured from the pointed end. As the penultimate protomer comoves with the tip of the filament, its age is given by eq. (6.7).

where $p_A(a)$ is the probability density function of the age $A(t)$. Let us recall chapter 3, where we have assessed different sources of stochasticity and concluded that random transitions within the filament lead to a much larger randomness in the system than the stochastic association and dissociation events. The release rate ω_{r}, however, is expected to be much larger than the respective dimerization rate ω: Photo-induced dimerization takes only place at very few protomers within the filament and leads to an interruption of depolymerization. Pi release, on the other hand, occurs at many protomers and leads to an increase of the dissociation rate of about one order of magnitude. In fact, we can estimate the release rate for the random mechanism by visual inspection of a typical depolymerization curve, where the initial slope decays on a time scale of 100 to 1000 s, leading to a rate ω_{r} of the order of 10^{-3}/s to 10^{-2}/s.

To assess the stochasticity of the polymerization and depolymerization, it is necessary to notice that the relative length fluctuations during growth are small and many association and dissociation events occur before a protomer appears at the penultimate position of a shrinking filament. Thus, along the lines of chapter 3, we neglect the randomness of the association and dissociation processes, and assign a deterministic age $a(t,x)$ to each protomer at the position x (measured from the pointed end) at the time t since the initiation of depolymerization. As filaments elongated with a constant velocity v_{pol} during the polymerization phase, the age of a protomer is a linear function of its position within the filament. Figure 6.3 visualizes that the deterministic age during depolymerization is given by

$$a(t,x) = t + t_{\mathrm{p}} - x/v_{\mathrm{pol}}, \tag{6.6}$$

where t_{p} is the known duration of polymerization. Moreover, as the penultimate protomer comoves with the tip of the filament, and the size of a single protomer is negligible compared to the filament length, the age of the penultimate protomer is a function of the filament length $L(t)$ and the time t:

$$a(t,L) = t + t_{\mathrm{p}} - L(t)/v_{\mathrm{pol}}, \tag{6.7}$$

and the probability $\mathcal{P}_2$ is given by

$$\mathcal{P}_2(t) = e^{-\omega_{\mathrm{r}} a(t,L)} = e^{-\omega_{\mathrm{r}}\left(t+t_{\mathrm{p}}-L(t)/v_{\mathrm{pol}}\right)}. \tag{6.8}$$

In consequence, the differential equation

$$\partial_t \mathcal{P}_1(t) = -\omega_{\mathrm{DPD}}\mathcal{P}_1(t) - \left(\omega_{\mathrm{D}} - \omega_{\mathrm{DPD}}\right)\mathcal{P}_1(t)e^{-\omega_{\mathrm{r}} a(t,L)} + \omega_{\mathrm{D}} e^{-\omega_{\mathrm{r}} a(t,L)}, \tag{6.9}$$

with the initial condition

$$\mathcal{P}_1(0) = 1, \tag{6.10}$$

describes the time-evolution of $\mathcal{P}_1(t)$ and via equation (6.3) the average depolymerization velocity. This leads to a second order differential equation for $L(t)$ which describes the depolymerization dynamics, see section A.6.1 in the appendix. In our case phosphate release within the filament is much slower than dissociation. Thus the asymptotic approximation

$$\frac{\partial_t \mathcal{P}_1(t)}{\omega_{\mathrm{DPD}}} \approx 0, \tag{6.11}$$

can be employed leading to

$$\mathcal{P}_1(t) \approx \frac{\omega_{\mathrm{D}} e^{-\omega_{\mathrm{r}} a(t,L)}}{(\omega_{\mathrm{D}} - \omega_{\mathrm{DPD}})\, e^{-\omega_{\mathrm{r}} a(t,L)} + \omega_{\mathrm{DPD}}}. \tag{6.12}$$

With eq. (6.3), and the identity $v_{\mathrm{dep}}(t) = -\partial_t L(t)$, we find the differential equation

$$\partial_t L(t) \approx \frac{-1}{\frac{1}{\omega_{\mathrm{D}}} + \left(\frac{1}{\omega_{\mathrm{DPD}}} - \frac{1}{\omega_{\mathrm{D}}}\right) e^{-\omega_{\mathrm{r}} a(t,L)}}. \tag{6.13}$$

This differential equation can not be solved explicitly, as $\partial_t L(t)$ depends in a non-algebraic way on $L(t)$. However, partial derivatives with respect to the parameters can be calculated in order to fit the resulting curve to the experimental length-vs-time data, see section 6.3. Furthermore, the following intuitive formula for the depolymerization velocity follows:

$$\frac{1}{v_{\mathrm{dep}}(a(t,L))} \approx \frac{1}{\omega_{\mathrm{D}}} + \left(\frac{1}{\omega_{\mathrm{DPD}}} - \frac{1}{\omega_{\mathrm{D}}}\right) e^{-\omega_{\mathrm{r}} a(t,L)}. \tag{6.14}$$

6.2.3 Vectorial phosphate release

In the vectorial model, the phosphate can only be released from an ADP-Pi-protomer adjacent to an ADP-protomer. Thus there is an interface between a segment of ADP-portomers at the pointed end side and another segment of ADP-Pi-protomers at the barbed end side, see figure 1.4 in the introduction. This interface moves with a velocity given by the release rate ω_{r} towards the barbed end. Meanwhile, the barbed end moves with a velocity that is given by the effective dissociation rate of ADP-Pi-actin ω_{DPD} in the opposite direction. When the interface reaches the barbed end at time τ_{D}, it vanishes and the filament continues to shrink with a velocity that is determined by the dissociation rate ω_{D} of ADP-actin. Thus the *typical* course of filament length $L(t)$ exhibits a kink when the interface reaches the end at time τ_{D}:

$$L(t) = \begin{cases} L_0 - \omega_{\mathrm{DPD}} t & \text{for} \quad t \leq \tau_{\mathrm{D}} \\ L_0 + (\omega_{\mathrm{D}} - \omega_{\mathrm{DPD}})\, \tau_{\mathrm{D}} - \omega_{\mathrm{D}} t & \text{for} \quad t > \tau_{\mathrm{D}}. \end{cases} \tag{6.15}$$

Note that the ensemble average $\langle L \rangle(t)$ is expected to exhibit a smooth transition from slope ω_{DPD} to ω_{D} as the period τ_{D} can vary within the filament ensemble due to the stochasticity of the association, dissociation, and release processes. However, to be experimentally detectable, the rate of phosphate release of the ADP-Pi-protomer at the interface must be of

the same order as the dissociation rate ω_{DPD}. Thus, for a vectorial transitions mechanism, the distribution of τ_{D} is expected to be very narrow, as we have argued in section 3.4. In fact, we can replace ω by ω_{r} in eq. (3.142) to estimate the theoretically expected standard deviation σ of the τ_{D} distribution. As the rate $\omega \equiv \omega_{\mathrm{r}}$ must be similar to ω_{off} for vectorial transitions and since $\omega_{\mathrm{on}} t_{\mathrm{p}}$ is less than 10^4, we can expect σ to be at most of the order of 10 s. Neglecting the randomness of the involved processes, the average value $\langle \tau_{\mathrm{D}} \rangle$ can be calculated from the equality between the filament length and the length of the ADP-actin segment at time τ_{D}. We find

$$v_{\mathrm{pol}} t_{\mathrm{p}} - \omega_{\mathrm{DPD}} \langle \tau_{\mathrm{D}} \rangle = \omega_{\mathrm{r}} \left(t_{\mathrm{p}} + \langle \tau_{\mathrm{D}} \rangle \right) \;\Leftrightarrow\; \langle \tau_{\mathrm{D}} \rangle = \frac{v_{\mathrm{pol}} - \omega_{\mathrm{r}}}{\omega_{\mathrm{DPD}} + \omega_{\mathrm{r}}}\, t_{\mathrm{p}}, \tag{6.16}$$

which is consistent with eq. (3.141). We will see below that the vectorial model does not fit the data.

6.2.4 Depolymerization velocity of a filament segment

In the previous sections, we have modeled both the Pi release, as well as the dissociation of protomers as stochastic processes and have derived asymptotic results which apply for realistic parameter values. Here, we will motivate the relation between the depolymerization velocity, and the Pi content within the filament in a rather different way.

Let us consider the general case of a filament segment consisting of n^{seg} protomers that may dwell in different states $i = 1, 2, \ldots, N_{\mathrm{s}}$. If there are no transitions between the states, the average time for the depolymerization of a segment is the sum of the inverse dissociation rates

$$\langle \tau_{\mathrm{seg}} \rangle = \sum_{i=1}^{N_{\mathrm{s}}} \frac{n_i^{\mathrm{seg}}}{\omega_i} = n^{\mathrm{seg}} \sum_{i=1}^{N_{\mathrm{s}}} \frac{q_i^{\mathrm{seg}}}{\omega_i}, \tag{6.17}$$

where n_i^{seg} is the number of state-i-protomers, q_i^{seg} the fraction of state-i-protomers, and ω_i the dissociation rate of a state-i-protomer. The average depolymerization velocity of the segment is defined as

$$v_{\mathrm{dep}}^{\mathrm{seg}} \equiv \frac{n^{\mathrm{seg}}}{\langle \tau_{\mathrm{seg}} \rangle} = \left(\sum_{i=1}^{N_{\mathrm{s}}} \frac{q_i^{\mathrm{seg}}}{\omega_i} \right)^{-1}. \tag{6.18}$$

If we now allow transitions between the states, $v_{\mathrm{dep}}^{\mathrm{seg}}$ becomes a time-dependent quantity. If these transitions occur rarely compared to the dissociation of *all* protomer species, they do not take place within a sufficiently *small* segment while this segment disassembles. In this case, $v_{\mathrm{dep}}^{\mathrm{seg}}(t)$ is solely determined by the time-dependent fractions $q_i^{\mathrm{seg}}(t)$ via eq. (6.18).

If the segment contains a significant number of protomers in each state i, that is the segment was chosen *large* enough, each fraction $q_i^{\mathrm{seg}}(t)$ fluctuates only little within the filament population, and can be approximated by the probability $Q_i^{\mathrm{seg}}(t)$ that a protomer is in state i at time t. Furthermore, if we neglect the fluctuations by the association and dissociation events, this probability is approximated by the (deterministic) age a of the filament segment. Therefore, for the discussed case of phosphate release, we obtain the age-dependent

depolymerization velocity

$$\frac{1}{v_{\mathrm{dep}}(a)} = Q_{\mathrm{DP}}(a)\left(\frac{1}{\omega_{\mathrm{DPD}}} - \frac{1}{\omega_{\mathrm{D}}}\right) + \frac{1}{\omega_{\mathrm{D}}}, \tag{6.19}$$

where $Q_{\mathrm{DP}}(a)$ is the probability that a protomer within the segment is in the ADP-Pi-state, and ω_{DPD} and ω_{D} are the effective dissociation rates of ADP-Pi-, and ADP-actin, respectively.

In case of random phosphate release, this equation is equivalent to the asymptotic result (6.13) which was inferred for phosphate release that is slow compared to dissociation. For a vectorial release mechanism, in contrast, we have argued that the rate of phosphate release of the ADP-Pi-protomer at the interface must be of the same order as the dissociation rate. However eq. (6.19) still applies in this case, if we choose the segment to have the size of a single protomer, and $Q_{\mathrm{DP}}(a)$ would suddenly drop from unity to zero, as there are no transitions within the segment of ADP-Pi-actin.

The intuitive formula (6.19) provides an alternative method to compare the experimental data with the theoretical models. However, as the transformation of the measured length-vs-time data into velocity-vs-age curves might be error-prone, the method is less accurate than the direct fit.

Note that for the analysis of intermittent depolymerization, see chapter 3, the presented considerations do not apply. Even in very long segments, there are typically no protomers in state 2, and a state-2-protomer has a very large dwell time at the barbed end.

6.2.5 The ATP cap

The presence – or absence – of an ATP-cap influences the dynamics of actin filaments. As mentioned, ATP cleavage is two orders of magnitude faster than Pi release. Thus, shortly after the initiation of depolymerization, no ATP-actin remains in the filament (see figure 6.8(c) and the depolymerization dynamics only depends on Pi release. During polymerization, however, the situation is entirely different since ATP-actin is constantly incorporated at the barbed end. As filament elongation was typically performed at a G-actin concentration of $2\,\mu$M, a lower limit for the association rate of about $\omega_{\mathrm{on}} \geq 15/\mathrm{s}$ can be assumed [41]. For the hypothetical case of a vectorial ATP cleavage mechanism, as proposed in [39,99], a cap of ATP-actin is present at the growing barbed end as the cleavage can not catch up with polymerization [39]. But also for random cleavage, the probability to find an ADP-Pi-protomer at the barbed end during elongation is negligible, if realistic values for the association and cleavage rates [49] are chosen. In fact, many theoretical works have estimated the length of the ATP-cap, that is the filament segment at the barbed end that consists entirely of ATP-actin, see for instance [51, 106]. However, usually only the steady state of a filament segment that comoves with the terminus is considered.

Here, we are only interested in an estimate for the probability that ATP-actin is at the barbed end. In analogy to eq. (6.4), the time evolution of this probability is governed by

$$\partial_t \mathcal{P}_1^{\mathrm{T}} = -\omega_{\mathrm{c}}\mathcal{P}_1^{\mathrm{T}} + \omega_{\mathrm{on}}\left(1 - \mathcal{P}_1^{\mathrm{T}}\right) - \omega_{\mathrm{T}}\mathcal{P}_1^{\mathrm{T}}\left(1 - \mathcal{P}_2^{\mathrm{T}}\right) + \omega_{\mathrm{DPD}}\mathcal{P}_1^{\mathrm{DP}}\mathcal{P}_2^{\mathrm{T}} + \omega_{\mathrm{D}}\mathcal{P}_1^{\mathrm{D}}\mathcal{P}_2^{\mathrm{T}}, \tag{6.20}$$

where $\mathcal{P}_1^{\mathrm{N}}$ denotes the probability that the nucleotide N = T, DP, D binds to the barbed end, and $\mathcal{P}_2^{\mathrm{N}}$ is the corresponding probability of the penultimate protomer. To our knowledge,

eq. (6.20) has not been solved in general. However, lower limits for both the steady state probability $\mathcal{P}_1^{\mathrm{T}}(t \to \infty)$ and the derivative $\partial_t \mathcal{P}_1^{\mathrm{T}}$ can be easily given:

$$\mathcal{P}_1^{\mathrm{T}}(t \to \infty) \geq \frac{\omega_{\mathrm{on}}}{\omega_{\mathrm{on}} + \omega_{\mathrm{T}} + \omega_{\mathrm{c}}}, \tag{6.21}$$

$$\partial_t \mathcal{P}_1^{\mathrm{T}} \geq \omega_{\mathrm{on}} - (\omega_{\mathrm{c}} + \omega_{\mathrm{on}} + \omega_{\mathrm{T}})\, \mathcal{P}_1^{\mathrm{T}}. \tag{6.22}$$

With realistic parameter values, this allows us to conclude that the probability that an ATP-cap is present at the barbed end exceeds 90% within less than a tenth of second. One could refine this estimate by successively estimating $\mathcal{P}_2^{\mathrm{T}}$, $\mathcal{P}_3^{\mathrm{T}}$, and so on. In fact, we will later see from stochastic simulations (see figure 6.8) that $\mathcal{P}_1^{\mathrm{T}}$ is virtually unity during filament growth.

In summary, an ATP-cap is typically present during filament elongation, since the cleavage rate ω_{c} is much smaller than the association rate ω_{on}. During depolymerization, we can neglect the presence of ATP-actin, because the rate ω_{c} is much larger than the Pi release rate ω_{r}. However, the presence ATP-cap during polymerization indirectly influences the dynamics of depolymerization: Since it prevents the exposure of ADP-Pi-protomers to the barbed end, the enhanced phosphate release does not take place during filament polymerization.

6.3 Comparison with experimental data

6.3.1 Vectorial versus random mechanism

In this section, we formally show that the depolymerization velocity is continuously increasing from $v_{\mathrm{DPD}} \equiv \omega_{\mathrm{DPD}}$ to $v_{\mathrm{D}} \equiv \omega_{\mathrm{D}}$, consistent with the random mechanism of phosphate release, rather than suddenly changing from v_{DPD} to v_{D}, as predicted by the vectorial mechanism. Thus we fit both a piecewise-linear function corresponding to the vectorial model and the nonlinear $L(t)$ as given by equation (6.13) – or equivalently by equation (a.9) in the appendix – of the random model to the experimental data. As mentioned, equation (6.13) cannot be solved explicitly, but partial derivatives of the right hand side with respect to the parameters ω_{DPD}, ω_{D}, and ω_{r} can be formally computed. These derivatives allow a nonlinear regression analysis via minimization of the sum of squared residuals. In practice, we have used the function `nlinfit.m` of the `matlab` statistics toolbox to perform this task. `nlinfit.m` employs the the Levenberg-Marquardt algorithm [107,108] to determine the least square deviations between the model and the data.

By inspection only, it is hardly possible to decide if the vectorial or the random model fits the data better, see figure 6.4(a) for an example. However, the sum of squared residuals SSR provides a relative measure to compare the quality of both fits [108]. For the $N_{\mathrm{f}} = 20$ observed filaments, we find that $\mathrm{SSR}_{\mathrm{vect}} > \mathrm{SSR}_{\mathrm{rand}}$ holds for almost all cases, indicating that the model of random phosphate release describes the data better, see figure 6.4(b).

Fitting the data from each filament with the piecewise linear function of the vectorial model also determines the time τ_{D} when the putative interface between ADP-Pi- and ADP-protomers reaches the barbed end. It turns out that the τ_{D} distribution is rather broad, with a standard deviation σ of the order of 100 s. However, we have argued above that the expected σ is at most of the order of 10 s, indicating another inconsistency of the data with the vectorial model.

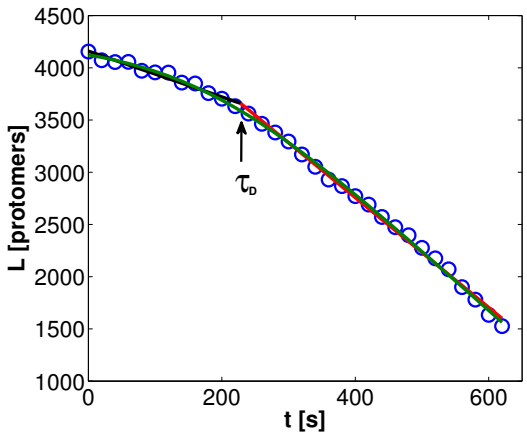

(a) Fits of the experimental depolymerization data (blue circles) by the random mechanism (green curve) as well as by the vectorial mechanism (black and red segments). The time τ_D denotes the sudden increase of the depolymerization velocity from v_{DPD} to v_D that occurs for the vectorial mechanism. By inspection only, it is hardly possible to decide which fit is better.

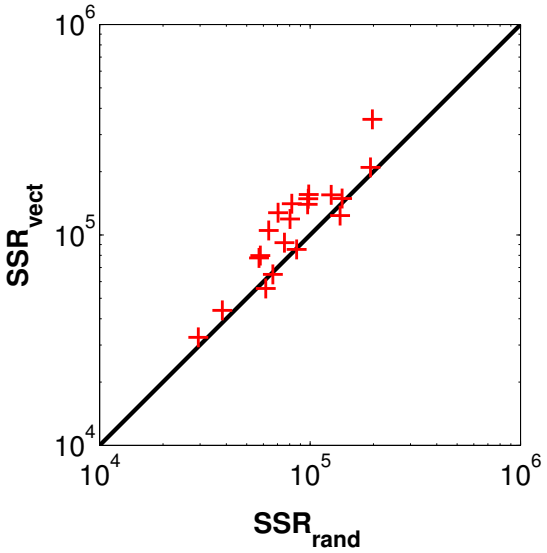

(b) Sum of square residuals (SSR) for fits of $N_f = 20$ filaments. The SSRs of the vectorial vs. the SSRs of the random mechanism are shown on a double-logarithmic scale. In most cases, $SSR_{vect} > SSR_{rand}$ holds, indicating that the model of phosphate release describes the data better.

Figure 6.4 : Vectorial versus random phosphate release mechanism.

Let us recall that equation (6.19) provides us with an alternative method to compare the experimental data with the theoretical models which is less accurate but more intuitive. Complete polymerization-depolymerization curves as in figure 6.3 were used to graphically determine the age $a(t, L)$ from the time t and the corresponding filament length $L(t)$. This corresponds to formally applying eq. (6.7). The local depolymerization velocity $v_{dep}(t)$ was estimated by fitting linearly the $L(t)$ plot around a given point, over a symmetrical window of 4-12 time intervals. We verified that, over these time ranges, increasing the window of the linear fit had no effect other than reducing the fluctuations of $v_{dep}(t)$. The plot of the inverse depolymerization velocity $1/v_{dep}$ vs. the age a, see figure 6.5(a), is well fitted by a single exponential decay, indicating that Pi release is governed by a random mechanism. A vectorial mechanism, in contrast, would result in a sudden drop in the $1/v_{dep}(a)$ plot.

6.3.2 Numerical values of kinetic parameters

In this section, we use the nonlinear regression method described above to fit the $L(t)$ curve of the random model, given by equation (6.13) – or equivalently by equation (a.9) in the appendix – to the experimental data. In the fitting procedure, the known values of t_p and

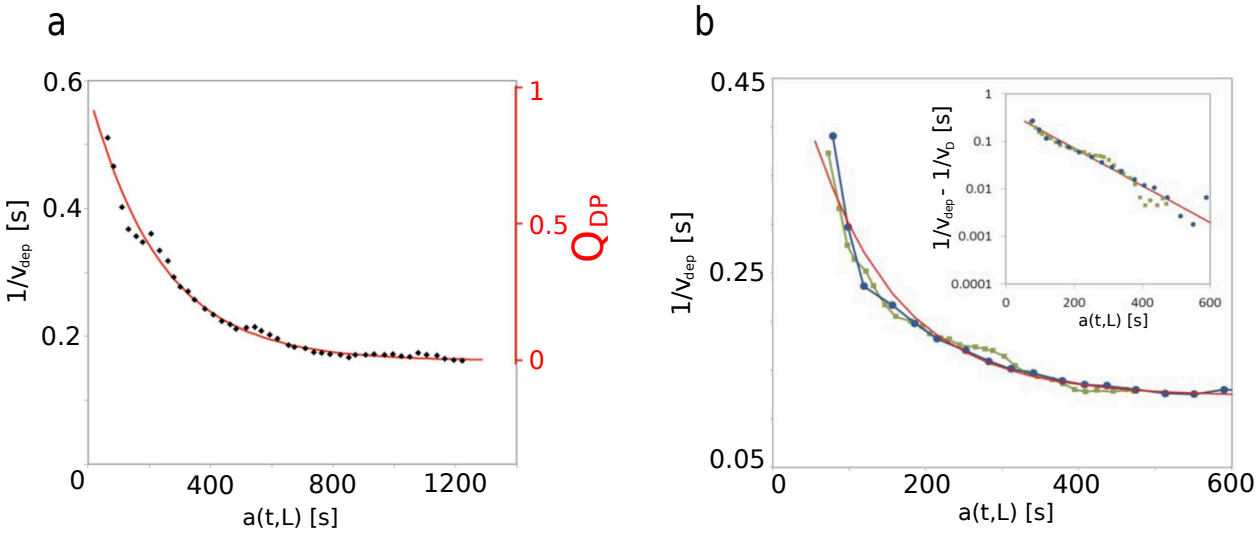

Figure 6.5 : (a) Inverse depolymerization velocity $1/v_{\mathrm{dep}}$ as a function of the age $a(t, L)$ for the filament shown in figure 6.1(a). The velocity $v_{\mathrm{dep}}(t)$ was obtained via linear fits of the $L(t)$ data and the age $a(t, L)$ was determined by eq. (6.7). The probability Q_{DP} that a protomer is in the ADP-Pi-state, when it reaches the barbed end, is proportional to $1/v_{\mathrm{dep}} - 1/v_{\mathrm{D}} = 1/v_{\mathrm{dep}} - 1/\omega_{\mathrm{D}}$, see eq. (6.19). Its exponential decay indicates a random release mechanism. (b) The $1/v_{\mathrm{dep}}$ vs. $a(t, L)$ plots for filaments grown with $2\,\mu$M actin during a short ($t_{\mathrm{p}} = 150\,$s, green) and a long ($t_{\mathrm{p}} = 600\,$s, blue) polymerization time match each other, confirming that the probability Q_{DP} depends only on the age. An exponential decay (red line) fits both data sets, as expected for a random Pi release mechanism. In the inset, a log-linear plot of $1/v_{\mathrm{dep}} - 1/v_{\mathrm{D}}$ is shown for the same data.

v_{pol} are fixed to determine the three unknown parameters ω_{DPD}, ω_{D}, and ω_{r}.

We proceed in two different ways. First, we fit individual curves to each of the $N_{\mathrm{f}} = 20$ filaments (cf. inset of figure 6.6), to obtain a set of 20 numerical values for each parameter. The means and standard deviations are given by $\omega_{\mathrm{DPD}} = 1.7 \pm 0.7/\mathrm{s}$, $\omega_{\mathrm{D}} = 6.3 \pm 1.5/\mathrm{s}$ and $\omega_{\mathrm{r}} = 8.3 \pm 4.3 \times 10^{-3}/\mathrm{s}$.

The other option for an analysis is to fit a single theoretical curve simultaneously to the data from all filaments. This gives the best estimate for the parameters. However, the $N_{\mathrm{f}} = 20$ data sets were not obtained from a single, but 5 individual experiments whose polymerization velocities v_{pol} and durations t_{p} differ. Thus only the filament data within one experiment can be fitted simultaneously, see figure 6.6. We obtain the following values for the weighted total averages of the parameters: $\omega_{\mathrm{DPD}} \simeq 1.5/\mathrm{s}$, $\omega_{\mathrm{D}} \simeq 6.0/\mathrm{s}$ and $\omega_{\mathrm{r}} \simeq 7.4 \times 10^{-3}/\mathrm{s}$, in agreement with the values determined above.

As an another alternative, we fit the transformed $1/v_{\mathrm{dep}}(a)$ data with a shifted exponential function as in figure 6.5. The intercept of the exponential at the vertical axis determines $1/v_{\mathrm{DPD}} = 1/\omega_{\mathrm{DPD}}$. For large ages a, $1/v_{\mathrm{dep}}(a)$ converges to $1/v_{\mathrm{D}} = 1/\omega_{\mathrm{D}}$, and the release rate ω_{r} is given by the decay constant of the exponential. For the $N_{\mathrm{f}} = 20$ analyzed filaments, we find $\omega_{\mathrm{DPD}} = 1.5 \pm 0.4/\mathrm{s}$, $\omega_{\mathrm{D}} = 6.2 \pm 0.4/\mathrm{s}$, and $\omega_{\mathrm{r}} = 6.8 \pm 2.1 \times 10^{-3}/\mathrm{s}$, in agreement with the more rigorous methods above.

The value of ω_{r} that we have determined is comparable to previous measurements from

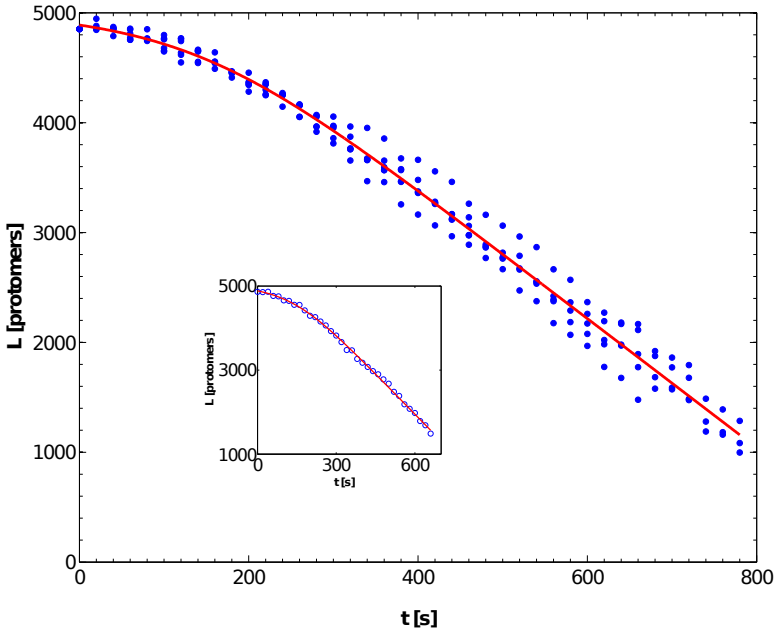

Figure 6.6 : Random release mechanism: Direct fit of the theoretical depolymerization curve, given by the differential eq. (6.13), to experimental data of six filaments from one experiment. The experimental curves were slightly shifted in a vertical direction to have a common initial length. In the inset, an example for a fit of the theoretical curve to a single experimental curve is shown.

bulk solution studies [46,48,99] or individual filament [49] studies, with ω_r ranging from 0.002 to 0.006/s. Our slightly higher value might be caused by the summery temperatures during the measurements in combination with the absence of an air conditioner in the laboratory. Filaments elongated at different actin concentrations, i.e. different velocities v_{pol}, or for different durations t_p all displayed the same age-dependence of depolymerization rate (see figure 6.5(b), confirming that the ADP-Pi content depends only on the age of the F-actin, as expected for a random Pi release mechanism.

As our model explicitly allows for Pi release at the barbed end (see section 6.2.1), the effective ADP-Pi-actin dissociation rate ω_{DPD} might be distinct from the dissociation rate ω_{DP} of an ADP-Pi-protomer. In fact, the value of $\omega_{DPD} \simeq 1.5/s$ differs by one order of magnitude from $\omega_{DP} \simeq 0.16/s$ which was measured in the presence of a saturating concentration of phosphate. As expected, the fitted dissociation rate $\omega_D \simeq 6.0/s$ agrees with $\omega_D \simeq 5.8/s$ which was determined from the depolymerization of ADP-actin filaments. These values for ω_D agree with bulk solution [48], as well as electron microscopy measurements of single filaments [41]. However, previous fluorescence microscopy experiments [52] found a significantly lower value, presumably because the intermittency of depolymerization was not correctly accounted for.

To determine the release rate at the barbed end ω_r^B, we reformulate eq. (6.2) to yield

$$\omega_r^B = \frac{(\omega_{DPD} - \omega_{DP})\,\omega_D}{\omega_D - \omega_{DPD}}, \tag{6.23}$$

and thus $\omega_r^B \simeq 1.8/s$. This confirms the enhancement of Pi release at the barbed end proposed by Fujiwara et al. [49] and our measurement corresponds to the lower limit of their estimated range for ω_r^B. Depolymerizing ADP-actin filaments rapidly switch to a slow depolymerization rate when exposed to Pi which indicates that, at least at the barbed end, Pi binds rapidly to a protomer and stabilizes its interactions with neighbors. Phosphate release in the core of the filament has been proposed to be kinetically limited by the slow conversion of the ATP hydrolysis transition state F-ADP-P* into F-ADP-Pi, see section 2.1.5 and [79].

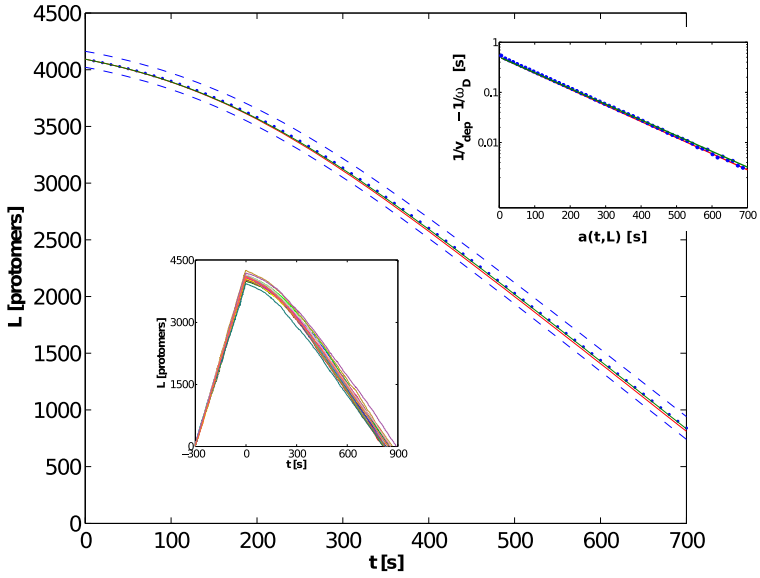

Figure 6.7 : Comparison of stochastic simulations with analytical results. We simulated the polymerization and depolymerization of 10^4 filaments with rates as specified in the text, i.e. including ATP cleavage. Average values (blue dots) ± standard deviations (blue dashed lines) are depicted. The continuous red line is the solution of eq. (6.13) for the same parameters as used in the simulations. The fit is sufficient for our purpose, since the deviation is much smaller than the optical resolution. The small error is mainly caused by neglecting the cleavage step: In a further improved approximation, we could consider ATP cleavage by an effective release rate which takes both cleavage and release into account. Thus, we replace ω_r by $\omega_c\omega_r/(\omega_c + \omega_r)$ in eq. (6.13). This yields the green line, which is in very good agreement with the simulations. In the upper inset, the exponential relation between $1/v_{dep} - 1/\omega_D$ and $a(t, L) = t + t_p - L(t)/v_{pol}$ is shown for the simulated and the calculated trajectories. In the lower inset, the length fluctuations within the filament population is indicated by 20 randomly chosen trajectories.

6.4 Stochastic simulations

In the analytical calculations for the random release mechanism which finally led to equation (6.13) the following simplifications were made.

- Only ADP-Pi- and ADP-actin protomers were considered, since we assumed that ATP-actin has an infinitely short lifetime within the filament. This assumption is justified by the large ratio ω_c/ω_r of the cleavage rate ω_c and the release rate ω_r, see section 6.2.5.

- Phosphate release at the barbed end does not take place during polymerization. A cap of ATP-actin is present during polymerization and prevents ADP-Pi-actin protomers from loosing their phosphate by being exposed at the barbed end. This assumption is justified by the small ratio ω_c/ω_{on} of the cleavage rate and the association rates ω_{on} in the experiment, see section 6.2.5.

- When considering the departure of ADP-Pi-protomers, we do not distinguish between the two possible pathways, see figure 6.2. Instead we use the effective dissociation rate ω_{DPD} given by eq. (6.2). However this can only lead to errors on the scale of single protomers.

- Instead of considering the distribution $p_A(a)$ of the age of protomers, we use a deterministic age function $a(t, L)$ which depends only on the average polymerization trajectory. This simplification is justified, since the length fluctuations, and thus the age fluctuations, are small compared to their corresponding average values, as we have argued in section 6.2.2.

- The phosphate release rate ω_r is much smaller than the dissociation rates ω_{DP} and ω_D. Thus, we assume that $\mathcal{P}_1(t)$ is constant on the time scale of single dissociation events, see eq. (6.11).

In order to validate these simplifications, we use the Gillespie algorithm to simulate the polymerization and depolymerization of filaments [90]. The following stochastic processes, which are known to play a role in actin dynamics, are taken into account. ATP cleavage with the rate $\omega_c = 0.3/\text{s}$ [49]; phosphate release with the rate $\omega_r = 7.4 \times 10^{-3}/\text{s}$; enhanced phosphate release at the barbed end with the rate $\omega_r^B = 1.8/\text{s}$; association of ATP-actin with the rate $\omega_{on} = 15/\text{s}$ (only during polymerization phase which lasted for $t_p = 300/\text{s}$); dissociation of ATP-actin with the rate $\omega_T = 1.4/\text{s}$ [41, 52]; dissociation of ADP-Pi-actin with the rate $\omega_{DP} = 0.16/\text{s}$; and dissociation of ADP-actin with the rate $\omega_D = 6/\text{s}$. Apart from ω_c and ω_T, the numerical values for the rates were taken from the last section.

It is shown in figure 6.7, that the simulations indeed justify the simplifications which were made to obtain the analytical results and especially eq. (6.13). The simulations also indicate the length fluctuations which follow from the stochasticity of the involved transitions. During the first instances of growth, the polymerization trajectories tend to diverge, leading to a spreading in the length at the beginning of depolymerization. During the depolymerization process, this spread varies only slightly. Figure 6.8 confirms the notion of the presence of an ATP-cap during polymerization and its absence during depolymerization.

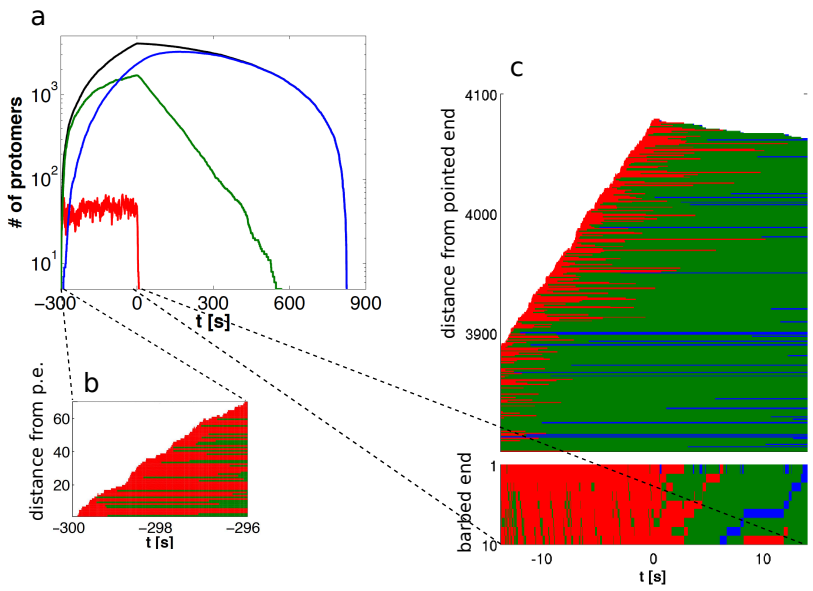

Figure 6.8 : Stochastic simulation of the composition of a single filament as a function of time t. The parameter values are as specified in the text. (a) Number of protomers during polymerization ($t < 0$) and depolymerization ($t > 0$). ATP-protomers are shown in red, ADP-Pi-protomers in green, and ADP-protomers in blue. The filament length is shown in black. After the initiation of depolymerization the number of ATP-protomers drops from 40 to 50 to zero on a time scale of few seconds. (b) Spatial composition of a filament after the start of polymerization from the seed (pointed end). Because the association of ATP-actin is much faster than the ATP cleavage, the probability $\mathcal{P}_1^{\mathrm{T}}$ to find ATP-actin at the barbed end is virtually unity during filament growth. (c) Spatial composition of a filament at the initiation of depolymerization. The lower graph displays the state of the 10 ultimate protomers that comove with the barbed end. During polymerization ATP-actin occupies the barbed end at almost all points in time. After the initiation of depolymerization $\mathcal{P}_1^{\mathrm{T}}$ drops to zero on a time scale of few seconds.

6.5 Effect of profilin

Actin polymerization is influenced by profilin, a low molecular weight protein [109]. Profilin specifically binds to monomeric ATP-actin at its barbed face [110]. This prevents both the formation of filament nuclei and the association of monomers to pointed ends. Association of profilin-actin to the barbed end enables filament growth, as profilin is released after each association step. However, the effect of profilin on ATP hydrolysis and the mechanism of filament growth from profilin-actin is still elusive [111]. We have addressed these issues using the microfluidic setup discussed in chapter 4 in combination with the presented theoretical analysis.

6.5.1 Depolymerization in presence of profilin

During depolymerization, the addition of profilin in the buffer accelerated the shrinking of actin filaments in a concentration-dependent manner, see figure a.14(a) in the appendix.

This acceleration vanished when removing the free profilin from the buffer, confirming that profilin does not bind to internal protomers. Consistently, the presence of profilin during depolymerization increases the dissociation rates ω_{DPD} and ω_{D} but does not affect the time-dependence of the probability that Pi is bound at a fixed protomer within the filament, which remains exponential with the same release rate ω_{r}.

To investigate the effect of profilin on ADP-Pi- and ADP-actin separately, the depolymerization of Cr-ATP-actin (which cannot release its bound phosphate) and (Mg-)ADP-actin filaments were monitored at different profilin concentrations. It was found that profilin increases ω_{DP}, see figure a.14(b), and that it also increases ω_{D} in agreement with earlier studies in solution [112]. Assuming that profilin is in rapid equilibrium with the barbed end, the probability that profilin binds to the terminus follows from the definition of the dissociation constant $\mathrm{K_D^{Pr\text{-}B}}$ of the barbed end and profilin:

$$\mathcal{P}_{\mathrm{Pr}} = \frac{c_{\mathrm{Pr}}}{c_{\mathrm{Pr}} + \mathrm{K_D^{Pr\text{-}B}}}, \tag{6.24}$$

where c_{Pr} is the profilin concentration in solution which can be precisely adjusted by the microflow setup. The concentration dependent depolymerization velocity is given by

$$v_{\mathrm{dep}} = (1 - \mathcal{P}_{\mathrm{Pr}})\,\omega_{\mathrm{off}} + \mathcal{P}_{\mathrm{Pr}}\;\omega_{\mathrm{off}}^{\mathrm{PrA}} = \omega_{\mathrm{off}} + \frac{\left(\omega_{\mathrm{off}}^{\mathrm{PrA}} - \omega_{\mathrm{off}}\right) c_{\mathrm{Pr}}}{c_{\mathrm{Pr}} + \mathrm{K_D^{Pr\text{-}B}}}, \tag{6.25}$$

where ω_{off} and $\omega_{\mathrm{off}}^{\mathrm{PrA}}$ are the barbed end dissociation rates of actin and profilin-actin, respectively. The dissociation rate ω_{off} was already determined in the absence of profilin: we found $\omega_{\text{Cr-DP}} \simeq 0.33/\mathrm{s}$ and $\omega_{\mathrm{D}} \simeq 5.8/\mathrm{s}$ for ADP-Pi- and ADP-actin, respectively. Thus $\omega_{\mathrm{off}}^{\mathrm{PrA}}$ and $\mathrm{K_D^{Pr\text{-}B}}$ are the free fitting parameters for both of the two concentration dependent depolymerization velocities, see figure a.14(b). For ADP-actin, we find $\mathrm{K_D^{Pr\text{-}B(D)}} = 28 \pm 5\,\mu\mathrm{M}$ and $\omega_{\mathrm{off}}^{\mathrm{PrA(D)}} = 52 \pm 3/\mathrm{s}$. For ADP-Pi-actin, the fitted values are $\mathrm{K_D^{Pr\text{-}B(DP)}} = 5.9 \pm 0.4\,\mu\mathrm{M}$ and $\omega_{\mathrm{off}}^{\mathrm{PrA(DP)}} = 4.7 \pm 0.4/\mathrm{s}$. Profilin has a higher affinity for ADP-Pi-actin than for ADP-actin at the barbed end, and the relative increase of the dissociation rate is also larger for ADP-Pi-actin. Having measured the concentration dependent impact of profilin on ω_{DPD}, ω_{DP}, and ω_{D}, we can compute $\omega_{\mathrm{r}}^{\mathrm{B}}$ as a function of profilin concentration following the reaction scheme of figure 6.2 and using eq. (6.23). We find that profilin also accelerates Pi release at the barbed end of actin filaments, see figure a.14(c). A saturation curve in analogy to eq. (6.25) given the dissociation constant $\mathrm{K_D^{Pr\text{-}B(DP)}} = 5.9 \pm 0.4\,\mu\mathrm{M}$ of profilin and ADP-Pi-actin at the barbed end leads to a Pi release rate $\omega_{\mathrm{r}}^{\mathrm{B,Pr}} = 6.1 \pm 0.3/\mathrm{s}$ of profilin-actin at the barbed end.

6.5.2 Polymerization from profilin-actin

We have monitored filaments elongated with various concentrations of actin (0.2 to 6 μM) and profilin (0 to 9 μM) and found that elongation from profilin-actin is 30% slower than from actin alone at the same concentration, as measured previously in bulk solution [113]. Filaments polymerized from profilin-ATP-actin exhibit the same depolymerization dynamics as filaments polymerized from ATP-actin, showing that the age-dependance of the probability to find bound Pi within the filament did not change. Thus, the polymerization from profilin-ATP-actin is not coupled to phosphate release.

We may also draw another, more indirect conclusion. We have seen in section 6.2.5 that the presence of an ATP-cap during polymerization prevents the ADP-Pi-protomers at the growing barbed end to release their Pi with the enhanced rate ω_r^B. This release would considerably decrease the probability to find bound Pi within the filament. Therefore, the unaltered composition of filaments grown from profilin-actin infers that such an ATP-cap also exists during the polymerization of these filaments. In consequence, the elongation from profilin-actin can not be coupled to ATP cleavage on the terminal protomer.

These findings seem to oppose the view that ATP hydrolysis is coupled to polymerization from profilin-(Mg)-ATP-actin [113, 114]. However, the possibility that the elongation is directly coupled to ATP cleavage at the penultimate protomer can not strictly be excluded from our findings. In fact, all proposed mechanisms for the elongation from profilin-ATP-actin – direct coupling [115], indirect coupling [116], and no coupling [105] – are consistent with our data, but the possible mechanisms for putative coupling are restricted.

6.6 Summary

The observation of the depolymerization of single actin filaments allowed us to infer the spatial distribution of bound phosphate along the filaments and the mechanism of phosphate release which is the rate-limiting step of ATP hydrolysis within filaments. We find that a random release mechanism describes the data best, meaning each ADP-Pi-protomer releases its Pi independently in a first-order reaction which is independent of the nucleotides bound to surrounding protomers. The best estimate for the transition rate is given by $\omega_r \simeq 7.4\times10^{-3}$/s which is comparable to previous measurements from bulk solution [46, 48, 99] or individual filament studies [49], with ω_r ranging from 0.002 to 0.006/s. At the barbed end, the phosphate release rate is strongly increased to $\omega_r^B \simeq 1.8$/s. This value corresponds to the lower limit of the estimated range [49]. For the dissociation rates of ADP-Pi- and ADP-actin, we found $\omega_{DP} \simeq 0.16$/s and $\omega_D \simeq 6.0$/s in agreement with all previously reported values.

We have seen that within certain limits of the growth velocity the phosphate composition of a filament is unchanged. This observation allows us to infer that under standard growth conditions, enhanced phosphate release at the barbed end is prevented by the presence of an ATP-actin cap. This means that during polymerization the probability that the terminal protomer binds ATP is effectively unity in agreement with the accepted values for ATP cleavage [49]. After the initiation of depolymerization this probability approaches zero on a time scale of seconds.

Our study also reveals that the binding of profilin to the barbed end strongly increases both the dissociation rates of ADP-Pi- and of ADP-actin. We also demonstrated that the rate ω_r^B of Pi release at the barbed end is increased by profilin, while the release rate ω_r of ADP-Pi-actin within the filament is unaffected, consistent with the notion that profilin only binds to the barbed face of actin. We found that the elongation of filaments from profilin-ATP-actin is not coupled to Pi release, as these filaments exhibit the same depolymerization dynamics as filaments polymerized from ATP-actin. Furthermore, we can indirectly conclude that the elongation of filaments from profilin-ATP-actin is not coupled to ATP cleavage at the terminal protomer.

7 Summary, discussion and perspectives

7.1 Summary

Intermittent depolymerization

In the main part of this thesis, which consists of the chapters 2 - 5 we approached a major controversy in the field of actin dynamics [117]: Do actin filaments indeed become more stable if they grow older, as recently reported, and what mechanism causes the surprising interruptions of depolymerization of single filaments? We resolved the problem by a combination of single filament experiments and stochastic modeling as follows.

We modified the single filament depolymerization experiments reported in [62] to circumvent their weak points, see chapter 2, and were able to confirm that the barbed end depolymerization of an individual actin filament is characterized by at least two dynamic phases. In the initial phase, the filament shrinks with a velocity of a few protomers per second, which is consistent with known barbed end dissociation rates. A few minutes after its initiation, the depolymerization is interrupted. We also demonstrated that the majority of protomers are already in the ADP-state when they dissociate and that the interruptions are not coupled to ATP cleavage. The duration τ, defined from the initiation of depolymerization until the occurrence of the first interruption, differs from filament to filament and represents a stochastic variable. The distribution of this duration τ turned out to be a fingerprint of the mechanism that causes the interruption.

Since the depolymerization pauses can not be explained by the nucleotide-induced protomer states known to date, we postulated a novel state, which is characterized by its very small barbed end dissociation rate. While being agnostic about the nature of the novel state, we considered various hypothetical mechanisms that lead to the appearance of such a state at the barbed end and thereby cause the interruption of depolymerization. These mechanisms include global filament transitions as proposed in [62], transitions of the shrinking end such as the transient anchoring of the barbed end at the cover slip surface [52], transitions that already occur during the polymerization process, and local transitions at random sites within the filament, see figure 3.2. These mechanisms cannot be distinguished directly, but they lead to distinct distributions of the duration τ, which can be compared with single filament experiments.

By modeling the underlying stochastic processes – the association and dissociation of protomers and putative transformations of these protomers – we computed the probability density functions of the duration τ for the considered transition mechanisms. We quantified the stochasticity of these processes in a quite intuitive way that also guides our calculations. The distributions are summarized in figure 3.6 for realistic parameter values for the polymerization time, and the association and dissociation rates. Global transitions of the whole

filament, transitions that occur only at the depolymerizing terminus, as well as transitions during polymerization all lead to exponentially distributed durations τ, see eq. (3.176). A vectorial transition mechanism, according to which the protomers successively undergo the transitions until the barbed end is reached, gives rise to a narrow Gaussian distribution around the average duration $\langle\tau\rangle$, see eq. (3.177). Local transitions of random protomers within the filament lead to a Rayleigh distribution, that grows linearly for small and decays slowly for large times with a broad maximum in-between, see eq. (3.180).

Comparing the cumulative distribution functions $P(t) \equiv \text{prob}\,(\tau \leq t)$ of the stochastic variable τ for the transformation mechanisms under discussion with the experimentally determined distribution revealed that only local transitions at random sites within the filament explain the observed interruptions, see figures 3.7 and 4.3. In particular, we could rule out the idea of a "dynamic stabilization" proposed in [62, 63].

Single filament experiments that employed a microfluidics setup, described in chapter 4, facilitate the imaging of filaments during the whole course of the experiment and the precise determination of the distribution of τ from the beginning of depolymerization, see figure 4.3. The microflow setup also allowed the direct demonstration of the local nature of the transition, see figure 4.4, and revealed the initial acceleration of depolymerization of filaments assembled from ATP-actin. This acceleration reflects the filament destabilization induced by ATP-hydrolysis, see figure 7.1. We generalized our analytical expression for the distribution of τ to account for the time-dependent depolymerization velocity, see eq. (4.8).

The combination of additional experiments with the microfluidics setup and our analytical results revealed a linear relation between the labeling fraction of actin and the local transition rate, see figure 5.1. This linearity allowed us to infer that transitions of single fluorescently labeled protomers lead to the transformed protomers, which have a very small barbed end dissociation rate and thus cause the interruptions of depolymerization. *In vivo* these transitions and the depolymerization intermittency are expected to be absent. The transitions appear to be photo-induced and irreversible on the experimental time scale. Every pause of depolymerization ends when the transformed protomer dissociates from the barbed end according to first order kinetics, see figure 5.3. Preformed, stable actin dimers that were incorporated into the filament by copolymerization with monomeric actin behaved like these transformed protomers. Their appearance at the barbed end during depolymerization caused very similar interruptions. These experiments demonstrate that our abstract notion of protomer transformations correspond to formations of stable dimers within the filament. Gel electrophoresis revealed that very stable dimers are indeed present in illuminated solutions of fluorescently labeled actin filaments. The excited state of the fluorophore can provide energy for the production of reactive molecular species [118] that may then lead to the dimerization of two nearby actin protomers. Control experiments with actin that was labeled with different fluorophores and on different residues exhibited very similar intermittent depolymerization, indicating the generality of our results.

In summary, we demonstrated that the pauses of depolymerization arise from photo-induced transitions of single fluorescently labeled protomers , which trigger the formation of covalent actin dimers within the filaments. The depolymerization process is interrupted as soon as such an actin dimer appears at the barbed end – see white arrow in figure 4.2(a) – and is continued when it dissociates from the filament – see black arrow in that figure. Thus, each

pause represents the delayed dissociation of a single dimer, which can directly be observed in the microscope. The measured distribution of pause durations provides the statistics of these single molecule events, see figure 5.3. The dissociation rate of the photo-induced dimers is found to be about 1.1×10^{-3}/s, which is much smaller than the dissociation rate of about 6/s for ADP-actin protomers. This reduced dissociation rate reflects the additional molecular bonds between the dimer and the neighboring protomers at the barbed end, see figure 3.1 and corresponds to an increase in the corresponding free energy barrier by about $8.6\,k_{\mathrm{B}}T$ compared to a terminal protomer, provided that the pre-exponential factor in the Arrhenius equation is equal in both cases. Because unlabeled filaments depolymerize without pauses, see figure 5.2, our results support the view that filament stability and turnover is controlled by ATP hydrolysis and that actin filaments become less stable as they grow older.

Mechanism of ATP hydrolysis

In the second part of the thesis, which is presented in chapter 6, we have investigated the mechanism of phosphate release, which is the rate limiting step of ATP hydrolysis within actin filaments. Since ADP-Pi- and ADP-actin dissociate from the barbed end with different rates, the time-dependent depolymerization velocity is an indicator of the spatial distribution of these species along the filament, see figure 7.1. A systematic analysis of the accelerated depolymerization of single filaments, see figure 6.4, shows that the rate of ATP hydrolysis is constant within the filament, corresponding to random, as opposed to a vectorial hydrolysis mechanism. Other crucial results of this second part, such as for instance the enhanced phosphate release at the barbed end, the ATP-cap during polymerization, and the function of profilin, are summarized in section 6.6.

7.2 Discussion

We demonstrated that the intermittent depolymerization of actin filaments is caused by the photo-induced dimerization of labeled actin protomers. The notions that the observed pauses reflect either (i) the transient attachment of the barbed end [52], (ii) strongly cooperative ATP cleavage followed by strongly cooperative Pi release [51], or (iii) the prominent "dynamic stabilization" of the filament helix [62, 63] are proved false.

In particular, we showed that the interruptions of depolymerization are not caused by the age-dependent rearrangement of actin filament architecture, see figure 1.6(c). Apart from the interruptions, single actin filaments depolymerize with velocities as expected from the dissociation rates of the known, nucleotide-induced protomer states, see for instance figure 6.1(b). Therefore the putative structural polymorphism or plasticity of actin filaments, which was reported in some [64, 65] but not all [16] electron microscopy studies, is not reflected in the depolymerization dynamics. Each of the protomer states, which are considered in actin dynamics (ATP-, ADP-Pi-, and ADP-actin) contains a set of substates which might be reflected in this polymorphism. Single-molecule fluorescence resonance energy transfer (FRET) experiments also indicate a dynamic polymorphism, as actin protomers switch between high- and low-FRET efficiency states on a time scale of seconds [119]. We disprove the appealing link between these structural data and *in vitro* function of actin proposed by

Kueh et al. [62,63]. The limited structural information about F-actin has, to our knowledge, so far prevented any other generally accepted structure function relation in actin dynamics.

The modified protomer state that we have predicted during the course of our investigations, turns out to be a photo-induced dimer that is merely an artifact from the fluorophore label rather than a novel actin "species". In the experiments described in this thesis, we primarily used the fluorophore Alexa488 bound to lysines, which are located on the surface of the actin filament, but we also observed intermittent depolymerization and photo-induced dimerization for filaments labeled with different fluorophores and on a different actin residue, see section 5.4. Likewise, Kueh et al. [62] labeled actin with Alexa647 on lysines, and in the earlier study [52], which also reported pauses in actin depolymerization, oregon green on Cysteine-374 was used. Photo-induced oligomerization of actin has also been found in solutions of fluorescein-labeled and rhodamine-labeled actin [118]. In summary, actin dimerization appears to be a general photo-chemical reaction occurring with all tested fluorescence labels.

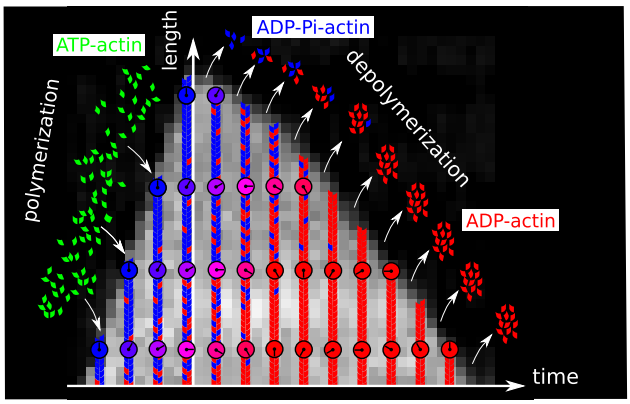

Figure 7.1 : Simplified sketch of the filament composition. The kymograph of the actin filament (shown in light grey) was obtained with the microfluidics setup. In the simplified description shown here, ATP is instantaneously cleaved upon incorporation of ATP-actin into the filament. The subsequent release of phosphate results in ADP-actin. The velocity of depolymerization increases over time, since ADP-actin dissociates more rapidly from the filament end than ADP-Pi-actin. The local composition of the filament – i.e. the fraction of ADP-Pi-actin – can be inferred from the time-dependence of the depolymerization velocity and is indicated by the coloring of the small clocks. These clocks measure the local time at the respective position within the filament, that is the time that has elapsed since the incorporation of the respective filament segment. The correlation between the color of the clocks and the local time indicates that the rate of phosphate release is constant along the filament.

The linear relation between the labeling fraction and the local transition rate, see figure 5.1(a), implies that the dimerization is triggered by the photo-induced transition of single, labeled protomers. However, it does not imply that the labeled protomer itself is covalently cross-linked to one of its neighbors, but only that a photo-induced reaction at single labeled protomers induces the formation of covalent cross-links between adjacent protomers. Control experiments have shown that photo-induced dimerization can also take place in illuminated solutions of labeled G-actin. In our single filament experiments, this reaction

should be negligible in conventional microscopy experiments and certainly played no role in our microfluidics experiments, as we argue in section 5.4.

The afore mentioned study [118] concluded from measurements of the viscosity that filaments undergo photo-induced fragmentation. However, the rate of the latter process was estimated to be a factor of $10^2 - 10^3$ smaller than the oligomerization [118]. The observation of rare fragmentation events in our study is consistent with this estimate. Based on the bulk measurements of the time-course of the amount of F-actin in [29], the local fragmentation rate of actin filaments was calculated [30] to be of the order of 10^{-8}/s. With Schmoller et al. [69], we found the very similar value of 5×10^{-9}/s from the time evolution of the length distribution of labeled actin reporter filaments in an unlabeled F-actin solution. The small relative difference between these two values seems to be a coincidence since in [29] a higher salt concentration (lowering the fragmentation rate), a higher temperature (increasing the fragmentation rate), and no fluorescent label (absence of label also should lower the rate) were used. Furthermore, Erickson [30] assumes 10^4 to be the average number of protomers in filaments. In the considered situation, this value is likely to be lower by a factor of about 100, which would lead to a fragmentation rate of 10^{-9}/s. In any case, the local fragmentation rate lies between 10^{-9}/s and 10^{-7}/s and is hence much smaller than the barbed end dissociation rate of a stable actin dimer, for which we found 4.3×10^{-4}/s in case of preformed dimers – see eq. (5.10) – and 1.1×10^{-3}/s for photo-induced dimers. As we know that the used pPDM-cross-linked dimers were lateral dimers, i.e. linked at the short interfaces shown in figure 3.1, the similarity of the two dissociation rates may indicate that photo-induced dimers are also such lateral dimers. The large difference between the fragmentation rate and these dissociation rates is inconsistent with the actin filament model shown in figure 3.1 and indicate that the actin-actin bonds between a covalently linked dimer at the barbed end and the adjacent protomers are substantially weaker than such bonds within the filament. Assuming again that the pre-exponential factor in the Arrhenius equation is equal in both cases implies that the free energy barriers for the dissociation of lateral dimers and for filament fragmentation differ by about $15\, k_{\mathrm{B}}T$.

This difference may arise from the tension caused by the covalent cross-link or by the water or ion contacts which modify the protomers at the terminus. An argument for the former is provided by the fact that fragmentation appears to be partially photo-induced, and the photo-induced dimerization may destabilize the filament helix in this manner. On the other hand, we found that phosphate release at the barbed end is accelerated more than 100-fold, see section 6.6. Since the nucleotide binding cleft is directing towards the pointed end of the filament, see figure 1.2(d), we believe that this enhanced rate does not merely arise from a steric effect, but reflects an conformational difference between protomers at the barbed end and those within the filament. Such differences also exist between pointed and barbed end protomers, as a simple bond model alone, see figure 3.1, may only explain the difference of the kinetics at the ends.

When copolymerizing actin monomers with preformed dimers, we found a linear relation between the fraction of dimers within the filament and the fraction of dimers in the polymerization solution, see inset of figure 5.5(a). The slope of the corresponding regression line is very close to one half which indicates that the association rate constant of dimers is about half as large as the monomer association rate constant. Therefore, the average time

for the association of a dimer equals the time for the association of two monomers, in case of identical concentrations. We believe that, even though this is an interesting observation, the association of a preformed dimer may not be envisaged as a succession of two monomer association events.

We have demonstrated that the rate of phosphate release in actin filaments is constant along the filament, corresponding to a random rather than the vectorial release mechanism. ADP-Pi- and ADP-actin are distributed according to figures 1.4(b,d) and not according to figures 1.4(a,c) along the filament. As discussed in the introduction, this local composition is important *in vivo*, as it may control or be affected by regulators of actin dynamics like profilin, capping proteins, or ADFs/cofilins that bind differently to ADP- or ADP-Pi-actin [10,44,45]. Furthermore, the local destabilization of the actin-actin bonds, caused by Pi release, leads to a lower rigidity of the polymer [76,104]. However, strictly speaking our result that phosphate release is constant along the filament – see figure 7.1 – does not imply a purely random release mechanism (i.e. an exactly identical rate at each protomer), but merely excludes a vectorial, or a strongly cooperative mechanism. The reason for this restriction lies in the limited optical resolution of the length measurement. In consequence, we might not detect small cooperativity effects: After the phosphate of one protomer has been released, the induced conformational change, which we indirectly detect by the increased dissociation rate of ADP-actin, may cause a small increase or decrease of the release rate of adjacent protomers. As long as the cooperativity is small, it does not give rise to filament segments that are highly enriched with ADP-actin and thus the cooperativity might not be detected in our experiment. However, such a cooperative effect is of minor importance, as for instance it changes the binding of ADFs only very locally.

7.3 Perspectives

We believe that the strong point of the presented work lies in the combination of experimental and theoretical methods and this path should be further explored. Here, we suggest a few possible routes.

In principle, we could transfer our investigation, which revealed the mechanism of phosphate release to the mechanism of ATP cleavage. However, since the cleavage rate is two orders of magnitude larger than the release rate, corresponding depolymerization experiments would require a very fast growth of filaments. In fact, under normal growth conditions, the ATP-actin cap is only present during filament growth, and rapidly vanishes upon initiation of depolymerization, see figure 6.8. The polymerization velocities that can be reached with the present microflow setup are limited by spontaneous nucleation (in the absence of profilin), and do not allow us to draw direct conclusions on the ATP cap. Furthermore, employing the filament length fluctuations near the critical concentration as suggested by theoretical studies appears unfeasible because these fluctuations are too similar for the vectorial [54] and random [59] cleavage mechanism, see section 1.1.7. Nevertheless, two alternative approaches might elucidate the mechanisms of ATP cleavage. One proposition to overcome the limitation of the microflow setup is to implement a "mixer", which allows to expose G-actin to KCl only seconds before reaching the spectrin-actin seeds.

The other approach is theory-driven and utilizes the fact that the presence of ATP-actin

instead of ADP-Pi-actin actin at the barbed end prevents the enhanced phosphate release discussed in section 6.2.1. The absence of enhanced phosphate release can be indirectly concluded from the phosphate composition of the filament that in turn is measured by depolymerization experiments, see chapter 6. Elongating the filaments with a very low actin concentration leads to an altered phosphate composition, which could be employed to infer the probability of ATP-actin at the barbed end. Knowing this probability as a function of the G-actin concentration would allow us to determine the mechanism of ATP cleavage.

The combined experimental and theoretical method, which we employed to elucidate the interruptions of depolymerization, provides a unique probe for the interactions between actin protomers. These interactions could be changed by a variety of actin-binding molecules and proteins. Of particular interest are proteins such as tropomyosin, heavy meromyosin, or the Arp2/3 complex that bind to more than one actin protomer and may induce additional pauses in depolymerization. Using the microfluidic setup in combination with the expression for the cumulative distribution function of τ as given by eq. 4.1 enables the determination of the transition rate ω which corresponds to the binding rate of these proteins. Putative binding cooperativity or competitive binding could also be studied along these lines. Tropomyosin, for example, prevents cofilin [120] as well as Arp2/3 [121] from binding to actin whereas fimbrin prevents the binding of tropomyosin [122]. The kinetics of these processes may be crucial for the coexistence of distinct actin networks within eukaryotic cells, see figure 1.1, a rather puzzling feature of the actin cytoskeleton [11, 66].

In our experiments, photo-induced transitions of fluorescently labeled actin protomers interrupt the depolymerization of filaments. These labeled molecules may be used as molecular switches when incorporated into large networks of actin filaments and illuminated by focussed laser beams. This would allow the "freezing" of the filament dynamics within localized regions of the networks. Using a procedure similar to fluorescence speckle microscopy [123], it may even be feasible to apply these molecular switches *in vivo* and, in this way, extend the method of "chromophore assisted laser inactivation" [124] from the protein to the filament level. One obvious obstacle on this path is the fact that photo-induced dimerization can also take place in illuminated solutions of labeled G-actin, albeit with a presumably much smaller rate. Therefore, much research effort is still needed.

Appendices

A.2 Appendix of chapter 2: Depolymerization experiments

A.2.1 Depletion of the monomer pool

In order to check whether the monomer concentration is constant during polymerization or depleted by the association reaction, preliminary experiments were performed. The same chemical conditions as in the standard assays were used, but the polymerization buffer was supplemented with methyl cellulose to allow for the observation of filament growth. We found that the growth velocity is rather constant during polymerization, indicating that no considerable depletion occurred. In the following, we argue why this result makes sense.

For incubation, we rinsed the chamber with about two times its volume with F*-buffer which contained at most 2 pM seeds. Even if all seeds were deposited in the chamber, the seed concentration during the later steps of the experiment should be not exceed 4 pM. Considering a concentration of monomeric actin of 5 μM, the monomer to seed ratio is at least 10^6. At the end of the polymerization process, the filament length is much less than 10^4 protomers. Therefore, less than 1% of monomers have been polymerized into filaments nucleated by the preformed seeds. From figure 4 of ref. [27], one can estimate that less than 10 % of the monomers are lost by spontaneous nucleation.

Here, we also make a rough estimate of the ratio between the number of seeds in the chamber and the number of filaments that stick to the coverslip during observation. The seed concentration of 2 pM and the chamber volume of 10 μl leads to an overall seed number of the order of 10^7. The area of the field of view is given by $(512\,\text{pixel} \times 167\,\text{nm/pixel})^2 \simeq 10^{10}\,\text{nm}^2$. On average, there are about 10 filaments in such a field of view. The area of the coverslip edge of the flow chamber is $3\,\text{mm} \times 26\,\text{mm} \simeq 100\,\text{mm}^2$. Therefore, only about $10 \times 100\,\text{mm}^2/10^{10}\,\text{nm}^2 = 10^5$ filaments stick to this edge. The discrepancy to the seed number can have several reasons. First, not all seeds can be expected to firmly attach to the coverslip during the 5 min incubation process. Second, the attachment has to occur in a certain angle to enable filament elongation. Third, most filaments are ripped of the chamber wall and flushed out during the rinsing procedure. This can be seen by the large number of filaments which are present near the edge of the chamber, where the flow velocity is much lower.

A.2.2 Computations

Actin concentration after sequestering by latrunculin

The F-actin which remains after rinsing provides some G-actin. In preliminary experiments without latrunculin, this led to very slow depolymerization with rates of 0.2 ± 0.1 subunits per

second. However, the "refilled" pool of G-actin remains below the critical concentration of the barbed ends, that is 0.1 μM [114]. Now, latrunculin A binds in a 1:1 stoichiometry to actin monomers: $\mathrm{L} + \mathrm{A} \rightleftharpoons \mathrm{LA}$. The equilibrium dissociation constant of this reaction was measured in ref. [77] as $K_\mathrm{D} \equiv c_\mathrm{L} c_\mathrm{A}/c_\mathrm{LA} = 0.2\,\mu$M, where $c_\mathrm{A} = c_\mathrm{A0} - c_\mathrm{LA}$ and $c_\mathrm{L} = c_\mathrm{L0} - c_\mathrm{LA}$ are the latrunculin and actin equilibrium concentrations, respectively. By combining the last three relations, we obtain $K_\mathrm{D} = (c_\mathrm{L0} - c_\mathrm{A0} + c_\mathrm{A})c_\mathrm{A}/(c_\mathrm{A0} - c_\mathrm{A})$. The positive solution of this quadratic equation for c_A is given by $c_\mathrm{A} = (c_\mathrm{A0} - c_\mathrm{L0} - K_\mathrm{D})/2 + \sqrt{(c_\mathrm{A0} - c_\mathrm{L0} - K_\mathrm{D})^2/4 + c_\mathrm{A0} K_\mathrm{D}}$. The addition of $c_\mathrm{L0} = 3\,\mu$M latrunculin A to $c_\mathrm{A0} < 0.1\,\mu$M actin results in $c_\mathrm{A} < 6.4$ nM. Therefore, we conclude that the amount of latrunculin that we use is sufficient to sequester practically all actin monomers.

Phosphate solution at pH 7

In order to get a phosphate solution at a given pH, we mixed solutions of K_2HPO_4 and KH_2PO_4 of the same concentrations. Here, we calculate the ratio of HPO_4^{2-} to $H_2PO_4^-$ which yields pH 7.0. As the acid dissociation constants of H_3PO_4 and HPO_4^{2-} are very high ($\mathrm{pK}_a = 2.13$) and very low ($\mathrm{pK}_a = 12.4$), respectively, one must consider the following equilibrium reaction only:

$$\mathrm{H_2PO_4^- + H_2O \rightleftharpoons HPO_4^{2-} + H_3O^+,\ pK_a = 7.2.} \tag{a.1}$$

For pH 7.0, a concentration ratio of $c_{\mathrm{HPO_4^{2-}}}/c_{\mathrm{H_2PO_4^-}} = 10^{7-\mathrm{pK_a}} = 0.63$, or equivalently $c_{\mathrm{HPO_4^{2-}}}/(c_{\mathrm{HPO_4^{2-}}} + c_{\mathrm{H_2PO_4^-}}) = 0.39$ is required. Therefore, 39% of K_2HPO_4 solution are mixed with 61% of KH_2PO_4 solution.

Ionic strength

As a control for the assays with ADP-Pi-actin, where we have used 25 mM phosphate at pH 7, another experiment with the same pH and the same ionic strength is needed. In this case, the potassium phosphate was replaced by potassium sulfate K_2SO_4. Here, we calculate the required concentration of K_2SO_4. As computed above, we need 39% of K_2HPO_4 solution and 61% of KH_2PO_4 solution to yield pH 7. In a phosphate solution of 25 mM, this gives an ionic strength of $I = \frac{1}{2}(c_{\mathrm{K^+}} + 4c_{\mathrm{HPO_4^{2-}}} + c_{\mathrm{H_2PO_4^-}}) = \frac{1}{2} \times 25\,\mathrm{mM}(2 \times 0.39 + 0.61 + 4 \times 0.39 + 0.61) \simeq 45\,\mathrm{mM}$. The ionic strength in the reference assay is given by $I = \frac{1}{2}(c_{\mathrm{K^+}} + 4c_{\mathrm{SO_4^{2-}}}) = 3c_{\mathrm{SO_4^{2-}}}$. Therefore 15mM of K_2SO_4 is needed for the same ionic strength.

A.2.3 Fitting piecewise linear functions

In standard experiments, most traces appear biphasic. We used a `matlab` code to determine a continuous and piecewise linear function that provided the best fit by minimizing the sum of square deviations. Increasing the number of segments in this function naturally improves the fit and lowers the mean square deviation (MSD). In most cases, the MSD drops sharply for choosing two instead of one segment, but than only decreases slowly for more then two segments, see figure a.1. This drop indicates that there is exactly one kink in the depolymerization trace. The kink of the fitted curve with two segments corresponds

to the duration τ of the initial shrinkage phase. In experiments with a lower pH, we also found filaments exhibiting four phases of depolymerization. In these cases, the MSD drops for four segments.

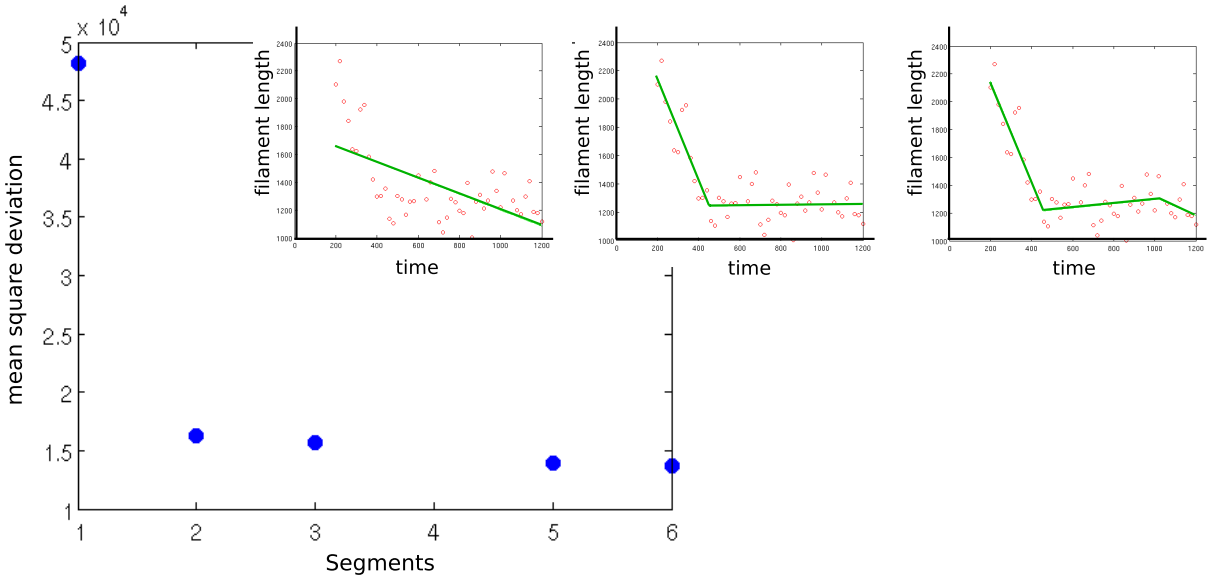

Figure a.1 : Mean square deviation (MSD) for the fits of continuous and piecewise linear functions. The three small panels show fits of such functions with one, two, and three segments to the length-vs-time data from of a single depolymerizing filament. Naturally the MSD decreases as the number of segments increases and approaches zero as the number of segments approaches the number of data points. The sharp drop of the MSD for two segments indicates that there is indeed exactly one kink in the depolymerization trace. The MSD for four segments is missing, as curiously our fitting procedure did not converge for this number of segments.

A.2.4 Failed experiment: Depolymerization of ADP-actin

In an ultimately failed approach to investigate the influence of the nucleotide, and to validate the hypothesis discussed in section 2.2.2, we probed the depolymerization of filaments assembled from ADP-actin. Here, we briefly report the details of the failed experiment.

We obtained ADP-actin by the following procedure: First, the divalent cation Ca^{2+} was exchanged for Mg^{2+}, i.e., ATP-Ca-actin at a concentration of 15.7 μM was converted into (ATP)-Mg-actin by initially adding 27 μM $MgCl_2$ and then 1 mM EGTA. Then, ATP-(Mg)-actin was converted into ADP-(Mg)-actin by addition of 2.5 mM glucose, 30 units/ml of a certain hexokinase and 10 μM diadenosine pentaphosphate (Ap_5A). As in living cells, glucose 6-phosphate is produced by phosphorylation of glucose, catalyzed by the hexokinase. The relevant point is that this reaction consumes one molecule of ATP and produces one molecule of ADP. Ap_5A is needed to prevent the contaminating myokinase from reconverting ADP into ATP and adenosine monophosphate (AMP) [125]. The initial concentrations of the discussed additives were chosen such to have an actin concentration of 15 μM in the final

solution. The buffers were also adjusted to 2.5 mM glucose, 30 units/ml hexokinase and 10 μM Ap_5A.

Because the association constant for ADP-actin is much smaller than the one for ATP-actin [41, 48, 49], we had to polymerize for a longer period (10 min) to get considerable filament lengths. Unfortunately, the filaments bleached very quickly. Within less than 2 s of exposure to the 473 nm laser, the filaments labeled with Alexa488 became invisible. To overcome this problem, we used actin which was labeled with Alexa596 and a 561 nm laser instead. Because of the smaller brightness of this dye, the image quality was poor in this case, but bleaching was not an issue and we were able to observe some filaments for about one hour (one image per minute, 40 ms exposure time per image). Because of the poor image quality, we were only able to analyze $N_\mathrm{f} = 5$ filaments. All filaments exhibited negligible shrinkage and the fluctuations seemed to be greatly hindered. Therefore, we consider this as a failed experiment.

After developing the microfluidic setup, the Carlier lab succeeded in investigating the depolymerization of individual filaments grown from ADP-actin, see chapter 4.

A.3 Appendix of chapter 3: Stochastic modeling

A.3.1 Distribution of duration τ for transitions during polymerization

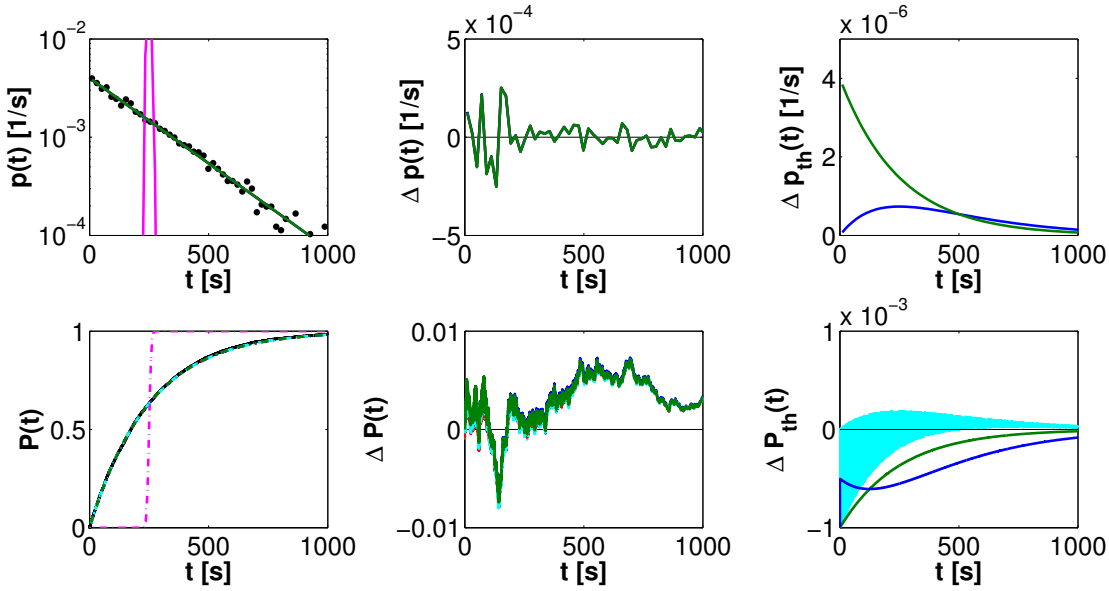

Figure a.2 : Transitions during polymerization: Comparison between theoretical results and simulations of the probability density function $p(t)$ (upper row), and the corresponding cumulative distribution $P(t)$ (lower row). For the pdfs containing δ-functions, only the corresponding cdfs are shown. Realistic values for the dissociation rate $\omega_{\text{off}} = 4/\text{s}$ and the probability $Q = 0.001$ were chosen and 10^4 filaments were simulated. In the left column, the pdfs $p(t)$, and the corresponding cdfs $P(t)$ are shown, encoded with the following colors. The simulation result is displayed in black, eq. (3.77) in red, eq. (3.78) in blue, and eq. (3.79) in magenta, eq. (3.80) in cyan, and eq. (3.81) in green, respectively. The red, blue, cyan, and green curves, as well as the simulation results lie on top of one another, whereas the magenta curve describes a qualitatively different distribution, see page 41 for a discussion. In the column in the middle, the magenta curve is omitted and the differences between the simulation result and the theoretical results are shown. The curves lie on top of one another, indicating that the fluctuations from the finite number of simulation runs are much larger than the difference between the theoretical results. In the right column, the differences between some approximations and the exact solution eq. (3.77) are shown as follows. Eq. (3.78) is shown in blue, (3.80) is shown in cyan, and eq. (3.81) shown in green. The cyan curve appears as an area, since the corresponding cdf involves many small, discrete steps. In summary, all analytical results for the distribution of τ successfully describe the simulations, except for eq. (3.79), where the randomness from the distribution of state-2-protomers along the filament is neglected.

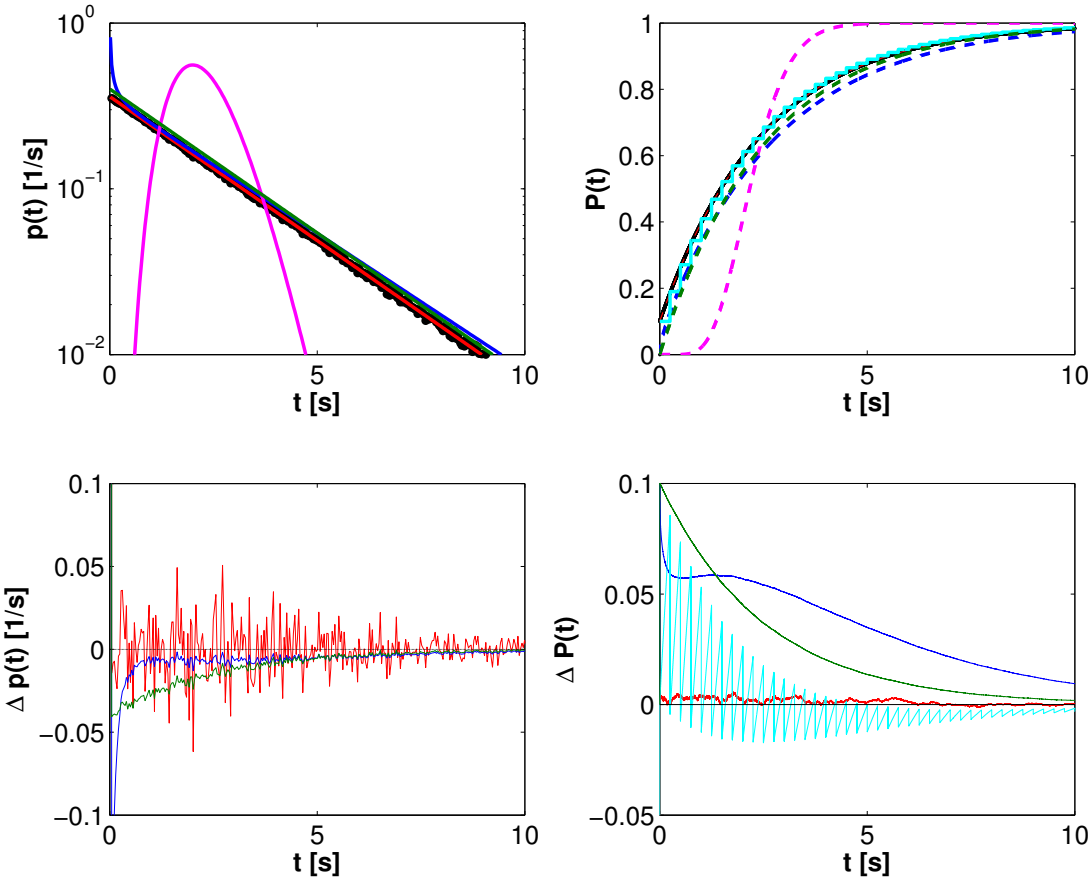

Figure a.3 : Transitions during polymerization: Comparison between theoretical results and simulations of the probability density function $p(t)$ and the corresponding cumulative distribution $P(t)$. The same value for the dissociation rate, $\omega_{\text{off}} = 4/\text{s}$, as in the previous figure was chosen, but the probability Q that a protomer is in state 2 is increased to $Q = 0.1$ in order to illustrate the limit of the theoretical results. 10^6 filaments were simulated. In the upper row, the pdfs $p(t)$, and the cdfs $P(t)$ are shown. In the lower row, the differences between the simulation result and the theoretical results are shown. The same color code as in the previous figure is used. The difference between the simulation and the exact result is enlarged tenfold in the lower graphs (shown in red). As before, eq. (3.79) (in magenta) completely fails to describe the simulations. The other three analytical results (blue, cyan and green) reasonably match the simulation result, but a certain deviation becomes apparent. This is because both approximations rely on the assumption that the typical number of protomers that dissociate is much larger than one, but, in the present case of $Q = 0.1$, the average number of protomers that dissociate is 9. This also leads to the appearance of the steplike shape of the cdf corresponding to eq. (3.80). The exact result (in red) match the simulations, with deviations arising merely from the finite number of simulated filaments.

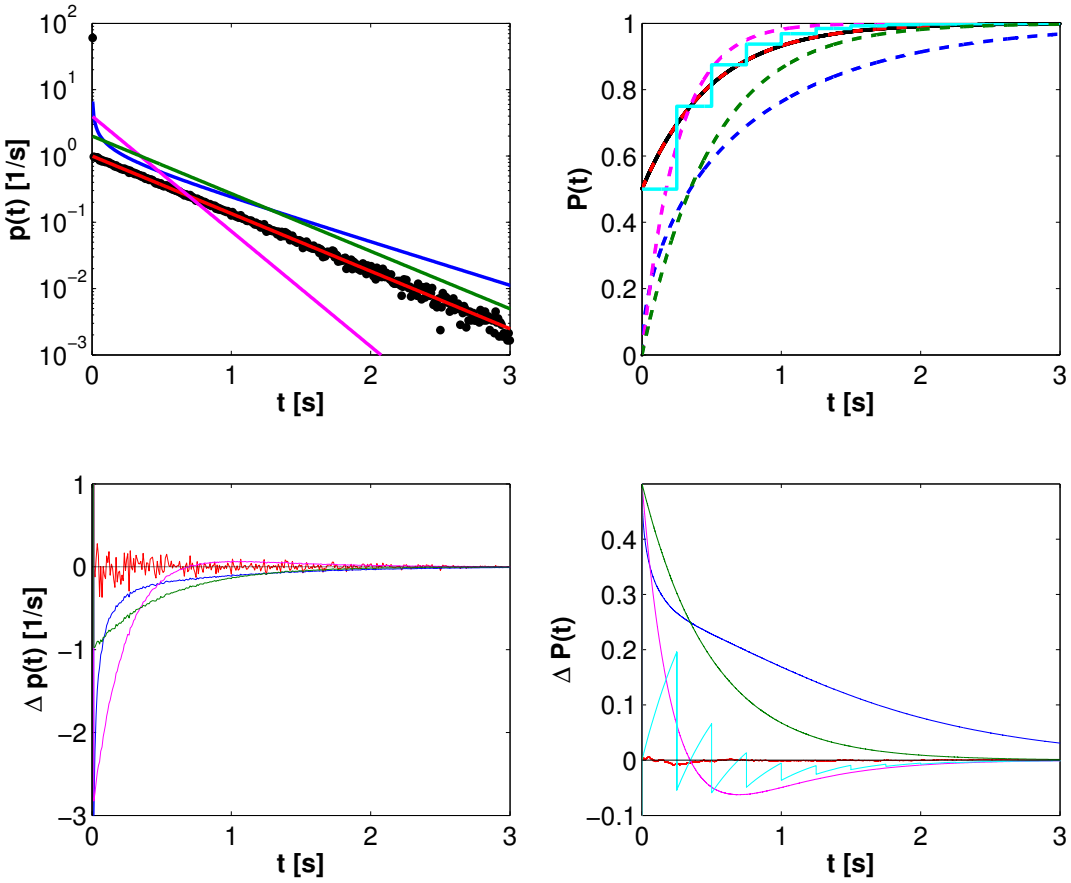

Figure a.4 : Transitions during polymerization: Comparison between theoretical results and simulations of the probability density function $p(t)$ and the corresponding cumulative distribution $P(t)$. The same value for the dissociation rate, $\omega_{\text{off}} = 4/\text{s}$, as in the previous figure was chosen, but the fraction Q of state-2-protomers is further increased to $Q = 0.5$ in order to illustrate the failure of the approximations. 10^6 filaments were simulated. The same quantities as in the previous figure are displayed, employing the same color code. Again, the difference between the simulation and the exact result is enlarged tenfold in the lower graphs (shown in red). For $Q = 0.5$, on average only one protomer dissociates before a state-2-protomer appears at the barbed end. The steplike shape and the decreasing step sizes of the cyan cdf that arises from the deterministic description of depolymerization is very demonstrative. Only the exact solution (shown in red) matches the simulation result.

A.3.2 Mean and variance via asymptotic expansion

Here, we use the asymptotic expansion, eq. (3.108), to calculate the mean μ and variance σ^2 of the duration τ for the case of a vectorial transition mechanism. However, we will first check the normalization of eq. (3.108) by calculating the integral $\int_0^\infty dt\, p(t)$. The corresponding integrals $\int_0^\infty dt\, t\, p(t)$ and $\int_0^\infty dt\, t^2\, p(t)$, which we need to compute μ and σ^2, are solved analogously.

The function $\gamma(t)$, as defined in section 3.4, can be resolved with the transformation

$$\int_0^\infty dt \frac{1}{\sqrt{\gamma^3(t)}}\, e^{-\omega_1 t+\beta_2\gamma(t)} = \frac{2\omega_3 t_\mathrm{p}}{\omega_1}\, e^{\omega_3 t_\mathrm{p}} \int_1^\infty d\gamma\, \gamma^{-1/2} e^{-\omega_3 t_\mathrm{p}\gamma^2+\beta_2\gamma}. \tag{a.2}$$

Now, since $\beta_2 \gg \omega_3 t_\mathrm{p}$, this integral can be approximated and then evaluated [89]:

$$\begin{aligned}\int_1^\infty d\gamma\, \gamma^{-1/2} e^{-\omega_3 t_\mathrm{p}\gamma^2+\beta_2\gamma} &\approx \int_0^\infty d\gamma\, \gamma^{-1/2} e^{-\omega_3 t_\mathrm{p}\gamma^2+\beta_2\gamma} \\ &= (2\omega_3 t_\mathrm{p})^{-1/4}\sqrt{\pi}\exp\left(\frac{\beta_2^2}{8\omega_3 t_\mathrm{p}}\right)\, D_{-\frac{1}{2}}\left(\frac{-\beta_2}{\sqrt{2\omega_3 t_\mathrm{p}}}\right),\end{aligned} \tag{a.3}$$

where $D_\nu(z)$ is a *parabolic cylinder function* [89]. Its asymptotic expansion for negative arguments z, with $|z| \gg 1$ and $|z| \gg |\nu|$ is given by:

$$D_\nu(z) \equiv -\frac{\sqrt{2\pi}}{\Gamma(-\nu)} e^{\nu\pi i} e^{z^2/4} z^{-\nu-1}(1 + O(\nu^2/z^2)). \tag{a.4}$$

With this result and with $\beta_2^2/(8\omega_3 t_\mathrm{p}) = \omega_2 t_\mathrm{p}/2$ and $\beta_2/\sqrt{2\omega_3 t_\mathrm{p}} = \sqrt{2\omega_2 t_\mathrm{p}} \gg 1$, the integral (a.3) is given by:

$$\int_0^\infty d\gamma\, \gamma^{-1/2} e^{-\omega_3 t_\mathrm{p}\gamma^2+\beta_2\gamma} \approx \sqrt{\frac{2\pi}{\beta_2}} e^{\omega_2 t_\mathrm{p}}, \tag{a.5}$$

and we find that $p(t)$ is indeed normalized in the considered limit:

$$\int_0^\infty dt p(t) \approx \sqrt{\frac{\omega_2}{\omega_3}} \frac{\omega_1}{\sqrt{2\pi\beta_2}} e^{-(\omega_2+\omega_3)t_\mathrm{p}} \frac{2\omega_3 t_\mathrm{p}}{\omega_1} e^{\omega_3 t_\mathrm{p}} \sqrt{\frac{2\pi}{\beta_2}} e^{\omega_2 t_\mathrm{p}} = 1. \tag{a.6}$$

Analogous approximations are employed to calculate the mean μ, and variance σ^2:

$$\mu \equiv \langle\tau\rangle \approx \frac{\omega_2 - \omega_3}{\omega_1} t_\mathrm{p}, \tag{a.7}$$

$$\sigma^2 \equiv \langle\tau^2\rangle - \langle\tau\rangle^2 \approx \frac{2\omega_2 t_\mathrm{p}}{\omega_1^2}. \tag{a.8}$$

A.3.3 Distribution of duration τ for vectorial transitions

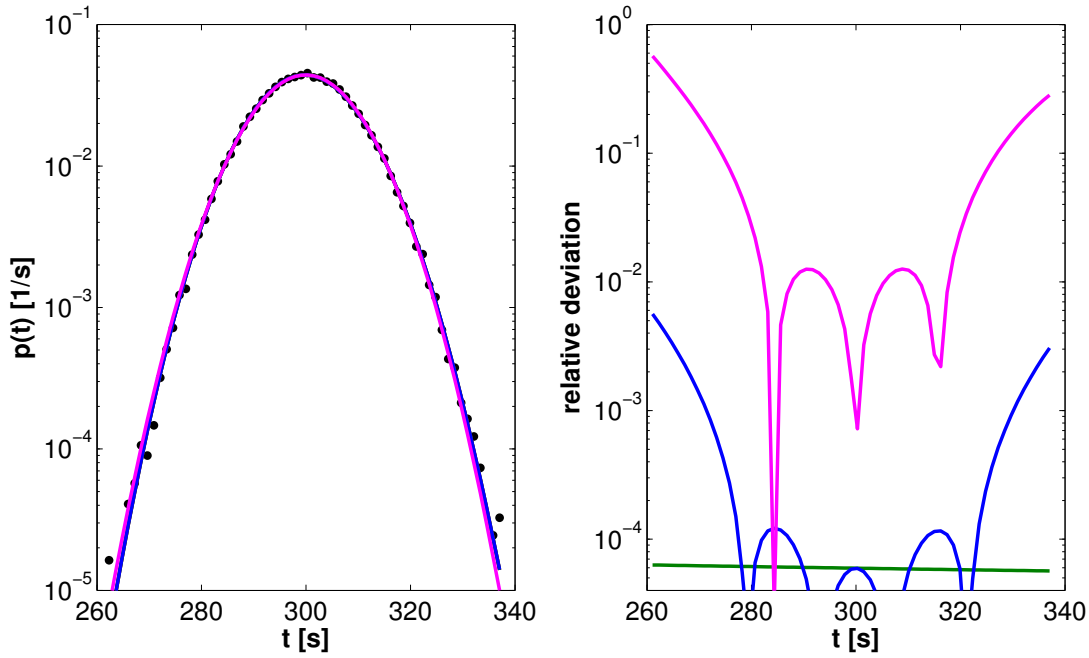

Figure a.5 : Probability density function $p(t)$ for vectorial transition mechanism with the following realistic parameter values. Association rate $\omega_{\text{on}} = 35/\text{s}$, dissociation rate during polymerization $\omega_{\text{off}}^{\text{pol}} = 1/\text{s}$, dissociation rate during depolymerization $\omega_{\text{off}} = 4/\text{s}$, duration of polymerization $t_{\text{p}} = 90$ s. As the average duration of phase I was about 5 min, we have fixed the unknown transition rate at $\omega = 4.77/\text{s}$ in order to satisfy eq. (3.110).
Left hand side: Simulation (black dots) of 10^5 filaments and theoretical results, encoded by the following colors. The analytical solution of the discrete model, eq. (3.136) in red, the asymptotic expansion, eq. (3.137), in green, and the solution of the continuous model, eq. (3.138), in blue, lie on top of one another. The parabolic shapes of the curves in this semilogarithmic plot indicate Gaussian-like functions. The approximation by a Gaussian, (3.139), is shown in magenta and mainly lies on top of the other curves. The simulation result also agrees very well.
Right hand side: Relative deviation of the theoretical results. We have plotted the quantity $|\tilde{p}(t) - p(t)|/p(t)$, where $p(t)$ is the analytical solution of the discrete model, eq. (3.136), and $\tilde{p}(t)$ is given by the asymptotic expansion (in green), the solution of the continuous model (blue), and the Gaussian approximation (magenta), respectively. As expected, the analytical expansion matches best, and the most simplistic approach, namely the Gaussian, is the crudest estimate of the analytical solution. However, within the region of significant density, that is between 280 s and 320 s, even the error from the Gaussian is only about 1%.

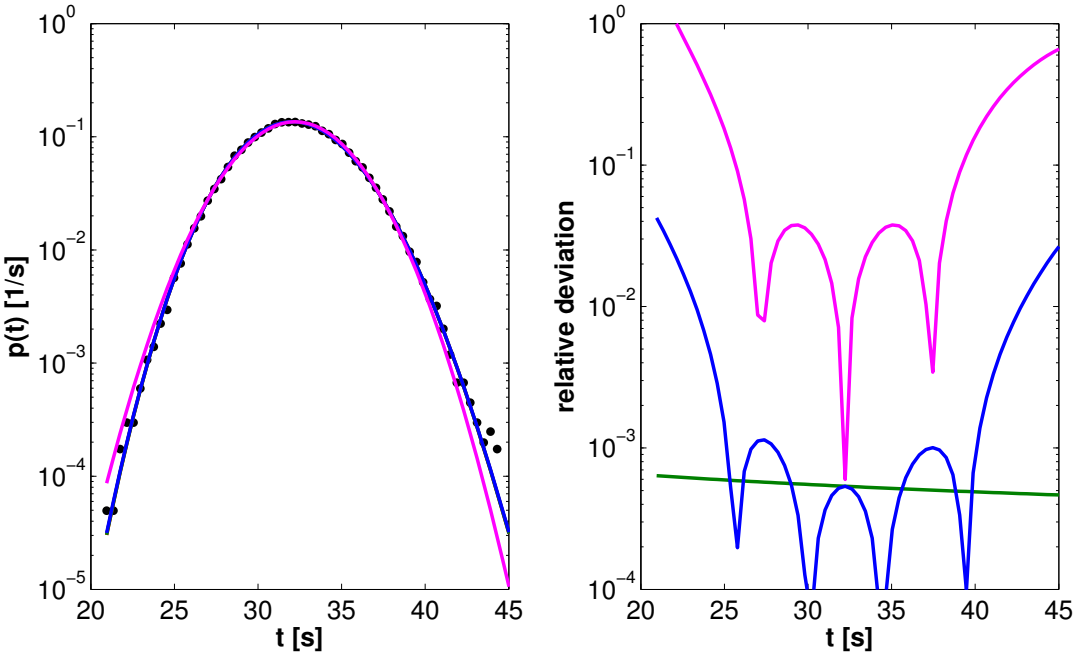

Figure a.6 : Probability density function $p(t)$ for vectorial transition mechanism with the parameter values as in the previous figure, but the duration of polymerization was reduced to the unrealistic value of $t_\mathrm{p} = 10$ s. The value of the transition rate was changed from 4.77/s to $\omega = 5$/s.
Left hand side: Simulation (black dots) of 10^5 filaments and theoretical results, encoded as in the previous figure. The analytical curves still fit the simulations well, but the Gaussian approximation exhibits some deviation.
Right hand side: Relative deviation of the theoretical results, as described in the previous figure. It becomes apparent that the deviation between the asymptotic expansion and eq. (3.136) decreases with increasing time t.

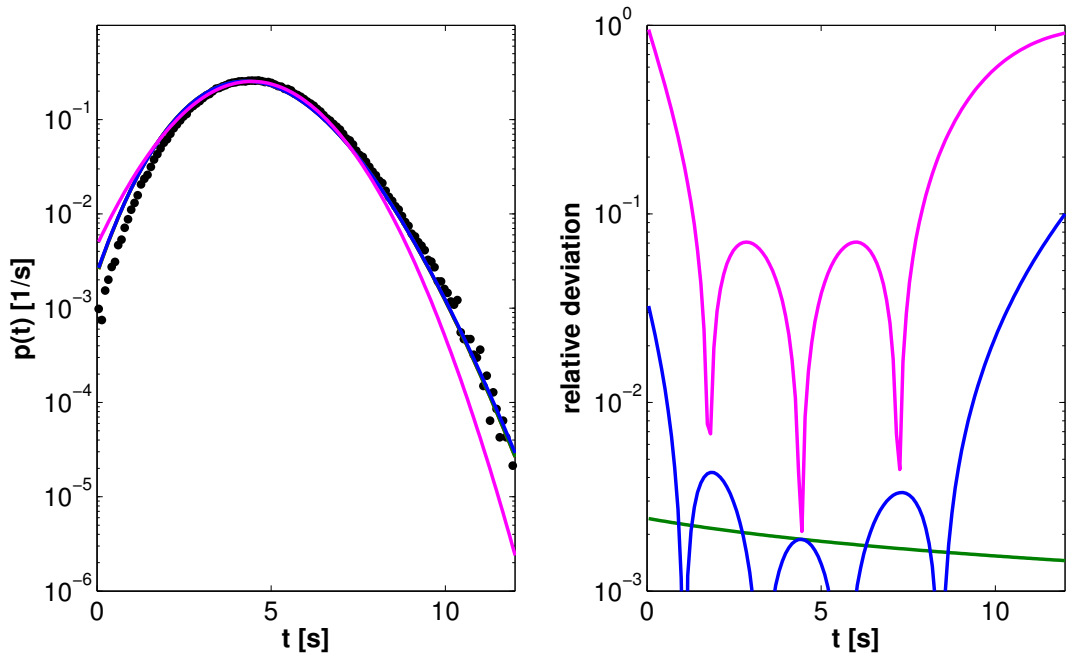

Figure a.7 : Probability density function $p(t)$ for vectorial transition mechanism with the parameter values as in the previous figure, but with an association rate that was reduced to the unrealistic value of $\omega_{\text{on}} = 10/\text{s}$.
Left hand side: Simulation (black dots) of 5×10^5 filaments and theoretical results, encoded as in the previous two figures. The Gaussian approximation fails completely. The other analytical results greatly overestimate the density for small times t. The reason for this is that, during polymerization, the association rate is not much larger than the sum of dissociation and transition rate, and moreover the duration of polymerization is not very large compared to ω_{on}^{-1}. In consequence, neglecting the boundary in the random walk described by eq. (3.87) is not feasible, but leads to an overestimation of the probability of small state-1-segments in eq. (3.91).
Right hand side: Relative deviation of the theoretical results, as described in the previous two figures. Apart form the Gaussian approximation (magenta), there is still good agreement between the other approximations.

A.3.4 Distribution of duration τ for random transitions

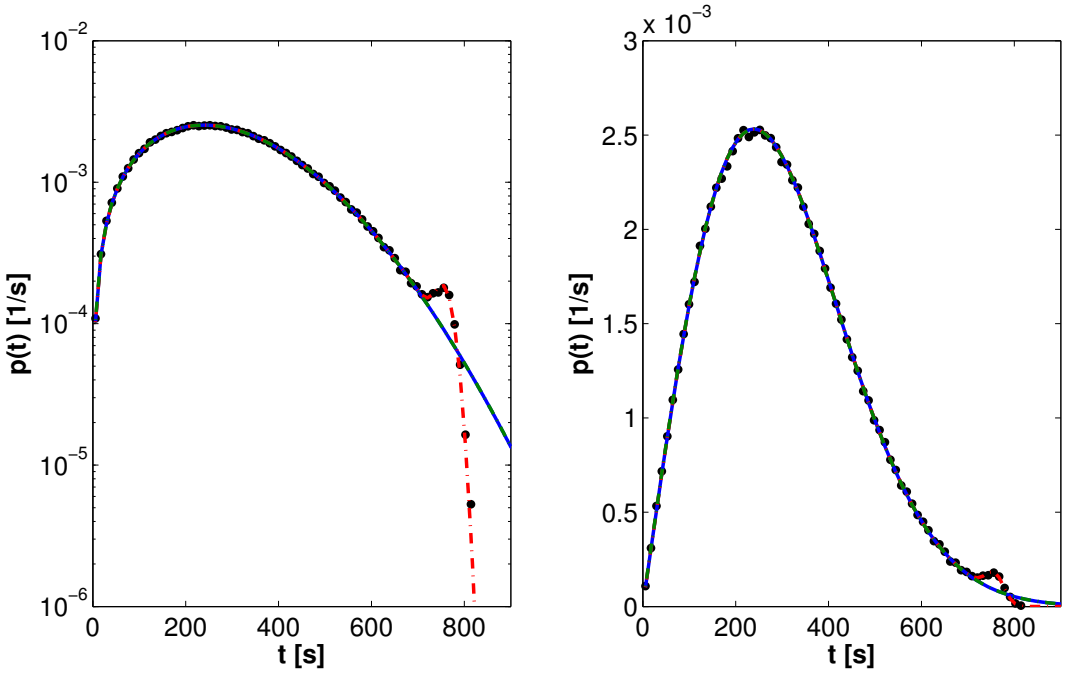

Figure a.8 : Probability density function $p(t)$ for the random transition mechanism, displayed on a logarithmic scale on the left hand side, and on a linear scale on the right hand side. The following realistic parameter values were chosen. Association rate $\omega_{\text{on}} = 35/\text{s}$, dissociation rate during polymerization $\omega_{\text{off}}^{\text{pol}} = 1/\text{s}$, dissociation rate during depolymerization $\omega_{\text{off}} = 4/\text{s}$, duration of polymerization $t_{\text{p}} = 90$ s. As the average duration of phase I was about 5 min, we have fixed the unknown transition rate at $\omega = 3.9 \times 10^{-6}/\text{s}$ in order to satisfy eq. (3.160). Shown are results from simulating 5×10^5 filaments (black dots) and theoretical results, encoded by the following colors: The approximation for small ω, eq. (3.157), is shown in blue, whereas the exact solution under the assumption of a deterministic age, eq. (3.154), is represented by the broken green line. Finally an extended expression – see below – is shown as broken red line.
For the chosen realistic parameter values, the eqs. (3.154) and (3.157) coincide. The agreement with the simulations is very good, except for $t > 700$s, where apparently a neglected effect leads to an additional small peak in the distribution. It turns out that this peak results from the fact that depolymerization also stops when the pointed end is reached, i.e. when a filaments has completely vanished. The peak is therefore centered around $t = v_{\text{pol}} t_{\text{p}} / v_{\text{dep}}$. In section 3.6, we derive an extension of eq. (3.157) which accounts for this effect. The result, eq. (3.170), is shown as broken red line. It agrees well with the simulations. For our experimental parameter values, the probability that a filament depolymerizes entirely is well below 1% – see eq. (3.175) – and thus eq. (3.157) is an appropriate approximation.

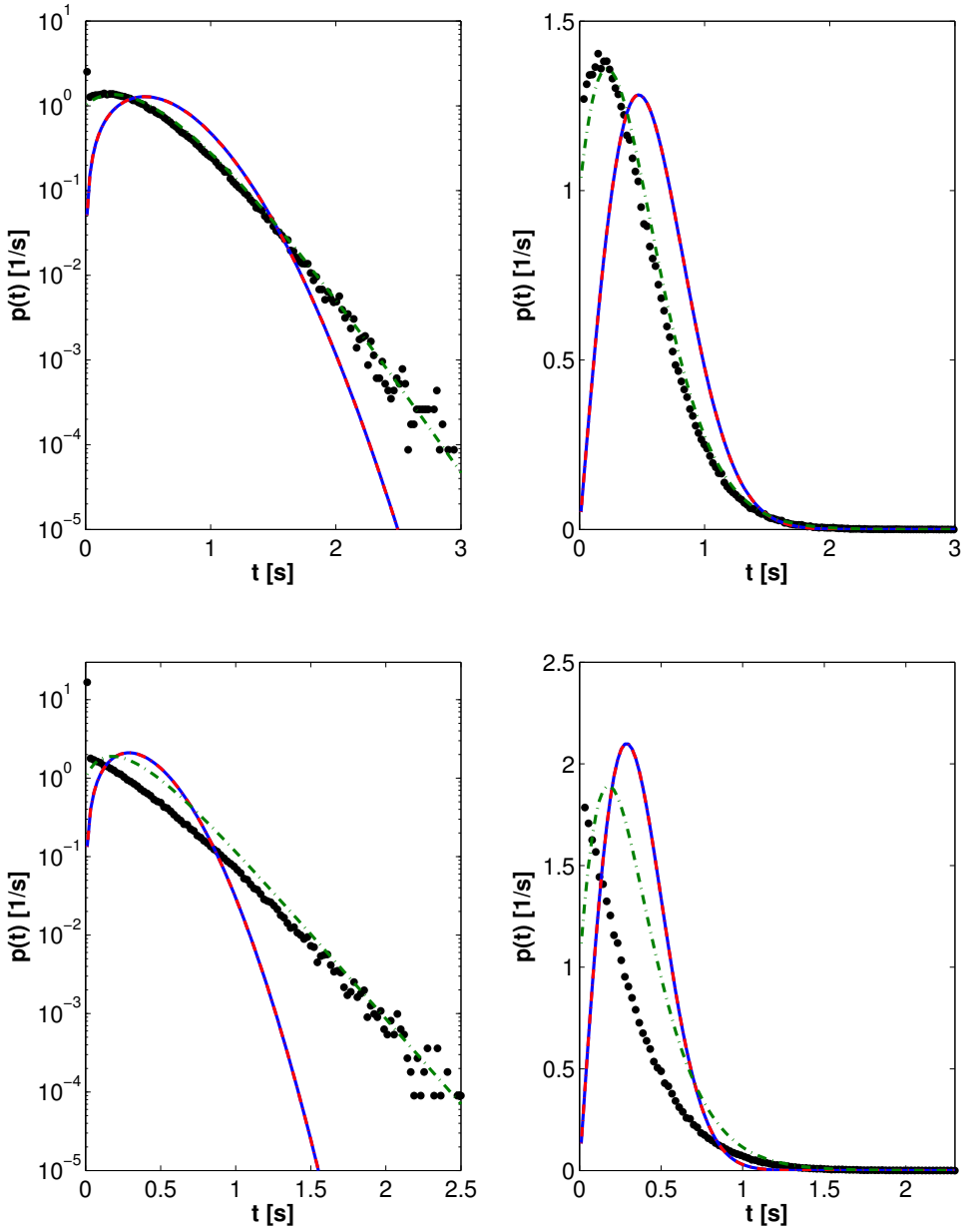

Figure a.9 : Failure of the deterministic age estimation for very large transition rate ω.
Shown is the probability density function $p(t)$ on a logarithmic scale on the left hand side, and on a linear scale on the right hand side. The same color code as in figure a.8 is used and the same parameter values were chosen, unless otherwise indicated.
Top: The transition rate was dramatically increased to the unrealistically large value $\omega = 1/\text{s}$. Eq. (3.157) fails completely, as it involves the simple estimate in eq. (3.156). But also the expression (3.154) exhibits a large deviation from the simulation results for small times t. This is because the stochasticity caused by the dissociation events is no longer small compared to the stochasticity caused by the transitions and thus the age of the penultimate protomer can no longer be describe by eq. (3.151).
Bottom: In addition to the increased transition rate, the association rate was decreased to $\omega_{\text{on}} = 3/\text{s}$. The analytical results completely fail to described the simulation results.

A.3.5 Distribution of duration τ for finite filament lengths

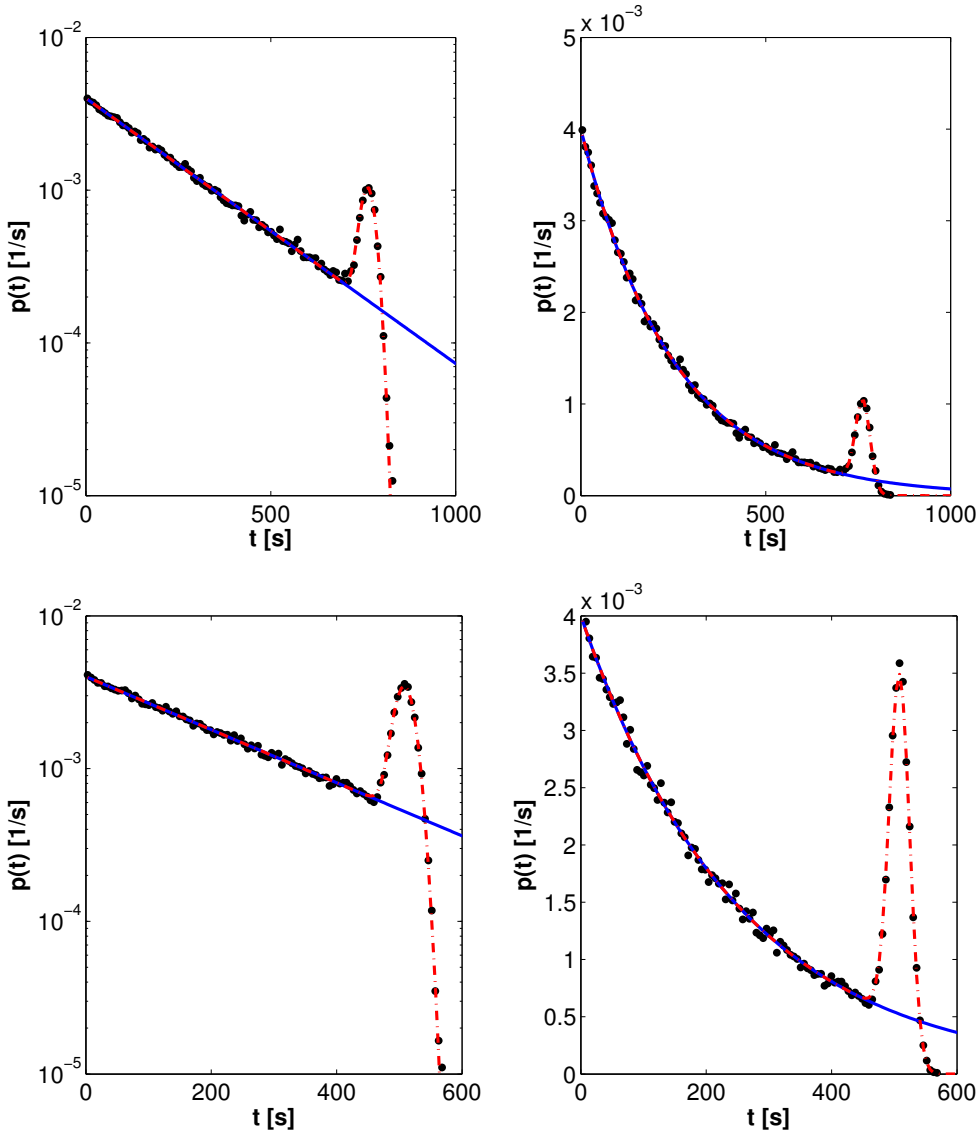

Figure a.10 : Finite size effects for transitions during polymerization.
Shown is the probability density function $p(t)$ on a logarithmic scale on the left hand side, and on a linear scale on the right hand side. Simulation results are shown as black dots, and the simple exponential, eq. (3.81), is shown in blue. The extended pdf in eq. (3.170) was applied for transitions that occur during polymerization – i.e. $p_1(t) = Q\,\omega_{\text{off}} \exp\left(-Q\,\omega_{\text{off}}\,t\right)$ was chosen – and then displayed as dashed red line. Our standard set of parameter values was used: $\omega_{\text{on}} = 35/\text{s}$, $\omega_{\text{off}}^{\text{pol}} = 1/\text{s}$, $\omega_{\text{off}} = 4/\text{s}$, and $Q = 0.001$. For the upper graphs, the realistic polymerization time of $t_{\text{p}} = 90$ s was chosen, for the lower ones we have decreased t_{p} to 60 s to increase the effect of complete depolymerization. In both cases, the extended expression, eq. (3.170) matches the simulations very well, as it correctly considers the finite filament lengths and thus the interruptions caused by complete depolymerization.

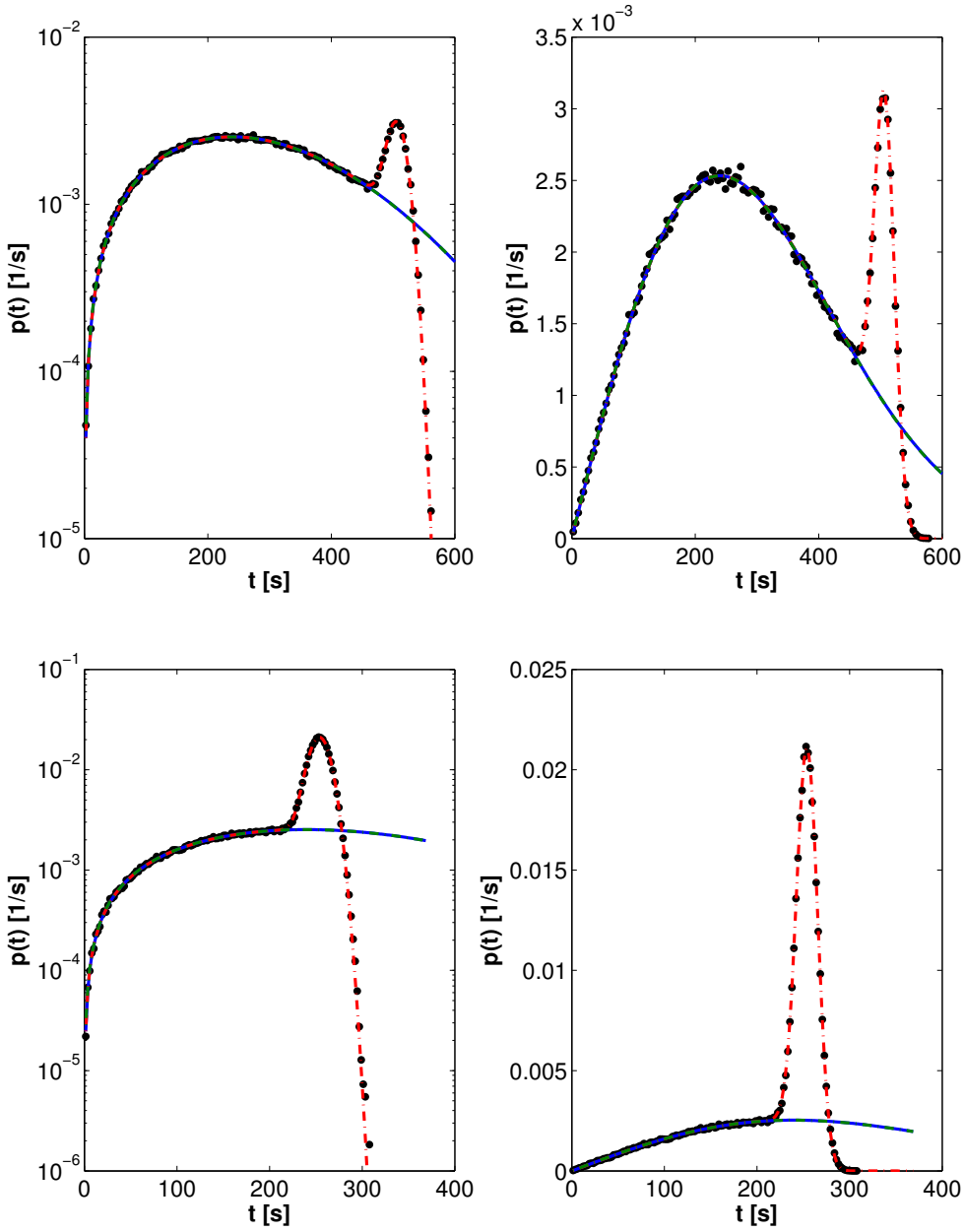

Figure a.11 : Finite size effects for the random transition mechanism.
Shown is the probability density function $p(t)$ on a logarithmic scale on the left hand side, and on a linear scale on the right hand side. The same color code as in figure a.8 is used and the same parameter values were chosen, apart from the polymerization time t_p which was decreased to 60 s for the upper plots and further to 30 s for the lower plots. Both eqs. (3.154) and (3.157) fail to describe the simulation results, since they neglect the increasingly important case of complete depolymerization. On the other hand, the extended expression for the pdf, eq. (3.170), where $p_1(t) = \alpha\,\omega\,t \exp\left(-\alpha\,\omega\,t^2/2\right)$ was inserted, matches the simulations very well.

A.4 Appendix of chapter 4: Filaments in a microflow

A.4.1 Proteins and buffers

Actin was purified from rabbit muscle [72] and labeled with Alexa488 succinimidyl ester. In standard experiments, a labeling fraction (defined as the fraction of Alexa488-actin on the total actin concentration) of 15% was chosen. Later, this fraction was varied between 7% and 20%. ADP-actin was obtained from ATP-actin using hexokinase and glucose, as described in the protocol in appendix A.2.4. Cr-ATP was made as described elsewhere [98]. Spectrin-actin seeds were purified from human red blood cells [74]. Recombinant Profilin I from mouse was expressed in Escherichia coli and purified as described elsewhere [126]. F-buffer contained 5mM TRIS pH 7.8, 0.2 mM ATP, 0.1 mM $CaCl_2$, 0.01% NaN_3, 100 mM KCl, 1 mM $MgCl_2$, 0.2 mM EGTA, and 1 mM DTT. Standard elongation and depolymerization of filaments were done in F-buffer, to which additionally 9 mM DTT and 1 mM DABCO were added to limit photobleaching. ATP-free buffer was used for experiments with ADP-actin.

A.4.2 Microfluidics setup

Flow cells were made with polydimethylsiloxane (PDMS) from Sylgard mounted on standard glass coverslips that were previously cleaned in 1 M NaOH. Molds made of SU-8 photoresist were built at the ESPCI clean room (Paris), with the assistance of Hélène Berthet. The microchambers used were Y- or trident-shaped, having two or three entry channels, respectively. The micro-channels were 42 μm high, and 200-800 μm wide. After adsorption of spectrin-actin seeds, the surface of the coverslip was passivated with bovine serum albumin (BSA) from Sigma. Flow rates were controlled and monitored using a MAESFLO system (Fluigent, Paris). For each channel, the flow rate could be changed instantly throughout the experiment, between zero and a few tens of μL/min. For flow rates below 1 μL/min, the filaments fluctuated thermally away from the surface and were difficult to image. For flow rates above 5 μL/min, the filaments aligned with the flow, and the amplitude of thermal fluctuations was reduced. Observations were carried out between 1 and 3 mm downstream of the entry channel junction. This microfluidics setup allows for fluorescence observation of the filaments during the whole experiment and buffer exchange within less than 1 s. All measurements were performed at room temperature.

A.4.3 Image acquisition and analysis

Observations were carried out using an inverted Olympus IX71 microscope, with a 60x objective (and an additional 1.6x magnification in some cases), using TIRF or epifluorescence. Images were acquired by a Cascade II camera (Photometrics). For TIRF microscopy, a 25 mW laser from Cobolt, emitting at 473 nm, was used for the fluorescence excitation. For epifluorescence microscopy, a X-Cite 120Q light source from Lumen Dynamics was used. The optical microscopy was controlled employing Metamorph. The time interval between images was 20 s, unless stated otherwise. Image stacks were analyzed using `ImageJ`. For the images as shown in figure 4.1(j), the contrast was enhanced using the KymoToolBox plugin (available from fabrice.cordelieres@curie.u-psud.fr). Filaments lengths were extracted from

the images using the tracking program [78]. In the computations, each actin protomer was taken to contribute 2.7 nm to the filament length. The duration τ of the initial shrinking phase was determined by inspection.

A.4.4 Unnoticed pauses

The depolymerization velocity during the initial shrinkage phase is a few protomers per second. Since the resolution of the optical microscope is about 100 protomers, pauses with a duration of less than a few tens of seconds remain unnoticed. In fact, with the chosen time interval between images of 20 s, we cannot reliably detect pauses with a duration of less than about 80 s. However, as the pause durations are exponentially distributed, with an average duration of about 1000 s, see figure 5.3, it can be concluded that at most 10% of the interruptions/pauses have been missed.

A.4.5 Control experiments

By performing the following measurements, it was verified that the microflow had no impact on the dynamics of the filaments. Filaments were elongated under various constant flow rates, ranging from a few tens of nL/min to a few tens of μL/min, and the resulting elongations were the same. Filaments were depolymerized under constant flow rates, ranging from two to a few tens of μL/min, and the resulting depolymerization curves were the same. Filaments were depolymerized with flow rates that oscillated over a period of 30 s (25 s at 200 nL/min, followed by 5 s at a few tens of μL/min, during which the image was acquired) and the resulting depolymerization curves were the same.

By monitoring the elongation of filaments, it was verified that filaments were growing with a constant polymerization velocity v_{pol} which was compatible with the association rate constant known from solution assays: $v_{\text{pol}} \simeq c_{\text{actin}}/\mu\text{M} \times 10/\text{s}$ and $v_{\text{pol}} \simeq c_{\text{actin}}/\mu\text{M} \times 7/\text{s}$ was measured for ATP-actin and profilin-ATP-actin, respectively.

In standard assays, fragmentation events were rare, and pauses during elongation or annealing events were not observed. In some experiments, the filaments were not monitored during elongation, and their growth rate was computed by measuring the length before and after elongation, and dividing the difference by the duration of elongation. In these experiments, we could verify that nearly all filaments exhibited the expected elongation rate. The few filaments that did not, presumably due to fragmentation, were discarded. In some assays, a certain fraction of filaments, between a few and 15%, did not depolymerize at all. When these non-depolymerizing filaments were not taken into account, very reproducible results were obtained. Therefore, the non-depolymerizing filaments were excluded from the data analysis.

A.5 Appendix of chapter 5: Elucidation of the local transition mechanism

A.5.1 Variation of labeling and illumination

The depolymerization of filaments labeled with various fractions of Alexa488-actin (7% - 20%) was monitored. As discussed in section 5.1, the labeling fraction has a crucial impact on the occurrence of interruptions/pauses, i.e. on the intermittency of depolymerization. On the other hand, no effect of the labeling fraction on the depolymerization velocity was detected.

By performing many control experiments with different exposure times (10 - 50 ms in TIRF, and 100 - 500 ms in epifluorescence) and with different time intervals between acquisitions (4 - 120 s), it was verified that illumination has no effect on the depolymerization velocity. However, the illumination seemed to have a strong influence on the occurrence of interruptions/pauses. The following experiments were performed to quantitate this.

An epifluorescence microscopy with a Lumen Dynamics X-Cite 120Q light source and a Semrock Brightline 482/35 filter was utilized. The setup ensures a very flat spectral density for wavelengths between 464.5 and 499.5 nm. This range of wavelengths contains 93% of the light intensity.

To determine the light intensity in the sample, the power entering the rear of the objective was separately measured with a laser power meter (Coherent, Fielm MAXII-TO). Assuming that there is almost no loss in the objective, in the microscope oil, and in the coverslip, this power corresponds to the overall power illuminating the sample. For the four data sets shown in figure 5.1(b), three different power settings of the light source, with a measured power of 1.80 mW, 0.66 mW, and 0.30 mW, were used. Since all light is focused by the objective to a spot with a diameter of 150 μm, corresponding to an illuminated area of 0.0177 mm^2, these values correspond to illumination intensities of 102 mW/mm^2, 37 mW/mm^2, and 17 mW/mm^2, respectively.

Apart from the lowest (magenta) curve in figure 5.1(b), the filaments were illuminated every 20 s with an exposure time of 0.5 s, leading to an average intensity of 2.54 mW/mm^2, 0.93 mW/mm^2, and 0.42 mW/mm^2, respectively. For the lowest magenta curve, the average intensity was further decreased to 0.21mW/mm^2 by doubling the interval to 40s, and keeping the illumination intensity at 17mW/mm^2.

The effect of photobleaching was estimated by repeatedly measuring the length of fluorescent segments embedded in non-labeled filaments (fabricated by sequentially polymerizing filaments with labeled and non-labeled actin) and was found negligible in our experiments.

A.5.2 Error bars for the transition rate ω

In figure 5.1, we specified the error bars for the single fitting parameter, provided by the transition rate ω, as follows. The upper and lower confidence bounds for the ecdf were determined by Greenwood's formula [101], where a confidence level of 70% was chosen. Both confidence bounds were fitted with eq. (4.1) and in each case, the 70% confidence interval for the parameter ω was determined. The lower bound of the error bar is chosen

to be the lower parameter bound of the lower confidence bound of the ecdf. Analogously, the upper bound of the error bar is chosen to be the upper parameter bound of the upper confidence bound of the ecdf. Thus, the probability that the true value of ω lies within the error bar is at least $0.7 \times 0.7 \simeq 50\%$.

A.5.3 Preformed covalent dimers

Cross-linked actin dimers were formed in F-actin by N,N′-p-phenylenedimaleimide (pPDM) [102] which forms a covalent bond between Cysteine-374 of one protomer and Lysine-191 of an adjacent protomer [103]. After depolymerization of the filaments, the resulting concentration of dimers was determined by SDS-PAGE. These preformed dimers were mixed with labeled actin for incorporation in the filaments shown in figure 5.5 and were used for comparison and calibration in the Western Blots shown in figure 5.6.

A.5.4 Copolymerization of actin monomers and preformed actin dimers

As shown in figure 5.5, we also studied the depolymerization of individual filaments that were copolymerized from G-actin monomers and preformed actin dimers. Since we were interested in the pauses caused by the preformed dimers and not in those caused by the photo-induced dimers, we used a low illumination intensity to observe the filaments. For these illumination conditions, we first determined the transition rate ω by studying the depolymerization of filaments grown from actin monomers with labeling fraction $X_{\mathrm{fl}} = 0.1$ in the absence of preformed dimers. As before, we identified those filaments that did not shrink at all. We excluded this small non-depolymerizing fraction R_0 and applied the Kaplan-Meier-estimator to obtain the empirical cumulative distribution function $\hat{P}(t)$. This distribution, which corresponds to the blue multi-step function in figure 5.5(a), was then fitted to eq. (4.1), from which we obtained the transition rate $\omega \simeq 4.9 \times 10^{-7}/\mathrm{s}$.

Next, we studied the depolymerization of filaments that were copolymerized from actin monomers, again with labeling fraction $X_{\mathrm{fl}} = 0.1$, and preformed dimers. The molar concentration of monomeric actin was kept close to 2μM (it varied between 2 and 2.1μM) whereas the molar concentration of the preformed dimers was chosen to be 2, 4, and 8 nM. In this case, the data analysis was performed as follows. First, we applied the Kaplan-Meier-estimator to the experimental data to obtain the experimental cumulative distribution function $P_{\mathrm{exp}}(t)$. These data still included a certain fraction R_0 of non-depolymerizing filaments. However, unlike in the absence of preformed dimers, we cannot directly detect R_0. In the presence of preformed dimers a considerable number of filaments might exhibit very early pauses. These filaments can not be distinguished experimentally from the non-shrinking filaments. Therefore, the multi-step function $P_{\mathrm{exp}}(t)$ was fitted by the distribution $R_0 + (1 - R_0)\, P(t)$, where the cumulative distribution function $P(t)$ is now given by eq. (5.9). The latter distribution function describes the combined effect of preformed and photo-induced dimers and depends on the fraction Q_0 of preformed dimers initially present in the filaments. In this analysis, we used both the fraction R_0 of non-depolymerizing filaments and the fraction Q_0 of preformed dimers as fit parameters. The reddish data shown in figure 5.5(a) represent the empirical cumulative distribution functions as given by $\hat{P}(t) = (P_{\mathrm{exp}}(t) - R_0) \,/\, (1 - R_0)$.

A.5.5 Quantification of photo-induced dimers by Western Blots

F-actin solutions were placed in a quartz cuvette, and exposed to collimated light from the Xcite lamp of the microscope, with an illumination intensity of 0.04 mW/mm^2. The dimer-to-monomer ratio in these samples was determined from the Western Blots, using the `gels` analysis function in `ImageJ`, and using the preformed dimer solutions for calibration. No dimers were found in the unexposed non-labeled actin sample. The dimer concentrations measured in the samples of labeled-actin were consistent with the transition rates ω_{fl} determined from the cumulative distributions of pauses: a dimer-to-monomer ratio of approximately 3×10^{-3} was measured in F-actin with 41.6 % Alexa488 exposed for 2.5 hours (sample shown in figure 5.6), and a ratio of approximately 4×10^{-4} was measured in F-actin with 10% Alexa488 exposed for 1 hour.

A.5.6 Different fluorescent labels

We performed additional experiments with Alexa594 or Atto594, bound to the surface lysines, and Alexa488 bound to Cysteine-374. In all cases, we again observed intermittent depolymerization with the characteristic cumulative distribution function of the duration τ. Taking differences in labeling fraction and illumination intensity into account, we estimate that labeling actin with Alexa594, Atto594, and Alexa488-Cysteine-374, leads to a fivefold, ninefold, and 30-fold increase of the protomer transition rate ω, compared to labeling with Alexa488 on lysines (data not shown). Gel electrophoresis and immunodetection of corresponding F-actin solutions directly confirm the formation of dimers for all three additionally tested species of fluorescently labeled actin. The corresponding dimer-to-monomer ratios are consistent with the estimates for ω obtained from the cumulative distribution functions of τ (data not shown).

A.5.7 Dimerization of G-actin

Photo-induced dimerization was also observed in illuminated solutions of labeled G-actin, see figure a.12. In contrast to actin filaments, in which the protomers are in permanent contact with their neighbors, monomers in G-actin buffer come into contact via collisions, with a frequency that depends quadratically on their concentration. Based on our results for 52 μM G-actin (see figure a.12), the dimerization rate in 1 μM G-actin is estimated to be about 30 times smaller than for F-actin, under identical illumination conditions. In conventional microscopy experiments, the relative importance of photo-induced G-actin dimerization is further reduced by the diffusive motion of monomers in and out of the illuminated region, hereby receiving less light than the protomers within the filaments. In our microfluidics experiments, photo-induced dimerization of G-actin is certainly irrelevant, because filaments elongate from fresh G-actin that constantly entered the flow cell without being previously illuminated. In fact, if G-actin dimers were present and incorporated into the filaments, they would affect the cdf $P(t)$ in the same way as the preformed dimers: this distribution would no longer have a sigmoidal shape as in figure 4.3 but rather a convex shape as the three upper curves in figure 5.5(a).

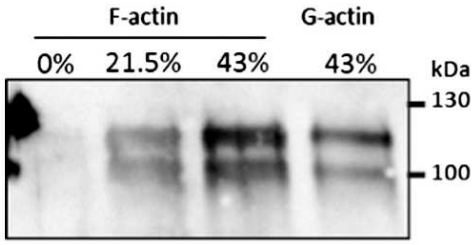

Figure a.12 : Additional Western blots for solutions of Alexa488-labeled actin. The first three columns display Western blots for actin filament solutions with labeling fraction $X_{\mathrm{fl}} = 0$, 0.215, and 0.43; the right column corresponds to G-actin solutions with labeling fraction $X_{\mathrm{fl}} = 0.43$. The filament solutions had an actin concentration of 50 μM and were exposed to an illumination intensity of 0.04 mW/mm^2 for 1 h. The G-actin solution had an actin concentration of 52 μM and was exposed to the same illumination protocol. For the F-actin buffer, the dimer-to-monomer ratio increases linearly with the labeling fraction X_{fl} according to $\rho \simeq 2.5 \times 10^{-3} X_{\mathrm{fl}}$. For the G-actin buffer, the dimer-to-monomer ratio is $\rho \simeq 1.45 \times 10^{-3}$.

A.6 Appendix of chapter 6: Mechanism of ATP hydrolysis

A.6.1 Additional theoretical results: Fast random transitions

As a supplement, we consider the theoretically interesting case that the time scale of the disassembly is not separated from the time scale of the random transitions within the filament, that is the asymptotic approximation (6.11) does not hold. From the equations (6.3) and (6.9), and the relation $\partial_t L(t) = -v_{\mathrm{dep}}(t)$ for the average filament length $L(t)$, the probability $\mathcal{P}_1(t)$ can be eliminated and a second order differential equation for $L(t)$:

$$\partial_t^2 L(t) = -\left((v_{\mathrm{D}} - v_{\mathrm{DP}})\, e^{-\omega_{\mathrm{r}}\left(t + t_{\mathrm{p}} - L(t)/v_{\mathrm{pol}}\right)} + v_{\mathrm{D}} \right) \partial_t L(t) - v_{\mathrm{DP}} v_{\mathrm{D}}, \tag{a.9}$$

with the initial conditions

$$\partial_t L(t)|_{t=0} = -v_{\mathrm{DP}} \tag{a.10}$$

$$L(0) = L_0 \tag{a.11}$$

follows. Again, the differential equation can not be solved explicitly, as $\partial_t^2 L(t)$ depends in a non-algebraic way on $L(t)$. However, partial derivatives with respect to the parameters can be calculated in order to fit the resulting curve to the experimental data, as discussed in section 6.3.

Note that the previous equation (6.13) is consistent with our general eq. (a.9), as it directly follows for vanishing $\partial_t^2 L(t)$, i.e. vanishing curvature of the shrinking curve on a time scale defined by the shrinking velocity.

Finally, we discuss another asymptotic approximation of the model. We consider the limit of instantaneous polymerization, i.e. $v_{\mathrm{pol}}/v_{\mathrm{dep}}(t) \to \infty$, or $t_{\mathrm{p}}/t \to 0$. In this case, the age of a protomer is simply given by the time t since the initiation of depolymerization, that is at $t = 0$ we effectively start from a filament containing only ADP-Pi-protomers. In

consequence, the dependence on $L(t)$ vanishes in eq. (6.9), and according to [127] the formal solution of the differential equation is given by:

$$\mathcal{P}_1(t) \approx f(t,0) + v_\mathrm{D} \int_0^t dt' \; f(t,t') e^{-\omega_\mathrm{r} t'}, \tag{a.12}$$

where

$$f(t,t') \equiv \exp\left(-v_\mathrm{DP} \; (t-t') + \frac{v_\mathrm{D} - v_\mathrm{DP}}{\omega_\mathrm{r}} \left(e^{-\omega_\mathrm{r} t} - e^{-\omega_\mathrm{r} t'} \right) \right). \tag{a.13}$$

The average length as a function of time can be formally written as

$$L(t) \approx L_0 - v_\mathrm{D} t + (v_\mathrm{D} - v_\mathrm{DP}) \int_0^t dt' \left(f(t',0) + v_\mathrm{D} \int_0^{t'} dt'' f(t',t'') e^{-\omega_\mathrm{r} t''} \right). \tag{a.14}$$

In our experiments, the polymerization is not particularly fast, and thus the asymptotic expansion does not apply. However, one can envisage experiments where either the polymerization is speeded up by a large actin monomer concentration, or – more realistically – the filaments are kept in the ADP-Pi-state during polymerization by an excess of phosphate in the buffer. We validated the equations (a.9) and (a.14) by extensive stochastic simulations similar to those discussed in section 6.4. Within their respective scope of application, the expressions match the simulated filament lengths $L(t)$.

A.6.2 Additional figures

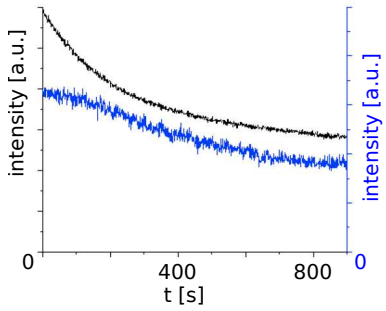

Figure a.13 : Time course of depolymerization in bulk solution. As the fluorescence of pyrene-F-actin is increased 25-fold compared to pyrene-G-actin [73], the pyrene fluorescence intensity represents the relative amount of polymerized actin in the bulk. Filaments were grown from 0.25 nM spectrin-actin seeds at 2μM actin (50% pyrene labeled) and depolymerized by 6-fold dilution in the presence of 5μM Latrunculin A. Blue curve, right y-axis: Depolymerization was initiated at times at which 20% of actin has polymerized. Black curve, left y-axis: Depolymerization was started at times at which 75% of actin has polymerized. Filaments that are switched to depolymerizing conditions in early stages of assembly displayed an accelerating depolymerization on a time scale of a few minutes. Because of our experimental conditions (relatively low actin concentration, many seeds), the barbed ends generated by spontaneous nucleation are negligible.

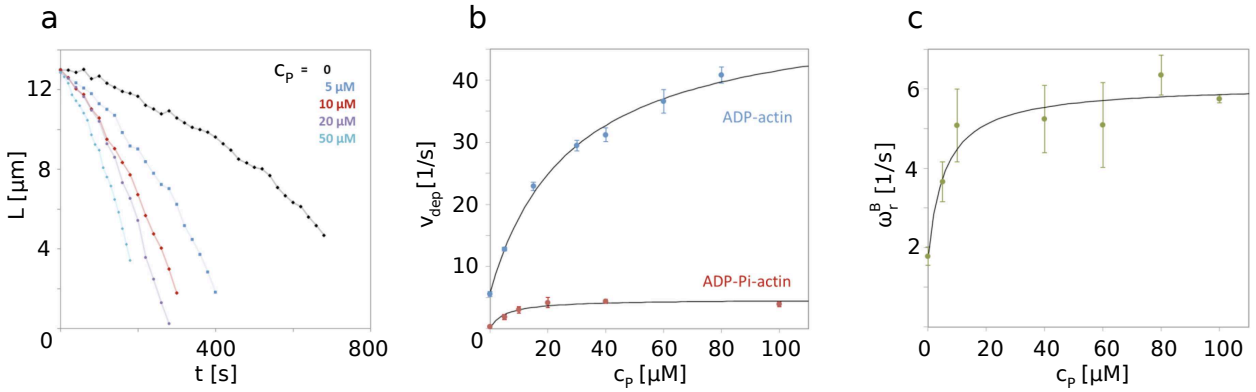

Figure a.14 : Effect of profilin during depolymerization. (a) Depolymerization curves in the presence of the indicated amount of profilin. Polymerization was performed with 1.5μM actin for 5min. The presence of profilin during depolymerization increases the dissociation rates ω_{DPD} and ω_{D} in a concentration dependent manner but does not affect the Pi release rate ω_{r}. (b) Effect of profilin on the depolymerization velocities v_{dep} of ADP-actin and ADP-Pi-actin (measured on CrATP-actin which does not release its phosphate). The lines are saturation curves, given by eq. (6.25), where a rapid equilibrium of profilin with the barbed end was assumed. We find $\mathrm{K}_{\mathrm{D}}^{\mathrm{Pr\text{-}B(DP)}} = 5.9 \pm 0.4\mu\mathrm{M}$, $\omega_{\mathrm{off}}^{\mathrm{PrA(DP)}} = 4.7 \pm 0.4/\mathrm{s}$ for the lower curve and $\mathrm{K}_{\mathrm{D}}^{\mathrm{Pr\text{-}B(D)}} = 28 \pm 5\mu\mathrm{M}$, $\omega_{\mathrm{off}}^{\mathrm{PrA(D)}} = 52 \pm 3/\mathrm{s}$ for the upper curve. (c) Rate of Pi release at the barbed end as a function of profilin concentration. The saturation curve gives a Pi release rate $\omega_{\mathrm{r}}^{\mathrm{B,Pr}} = 6.1 \pm 0.3/\mathrm{s}$ of profilin-actin at the barbed end.

List of symbols

A	(stochastic) protomer age
α	auxiliary variable defined in eq. (3.158), characterizes the polymerization and depolymerization curve
$a(t)$	(deterministic) protomer age as a function of time
$\beta_1(t)$	auxiliary variable defined as $\beta_1(t) \equiv \sqrt{\omega_2/\omega_3}\, \omega_1 t$
β_2	auxiliary variable defined as $\beta_2 \equiv 2\sqrt{\omega_2\omega_3}\, t_\mathrm{p}$
$\Gamma(\nu)$	Gamma function, defined in eq. (3.93)
c_x	concentration of X
$\gamma(t)$	auxiliary variable defined as $\gamma(t) \equiv \sqrt{1 + 2\beta_1(t)/\beta_2} = \sqrt{1 + \omega_1 t/\omega_3 t_\mathrm{p}}$
c^crit	critical concentration
D	diffusion coefficient
D_+	diffusion coeff. for growth of state-1-segment during polymerization
D_-	diffusion coefficient for shrinkage of state-1-segment during phase I
$\delta(z)$	Dirac delta function
∂_x	partial derivative with respect to x
Δ_i	distance of the i-th state-2-site to the barbed end
$D_\nu(z)$	parabolic cylinder function [89]; asympt. expansion given in eq. (a.4)
E	time-averaged illumination intensity
$\mathrm{erf}(z)$	error function, $\mathrm{erf}(z) \equiv \frac{2}{\sqrt{\pi}} \int_0^z dt\; e^{-t^2}$
$\mathrm{erfc}(z)$ . . .	complimentary error function, $\mathrm{erfc}(z) \equiv \frac{2}{\sqrt{\pi}} \int_z^\infty dt\; e^{-t^2} = 1 - \mathrm{erf}(z)$
$G^{(m)}(z,t)$ . .	generating function for $P_n^{(m)}(t)$; defined in eq. (3.31)

$\tilde{G}(z,t)$ . . .	generating function for $\tilde{P}_m(t)$; defined in eq. (3.89)
$I_\nu(z)$	modified Bessel function of the first kind, defined in eq. (3.92)
I	ionic strength
k_{on}	barbed end association rate constant of ATP-actin
k_{B}	Boltzmann constant
$k_{\mathrm{on}}^{\mathrm{cap}}$	barbed end association rate constant of capping protein
$\mathrm{K_D}$	dissociation constant
$\mathrm{K_D^{Pr\text{-}B}}$	dissociation constant of profilin and the barbed end of actin
$\mathrm{K_D^{Pr\text{-}B(DP)}}$ . .	dissociation constant of profilin and the barbed end of ADP-Pi-actin
$\mathrm{K_D^{Pr\text{-}B(D)}}$ . . .	dissociation constant of profilin and the barbed end of ADP-actin
$L, L(t)$ . . .	filament length
ℓ	extend of one protomer within filament, $\ell = 2.7\,\mathrm{mn} \equiv 1$
μ	mean duration of phase I, $\mu \equiv \langle\tau\rangle$
μ_{cd}	mean duration for complete depolymerization, $\mu_{\mathrm{cd}} \equiv \langle\tau_2\rangle$
$N(t)$	length of state-1-segment in discrete description, whole-number random variable
N_0	number of protomers that dissociate before a state-2-protomer appears at the barbed end
$N_1(t)$	number of protomers in state 1
$N_2(t)$	number of protomers in state 2
m, n, n_0 . . .	integral variables
N_{f}	number of filaments in particular experiment
$P(t)$	cumulative distribution function (cdf) of the random variable τ, defined in eq. (3.2)
$\hat{P}(t)$	empirical cumulative distribution function (ecdf) of a sample
$P_1(t)$	cumulative distribution function (cdf) of τ_1

$\mathcal{P}_1(t)$ . . . . probability that terminal protomer is in the ADP-Pi-state when it appears at the barbed end

$P_2(t)$ . . . . cumulative distribution function (cdf) of τ_2

$\mathcal{P}_2(t)$ . . . . probability that the penultimate protomer is in the ADP-Pi-state

$p_A(a)$ . . . . probability density function (pdf) of the stochastic protomer age A

$p(t)$ . . . . . probability density function (pdf) of the random variable τ, defined in eq. (3.3)

$p_1(t)$ . . . . . probability density function (pdf) of τ_1

$p_2(t)$ . . . . . probability density function (pdf) of τ_2

$P(t\,|B)$ . . . conditional cdf of τ, defined in eq. (3.4)

$p(t\,|B)$ . . . conditional pdf of τ, defined in eq. (3.5)

$\Phi(z)$ . . . . . standard normal integral, defined as $\Phi(z) \equiv 1/\sqrt{2\pi}\int_{-\infty}^{z} dy\; e^{-y^2/2}$

$\mathrm{pK_a}$ . . . . . negative logarithm of acid dissociation constant

$\tilde{P}_m(t)$ . . . . length distribution of state-1-segments at the beginning of depolymerization, defined in eq. (3.84)

$P_n^{(m)}(t)$ . . . probability for $N(t) = n$, given that $N(0) = m$; defined in eq. (3.26)

$P_n(t)$ . . . . probability for $N(t) = n$

$\mathcal{P}_{\mathrm{Pr}}$ . . . . . probability that profilin binds to the barbed end

$\mathrm{prob}\,(A)$ . . probability of event A

$\mathrm{prob}\,(A \mid B)$ conditional probability of event A given event B

$p_{X_0}(x_0)$ . . . probability density function (pdf) of the random variable X_0

$p(x,t)$ . . . . probability density function (pdf) of the random variable $X(t)$

$p(x,t\,|x_0)$. solution of the diffusion equation for the initial pdf $p(x,0) = \delta(x - x_0)$

$\hat{p}(x,t\,|x_0)$. solution of the diffusion equation for the initial pdf $p(x,0) = \delta(x - x_0)$ and an absorbing boundary at the origin

$Q(t)$ . . . . . time-dependent probability for a protomer to be in state 2

q . . . . . number density for state 2 in a continuous filament description

Q_0 . . . . . time-independent probability for a protomer to be in state 2, i.e. fraction of preformed dimers in filament

$S(t)$ . . . . . survival function

σ . . . . . variance of duration of phase I, $\sigma \equiv \langle \tau^2 \rangle - \langle \tau \rangle^2$

σ_{cd} . . . . . variance of duration of complete depolymerzation, $\sigma_{\mathrm{cd}} \equiv \langle \tau_2^2 \rangle - \langle \tau_2 \rangle^2$

$\mathfrak{S}(t)$ . . . . . filament state, defined in eq. (3.1)

$\mathfrak{s}_i(t)$ . . . . . state of i-th protomer, with $i = 1$ denoting the pointed end, and $i = L$ the barbed end

T . . . . . thermodynamic temperature

τ . . . . . duration of depolymerization phase I

τ_1 . . . . . duration until protomer in state 2 appears at the barbed end

τ_2 . . . . . duration until filament has completely depolymerized

τ_{II} . . . . . duration of depolymerization phase II

$\langle \tau \rangle$ . . . . . mean of τ, averaged over filament population

$\langle \tau \rangle_{\mathrm{obs}}$ . . . . observed mean duration $\langle \tau \rangle$, averaged only over filaments with two observed phases of depolymerization

t_{cc} . . . . . duration of delay, i.e. the time that the filaments are kept at the critical concentration

τ_{D} . . . . . for vectorial Pi release mechanism: time until segment of ADP-actin reaches the barbed end

τ_{df} . . . . . time of filament detachment or fragmentation

$\Theta(z)$ . . . . . Heaviside step function with $\Theta(0) \equiv 1$

t_{lag} . . . . . lag time after the initiation of depolymerization

t_{p} . . . . . duration of polymerization

u . . . . . drift coefficient in diffusion equation

u_+ . . . . . drift coefficient for growth of state-1-segment during polymerization

u_- . . . . . drift coefficient for shrinkage of state-1-segment during phase I

v . . . . . shrinkage velocity

v_{I} . . . . . apparent shrinkage velocity during depolymerization phase I

v_{II} . . . . . apparent shrinkage velocity during depolymerization phase II

v_{dep} . . . . . barbed end depolymerization velocity during phase I

v_{D} . . . . . depolymerization velocity caused by barbed end dissociation of ADP-actin with rate ω_{D}

v_{DP} . . . . . depolymerization velocity caused by barbed end dissociation of ADP-Pi-actin with rate ω_{DP}

v_{DPD} . . . . depolymerization velocity caused by barbed end dissociation with effective rate ω_{DPD}

v_{pol} . . . . . barbed end polymerization velocity

$X(t)$ . . . . . length of state-1-segment in continuous description, real-valued random variable

X_{fl} . . . . . labeling fraction

X_0 . . . . . length of filament segment that depolymerized, before state-2-site appears at the barbed end

x, x_0 . . . . . real-valued variables

Ω . . . . . pause termination rate

ω . . . . . transition rate for transitions from state 1 to state 2

ω_{21} . . . . . reverse transition rate, i.e. transition rate from state 2 to state 1

$\hat{\omega}$ . . . . . transition rate for transitions from filament state with state-1-protomer at the barbed end to state with state-2-protomer at the barbed end

ω_{c} . . . . . ATP cleavage rate

$\omega_{\mathrm{Cr\text{-}DP}}$ . . . . barbed end dissociation rate of Cr-ADP-Pi-actin

ω_{D} . . . . . barbed end dissociation rate of ADP-actin

ω_{DP} . . . . . barbed end dissociation rate of ADP-Pi-actin

ω_{DPD} . . . . effective barbed end dissociation rate of ADP-Pi-actin, given by eq. (6.2)

$\omega_{\mathrm{N}}^{\mathrm{E}}$ . . . . . dissociation rate of actin with bound nucleotide N (= T, DP, P) from the end E (= B, P)

$\omega_{\mathrm{on,\,N}}^{\mathrm{E}}$ . . . . association rate of actin with bound nucleotide N (= T, DP, P) at the end E (= B, P)

ω_{fl} . . . . . transition rate of fluorescently labeled protomers

ω_{off} . . . . . barbed end dissociation rate of state 1 during depolymerization

$\omega_{\mathrm{off,2}}$ . . . . . barbed end dissociation rate of state 2, i.e. barbed end dissociation rate of photo-induced dimer

ω_{on} . . . . . barbed end association rate of state 1 during polymerization, $\omega_{\mathrm{on}} \equiv \kappa_{\mathrm{on}} c_{\mathrm{actin}}$

$\omega_{\mathrm{off}}^{\mathrm{pol}}$ . . . . . barbed end dissociation rate of state 1 during polymerization

$\omega_{\mathrm{off}}^{\mathrm{PrA}}$ . . . . . barbed end dissociation rate of profilin-actin

$\omega_{\mathrm{off}}^{\mathrm{PrA(DP)}}$ . . barbed end dissociation rate of profilin-ADP-Pi-actin

$\omega_{\mathrm{off}}^{\mathrm{PrA(D)}}$ . . . barbed end dissociation rate of profilin-ADP-actin

$\tilde{\omega}_{\mathrm{pre}}$ . . . . . pause termination rate for filaments containing preformed dimers

ω_{pre} . . . . . dissociation rate (= pause termination rate) of preformed dimer

ω_{r} . . . . . phosphate release rate

$\omega_{\mathrm{r}}^{\mathrm{B}}$ . . . . . phosphate release rate at the barbed end

$\omega_{\mathrm{r}}^{\mathrm{B,Pr}}$ . . . . phosphate release rate at the barbed end for profilin-actin

ω_{T} . . . . . barbed end dissociation rate of ATP-actin

ω_1 . . . . . shrinkage rate of state-1-segment during depolymerization (for vectorial transition mechanism): $\omega_1 \equiv \omega + \omega_{\mathrm{off}}$

ω_2 . . . . . growth rate of state-1-segment during polymerization (for vectorial transition mechanism): $\omega_2 \equiv \omega_{\mathrm{on}}$

ω_3 . . . . . shrinkage rate of state-1-segment during polymerization (for vectorial transition mechanism): $\omega_3 \equiv \omega + \omega_{\mathrm{off}}^{\mathrm{pol}}$

ω_{L} . . . . . transition rate to the left for random walk on a lattice

ω_{R} . . . . . transition rate to the rigth for random walk on a lattice

$\lceil z \rfloor$ . . . . . rounded value of z

$\lfloor z \rfloor$ . . . . . floor function, $\lfloor z \rfloor$ is the largest integer not greater than z

$\lceil z \rceil$ . . . . . ceiling function, $\lceil z \rceil$ is the smallest integer not smaller than z

List of abbreviations and glossary

ABP	actin-binding protein
ADFs	actin depolymerizing factors
ADP	adenosine diphosphate
Alexa	Alexa Fluor, family of fluorescent dyes
AMP	adenosine monophosphate
Ap_5A	diadenosine pentaphosphate
ATP	adenosine triphosphate
Atto	Atto Dye, family of fluorescent dyes
BSA	bovine serum albumin
cdf	cumulative distribution function
DABCO	1,4-diazabicyclo[2.2.2]octane
DTT	dithiothreitol
ecdf	empirical cumulative distribution function
EGTA	ethylene glycol tetraacetic acid
EM	electron microscopy
EMCCD	electron-multiplying charge-coupled device
F-actin	filamentous actin
F-buffer	high salt buffer, used to polymerize actin into F-actin
G-actin	monomeric (globular) actin
G-buffer	low salt buffer, used to store G-actin
GTP	guanosine triphosphate; binds to tubulin

HEPES . . .	4-(2-hydroxyethyl)-1-piperazineethanesulfonic acid
latrunculin A	toxin that bind to G-actin and prevents polymerization
monomer . .	actin protein in solution
MSD	mean square deviation
NEM	N-ethyl-maleimide
pdf	probability density function
PDMS . . .	polydimethylsiloxane
phase I . . .	first phase of depolymerization, characterized by barbed end shrinkage of a few protomers per second
phase II . .	second phase of depolymerization, characterized by vanishing barbed end shrinkage
Pi	inorganic phosphate
pPDM . . .	N,N′-p-phenylenedimaleimide
protomer . .	actin protein within actin filament
pyrene . . .	n-(1-pyrenyl)iodoacetamid
SDS-PAGE	sodium dodecyl sulfate polyacrylamide gel electrophoresis
seed	spectrin-actin seed, nucleus that triggers the barbed end polymerization of actin
SSR	sum of squared residuals
state 1 . . .	protomer state with dissociation rate ω_{off}, present at the barbed end during phase I
state 2 . . .	protomer state with vanishing dissociation rate, present at the barbed end during phase II
TIRFM . . .	total internal reflection fluorescence microscopy
Tris	$(HOCH_2)_3CNH_2$

Bibliography

[1] Pollard, T., Earnshaw, W. & Lippincott-Schwartz, J. *Cell Biology* (Saunders, 2007), 2 edn.

[2] Alberts, B., Johnson, A., Lewis, J., Raff, M., Roberts, K. & Walter, P. *Molecular Biology of the Cell* (Garland Science, 2007), 5 edn.

[3] Straub, F. Actin. *Stud. Inst. Med. Chem. Univ. Szeged.* **II**, 3–15 (1942).

[4] Bray, D. *Cell Movements: From Molecules to Motility* (Garland Publ., 2001).

[5] Pollard, T. & Cooper, J. Actin, a central player in cell shape and movement. *Science* **326**, 1208–1212 (2009).

[6] Pollard, T. & Borisy, G. Cellular motility driven by assembly and disassembly of actin filaments. *Cell* **112**, 453–465 (2003).

[7] Bugyi, B. & Carlier, M.-F. Control of actin filament treadmilling in cell motility. In *Annual Review of Biophysics*, vol. 39, 449–470 (Annual Reviews, 2010).

[8] Engqvist-Goldstein, Å. & Drubin, D. Actin assembly and endocytosis: from yeast to mammals. *Annual review of cell and developmental biology* **19**, 287–332 (2003).

[9] Girao, H., Geli, M. & Idrissi, F. Actin in the endocytic pathway: from yeast to mammals. *FEBS letters* **582**, 2112–2119 (2008).

[10] Dos Remedios, C., Chhabra, D., Kekic, M., Dedova, I., Tsubakihara, M., Berry, D. & Nosworthy, N. Actin binding proteins: regulation of cytoskeletal microfilaments. *Physiological reviews* **83**, 433–473 (2003).

[11] Michelot, A. & Drubin, D. Building distinct actin filament networks in a common cytoplasm. *Current Biology* **21**, R560–R569 (2011).

[12] Otterbein, L., Graceffa, P. & Dominguez, R. The crystal structure of uncomplexed actin in the ADP state. *Science* **293**, 708–711 (2001).

[13] Graceffa, P. & Dominguez, R. Crystal structure of monomeric actin in the ATP state - Structural basis of nucleotide-dependent actin dynamics. *Journal of Biological Chemistry* **278**, 34172–34180 (2003).

[14] Dominguez, R. & Holmes, K. Actin structure and function. *Annual Review of Biophysics* **40**, 169 (2011).

[15] Reisler, E. & Egelman, E. H. Actin structure and function: What we still do not understand. *Journal of Biological Chemistry* **282**, 36133–36137 (2007).

[16] Fujii, T., Iwane, A., Yanagida, T. & Namba, K. Direct visualization of secondary structures of F-actin by electron cryomicroscopy. *Nature* **467**, 724–728 (2010).

[17] Kabsch, W., Mannherz, H., Suck, D., Pai, E. & Holmes, K. Atomic structure of the actin: Dnase I complex. *Nature* **347**, 37–44 (1990).

[18] Carlier, M.-F., Pantaloni, D. & Korn, E. The effects of Mg2+ at the high-affinity and low-affinity sites on the polymerization of actin and associated ATP hydrolysis. *Journal of Biological Chemistry* **261**, 10785–10792 (1986).

[19] Carlier, M.-F. Actin: Protein structure and filament dynamics. *The Journal of Biological Chemistry* **266**, 1–4 (1991).

[20] Moore, P., Huxley, H. & DeRosier, D. Three-dimensional reconstruction of F-actin, thin filaments and decorated thin filaments. *Journal of Molecular Biology* **50**, 279–292 (1970).

[21] Jakus, M. & Hall, C. Studies of actin and myosin. *Journal of Biological Chemistry* **167**, 705–714 (1947).

[22] Hanson, J. & Lowy, J. The structure of F-actin and of actin filaments isolated from muscle. *Journal of Molecular Biology* **6**, 46–IN5 (1963).

[23] Holmes, K., Popp, D., Gebhard, W. & Kabsch, W. Atomic model of the actin filament. *Nature* **347**, 44–49 (1990).

[24] Toshiro Oda and Mitsusada Iwasa and Tomoki Aihara and Yuichiro Maeda and Akihiro Narita. The nature of the globular-to fibrous-actin transition. *Nature* **457**, 441–445 (2009).

[25] Gershman, L., Selden, L. & Estes, J. High affinity binding of divalent cation to actin monomer is much stronger than previously reported. *Biochemical and biophysical research communications* **135**, 607–614 (1986).

[26] Pollard, T. & Cooper, J. Actin and actin-binding proteins. A critical evaluation of mechanisms and functions. *Annual Review of Biochemistry* **55**, 987–1035 (1986).

[27] Sept, D. & McCammon, J. Thermodynamics and kinetics of actin filament nucleation. *Biophysical Journal* **81**, 667–674 (2001).

[28] Howard, J. *Mechanics of Motor Proteins and the Cytoskeleton* (Sinauer Associates, Inc., 2001).

[29] Wegner, A. Spontaneous fragmentation of actin filaments in physiological conditions. *Nature* **296**, 266–267 (1982).

[30] Erickson, H. Co-operativity in protein-protein association: The structure and stability of the actin filament. *Journal of Molecular Biology* **206**, 465–474 (1989).

[31] Bonder, E., Fishkind, D., Mooseker, M. *et al.* Direct measurement of critical concentrations and assembly rate constants at the two ends of an actin filament. *Cell* **34**, 491 (1983).

[32] Gordon, D., Yang, Y. & Korn, E. Polymerization of acanthamoeba actin. Kinetics, thermodynamics, and co-polymerization with muscle actin. *Journal of Biological Chemistry* **251**, 7474 (1976).

[33] Nicholls, D. & Ferguson, S. *Bioenergetics 2* (Academic Press, 1992).

[34] Wanger, M. & Wegner, A. Similar affinities of ADP and ATP for G-actin at physiological salt concentrations. *FEBS letters* **162**, 112–116 (1983).

[35] Straub, F. & Feuer, G. Adenosinetriphosphate the functional group of actin. *Biochimica et Biophysica Acta* **4**, 455–470 (1950).

[36] De La Cruz, E., Mandinova, A., Steinmetz, M., Stoffler, D., Aebi, U. & Pollard, T. Polymerization and structure of nucleotide-free actin filaments. *Journal of Molecular Biology* **295**, 517–526 (2000).

[37] Korn, E., Carlier, M.-F. & Pantaloni, D. Actin polymerization and ATP hydrolysis. *Science* **238**, 638–644 (1987).

[38] Carlier, M.-F., Pantaloni, D. & Korn, E. Evidence for an ATP cap at the ends of actin filaments and its regulation of the F-actin steady state. *Journal of Biological Chemistry* **259**, 9983–9986 (1984).

[39] Carlier, M.-F., Pantaloni, D. & Korn, E. The mechanisms of ATP hydrolysis accompanying the polymerization of Mg-actin and Ca-actin. *Journal of Biological Chemistry* **262**, 3052–3059 (1987).

[40] Pollard, T. Polymerization of ADP-actin. *The Journal of Cell Biology* **99**, 769–777 (1984).

[41] Pollard, T. Rate constants for the reactions of ATP- and ADP-actin with the ends of actin filaments. *The Journal of Cell Biology* **103**, 2747–2754 (1986).

[42] Wegner, A. Head to tail polymerization of actin. *Journal of Molecular Biology* **108**, 139–150 (1976).

[43] Fujiwara, I., Takahashi, S., Tadakuma, H., Funatsu, T. & Ishiwata, S. Microscopic analysis of polymerization dynamics with individual actin filaments. *Nature Cell Biology* **4**, 666–673 (2002).

[44] Carlier, M.-F., Laurent, V., Santolini, J., Melki, R., Didry, D., Xia, G., Hong, Y., Chua, N. & Pantaloni, D. Actin depolymerizing factor (ADF/cofilin) enhances the rate of filament turnover: implication in actin-based motility. *The Journal of Cell Biology* **136**, 1307–1322 (1997).

[45] Blanchoin, L. & Pollard, T. Interaction of actin monomers with acanthamoebaactophorin (ADF/cofilin) and profilin. *Journal of Biological Chemistry* **273**, 25106–25111 (1998).

[46] Carlier, M.-F. & Pantaloni, D. Direct evidence for ADP-inorganic phosphate-F-actin as the major intermediate in ATP-actin polymerization. rate of dissociation of inorganic phosphate from actin filaments. *Biochemistry* **25**, 7789–7792 (1986).

[47] Carlier, M.-F., Pantaloni, D., Evans, J., Lambooy, P., Korn, E. & Webb, M. The hydrolysis of ATP that accompanies actin polymerization is essentially irreversible. *FEBS letters* **235**, 211–214 (1988).

[48] Carlier, M.-F. & Pantaloni, D. Binding of phosphate to F-ADP-actin and role of F-ADP-Pi-actin in ATP-actin polymerization. *The Journal of Biological Chemistry* **263**, 817–825 (1988).

[49] Fujiwara, I., Vavylonis, D. & Pollard, T. Polymerization kinetics of ADP- and ADP-Pi-actin determined by fluorescence microscopy. *Proceedings of the National Academy of Sciences of the United States of America* **104**, 8827–8832 (2007).

[50] Ohm, T. & Wegner, A. Mechanism of ATP hydrolysis by polymeric actin. *Biochimica et Biophysica Acta - Protein Structure and Molecular Enzymology* **1208**, 8–14 (1994).

[51] Li, X., Kierfeld, J. & Lipowsky, R. Actin polymerization and depolymerization coupled to cooperative hydrolysis. *Physical Review Letters* **103**, 048102–1–048102–4 (2009).

[52] Kuhn, J. & Pollard, T. Real-time measurements of actin filament polymerization by total internal reflection fluorescence microscopy. *Biophysical Journal* **88**, 1387–1402 (2005).

[53] Halavatyi, A., Nazarov, P., Medves, S., Van Troys, M., Ampe, C., Yatskou, M. & Friederich, E. An integrative simulation model linking major biochemical reactions of actin-polymerization to structural properties of actin filaments. *Biophysical Chemistry* **140**, 24–34 (2009).

[54] Stukalin, E. & Kolomeisky, A. ATP hydrolysis stimulates large length fluctuations in single actin filaments. *Biophysical Journal* **90**, 2673 (2006).

[55] Hill, T. & Kirschner, M. Bioenergetics and kinetics of microtubule and actin filament assembly-disassembly. *International Review of Cytology* **78**, 1–125 (1982).

[56] Pantaloni, D., Hill, T., Carlier, M.-F. & Korn, E. A model for actin polymerization and the kinetic effects of ATP hydrolysis. *Proceedings of the National Academy of Sciences of the United States of America* **82**, 7207 (1985).

[57] Hill, T. Theoretical study of a model for the ATP cap at the end of an actin filament. *Biophysical Journal* **49**, 981–986 (1986).

[58] Flyvbjerg, H., Holy, T. & Leibler, S. Stochastic dynamics of microtubules: A model for caps and catastrophes. *Physical Review Letters* **73**, 2372–2375 (1994).

[59] Vavylonis, D., Yang, Q. & O'Shaughnessy, B. Actin polymerization kinetics, cap structure, and fluctuations. *Proceedings of the National Academy of Sciences of the United States of America* **102**, 8543 (2005).

[60] Ranjith, P., Lacoste, D., Mallick, K. & Joanny, J. Nonequilibrium self-assembly of a filament coupled to ATP/GTP hydrolysis. *Biophysical Journal* **96**, 2146–2159 (2009).

[61] Van Kampen, N. *Stochastic Processes in Physics and Chemistry* (Elsevier, 1992).

[62] Kueh, H., Brieher, W. & Mitchison, T. Dynamic stabilization of actin filaments. *Proceedings of the National Academy of Sciences of the United States of America* **105**, 16531–16536 (2008).

[63] Kueh, H. Y. & Mitchison, T. J. Structural plasticity in actin and tubulin polymer dynamics. *Science* **325**, 960–963 (2009).

[64] Egelman, E., Francis, N. & DeRosier, D. F-actin is a helix with a random variable twist. *Nature* **298**, 131 (1982).

[65] Galkin, V., Orlova, A., Schröder, G. & Egelman, E. Structural polymorphism in F-actin. *Nature structural & molecular biology* **17**, 1318–1323 (2010).

[66] Chhabra, E. & Higgs, H. The many faces of actin: matching assembly factors with cellular structures. *Nature Cell Biology* **9**, 1110–1121 (2007).

[67] Niedermayer, T., Jégou, A., Chièze, L., Guichard, B., Helfer, E., Romet-Lemonne, G., Carlier, M.-F. & Lipowsky, R. Intermittent depolymerization of actin filaments is caused by photo-induced dimerization of actin protomers. *Proceedings of the National Academy of Sciences of the United States of America* **109**, 10769–10774 (2012).

[68] Jégou, A., Niedermayer, T., Orbán, J., Didry, D., Lipowsky, R., Carlier, M.-F. & Romet-Lemonne, G. Individual actin filaments in a microfluidic flow reveal the mechanism of ATP hydrolysis and give insight into the properties of profilin. *PLoS Biology* **9**, e1001161 (2011).

[69] Schmoller, K., Niedermayer, T., Zensen, C., Wurm, C. & Bausch, A. Fragmentation is crucial for the steady-state dynamics of actin filaments. *Biophysical Journal* **101**, 803–808 (2011).

[70] Kovar, D. & Pollard, T. Insertional assembly of actin filament barbed ends in association with formins produces piconewton forces. *Proceedings of the National Academy of Sciences of the United States of America* **101**, 14725 (2004).

[71] Schmoller, K., Semmrich, C. & Bausch, A. Slow down of actin depolymerization by cross-linking molecules. *Journal of Structural Biology* **173**, 350–357 (2011).

[72] Spudich, J. A. & Watt, S. The regulation of rabbit skeletal muscle contraction. I. Biochemical studies of the interaction of the tropomyosin-troponin complex with actin and the proteolytic. *Journal of Biological Chemistry* **246**, 4866–4871 (1971).

[73] Kouyama, T. & Mihashi, K. Fluorimetry study of N-(1-pyrenyl) iodoacetamide-labelled F-actin. *European Journal of Biochemistry* **114**, 33–38 (1981).

[74] Lin, D. & Lin, S. Actin polymerization induced by a motility-related high-affinity cytochalasin binding complex from human erythrocyte membrane. *Proceedings of the National Academy of Sciences of the United States of America* **76**, 2345 (1979).

[75] Ono, S., Mohri, K. & Ono, K. Microscopic evidence that actin-interacting protein 1 actively disassembles actin-depolymerizing factor/cofilin-bound actin filaments. *Journal of Biological Chemistry* **279**, 14207 (2004).

[76] Isambert, H., Venier, P., Maggs, A., Fattoum, A., Kassab, R., Pantaloni, D. & Carlier, M.-F. Flexibility of actin filaments derived from thermal fluctuations. Effect of bound nucleotide, phalloidin, and muscle regulatory proteins. *Journal of Biological Chemistry* **270**, 11437 (1995).

[77] Coué, M., Brenner, S., Spector, I. & Korn, E. Inhibition of actin polymerization by latrunculin A. *FEBS Letters* **213**, 316–318 (1987).

[78] Li, H., Shen, T., Smith, M., Fujiwara, I., Vavylonis, D. & Huang, X. Automated actin filament segmentation, tracking, and tip elongation measurements based on open active contour models. In *Proc. of the IEEE Int'l Symposium on Biomedical Imaging: From Nano to Macro, ISBI'09* (Boston, 2009).

[79] Combeau, C. & Carlier, M.-F. Probing the mechanism of ATP hydolysis on F-actin using vanadate and the structural analogs of phosphate BeF_3^- and AlF_4^-. *The Journal of Biological Chemistry* **263**, 17429–17436 (1988).

[80] Combeau, C. & Carlier, M.-F. Characterization of the aluminium and beryllium fluoride species bound to F-actin and microtubules at the site of the γ-phosphate of the nucleotide. *The Journal of Biological Chemistry* **264**, 19017–19021 (1989).

[81] Oda, T., Makino, K., Yamashita, I., Namba, K. & Maéda, Y. Distinct structural changes detected by X-ray fiber diffraction in stabilization of F-actin by lowering pH and increasing ionic strength. *Biophysical Journal* **80**, 841–851 (2001).

[82] Kasai, M., Asakura, S. & Oosawa, F. The G-F equilibrium in actin solutions under various conditions. *Biochimica et Biophysica Acta* **57**, 13–21 (1962).

[83] Tsuboi, K., Markel, R. & Tomita, J. The pH-dependent nature of actin transformation. *Archives of Biochemistry and Biophysics* **112**, 82–88 (1965).

[84] Zimmerle, C. & Frieden, C. Effect of pH on the mechanism of actin polymerization. *Biochemistry* **27**, 7766–7772 (1988).

[85] Wang, F., Sampogna, R. & Ware, B. pH dependence of actin self-assembly. *Biophysical Journal* **55**, 293–298 (1989).

[86] Sampath, P. & Pollard, T. Effects of cytochalasin, phalloidin and pH on the elongation of actin filaments. *Biochemistry* **30**, 1973–1980 (1991).

[87] Gross, D. & Harris, C. *Fundamentals of Queuing Theory* (Wiley & Sons, 1974).

[88] Cox, D. & Miller, H. *The Theory of Stochastic Processes* (Chapman & Hall/CRC, 1965).

[89] Gradshteyn, I. & Ryzhik, I. *Table of Integrals, Series, and Products* (Academic Press, 1994), 5 edn.

[90] Gillespie, D. T. Exact stochastic simulation of coupled chemical-reactions. *Journal of Physical Chemistry* **81**, 2340–2361 (1977).

[91] Ledermann, W. & Reuter, G. Spectral theory for the differential equations of simple birth and death processes. *Philosophical Transactions of the Royal Society of London. Series A, Mathematical and Physical Sciences* **246**, 321–369 (1954).

[92] Bailey, N. A continuous time treatment of a simple queue using generating functions. *Journal of the Royal Statistical Society. Series B (Methodological)* **16**, 288–291 (1954).

[93] Sharma, O. *Markovian Queues* (Ellis Horwood Ltd., 1990).

[94] Abramowitz, M. & Stegun, I. A. *Handbock of Mathematical Functions* (Dover, 1970).

[95] Skellam, J. The frequency distribution of the difference between 2 Poisson variates belonging to different populations. *Journal of the Royal Statistical Society Series A - Statistics in Society* **109**, 296 (1946).

[96] Prudnikov, A., Brychkov, Y. & Marichev, O. *Integrals and Series*, vol. 2: Special Functions (Taylor & Francis, 1986).

[97] Brewer, L. & Bianco, P. Laminar flow cells for single-molecule studies of DNA-protein interactions. *Nature Methods* **5**, 517–525 (2008).

[98] Valentin-Ranc, C. & Carlier, M.-F. Evidence for the direct interaction between tightly bound divalent metal ion and ATP on actin. binding of the lambda isomers of beta gamma-bidentate Cr-ATP to actin. *Journal of Biological Chemistry* **264**, 20871–20880 (1989).

[99] Melki, R., Fievez, S. & Carlier, M.-F. Continuous monitoring of Pi release following nucleotide hydrolysis in actin or tubulin assembly using 2-amino-6-mercapto-7-methylpurine ribonucleoside and purine-nucleoside phosphorylase as an enzyme-linked assay. *Biochemistry* **35**, 12038–12045 (1996).

[100] Kaplan, E. L. & Meier, P. Nonparametric estimation from incomplete observations. *Journal of the American Statistical Association* **53**, 457–481 (1958).

[101] Kalbfleisch, J. & Prentice, R. *The Statistical Analysis of Failure Time Data* (Wiley & Sons, 2002), 2 edn.

[102] Knight, P. & Offer, G. p-NN'-phenylenebismaleimide, a specific cross-linking agent for F-actin. *Biochemical Journal* **175**, 1023 (1978).

[103] Elzinga, M. & Phelan, J. F-actin is intermolecularly crosslinked by N, N'-p-phenylenedimaleimide through lysine-191 and cysteine-374. *Proceedings of the National Academy of Sciences of the United States of America* **81**, 6599 (1984).

[104] Janmey, P., Hvidt, S., Oster, G., Lamb, J., Stossel, T. & Hartwig, J. Effect of ATP on actin filament stiffness. *Nature* **347**, 95–99 (1990).

[105] Blanchoin, L. & Pollard, T. Hydrolysis of ATP by polymerized actin depends on the bound divalent cation but not profilin. *Biochemistry* **41**, 597–602 (2002).

[106] Li, X., Lipowsky, R. & Kierfeld, J. Coupling of actin hydrolysis and polymerization: Reduced description with two nucleotide states. *Europhysics Letters* **89**, 38010 (2010).

[107] Press, W., Teukolsky, S., Vetterling, W. & Flannery, B. *Numerical Recipes: The Art of Scientific Computing* (Cambridge University Press, 2007), 3 edn.

[108] Seber, G. A. F. & Wild, C. J. *Nonlinear Regression* (Wiley-Interscience, 2003).

[109] Carlsson, L., Nyström, L., Sundkvist, I., Markey, F., Lindberg, U. *et al.* Actin polymerizability is influenced by profilin, a low molecular weight protein in non-muscle cells. *Journal of Molecular Biology* **115**, 465 (1977).

[110] Schutt, C., Myslik, J., Rozycki, M., Goonesekere, N. & Lindberg, U. The structure of crystalline profilin-ß-actin. *Nature* **365**, 810–816 (1993).

[111] Yarmola, E. & Bubb, M. Profilin: Emerging concepts and lingering misconceptions. *Trends in biochemical sciences* **31**, 197–205 (2006).

[112] Bubb, M., Yarmola, E., Gibson, B. & Southwick, F. Depolymerization of actin filaments by profilin. *Journal of Biological Chemistry* **278**, 24629 (2003).

[113] Gutsche-Perelroizen, I., Lepault, J., Ott, A. & Carlier, M.-F. Filament assembly from profilin-actin. *Journal of Biological Chemistry* **274**, 6234–6243 (1999).

[114] Pantaloni, D. & Carlier, M.-F. How profilin promotes actin filament assembly in the presence of thymosin $\beta 4$. *Cell* **75**, 1007–1014 (1993).

[115] Romero, S., Didry, D., Larquet, E., Boisset, N., Pantaloni, D. & Carlier, M.-F. How ATP hydrolysis controls filament assembly from profilin-actin. Implication for formin processivity. *Journal of Biological Chemistry* **282**, 8435–8445 (2007).

[116] Yarmola, E., Dranishnikov, D. & Bubb, M. Effect of profilin on actin critical concentration: A theoretical analysis. *Biophysical Journal* **95**, 5544–5573 (2008).

[117] Mullins, R. The instability of stabilization. *Proceedings of the National Academy of Sciences of the United States of America* **109**, 10743–10744 (2012).

[118] Simon, J., Gough, A., Urbanik, E., Wang, F., Lanni, F., Ware, B. & Taylor, D. Analysis of rhodamine and fluorescein-labeled F-actin diffusion in vitro by fluorescence photobleaching recovery. *Biophysical Journal* **54**, 801–815 (1988).

[119] Kozuka, J., Yokota, H., Arai, Y., Ishii, Y. & Yanagida, T. Dynamic polymorphism of single actin molecules in the actin filament. *Nature Chemical Biology* **2**, 83–86 (2006).

[120] DesMarais, V., Ichetovkin, I., Condeelis, J. & Hitchcock-DeGregori, S. Spatial regulation of actin dynamics: A tropomyosin-free, actin-rich compartment at the leading edge. *Journal of Cell Science* **115**, 4649–4660 (2002).

[121] Bugyi, B., Didry, D. & Carlier, M.-F. How tropomyosin regulates lamellipodial actin-based motility: A combined biochemical and reconstituted motility approach. *The EMBO journal* **29**, 14–26 (2010).

[122] Skau, C. & Kovar, D. Fimbrin and tropomyosin competition regulates endocytosis and cytokinesis kinetics in fission yeast. *Current Biology* **20**, 1415–1422 (2010).

[123] Danuser, G. & Waterman-Storer, C. Quantitative fluorescent speckle microscopy of cytoskeleton dynamics. *Annu. Rev. Biophys. Biomol. Struct.* **35**, 361–387 (2006).

[124] Jacobson, K., Rajfur, Z., Vitriol, E. & Hahn, K. Chromophore-assisted laser inactivation in cell biology. *Trends in cell biology* **18**, 443–450 (2008).

[125] Pantaloni, D., Carlier, M.-F., Coué, M., Lal, A., Brenner, S. & Korn, E. The critical concentration of actin in the presence of ATP increases with the number concentration of filaments and approaches the critical concentration of ADP-actin. *The Journal of Biological Chemistry* **259**, 6274–6283 (1984).

[126] Gieselmann, R., Kwiatkowski, D., Janmey, P. & Witke, W. Distinct biochemical characteristics of the two human profilin isoforms. *European Journal of Biochemistry* **229**, 621–628 (1995).

[127] Polyanin, A. & Zaitsev, V. *Handbook of exact solutions for ordinary differential equations* (CRC Press, 1995).

Danksagung

Ich hatte mich sehr darauf gefreut, zum Schluss noch mal allen Mitwirkenden für ihre Hilfe zu danken, und die letzten Jahre Revue passieren zu lassen. Ich gebe zu, die Dinge nun – nach einer Nacht am Schreibtisch – ganz anders zu sehen und mich auf viel profanere Unternehmungen zu freuen.

Mein Dank gilt zuallererst meinem Betreuer, Herrn Reinhard Lipowsky, der mir vieles ermöglicht hat. Insbesondere danke ich Herrn Lipowsky für die Zeit, die er sich auch für längere Diskussionen genommen hat und die Freiheit, die er mir in vielen Dingen gewährt hat. Ausserdem bedanke ich mich für die freundliche Mac-Leihgabe, die Vertragsverlängerung in einer für mich schwierigen Zeit, und den Tipp, doch endlich mal die Diss abzuschliessen. Dank gebührt auch Jan Kierfeld, der mich bei meinem ursprünglichen (Stäbchen-)Thema betreut und mich auch sonst bei vielem unterstützt hat. Weiterhin gilt mein Dank Peter Lenz, er hat mir empfohlen, bei Herrn Lipowsky nach einem Thema zu fragen.

Besonderer Dank gilt Marie-France Carlier, die mich sehr herzlich in ihrer Gruppe aufgenommen hat, mir vieles persönlich erklärt, und mich mit ihrem Enthusiasmus begeistert hat. Die unheimliche Hilfsbereitschaft ihrer Gruppe in Gif-sur-Yvette hat es mir erst ermöglicht, im Labor mehr als nur herumzustehen. Insbesondere sei Emmanuèle Helfer für die Einfürung in die Mikroskopie erwähnt. Ich danke auch Veronika Wanner, die nicht nur den Aufenthalt in Frankreich angenehmer gemacht hat. Guillaume Romet-Lemonne möchte ich für die gute Kooperation und unsere stundenlangen Telefonate danken, bei denen ich viel gelernt habe. Ohne ihn und Antoine Jégou hätte es die besprochenen Resultate nicht gegeben.

Ich danke auch der gesamten Theorieabteilung für die Diskussionsbereitschaft, nicht nur über das Thema Wissenschaft. Es fällt mir schwer, hier einzelne hervorzuheben. Weiterhin danke ich Marco Ehlert und René Genz für hervorragenden IT-support. Ausserdem möchte ich Alida Babel nicht unerwähnt lassen, deren Kantine den eigentlichen “Standortvorteil” von Golm darstellt. Weiterhin danke ich meinen Freunden, die mich in den letzten Jahren unterstützt haben, insbesondere jedoch Nikolai Becker, Florian Berger und Veronika Bierbaum für den Unterschlupf während der stürmischen Wochen im Frühling. Ich habe das Glück, Eltern zu haben, die in jeder Situation hinter mir standen. Ihnen gebührt mein besonderer Dank. Zum Schluss möchte ich Sophia Rudorf, Veronika Bierbaum, Andrea Grafmüller, Carlus Deneke und Florian Berger nicht nur für das Korrekturlesen in letzter Minute danken.

Erklärung

Ich erkläre, dass ich diese Arbeit an keiner anderen Hochschule eingereicht, sowie selbstständig verfasst und keine anderen als die angegebenen Quellen und Hilfsmittel verwendet habe.

Thomas Niedermayer,
Potsdam, im Juli 2012